FLORIDA SOLAR ENERGY CENTER®

Latent and Sensible Load Distributions in Conventional and Energy Efficient Residences

Authors

Philip Fairey
Alp Keresteciogl u
Robin Vieira
Muthusamy Swami
Subrato Chandra

Original Publication

Fairey, P., Keresteciogl u, A., Vieira, R., Swami, M., Chandra, S., "Latent and Sensible Load Distributions in Conventional and Energy Efficient Residences", prepared for Gas Research Institute, May 1986.

Publication Number

FSEC-CR-153-86

A Research Institute of the University of Central Florida
1679 Clearlake Road, Cocoa, FL 32922-5703 • Phone: 321-638-1000 • Fax: 321-638-1010
www.fsec.ucf.edu

GRI-86/0056

LATENT AND SENSIBLE LOAD DISTRIBUTIONS IN CONVENTIONAL AND ENERGY EFFICIENT RESIDENCES

FINAL REPORT

JANUARY 1983 - JANUARY 1986

GRI CONTRACT NO. 5082-243-0727

By

FLORIDA SOLAR ENERGY CENTER
300 State Road 401
Cape Canaveral, Florida 32920

FSEC-CR-153-86

For

GAS RESEARCH INSTITUTE
8600 West Bryn Mawr Avenue
Chicago, Illinois 60631

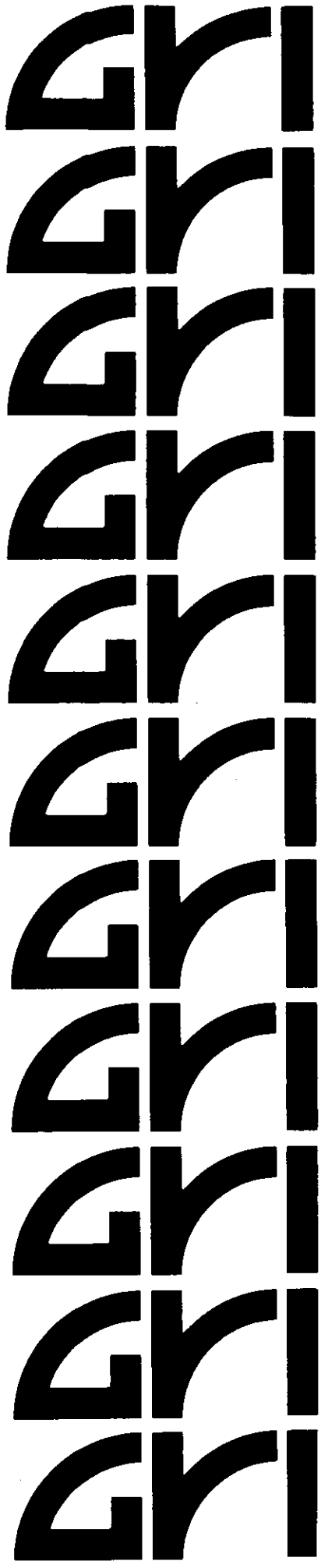

LATENT AND SENSIBLE LOAD DISTRIBUTIONS IN CONVENTIONAL AND ENERGY EFFICIENT RESIDENCES

FINAL REPORT
(January 1983 - January 1986)

Prepared by

Philip Fairey
Alp Keresteciogl u
Robin Vieira
Mathusamy Swami
Subrato Chandra

Florida Solar Energy Center
300 State Road 401
Cape Canaveral, FL 32920

FSEC-CR-153-86

for

GAS RESEARCH INSTITUTE
Contract No. 5082-243-0727

GRI Project Manager

Douglas R. Kosar
Cooling Systems

May 1986

LEGAL NOTICE This report was prepared by the Florida Solar Energy Center (FSEC) as an account of work sponsored by the Gas Research Institute (GRI). Neither GRI, members of GRI, nor any person acting on behalf of either:

a. Makes any warranty or representation, express or implied, with respect to the accuracy, completeness, or usefulness of the information contained in this report, or that the use of any apparatus, method, or process disclosed in this report may not infringe privately owned rights; or

b. Assumes any liability with respect to the use of, or for damages resulting from the use of, any information, apparatus, method, or process disclosed in this report.

ACKNOWLEDGEMENTS

The authors are indebted to the many people who have provided their assistance and expertise during this study. They are so many and scattered that it would not be possible to acknowledge them all. Most of the FSEC staff have assisted in one manner or another. The FSEC graphics department is responsible for many of the illustrations, and we are especially grateful to Ms. Mable Flumm, Ms. Didem Keresteciogl u and Mrs. Ann Fay who patiently and cheerfully provided all the word processing support for the project.

We are grateful to George Walton of the National Bureau of Standards who created the basic TARP computer code upon which we have built. He also helped the project team with advice during the debugging phase of our code work. Many thanks also go to Doug Kosar, the GRI manager for this project, for his patience and guidance.

50272-101

REPORT DOCUMENTATION PAGE	1. REPORT NO. GRI-86/0056	2.	3. Recipient's Accession No

4. Title and Subtitle
Latent and Sensible Load Distributions in Conventional and Energy Efficient Residences

5. Report Date
May 1986

6.

7. Author(s)
P. Fairey, A. Keresteciogl u, R. Vieira, M. Swami, and S. Chandra

8. Performing Organization Rept. No
FSEC-CR-153-86

9. Performing Organization Name and Address
Florida Solar Energy Center (FSEC)
300 State Road 401
Cape Canaveral, Florida 32920

10. Project/Task/Work Unit No.

11. Contract(C) or Grant(G) No.
(C) GRI/5082-243-0727
(G)

12. Sponsoring Organization Name and Address
Gas Research Institute (GRI)
8600 West Bryn Mawr Avenue
Chicago, Illinois 60631

13. Type of Report & Period Covered
Final (Jan 83-Jan 86)

14.

15. Supplementary Notes

16. Abstract (Limit: 200 words)

The effects of moisture adsorption and desorption in residential buildings is studied in detail. Energy conserving and conventional residences are examined and building loads are disaggregrated into their thermal, moisture and source components.

The report covers significant new analytical and experimental work. A detailed building moisture analysis technique is developed to be incorporated into the NBS building analysis program TARP. The model is validated against field and laboratory data with good results. The new code, MADTARP, is used to parametrically examine residential load distributions under a variety of climate, cooling strategy, and building construction conditions. At the conclusion the economies of gas and electrical dehumidification/cooling equipment are explored.

17. Document Analysis a. Descriptors
Cooling loads, building analysis, humidity, mass transfer, dehumidification, moisture adsorption, energy conservation, passive cooling, desiccant cooling.

b. Identifiers/Open-Ended Terms

c. COSATI Field/Group

18. Availability Statement:	19. Security Class (This Report)	21. No. of Pages
Release Unlimited	Unclassified	249
	20. Security Class (This Page) Unclassified	22. Price

(See ANSI-Z39.18) See Instructions on Reverse OPTIONAL FORM 272 (4-77) (Formerly NTIS-35) Department of Commerce

Research Summary

Title	Latent and Sensible Load Distributions in Conventional and Energy Efficient Residences
Contractor	Florida Solar Energy Center
Principal Investigators	Philip Fairey, Alp Keresteciogl u, Robin Vieira, Mathusamy Swami, Subrato Chandra
Report Period	January 1983 - January 1986 Final Report
Objective	To develop a method to characterize the cooling load distributions in conventional and energy efficient residences, specifically as related to building dehumidification loads, as they pertain to the potential for the use of gas-fired dehumidification and cooling equipment.
Technical Perspective	Prior to this work no detailed effort to understand and predict the effect of moisture on building cooling loads had been attempted. The behavior of moisture is particularly problematic because there is a limited phenomenological knowledge base and material moisture property data is sketchy. Combined heat and mass transfer methods first proposed by Luikov are used in this analysis. These methods are amenable for use in detailed models but not directly usable in the conduction transfer function models used in building energy analysis. Therefore, moisture migration in buildings must first be characterized through detailed modeling techniques and those characteristics carried over to the building energy analysis codes.
Results	The analysis has shown that typical buildings have surprisingly high capacities to store and release moisture. Analysis techniques that ignore this fact exhibit significant errors in the prediction of dehumidification loads and room humidity conditions in buildings. These errors are quite high for ventilated buildings and can lead to inaccurate estimates of cooling loads and room humidity conditions. The analysis has shown the potential for the use of gas-fired dehumidification systems to be warranted and economically viable in many of the climates for the more energy efficient residences.

Technical Approach

Through detailed finite element modeling methods and experimental field measurements the research has characterized mass transfer potentials in typical residences. Algorithms that predict this characteristic behavior are incorporated in a conduction transfer function analysis code (TARP) and a detailed moisture adsorption and desorption building analysis code (MADTARP) is developed. The code is used to parametrically analyze the performance and cooling and heating loads for a variety of building strategies in nine southeastern climates. Results of the analysis are then used to estimate the requirements and economic feasibility of gas-fired desiccant dehumidification systems as compared to competing electrical systems.

Project Implications

This project represents the first comprehensive effort to accurately examine moisture transfer in buildings and its resultant effect on latent and sensible cooling loads. Performance requirements for air conditioning systems are significantly impacted by moisture adsorption and desorption in building materials and furnishings. Gas fired desiccant dehumidification and cooling systems under development at GRI will benefit greatly from a more accurate representation of building loads. Further development and validation of these modeling capabilities is required though, including generation of a data base of building material moisture properties, verification of algorithms in the field, and documentation of the computer program for public use. GRI plans to continue support for this development and validation in coordination with cognizant national engineering organizations and federal government agencies sponsoring research in this area.

GRI Project Manager
Doug Kosar
Project Manager, Cooling Systems

TABLE OF CONTENTS

LIST OF FIGURES

List of Tables

SECTION ONE
INTRODUCTION

During the past ten to fifteen years there has been an effort to reduce the level of energy use in the United States. A significant portion of this effort has concentrated on building energy consumption. Passive design and energy-efficient buildings have been an outgrowth of these efforts. The major part of the buildings effort, however, has concentrated on methods of providing heat for buildings. Unlike much of the past work, this study represents an extensive effort in building cooling research.

The primary objective of the study has been to characterize the auxilary cooling requirements of conventional and efficient buildings that are located in the rapidly growing Sunbelt portion of the U.S. Of the 1.7 million new housing starts in 1983, almost 68 percent were in the south. Approximately 62 percent of these were in the hot, humid southeastern United States. Figure 1-1 illustrates this shift in population growth and identifies the cities chosen for use in this study.

The Atlantic and Gulf Coast climates of the Sunbelt are characterized by long, hot and excessively humid summers, and cooling loads often dominate the annual load. Energy conservation techniques and passive building design are capable of reducing the thermal loads on these buildings. But to date, no effective means, short of mechanical systems, have been developed to remove moisture loads. As thermal loads are reduced, moisture loads tend to rise as a percentage of the total building cooling load. Typical mechanical systems (i.e., vapor compression air conditioners) are not well equipped to remove moisture in the absence of a thermal load. As a result, building humidity levels have a tendency to rise above traditionally acceptable levels in efficiently designed

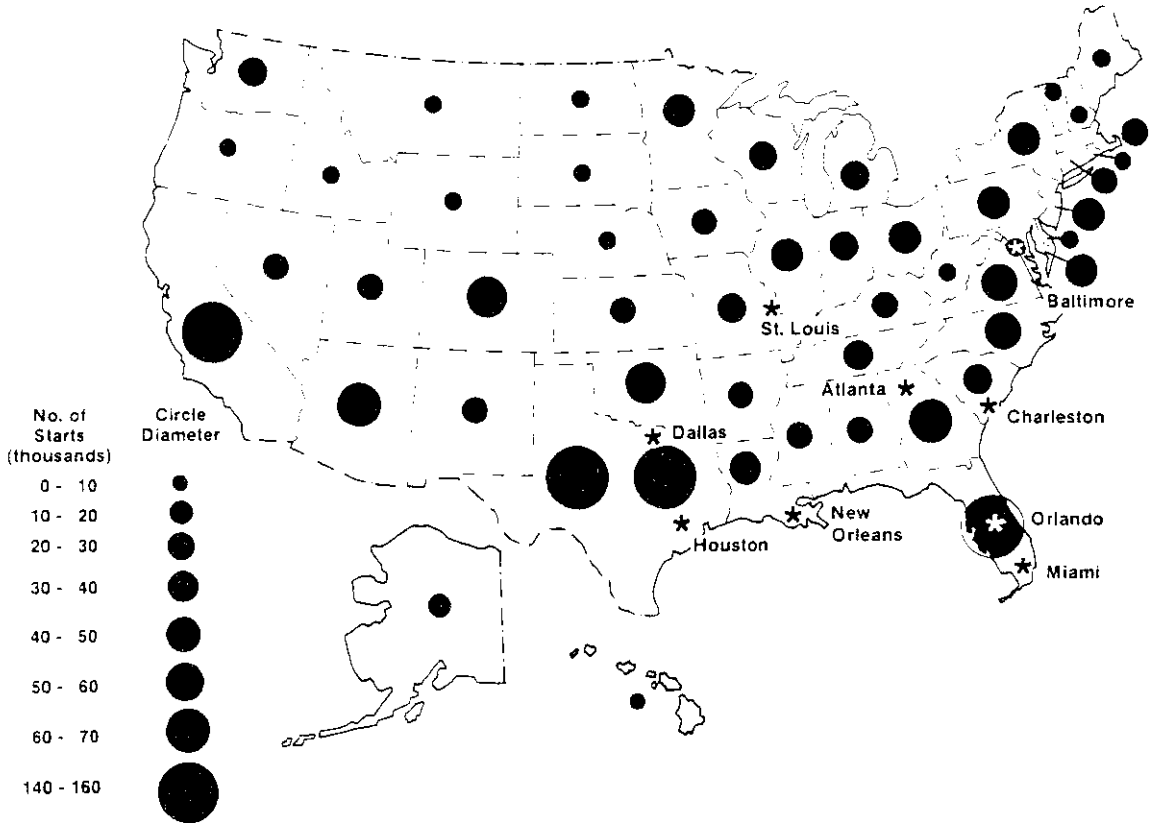

Figure 1-1 1983 single family residential housing starts. Source: USA TODAY, Jan. 19, 1984.

buildings that are located in humid climates.

The excessive humidity in such climates not only limits the efficiency of natural cooling techniques but also severely complicates building energy analysis. The thermal behavior of a building can be modeled in considerable detail with publicly available software, but conventional building energy analysis techniques do not consider the detailed behavior of moisture in buildings. When moisture enters (or is generated in) a building, it may either increase the moisture content of the room air, be absorbed by the materials in the room, be removed by the mechanical cooling system, or experience a combination of the three. Conventional building energy analysis techniques assume that all moisture entering the room results in an increase in the moisture content of the room air only.

In reality part of this moisture will be absorbed by the room materials and part will be removed by the cooling system.

Many building materials and furnishings have a large propensity to absorb and desorb moisture. Building energy analysis models that do not include analysis of moisture absorption and desorption (MAD) will inaccurately predict both cooling loads and room humidity conditions, and thus, the performance of the air conditioner. When passive cooling options (especially ventilation) are used in combination with thermally efficient building envelopes, this phenomena results in large errors in predicted cooling loads.

Until this study, no comprehensive effort to accurately examine the effects of moisture transfer in buildings had been attempted. An extensive search of the literature has been conducted to determine the state-of-the-technology of moisture transfer into and through solid materials and the behavior of moisture in buildings on the whole.

Two recent researchers, Kusuda [1984] and Miller [1985], have addressed the effects of MAD on building conditions and loads. Their initial work illustrated the potential importance of MAD in whole buildings. This study builds upon their initial findings in monitored buildings. Additional whole-building monitoring has been conducted by FSEC during this study and has contributed extensively to our confidence in the analytical tools that are used.

The physical and analytical theory that forms the core of this study comes largely from the work of Luikov [1966, 1975]. Luikov has considerably advanced the theory of combined heat and mass transfer and the serious reader should consult his work.

The literature, however, reveals no comprehensive analytical method of evaluating moisture transport in buildings, so one was developed called MADAM (**M**oisture **A**bsorption and **D**esorption **A**nalysis **M**ethod). It is shown in Section 2 of the report to be a well validated and highly accurate method. Results from MADAM have produced an accurate moisture prediction algorithm that has been included in TARP [Walton, 1983], a detailed hourly building energy analysis program. The new program is called MADTARP (**M**oisture **A**bsorption/**D**esorption and **T**hermal **A**nalysis **R**esearch **P**rogram). The algorithms incorporated in MADTARP have been separately compared against monitored data from an unoccupied residence to determine appropriate whole-building moisture holding capacities for "typical" buildings. This work is also well documented in Section 2 of the report.

MADTARP was subsequently used to parametrically analyze the energy requirements of typical (new construction), energy efficient, and passively cooled buildings in nine cities. Of these cities, five can be classified as hot and humid, three as warm and moderately humid, one as temperate and moderately humid, and one as temperate with normal humidity. It was found that buildings have far more capacity to adsorb and desorb moisture in all climates than any previous building analysis method could account for. This fact considerably affected the predicted cooling loads and/or space conditions in all the buildings and climates analyzed.

It has become apparent through this study that even typical buildings in humid climates, cooled by conventional mechanical cooling equipment (i.e., vapor compression air conditioners and heat pumps), are not capable of maintaining the conditions of the ASHRAE Standard 55-1981 for human comfort. As the thermal performance of these buildings is improved the moisture problem is exacerbated, and if passive or hybrid

cooling systems are added, building moisture problems can become critical.

With respect to the ASHRAE comfort standard, typical residences in the five most humid climates using traditional mechanical cooling systems have annual moisture removal shortfalls between 3,500 and 6,000 pounds. If energy conservation measures are employed and infiltration levels are reduced to their lowest reasonable (for health reasons) levels, this shortfall can be somewhat reduced to 3,000 to 4,500 pounds (see Figure 2-2). If passive or hybrid cooling systems are added to residences to reduce the thermal cooling load the annual shortfall will rise to between 4,000 and 8,000 pounds.

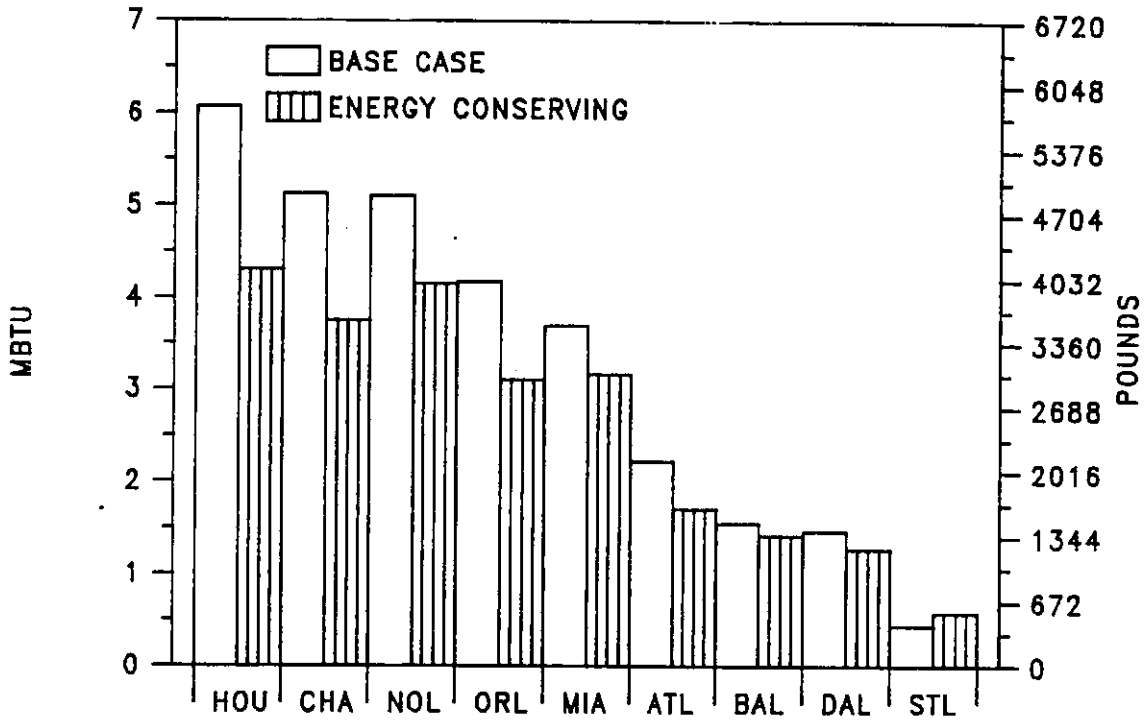

Figure 1-2 Annual latent load shortfall to maintain ASHRAE comfort conditions for the basecase and energy conserving frame residences.

Nonetheless, 30-40 percent savings in cooling energy consumption with bearable humidity liabilities (<68% RH) were found possible in southern homes. The results, reported in

Section 4, indicate that if infiltration is kept low, the high humidity levels (>68% RH) associated with mold and mildew growth are limited primarily to passively cooled residences and residences that are vented on a daily cycle (e.g., night venting with air conditioning during the day).

However, as energy conservation measures were added to the basecase (typical) residence, room relative humidity tended to rise. If infiltration was not simultaneously reduced to 0.5 air changes per hour from the basecase rate of 0.75, room relative humidities climbed above 68% in the energy conserving residences as well. The only conservation strategy investigated that did not have a strong tendency to raise indoor RH was increased thermostat settings. In this case the temperature rose along with the humidity ratio of the buildings and room RH remained relatively stable. Although they saved energy, all other strategies except reduced infiltration resulted in an attendant increase in indoor RH.

Because buildling RH tends to rise with increases in the thermal integrity of the envelope, the economic feasibility of using gas dehumidification equipment to meet moisture loads in buildings has been examined in Section 5 of the report. As in all analysis the results are driven by the basic assumptions. For this study the room moisture limits of the ASHRAE Standard 55-1981 for human comfort constitute a major assumption that, if relaxed, will significantly alter the results.

The base alternative against which the gas dehumidification equipment is compared is the stand-alone electric vapor-compression dehumidifier. The reasoning for this choice is rooted in the fact that over 591,000 electric dehumidification units were sold in 1984. Results of any comparative analysis are a strong function of the basis for comparison and, again, the results presented here may be greatly altered by the choice of an alternative base system.

Accepting these assumptions, there are significant economic advantages to be gained through the use of gas rather than electric dehumidification systems. The analysis shows that simple paybacks of one and one-half years are obtained in passively cooled buildings in eight of the nine climates examined. Even in energy conserving buildings paybacks of under one and one-half years were realized in six of the nine climates, and eight of the nine climates analyzed had simple paybacks of three and one-half years or less for the energy conserving building.

Improvements in building thermal design are becoming more and more popular. Good thermal building practices are now being encouraged through building codes, utility incentives or both in many states. The success and popularity of passive building design for heating in northern climates will undoubtedly lead to a desire on the part of the public to increase building efficiency and incorporate as many passive building techniques as practicable in southern climates as well. This study indicates that traditional mechanical cooling systems will not be appropriately matched to the auxiliary cooling loads found in these improved buildings because of the inability of vapor compression machines to remove moisture in the absence of a thermal load. As a result, the marketplace will seek alternative mechanical equipment that is capable of removing the residual moisture loads in good buildings. Desiccant and hybrid cooling equipment currently under development by GRI and others offers a realistic alternative to meet this potential marketplace demand.

SECTION TWO
DEVELOPMENT OF MADTARP

2.1 BACKGROUND

The major objective of this research is to characterize the interface between conventional and energy efficient building techniques and the mechanical cooling requirements of residences in hot, humid climates. Four specific types of energy efficient building techniques are studied in detail.

- Load avoidance through radiant barriers, window shading, and increased thermal insulation.
- Building cooling through natural ventilation.
- Passive/hybrid cooling through night sky roof radiation.
- Passive/hybrid cooling through earth-coupled cooling tubes.

The analysis is conducted primarily in humid climates of the southeastern United States. It consists of the detailed hourly building simulation and analysis of six different building "types" in nine different climates. Each of these is analyzed for performance with respect to two mechanical cooling scenarios: a "typical" vapor compression air conditioning system and what we term an "ideal" machine. The typical a/c is modeled after a two-ton, "split" system (SEER=8.0/SHF=0.76 @ ARI test conditions of 95°F db outside air and 80°F db/67°F wb room return air). The ideal machine is assumed to be capable of maintaining an upper limit on room temperature **and** relative humidity. The building loads imposed on both mechanical systems are carefully evaluated for their separate sensible and latent components and the sources of these loads are separately tracked.

At the inception of the research a detailed hourly building energy analysis computer code called TARP (**T**hermal **A**nalysis **R**esearch **P**rogram), written by George Walton [1983] at the

National Bureau of Standards, was chosen to perform the building simulations. The TARP was selected for two primary reasons:

- First, the technical and scientific basis of the thermal code is well documented. The TARP is a derivative of the BLAST, and more indirectly, the NBSLD computer codes. NBSLD was written by a team led by Kusuda [1976] at NBS and Walton (the author of TARP) was a major contributor to the BLAST code development under Hittle [1981]. The TARP is well documented in terms of its thermal algorithms and both BLAST and NBSLD have survived the close scrutiny of the building energy research community for a number of years. The TARP is currently being used at NBS for a number of detailed validation studies. The fact that the TARP performs zone energy balances was an important consideration in the final choice.

- Second, the TARP is highly portable. Unlike its predecessors the TARP is written entirely in FORTRAN-77 and can be installed on a large number of main-frame and minicomputer systems. We have installed and run the code on a 1 MByte microcomputer using 16 bit architecture but that practice, although achievable, is not recommended.

The TARP, however, does not come equipped to perform the moisture analysis required by this research. It has been significantly altered and the version used here is called MADTARP (**M**oisture **A**bsorption/**D**esorption and **T**hermal **A**nalysis **R**esearch **P**rogram). The biggest alterations are the addition of computer code that allows analysis of moisture absorption and desorption (MAD) by materials and the analysis of passive and hybrid cooling systems. The capability to model mechanical system performance and provide for control logic

have also been included in the code. A method of evaluating slab-on-grade heat transfer has been included in the analysis and a number of improvements have been made to existing TARP algorithms. Each of the alterations is discussed in detail in this and the following section of the report. Figure 2-1 illustrates the general structure of the model used in this study.

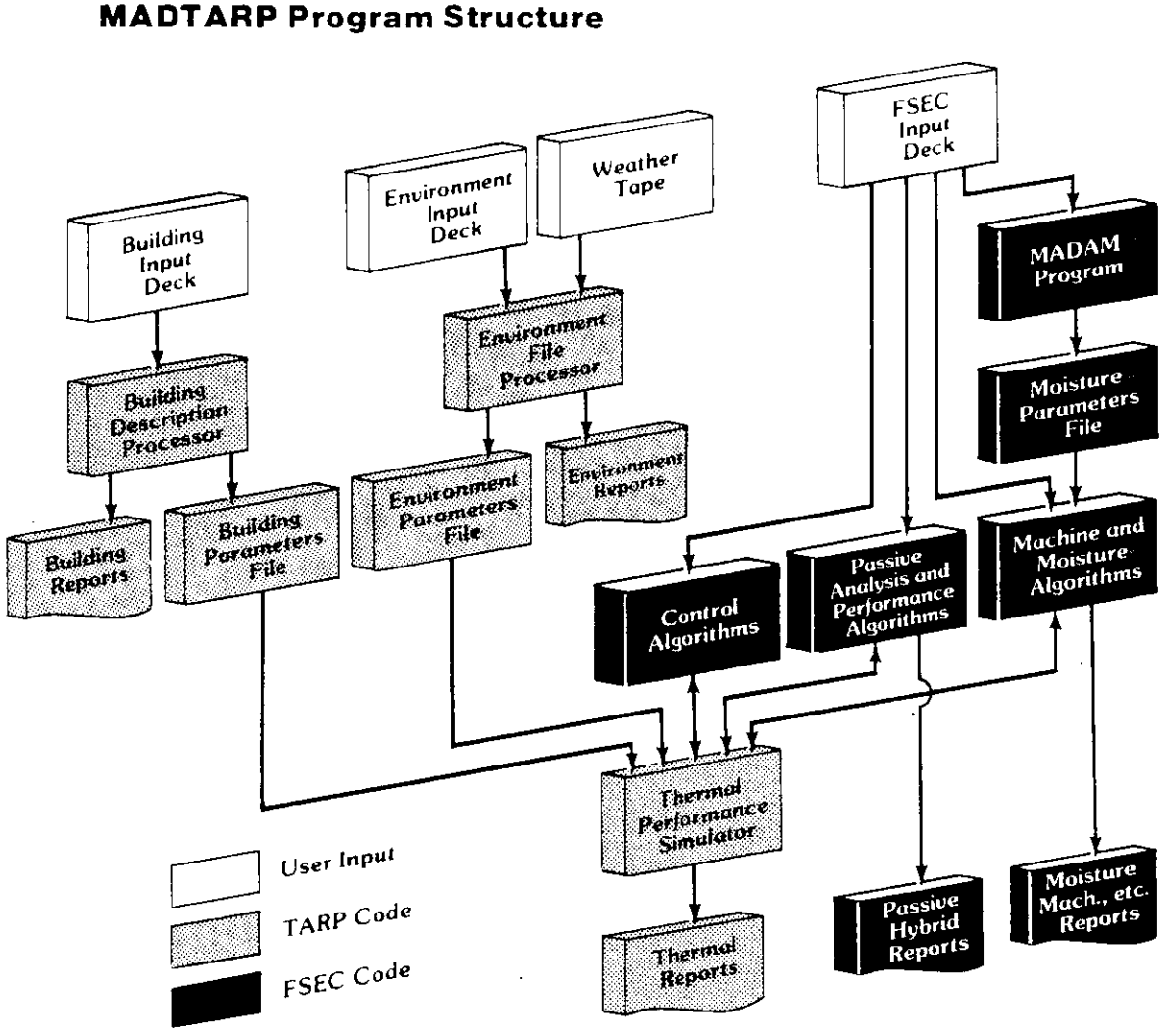

Figure 2-1 Structural diagram showing interface between original TARP code and the modifications that make up MADTARP.

In terms of building energy predictions the most significant of these changes is the detailed modeling of MAD. Research of building moisture problems has been primarily limited to northern cold-weather problems. As a result, the emphasis has been on the problem of condensation on or within building components. The research has concentrated on vapor diffusion through building materials and has resulted in recommendations for the placement of vapor barrier materials within building envelopes.

In humid climates under summer conditions, vapor diffusion through opaque building envelope (e.g., walls) is not a significant loads analysis problem. The overwhelming majority of building moisture arrives in the conditioned zone through infiltration and internal generation [ASHRAE 1981, p. 26.31]. Additionally, where a good outside weather skin is provided, condensation of moisture in building materials in summer is an extremely rare occurrence that should not constitute a serious problem [Sherwood, 1985]. Ambient dew-point temperatures rarely exceed internal set-point temperatures, and then only for relatively short periods of time.

There are, however, significant moisture problems associated with warm, humid climates. It is not uncommon in severely humid climates to have a moisture load in excess of 50 pounds per day. In typical residences, much of this load is removed by the air-conditioning system and does not generally cause serious problems. In passively cooled or energy-efficient buildings with traditional air conditioners where sensible loads have been significantly reduced, these moisture loads may result in excessive relative humidity levels, even in air conditioned buildings. Sustained relative humidities of 70% or greater will lead to the growth of molds and mildews [Humphries 1972].

Methods of accurately evaluating moisture effects in buildings

are generally lacking in building energy analysis procedures. Typically, simple procedures call for the calculation of sensible loads and the subsequent application of some percentage of that load to represent the additional moisture load of the zone. Where moisture loads are calculated by detailed procedures, the assumption is usually made that all moisture entering the zone is added to the zone air.

This assumption can produce severe inaccuracies. In reality, the moisture that is added to a conditioned zone will be distributed in some manner between the zone air, the zone materials and the zone mechanical system. The significant impact of moisture adsorption and desorption in this balance has been recently recognized by other researchers as well [Kusuda 1984, and Miller 1984].

In humid climates, savings from ventilative cooling can be significantly effected if MAD in buildings is not accounted for in the analysis. The outdoor air can have a high moisture content, especially at cool temperatures. Buildings ventilated under these conditions will experience a high room air moisture level. This moisture is in turn adsorbed by the room materials. When the temperature increases and the a/c is turned on, the room moisture content will be high. Under these conditions the a/c does less sensible cooling per unit of energy use. The net result is that the a/c must run longer to meet the sensible building cooling load. As the a/c runs it removes moisture from the room air creating a moisture transfer potential imbalance between the room air and room material surfaces. Moisture is then desorbed from the room materials and the a/c must run even longer. So, over the course of days, the a/c will remove moisture which was absorbed at inside surfaces much earlier while the building was being ventilated.

The moisture removal rate of an air conditioner is heavily

dependent on the evaporator coil inlet wet-bulb temperature. If all moisture loads are assumed to go to the zone air, errors in machine performance characteristics will be made, even in detailed machine analysis procedures. Depending on building control strategies, these errors can produce significant prediction inaccuracies, particularly for hourly calculations of zone loads humidities and ultimately human comfort parameters.

For accurate modeling of moisture loads and zone conditions two criteria need to be met:

- Building material moisture absorption and desorption properties must be modeled to correctly account for the complete effective building moisture capacity in the zone moisture balance. The infiltration load and resulting zone humidity levels will otherwise be in error.

- Machine sensible and latent cooling performance must be calculated during the building simulation **at each time-step** in the analysis, accounting for the **variation within the time-step** of the air conditions entering and leaving the cooling coil as it removes moisture. If this is not done, zone humidity levels at the end of the hour will be incorrectly predicted. This, in turn, will adversely effect predictions of the machine performance, infiltration loading and moisture absorption/desorption in the following time-step of the analysis.

2.2 MADAM

MADAM is an acronym for **M**oisture **A**bsorption/**D**esorption **A**nalysis **M**ethod. It refers to an analysis of surface and boundary layer mass transfer potentials with respect to changes in their driving forces. The method uses a validated,

extremely detailed finite element program called FEMALP (**F**inite **E**lement **M**ethod **A**pplications **L**anguage **P**rogram) [Keresteciogl u 1985].

2.2.1 Structure and Capabilities

FEMALP has been developed at FSEC over the past four years. In its development two major objectives were realized.

- The capability of solving most systems of simultaneous ordinary or partial differential equations with any boundary conditions.

- The capability of using either hard-built, user selectable and/or user-defined equation and boundary condition libraries.

The general capabilities of FEMALP are illustrated in Figure 2-2. Possible boundary conditions for use in FEMALP are given in Figure 2-3.

MADAM uses FEMALP to determine the coupled heat and mass transfer potential between single layer or composite materials and the cavities they bound. Solutions are accomplished with respect to variations in temperature, vapor pressure and fluid flow regimes. MADAM converts the results of this analysis into a set of algebraic moisture transfer potential characteristics which can be used with building thermal analysis programs to predict the behavior of moisture absorption and desorption at those material surfaces. In MADTARP the material characteristics are incorporated in a zone moisture balance through a set of ordinary differential equations describing the characteristic behavior of the elements making up the balance. The development and validation of the moisture balance are discussed in Section 2.3 of this report.

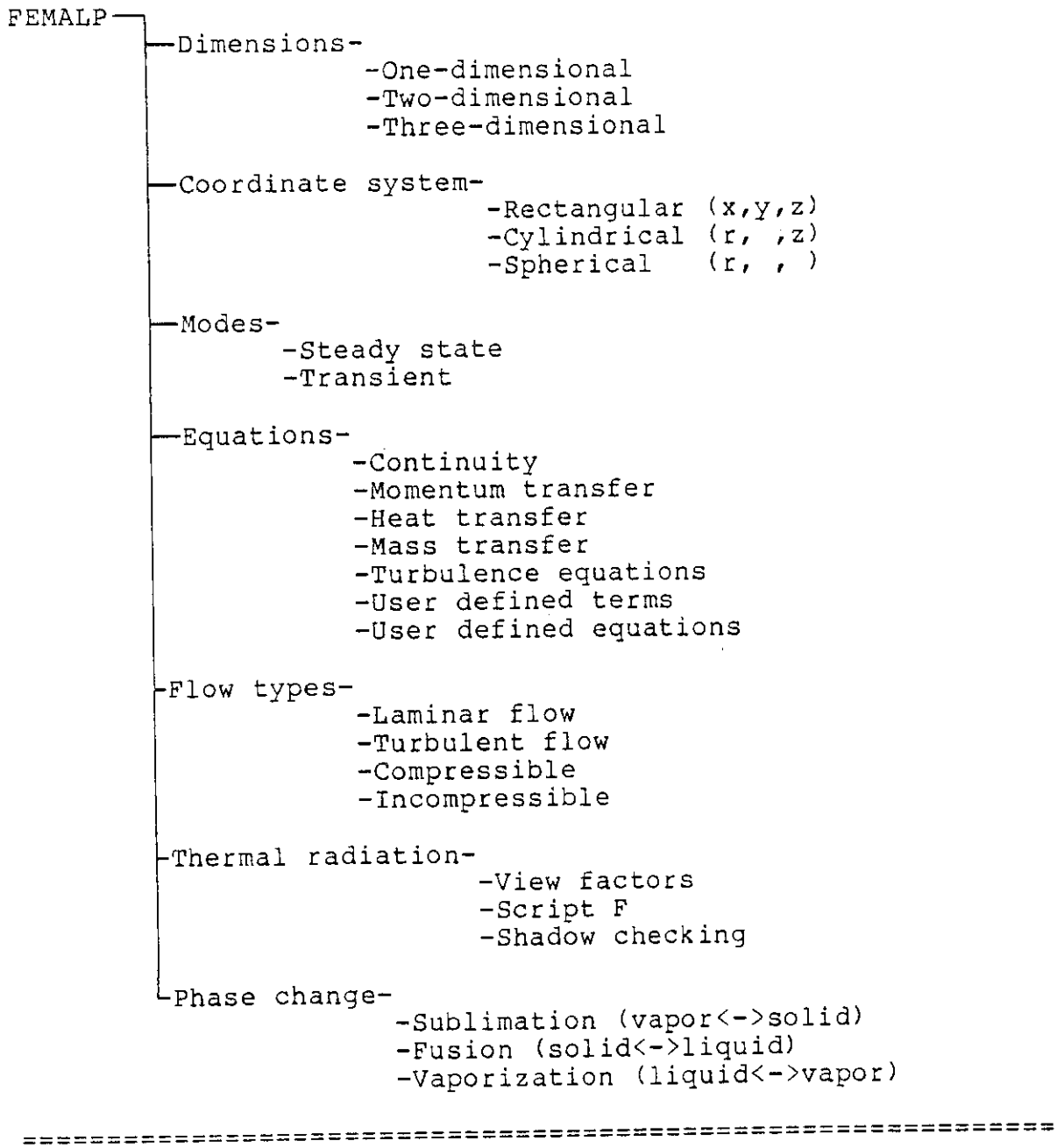

Figure 2-2 General capabilities of FEMALP.

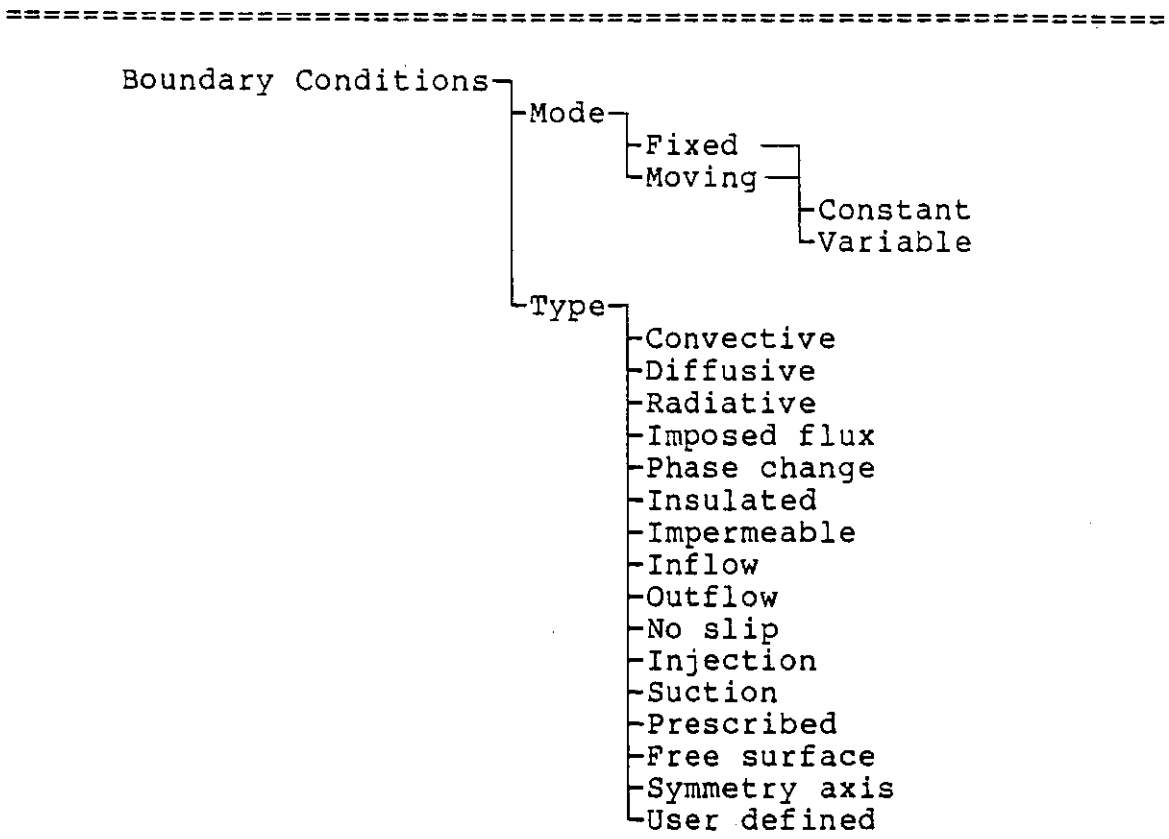

Figure 2-3 Possible boundary conditions in FEMALP.

2.2.2 Theoretical Approach

Moisture Absorption and Desorption (MAD) are material-dependent surface phenomena. The study of MAD can best be approached through physical chemistry. Colloidal chemistry describes the physical principles of the moisture-solid bond in disperse systems. Moist materials can be classified as colloidal disperse systems formed by moisture and solids.

Due to the nature of moisture-solid bonding in colloidal mixtures, the simultaneous heat and mass transfer through moist disperse solids is a complex, irreversible process. In other words, the adhesive bonding potentials are different for wetting and drying. MAD rates, therefore, will be different

Figure 2-5 shows the variation in normalized absorption rates for wood with changes in the relative vapor pressure difference between the air and the material surface (analagous to w). Changes in the convective mass transfer coefficient (h_m) produce a similar rate shift.

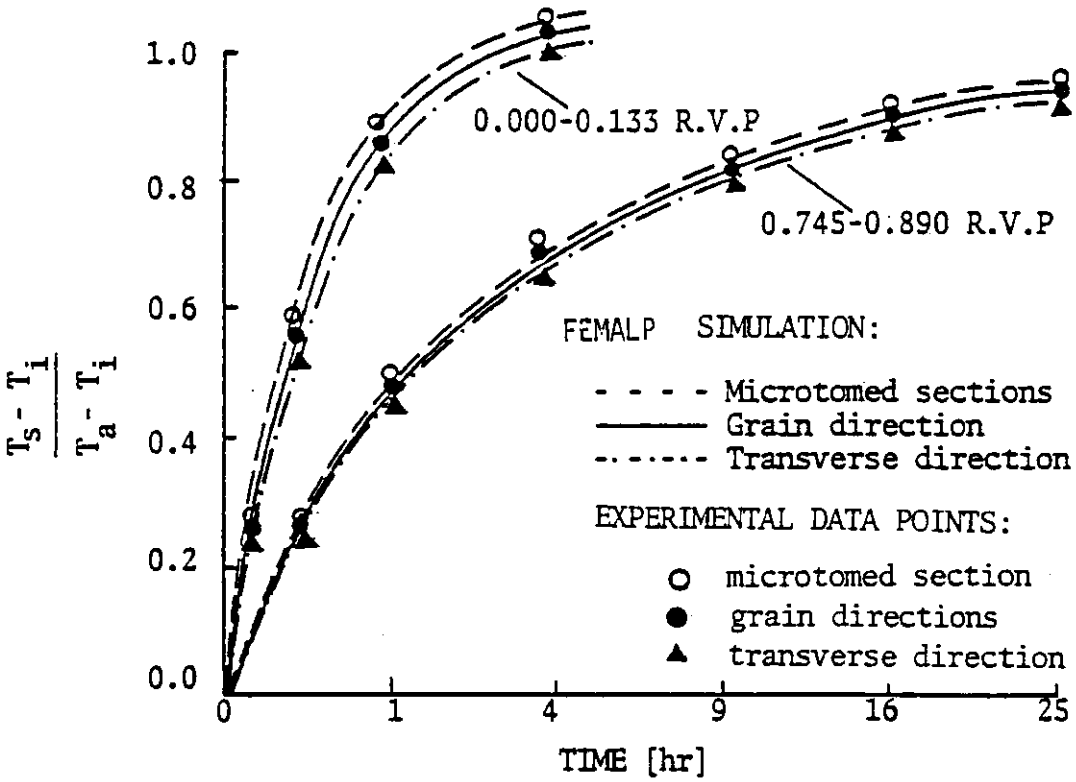

Figure 2-5 Comparison of measured laboratory data with FEMALP Predictions for three cross sections of Kilinki pine at two different relative vapor pressures. (T_s=dew-point of surface; T_i=initial dew-point of surface; T_a=dew-point of room air; RVP=Relative Vapor Pressure difference between surface and room air).

2.2.2.1 Analytical Solution

There is a direct interrelation between moisture and heat transfer in capillary porous bodies because liquid motion is generally accompanied by enthalpy transfer. This interrelation is compounded by the fact that liquids are transferred not only by the forces attributable to volumetric liquid concentration gradients but also by the forces

attributable to temperature gradients. The interrelation between liquid motion and heat transfer becomes even more complex when the liquid is evaporated or condensed inside the porous body. In this case mass within the capillary porous body transfers not only in the form of liquid but also in the form of vapor. For this reason, the use of separate differential equations (Fourier's equation for heat transfer and Fick's equation for mass transfer) cannot define a solution to the problem. Interrelated differential equations for heat and mass transfer in capillary porous bodies, first proposed by Luikov [1966, 1975], must be employed for proper solution.

Luikov has shown that it is mass transfer potential (M) and not moisture content (U) that defines the liquid transfer potential in capillary-porous bodies. Moisture content in mass transfer theory is the analog of heat content (enthalpy) in heat transfer theory.

Figure 2-6 is used here to show the analogous nature of this concept. The figure illustrates the discontinuity of both enthalpy and moisture content in dissimilar materials. Figure 2-6a depicts the enthalpy (heat content) of two materials at a uniform temperature. A large enthalpy difference that is discontinuous at the boundary exists between the materials. Figure 2-6b illustrates the effect of an applied temperature gradient on the two materials. It is noted that the flow of thermal energy occurs in a direction opposite to the enthalpy difference, from the higher potential (temperature) to a lower one.

Figure 2-6c and d illustrate the analogous phenomenon for mass transfer. In this case the driving force of the transfer is the difference in mass transfer potential (^{o}M) rather than the moisture content difference.

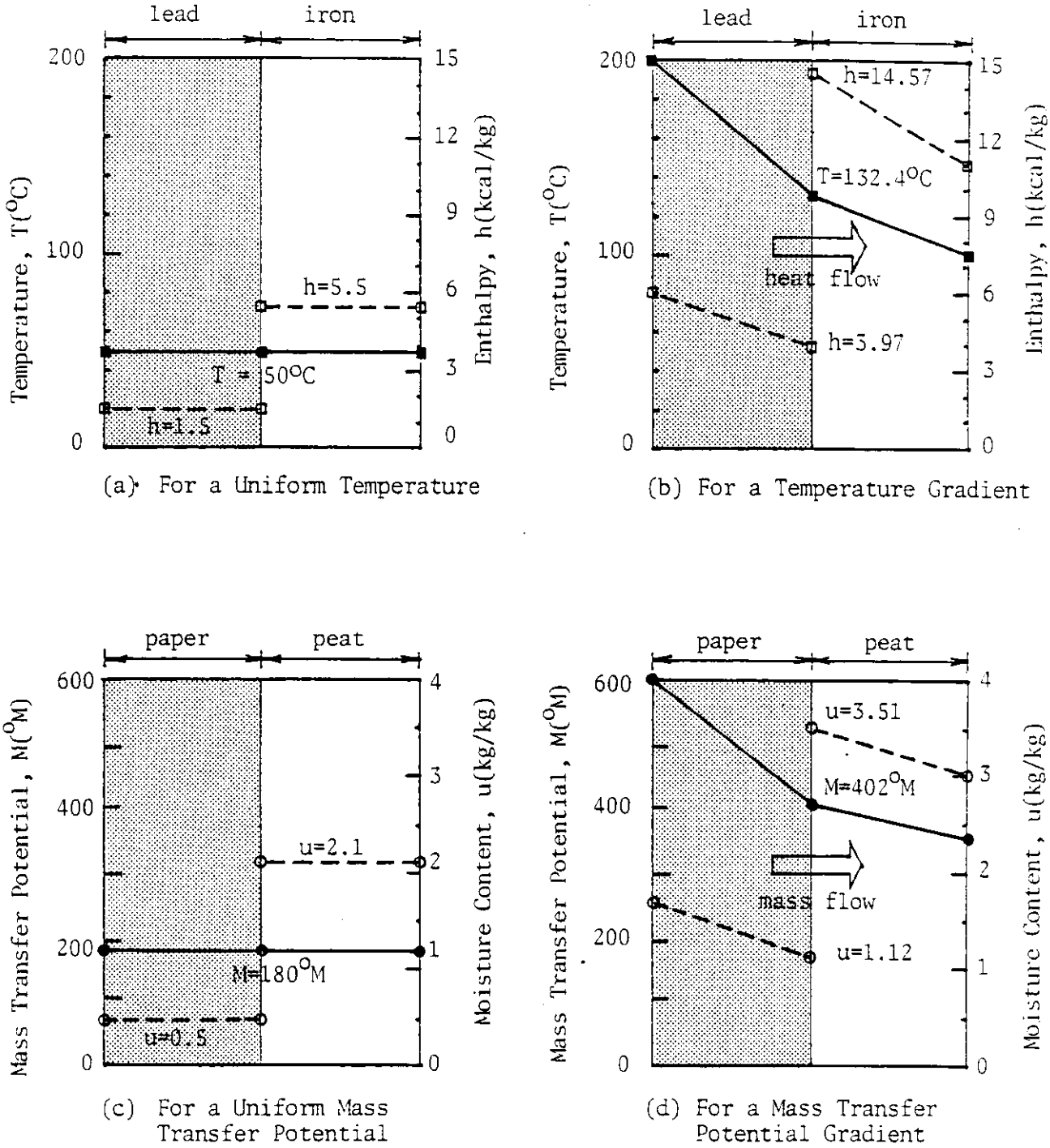

Figure 2-6 Distribution of enthalpy (heat content) (a) and moisture content (c) in dissimilar materials having no thermal or moisture transfer potential; (b) and (d) illustrate the direction of heat and mass transfer, respectively, when a thermal gradient (b) and mass transfer potential gradient (d) are applied.

Luikov [1975] has suggested the use of ^{o}M concept as a normalizing function for mass transfer and has experimentally determined its validity in the analytical description of combined heat and mass transfer. As a result, a system of heat and mass transfer equations using continiuous heat (T) and mass (M) transfer potentials may be written as proposed by Luikov [1975].

If T and M are taken as the heat and moisture transfer potentials respectively, then the system of differential heat and mass transfer equations can be written in the following form [Luikov, 1975].

$$C_T \partial T/\partial \tau = K_{11}\nabla^2 T + K_{12}\nabla^2 M \qquad (2\text{-}1a)$$

$$C_M \partial M/\partial \tau = K_{21}\nabla^2 T + K_{22}\nabla^2 M \qquad (2\text{-}1b)$$

with

$$\begin{aligned} K_{11} &= k_T + \gamma\, h_{ig}\, k_M\, \delta_M \\ K_{12} &= \gamma\, h_{ig}\, k_M \\ K_{21} &= k_M \\ K_{22} &= k_M \end{aligned} \qquad (2\text{-}2)$$

In Equations 2-1, T and M denote the temperature and the moisture transfer potentials, respectively. The moisture transfer potential M is a function of the moisture content (U) and temperature (T) of the body

$$M = M\,(U,T)$$

and

$$d_M = (\partial M/\partial U)_T\, dU + (\partial M/\partial T)_U\, dT = (1/c_M)\, dU + M dT \qquad (2\text{-}3)$$

where

$c_M = (\partial U/\partial M)_T$ is the specific isothermal moisture capacity (the amount of moisture increase or decrease for a unit change in mass transfer potential at a given temperature) and $M_T = (M/T)_U$ is the temperature coefficient of the mass-transfer potential. The moisture content of the body can be expressed by the following relation:

$$U = (m_1 + m_2 + m_3)/m_o$$

where m_1, m_2 and m_3 are used to denote the mass of vapor,

liquid and solid, respectively, within the capillary porous body and m_o denotes the dry mass of the body.

The derivation of Equations 2-1 can be found in Luikov [1966]. For further details the reader is referred to Luikov [1966, 1975] and Luikov and Mikhailov [1965]. Only the variables appearing directly in the equations are explained.

h_{ig} is the heat of phase change [J/kg],

k_M is the moisture conductivity of the moist material [kg_w/m.s.^oM],

k_T is the thermal conductivity of the moist material [W/m·K],

M is the mass transfer potential [^oM],

δ_M is the thermogradient coefficient based on the potential difference [^oM/K],

γ is the ratio of the vapor diffusion coefficient to the coefficient of total diffusion [unitless].

c_M is the specific isothermal mass capacity of the moist body [kg_w/kg·^oM],

$$c_M = U/M$$

C_T is the specific heat of the moist body [J/kg·K],

$$C_T = C_{To} + \sum_{i=1}^{3} C_i U_i$$

where C_i, U_i are the specific heat and the moisture content, respectively, of the i-th phase of the mass (i.e., m_1, m_2 and m_3)

2.2.2.2 Calculation of Specific Isothermal Moisture Capacity

A relation exists between the moisture content of a body (U) and its mass transfer potential (M) in the form of the expression:

$$c_M = (\partial U/\partial M)_T \qquad (2\text{-}4)$$

where c_M is defined as the specific isothermal moisture capacity. Therefore, the moisture capacity of a material is equal to the slope of the line tangent to the curve U=f(M). Consequently, the experimental determination of the specific isothermal moisture capacity reduces to finding the

equilibrium moisture content, under which thermodynamic and molecular equilibrium exists between the moisture content of the body and the humidity of the air and hence, also, the mass transfer potential.

If the equilibrium moisture content (U_e) of the material is divided by the mass transfer potential of air at a given relative humidity, the specific isothermal moisture capacity of the material can be calculated. Hence, the following equation may be used to determine the specific isothermal moisture capacity of the material.

$$c_M(RH)_T = [U_e(RH)/M_{air}(RH)_T] \qquad (2\text{-}5)$$

The mass transfer potential of air has been experimentally determined by Luikov [1966] to be a function of relative humidity and is shown in Figure 2-7. Unlike equilibrium moisture content in materials, the mass transfer potential of air has been shown to be independent of air temperataure [Luikov 1966].

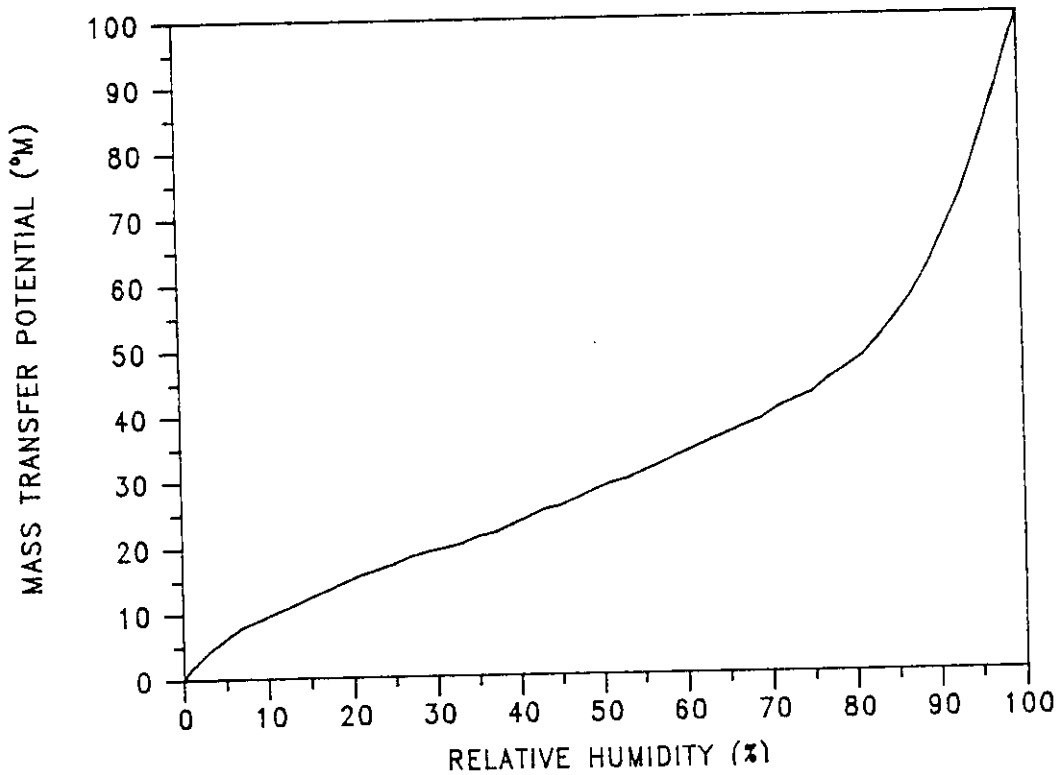

Figure 2-7 Mass transfer potential versus relative humidity of air.

The product of the specific isothermal moisture capacity c_M and the mass of the perfectly dry body m_o is called the moisture capacity of the body (C_M).

$$C_M = c_M \, m_o$$

After the mass transfer potential field is solved the concentration of water vapor can be calculated from the following relation

$$C = \rho \, c_m \, M \qquad (2\text{-}6)$$

where ρ is the dry body density in (kg/m^3), c_m is the specific isothermal moisture capacity of the body in ($kg_w/kg.^oM$) and M is the moisture transfer potential in (^oM). Consequently, the unit of moisture concentration is kg_w/m^3.

A system consisting of differential equations is fully described when the boundary conditions (i.e., the values along the boundary of the enclosure of integration) are known.

Boundary conditions for Equations 2-1a and 2-1b are:

$$k_T(\partial T/\partial n) - g''_{Tp} + h_{Tp}(T-T_{ap}) + (1-\gamma) h_{ig} h_{MP}(M-M_{ap}) + \varepsilon_p \sigma (T^4 - T^4_{rp}) + \sum_{\substack{j=1 \\ j \neq i}}^{n} \mathcal{F}_{ij,p} \, \sigma (T^4 - T_j^4, rp) = 0 \qquad (2\text{-}7a)$$

$$k_m \, \partial M/\partial n - g''_{MP} + k_M \delta_M (\partial T/\partial n) + h_{MP}(M-M_{ap}) = 0 \qquad (2\text{-}7b)$$

Figure 2-8 presents a schematic diagram of the set of boundary conditions that are used by the problem.

Equations 2-1 through 2-7 can be solved under differing conditions to obtain sets of temperature and moisture transfer potential distributions within materials. The solutions of these equations are given by Keresteciogiu [1985] in detail.

2.2.2.3 Incorporating MADAM Results in MADTARP

With respect to MAD, a certain portion of the surface material

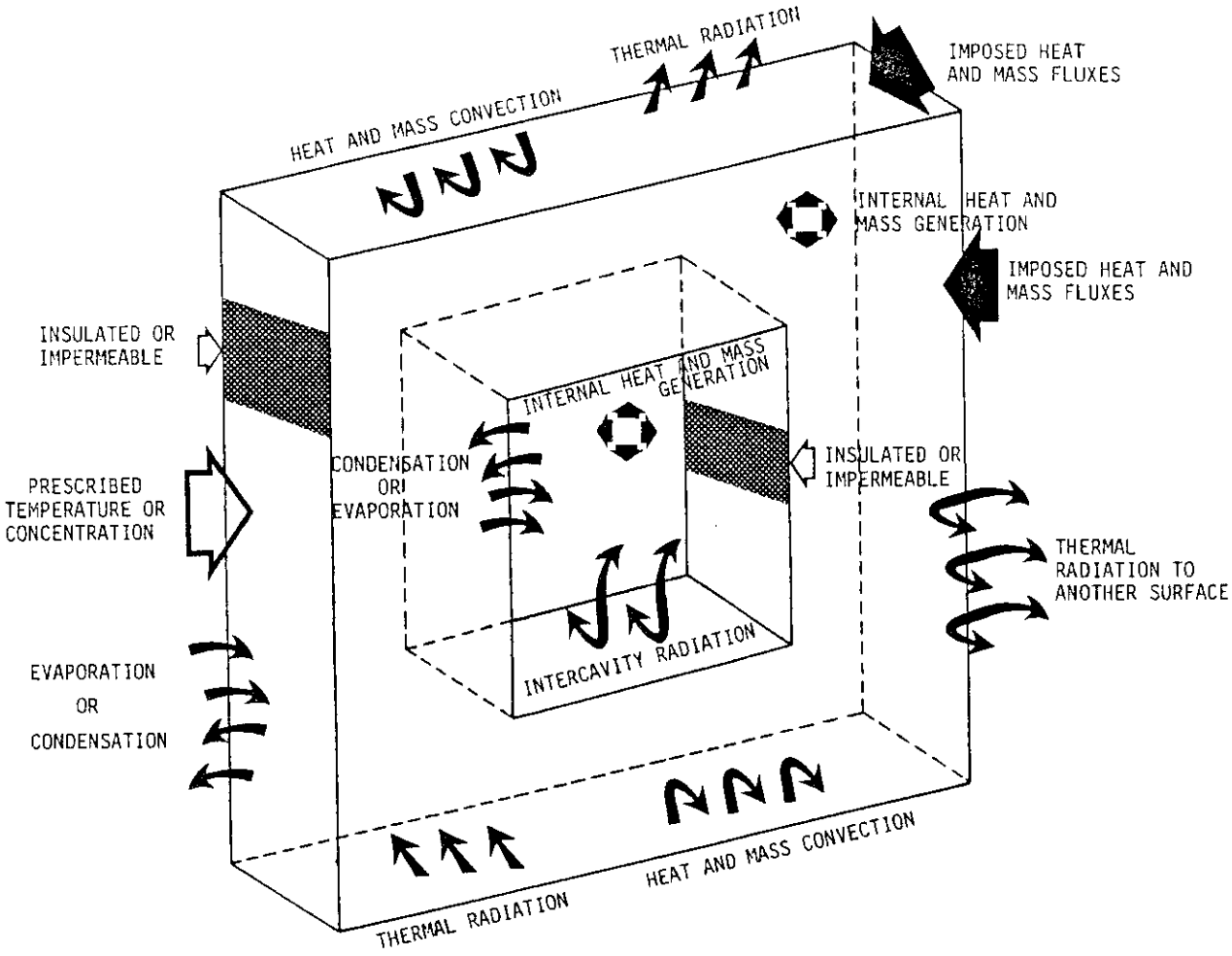

Figure 2-8 Diagram of the boundary conditions (see Eqs. 2-7a and b) used in combined heat and mass transfer analysis to determine the MAD characteristics of materials.

will come into equilibrium with the environment. If equilibrium moisture content data are available, then the surface moisture content of this layer can be related to the surface humidity ratio W_s. Equilibrium moisture content data are given in terms of environment relative humidity and material temperature such that,

$$W_s = f(u, W_{sat}, T) \qquad (2\text{-}8)$$

The moisture content of the surface layer and the amount of moisture absorbed or desorbed are known from the solution of Equation 2-1b, and W_{sat} is the humidity ratio of saturated air at temperature T, which is also known. Therefore, the equilibrium moisture content data for the surface layer may be

written in the following format with piece wise linearization:

$$W_s = A_1 M_c + A_2 \quad (2\text{-}9)$$

where:

$$A_1 = f(W_{sat}, M_d, T) \quad (2\text{-}10a)$$

$$A_2 = f(W_{sat}, T) \quad (2\text{-}10b)$$

The moisture content of the effective MAD surface layer is defined by the ratio of the absolute moisture content (M_c) and the dry weight (M_d) of the layer. Therefore, in MADTARP the dry weight (M_a) represents only the weight of the material layer that effectively participates in absorption and desorption. MADAM gives an effective M_d for a MADTARP analysis that is dependent upon the structure and boundary conditions of the problem.

2.2.3 MADAM Validation

The analysis method used by MADTARP has been validated against both laboratory and field data. Where material moisture characteristics are well known, MADAM can accurately predict both moisture contents and their rates of change. Figure 2-5 shows a set of validation results from the base finite element model (FEMALP) used by the method plotted against laboratory measurements [Wexler, 1965] for various sections of Kilinki pine wood under two conditions of relative vapor pressure. Laboratory data from gypsum wallboard [Kusuda, 1983] and brick [Luikov, 1965] are also well predicted by FEMALP (Figure 2-9).

Field data have been obtained from the attic of a multifamily living unit located in Oroville, CA monitored by Lawrence Berkeley Laboratories [Cleary, 1984]. The monitoring effort by LBL was accurate and detailed to the point that even infiltration/ventilation rates are well described. Good agreement with measured moisture data would not be possible otherwise. The effective mass transfer coefficient (h_m) is strongly related to surface boundary layer velocities and very accurate results are only possible when fluid flow parameters

can be accurately estimated. The primary attic material (wood) also has well-defined moisture and thermal transfer characteristics. Therefore, the results depicted in Figure 2-10 are excellent. There is a high degree of confidence in MADAM where the required modeling parameters are known.

2.3 MACHINE AND MOISTURE ALGORITHMS (MAMA)

The detailed calculation techniques used by FEMALP cannot be used directly in an hourly building energy analysis model without paying a significant computer run time penalty. The parameters of Equation 2-10, however, may be calculated for different materials over the range of temperatures 0-40°C and humidity ratios (0.001-0.040 kg/kg) that relate to buildings. Once this is accomplished through MADAM, the coefficients of Equation 2-10 may be found and the equation may be used in detailed hourly building energy analysis programs with a high degree of confidence and very little run time penalty.

2.3.1 Capablities of MAMA

Equation 2-9 must, of necessity, participate in a zone moisture balance that accounts for all moisture sources and sinks that affect the zone moisture balance (see Figure 2-11). In general the sources consist of the infiltration rate in air changes per hour (ACH), the internal moisture generation rate (MGR) and MAD. The moisture sinks usually consists of only the moisture removal rate of the a/c (MAC). The internal moisture generation rate is usually an independent constant and does not present a significant calculation problem. Infiltration rate, however, is a dependent variable that is a function of both the exterior humidity ratio as a source and the mechanical system and MAD potentials as a moisture sink. In the event moisture condensation or vaporization potentials exist (CON) they too must be considered as a sink or source, respectively, for moisture in the zone.

The rate of change in room moisture content is a complex

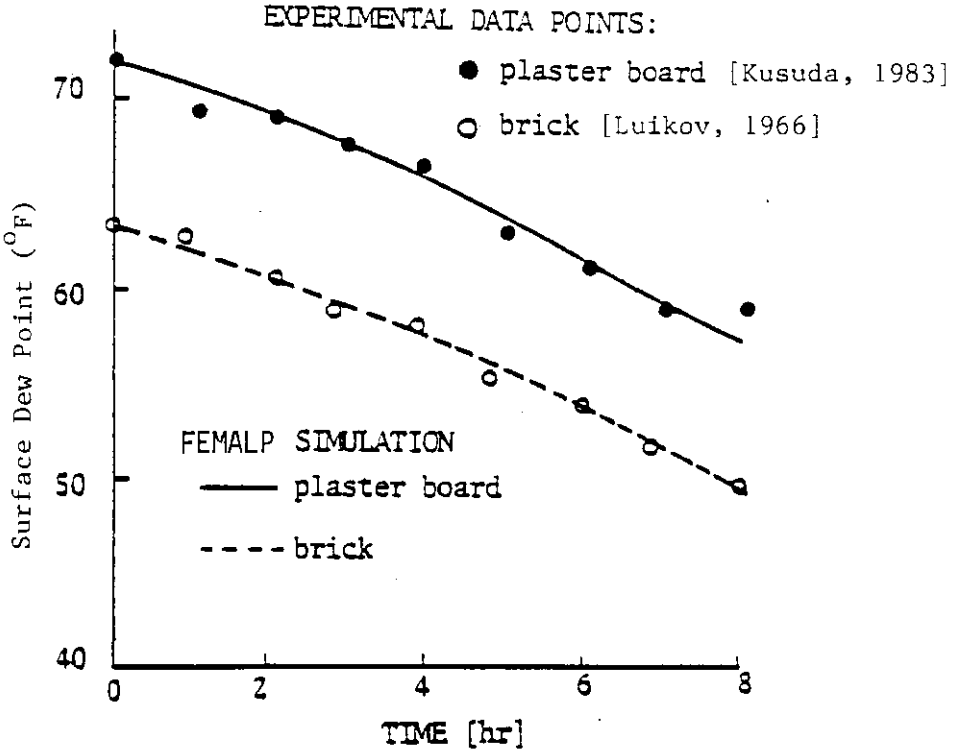

Figure 2-9 Experimental versus simulated drying rates of plaster board and brick.

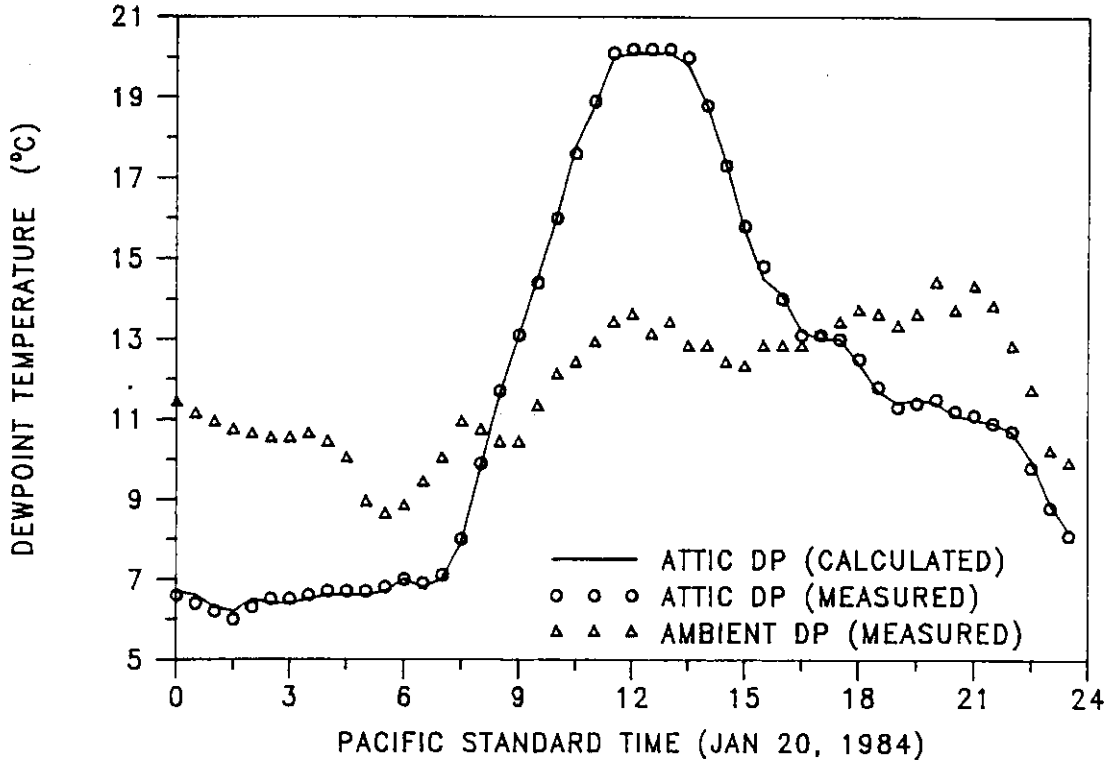

Figure 2-10 Measured ambient air and attic air dew-point compared with FEMALP prediction of attic air dew-point for residence in Oroville, CA.
Data source: P. Cleary, Lawrence Berkeley Laboratories

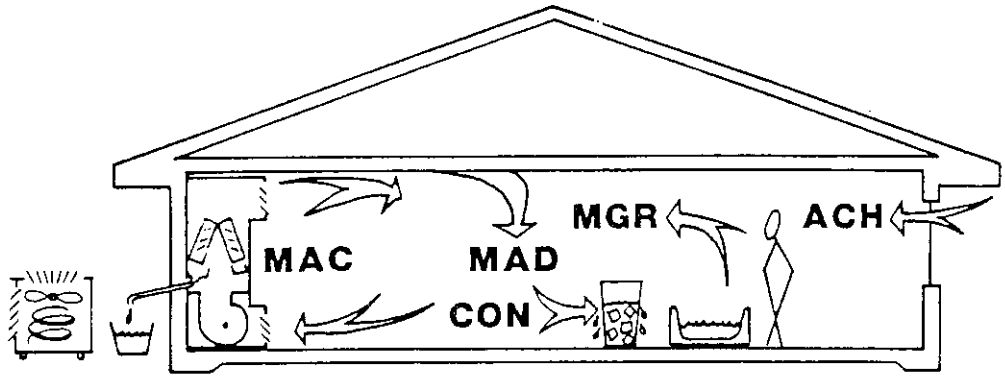

Figure 2-11 Schematic showing principal components of room moisture balance. Diffusion through the envelope is accounted for through the MAD term.

phenomenon. Infiltration rate, for instance, is highly sensitive to both the latent machine performance characteristics and the MAD rates of the room materials. As the machine removes moisture from the zone, the difference in moisture content between the zone and ambient increases, thereby increasing the rate of change of the room moisture content due to infiltration. As the machine removes moisture it also increases the vapor pressure difference between the room air and room material surfaces, resulting in an increase in moisture desorption from materials to the room air. Therefore, the room air moisture level is prohibited from dropping too rapidly by these additional moisture sources. The sensible cooling performance of the machine is usually highly dependent on zone moisture content. If the zone moisture content remains high the machine must run longer and consume more power to accomplish the required sensible cooling. If machine run time increases, total moisture removal increases, in turn increasing both the relative moisture infiltration and material desorption rates.

Mathematical problems of this type can be handled precisely through differential equations. MADTARP uses an exact solution of a set of differential equations (referred to as MAMA) to solve this problem and predict the performance of

building systems with respect to moisture transfer.

2.3.2 Theoretical Approach

The governing moisture balance equations for a given control volume may be written as:

$$m\ dW_r/dt=MGR+MAC+ACH\ m\ (W-W_r)-CON-MAD \quad (2\text{-}11)$$

where:

$$CON=h_{cd}\ A_{cd}\ (W_r-W_c) \quad (2\text{-}12)$$

and

$$MAD=dM_c/dt=h_m\ A_m\ (W_r-W_s) \quad (2\text{-}13)$$

and

$$W_s=A_1\ M_c+A_2 \quad (2\text{-}14)$$

Equation 2-11 describes the conservation of moisture in a control volume. The first term on the right-hand side (MGR) is the internal moisture generation rate and, in the case of humidification modeling, the desired amount of moisture input is added through this term. The second term (MAC) is the amount of moisture that is removed by the cooling equipment. It corresponds to the latent cooling performed by the equipment. The third term (ACH) represents the amount of moisture that is brought to or removed from the zone by infiltration and/or ventilation. The fourth term (CON) represents the amount of moisture that is condensing over cold surfaces and is described by Equation 2-12. Finally, the last term (MAD) represents the amount of moisture that is absorbed or desorbed by the envelope and internal furnishings and is described by Equations 2-13 and 2-14. For a MADTARP analysis h_m, A_1, M_c and A_2 are prescribed based on MADAM analysis (see Section 2.2).

MAC is defined by functional relationship. In this case the amount of latent and sensible cooling performed by the cooling equipment is a function of the outdoor dry-bulb temperature and the indoor dry-bulb and wet-bulb temperatures. Mechanical performance characteristics can normally be obtained from

manufacturer's data. Generally the equipment performance data are given in tabular format. Therefore, the data usually have to be curve fit for functional relations that can be used in Equation 2-11. The amount of moisture removed by the cooling equipment can be represented by the following equation:

$$MAC=(LMC1+LMC2\ W_r)\ CF \tag{2-15}$$

In Equation 2-15, LMC1 and LMC2 are the machine latent load performance functions. Consequently, Equations 2-11 through 2-15 combined with the correct initial boundary conditions constitute a system of differential equations. The initial boundary conditions for the system are:

$$\text{at } t=0 \quad W_r(0)=W_{ro}$$

and (2-16)

$$\text{at } t=0 \quad M_c(0)=M_{co}$$

The exact solutions of the differential equations are given as:

$$W_r(t)=C_1\ \exp(m_1 t)+C_2\ \exp(m_2 t)+\bar{E}_3/\bar{E}_2 \tag{2-17}$$

and

$$M_c(t)=[E_5/(m_1-E_6)]\ C_1\ \exp(m_1 t)+[E_5/(m_2-E_6)]\ C_2\ \exp(m_2 t)+\bar{E}_4/\bar{E}_2 \tag{2-18}$$

In Equations 2-17 and 2-18, m_1 and m_2 denote the roots of the characteristic equation of this system of differential equations and the are described as:

$$m_{1,2}=-E_1\pm(\bar{E}_1^2-4\bar{E}_2)^{0.5} \tag{2-19}$$

The constants C_1 and C_2 used in Equations 2-17 and 2-18 are defined as:

$$C_1 = - C_2-\bar{E}_3/\bar{E}_2+W_{ro} \tag{2-20a}$$

$$C_2=(m_2-E_6)\ [W_{ro}-(\bar{E}_3/\bar{E}_2)]\ [1/(m_2-m_1)] -(m_2-E_6)/[E_5\ (m_2-m_1)]\ [M_{co}-(\bar{E}_4/\bar{E}_2)] \tag{2-20b}$$

The functions E_1 through E_5 used in Equations 2-17 through 2-20 are given with the following relations:

$$E_1=(MGR+ACH\ M\ W_r+LMC1\ CF+h_{cd}\ A_{cd}\ W_c)/m$$

$$E_2=(LMC2\ CF-ACH\ M-h_{cd}\ A_{cd})/m$$

$$E_3=-1/m$$

$$E_4=-h_m\ A_m\ A_2$$

$$E_5=h_m\ A_m$$

$$E_6=-h_m\ A_m\ A_1$$

and

$$\bar{E}_1=-(E_2+E_3\ E_5+E_6)$$

$$\bar{E}_2=E_2\ E_6$$

$$\bar{E}_3=-E_1\ E_6$$

$$\bar{E}_4=E_1\ E_5-E_2\ E_4 \qquad (2\text{-}21)$$

From the solution of Equation 2-17 the indoor humidity ratio can be calculated, and from the solution of Equation 2-18 the moisture content of the material can be calculated. Since Equations 2-17 and 2-18 are the exact solutions of the system, no complex numerical technique need be employed.

The calculation of cooling equipment run time is based on a known sensible load. Therefore, before calculating the equipment run time, the hourly sensible load must be obtained from another source (the TARP thermal processor). Consequently, if the required hourly zone sensible load is designated by Q_{rs} the following equation may be written:

$$Q_{rs} = \int_0^{trt} (SMC1+SMC2\ W_r)\ dt \qquad (2\text{-}22)$$

The right-hand side of Equation 2-22 is similiar to Equation 2-15. SMC1 and SMC2 are the sensible equipment performance functions. By integrating Equation 2-22, the following equation in terms of required equipment run time is obtained:

$$Q_{rs}=(SMC1+SMC2\ \bar{E}_3/\bar{E}_2)t_{rt}+(SMC2\ C_1/m_1)$$
$$[\exp(m_1t_{rt})-1](SMC2\ C_2/m_2)[\exp(m_2t_{rt})-1] \qquad (2\text{-}23)$$

Since t_{rt} appears in both the linear and exponential terms, Equation 2-23 has to be solved iteratively for the required cooling run time.

With a known equipment run time the amount of moisture removal

as a function of indoor humidity ratio can be calculated from the following equation:

$$Q_{rl} = \int_{o}^{trt} (LMC1+LMC2\ W_r)\ dt \qquad (2\text{-}24)$$

Substituting Equation 2-17 into Equation 2-24 and integrating over the equipment run time yields the following latent load removal equation:

$$Q_{rl}=(LMC1+LMC2\ \bar{E}_3/\bar{E}_2)t_{rt}+(LMC2\ C_1/m_1)$$
$$[\exp(m_1 t_{rt})-1]\ (LMC2\ C_2/m_2)\ [\exp(m_2 t_{rt})-1] \qquad (2\text{-}25)$$

Using multivariable regression analysis, mechanical system performance parameters can be reduced to regression equations. In this study, the following equations are used to represent equipment performance:

$$Q_{rl}=a_0+a_1\ T_o+a_2\ T_o^2+a_3\ T_i+a_4\ T_i^3+a_5$$
$$T_i^2 T_o+a_6\ \cos(T_i)+a_7\ \sin(T_i)+a_8\ \cos(T_o)+a_9\ W_r \qquad (2\text{-}26)$$

$$Q_{rs}=a_0+a_1\ T_o+a_2\ T_o^2+a_3\ T_i+a_4\ T_i^3+a_5$$
$$T_i^2 T_o+a_6\ \cos(T_i)+a_7\ \sin(T_i)+a_8\ \cos(T_o)+a_9\ W_r \qquad (2\text{-}27)$$

The constants used in the preceding equations for a typical two-ton condensing unit with an 850 cfm evaporator unit are tabulated in Table 2-1. Table 2-2 gives the manufacturers data from which the constants are developed.

The equations developed up to this point apply particularly for real mechanical systems with a priori performance conditions. If an ideal system is to be modeled, some of the described equations must be altered. Equations 2-11 and 2-13 remain the same but the MAC term in Equation 2-11 reduces to zero. In the modeling of ideal systems the room relative humidity as well as temperature conditions can be maintained at a predefined upper limit, which means the machine is capable of removing any excessive moisture or thermal load instantly. However, when the room humidity or temperature condition drops below the set point the system does not

operate. With the ideal machine the indoor humidity condition fluctuates between the set point and a lower value. Consequently, MAD has to be taken into account.

If the room conditions are below the set point, Equations 2-11 through 2-14 can be used by setting

$$MAC = 0$$

However, when the room humidity conditions climb above the set point plus a user-defined humidistat hysteresis (HY_h), the Wr term used in Equations 2-11 through 2-13 must be replaced by ($Wr-HY_h$), representing the new set point accounting for the lower hysteresis condition.

With the new conditions, Equation 2-13 is replaced with the following equation:

$$M_c(t) = [M_{co} - (Z_2/Z_1)] \exp(-Z_1 t) + (Z_2/Z_1) \qquad (2\text{-}28)$$

where

$$Z_1 = h_m A_m A_1$$

$$Z_2 = h_m A_m (Wr - Wr) - h_m A_m A_2$$

2.3.3 Validation of MAMA

Equation 2-11 represents the energy balance on a conditioned room (also see Figure 2-11). The balance evaluates the moisture flows in the zone by component. However, very little MAD data exists for real buildings. The MAD term in Equation 2-11 is defined by the relation given in Equation 2-14. Its functional coefficients (see Eqs. 2-10a and 2-10b) are derived from MADAM given the known characteristics of only two representative building materials: gypsum drywall to represent wall materials and "rag felt" to simulate furnishings, clothing, linens, rugs, etc. In order to have confidence in this relationship it is necessary to confirm it through measured data.

A two-story townhouse in Cocoa, FL (see photograph in Figure

Table 2-1 Regression analysis coefficients for two-ton air conditioner used in equations 2-26 and 2-27.

	a^0	a^1	a^2	a^3	a^4	a^5	a^6	a^7	a^8	a^9
	const.	T_o	T_o^2	T_i	T_i^3	$T_i^2*T_o$	$\cos(T_i)$	$\sin(T_i)$	$\cos(T_o)$	XI
SENSIBLE CAP. (dry coil)	-10.03075	0.00000	0.00000	0.56991	0.000000	$-1.21247\ 10^{-5}$	0.00000	0.00000	0.00000	-1035.50697
SENSIBLE CAP.	-3.29319	-0.05495	0.00000	0.49448	0.000000	0.00000	0.00000	0.14932	0.05469	-1220.75141
LATENT CAP. (dry coil)	-3.12778	0.00000	0.00000	0.00000	0.000000	$-1.38935\ 10^{-5}$	0.00000	0.00000	0.00000	1597.46057
LATENT CAP.	4.90300	0.00000	0.00000	-0.12352	0.000000	$-1.57418\ 10^{-5}$	-0.08620	-0.21076	0.00000	1772.16944
TOTAL CAP.	18.95332	0.00000	$-7.12816\ 10^{-4}$	0.00000	$7.816633\ 10^{-6}$	0.00000	0.00000	-0.05443	0.00000	554.00196
TOTAL CAP.	19.07280	0.00000	$-7.27426\ 10^{-4}$	0.00000	$7.952917\ 10^{-6}$	0.00000	0.00000	-0.04540	0.00000	551.25387

Table 2-2 Manufacturer's performance data for two-ton condensing unit with 850 cfm evaporator coil.

O.D. D.B.	I.D. I.D.	TOTAL CAP.	SENS. CAP. AT ENTERING D.B. TEMP 72	74	76	78	80	COMPR. KW	APP. DEW PT
85	59	20.9	18.1	19.7	21.1*	21.6*	22.1*	2.07	49.0
	63	22.5	14.9	16.5	18.1	19.7	21.3	2.13	53.0
	67	24.1	11.4	13.0	14.6	16.2	17.8	2.21	57.2
	71	25.8	7.8	9.5	11.1	12.7	14.3	2.28	16.6
90	59	20.3	17.8	19.4	20.6*	21.1*	21.6*	2.15	49.4
	63	21.8	14.6	16.2	17.8	19.4	21.0	2.22	53.3
	67	23.5	11.2	12.8	14.4	16.0	17.6	2.29	57.6
	71	25.1	7.6	9.2	10.8	12.4	14.0	2.36	61.9
95	59	19.7	17.6	19.2	20.1*	20.6*	21.1*	2.23	49.7
	63	21.2	14.4	16.0	17.6	19.2	20.8	2.30	53.7
	67	22.8	10.9	12.5	14.1	15.7	17.3	2.37	57.9
	71	24.4	7.4	9.0	10.6	12.2	13.8	2.44	62.2
100	59	19.1	17.3	18.9	19.5*	20.0*	20.5*	2.31	5.01
	63	20.5	14.1	15.7	17.3	18.9	20.5	2.38	64.0
	67	22.0	10.6	12.2	13.8	15.4	17.0	2.46	58.3
	71	23.6	7.1	8.7	10.3	11.9	13.5	2.53	62.6
105	59	18.4	17.0	18.5	19.0*	19.4*	19.9*	2.40	50.4
	63	19.8	13.8	15.4	17.0	18.6	19.9	2.47	64.4
	67	21.3	10.3	11.9	13.6	15.2	16.8	2.54	5.86
	71	22.8	6.8	8.4	10.0	11.6	13.2	2.62	6.30
115	59	17.0	16.4	17.3	17.8*	18.3*	18.7*	2.58	51.2
	63	18.3	13.2	14.8	16.5	18.1	18.7	2.64	55.1
	67	19.7	9.8	11.4	13.0	14.6	16.2	2.72	59.4
	71	21.2	6.3	7.9	9.5	11.1	12.7	2.79	63.7

2-12) known as Rangewood Villas is being monitored by FSEC under separate contract.

Figure 2-12 Photo of Rangewood Villas townhouses showing south facade. Two westernmost units in the fourplex are monitored by FSEC.

The monitoring system was designed to collect as much moisture data as practicable. Dry-bulb and dewpoint temperatures are measured on both sides of the a/c evaporator coil (return air and supply air) and the coil condensate is measured through a calibrated rain gauge. Coil measurements are taken only when the condensing unit and evaporator coil blower are operating. Total machine run times are recorded at fifteen minute intervals and power consumption of compressors and blowers are recorded through automated kWh pulse counters. Room dry-bulb and wet-bulb or RH measurements are taken both upstairs and downstairs in the townhouse. A full set of site metereological data are also taken: dry-bulb, RH, solar radiation, net sky (far-infrared) radiation, wind speed, wind

direction and ground temperatures to three feet below the surface are monitored. All data are scanned at rapid (10 second) intervals and the average is recorded at fifteen minute time increments.

A data-set from September 14-25, 1984, was chosen for the analysis presented here. During this period the building was ventilated on the nights of September 21-22 and September 22-23 and the a/c ran the remainder of the time.

No continuous infiltration measurements are taken on the townhouse due to the expense of such monitoring devices. Therefore, the ACH term in Equation 2-11 is not precisely known. Two sets of one-time infiltration measurements using SF_6 gas chromatograph techniques were performed on September 21. The resulting air change rates were between 0.25 and 0.4 ACH (air changes per hour). Two separate mechanical system air volume flow rate measurements have also been made.

Given the volumetric airflow rate of the machine and the measured dewpoint temperature difference across the evaporator coil, the machine latent performance characteristics may be determined. The volumetric airflow rate of the system was measured by airflow measurement devices to be between 980 and 1005 CFM. Since the condensate was also measured the airflow rate may be separately calculated as:

$$CFM = (CON+C_{res})/ (W_i-W_o)* *rt)$$

where

CFM = volumetric flow rate across evaporator coil
CON = measured condensate
C_{res} = residual coil moisture (not measured)
W_i = evaporator coil inlet humidity ratio
W_o = evaporator coil outlet humidity ratio
= density of air
rt = runtime

Since C_{res} is an unmeasured term in the equation and accurate

estimation is difficult, the data-set used in the calculation of CFM was reduced to only those hours when the machine run-time was greater than 48 minutes (0.8 hour). From this data-set only the second and following hours of continuous machine operation were chosen for the analysis. The first hour in each series of hours was eliminated to obviate any time lag problems associated with condensate measurements. The evaporator coil volumetric flow-rate was calculated by this technique to be 995 CFM. This is in good agreement with the measured values. A flow-rate of 1000 CFM was chosen for use in the validation.

In order to validate MAMA it is necessary to know all but one of the values on the right hand side of Equation 2-11. MAD is the term of interest but ACH is not continuously measured, so some accurate estimation of ACH must be made. To do this, a reasonable estimate of the effective MAD surface area was assumed and an hourly infiltration schedule was determined through back substitution in Equation 2-11 using the first day's (September 14, 1985) measured data. This infiltration rate was found to vary between 0.25 and 0.40. The pattern of the variation in infiltration was found to correspond well with the measured environmental windspeeds, with the lower ACH at night when windspeed was low and the higher ACH during the day when windspeed was high. Examination of external windspeeds showed very similar windspeed patterns for the entire period of the data set. Thus, the ACH schedule calculated for the first day was assumed reasonable for the entire period.

Next, a set of analysis was performed using this calculated hourly ACH schedule to determine the optimum effective MAD surface area (A_m) for use in Equation 2-13. This optimization was accomplished using the calculated ACH schedule from the first day for all 12 days of the data-set. Upon optimization the most effectiv e MAD surface area was found to be 2798 ft^2.

Figure 2-13 shows the measured and calculated room humidity ratio for the entire period using this effective MAD surface area.

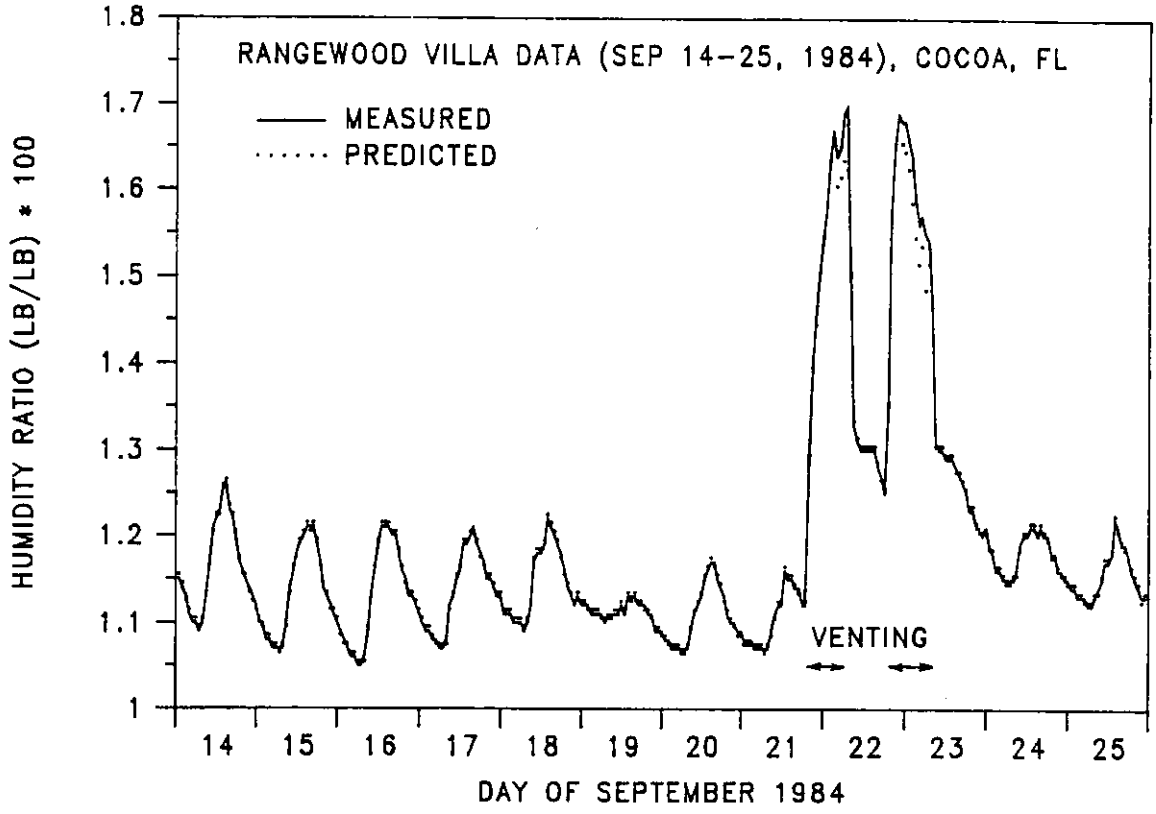

Figure 2-13 Room humidity ratio as measured and as predicted.

Next, the analysis was performed with the effective MAD surface area set equal to zero to examine results when no MAD is possible. Results are given in Figure 2-14 as the error in predicted room humidity ratio with respect to the measured data.

For convenience and for use in MADTARP, a ratio between the effective MAD surface area and the heat transfer surface area of the building was calculated. For the material moisture capacity that optimized the townhouse case, this effective surface area multiplier (ESAM) was calculated to be 0.5. The townhouse contained minimal furnishings (one bed and one sofa)

and was unoccupied. As a result, this ESAM is probably too low for typical occupied residences since they contain much more moisture absorbing material (clothing, linens, towels, additional furnishings, etc.).

A brief parametric analysis using additional ESAMs of 0.25 (half optimum) and 1.0 (double optimum) was performed to observe the sensitivity of material moisture capacity. Results from this analysis are given in Figure 2-15. Note that y-axis scales in Figures 2-14 and 2-15 are almost identical, resulting in an interesting observation. If the effective surface area (and thus, the moisture capacity) is set to zero in the model, large errors in prediction of room humidity ratio result. However, if MAD is modeled even with incorrect effective MAD surface areas, room humidity ratio errors are relatively small. It is also interesting to note that after ventilation periods, errors in humidity ratio are either consistently high or consistently low and in opposite directions for ESAMs of 0.25 and 1.00, respectively. Therefore, if ESAM is incorrectly estimated it will primarily affect results following a step change in room moisture conditions. In typical ventilated residences this effect has been estimated to last for two to five days depending on the moisture holding capacity of the building.

The ventilation periods in the data-set (September 21-23) provide for a step function increase in the room air moisture content. This gives an additional means of evaluating the validity of the MAD analysis. If the rate or capacity terms are significantly in error, the model should have difficulty predicting room humidity ratios after the vent period even if they can be matched before ventilation occurs. Figure 2-15 points out that this is indeed the case. If we look in detail at the data-set before and after these vent periods the effect becomes more clear. Figure 2-16 is a plot of the predictions of room humidity ratio for each ESAM plotted over the measured

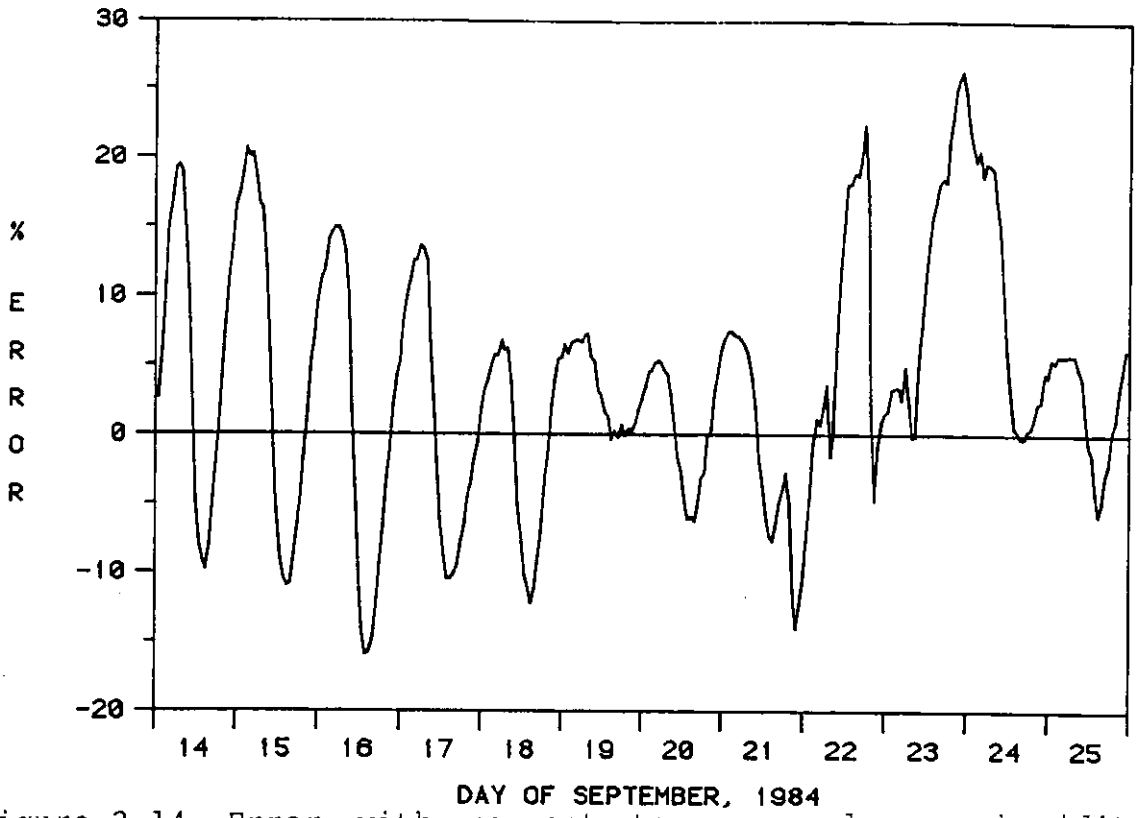

Figure 2-14 Error with respect to measured room humidity ratio for no MAD.

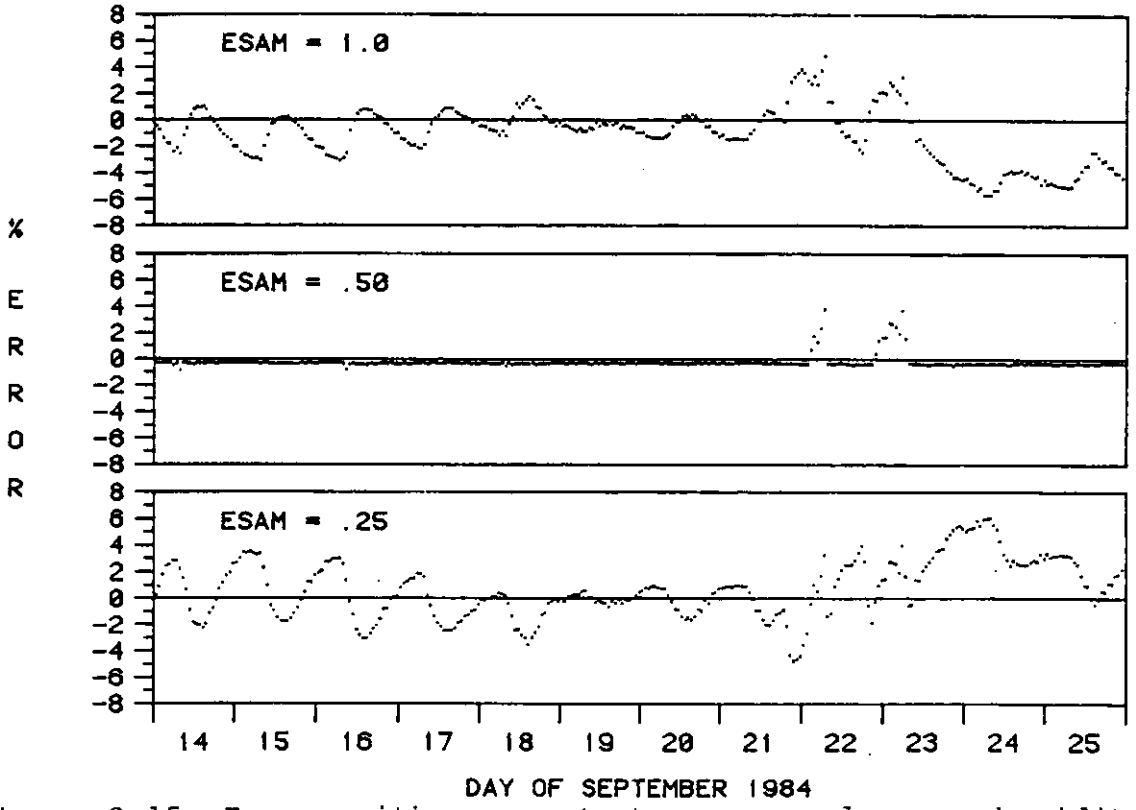

Figure 2-15 Error with respect to measured room humidity ratio for three effective surface area multipliers (ESAM).

data for September 20 before the building is vented. Note that when ESAM decreases, the humidity ratio amplitude increases; and that when ESAM increases, the amplitude decreases. This amplitude shift is related to the rate of MAD as it is controlled by available surface area. (The thickness of the MAD surface remains constant regardless of the area used in the analysis. Thus, the area available for MAD to some extent also controls the net moisture capacity of the building.)

Figure 2-17 shows the same data plotted after the vent period on September 24. There is now a much greater discrepancy in the curves. It is somewhat more difficult to see but the amplitude shift remains. Superimposed on the amplitude shift is a magnitude shift. The magnitude shift relates to a discrepancy in the total moisture capacity of the building and is also controlled by the available surface area. One can see that **as ESAM increases,** room humidity ratio increases in magnitude but decreases in amplitude; and **as ESAM decreases** room humidity ratio decreases in magnitude but increases in amplitude. Both shifts are the result of a moisture capacitance effect. It was gratifying to know that if the value of the effective moisture surface area (and therefore, the room moisture capacitance) can be accurately estimated, the model can accurately predict the behavior of the room humidity ratio before, during and after a step change (i.e., ventilation) in room humidity ratio even when the room materials are represented by only two characteristic materials acting in parallel.

To determine an ESAM value that is likely to be "typical" of real, occupied buildings, a sensitivity analysis using annual MADTARP runs was performed. The passive building (see Section 3.5 for detailed building descriptions) was used in the analysis and ESAM was varied from 0.0001 to 5 for both an unvented and a vented building. Results of the analysis

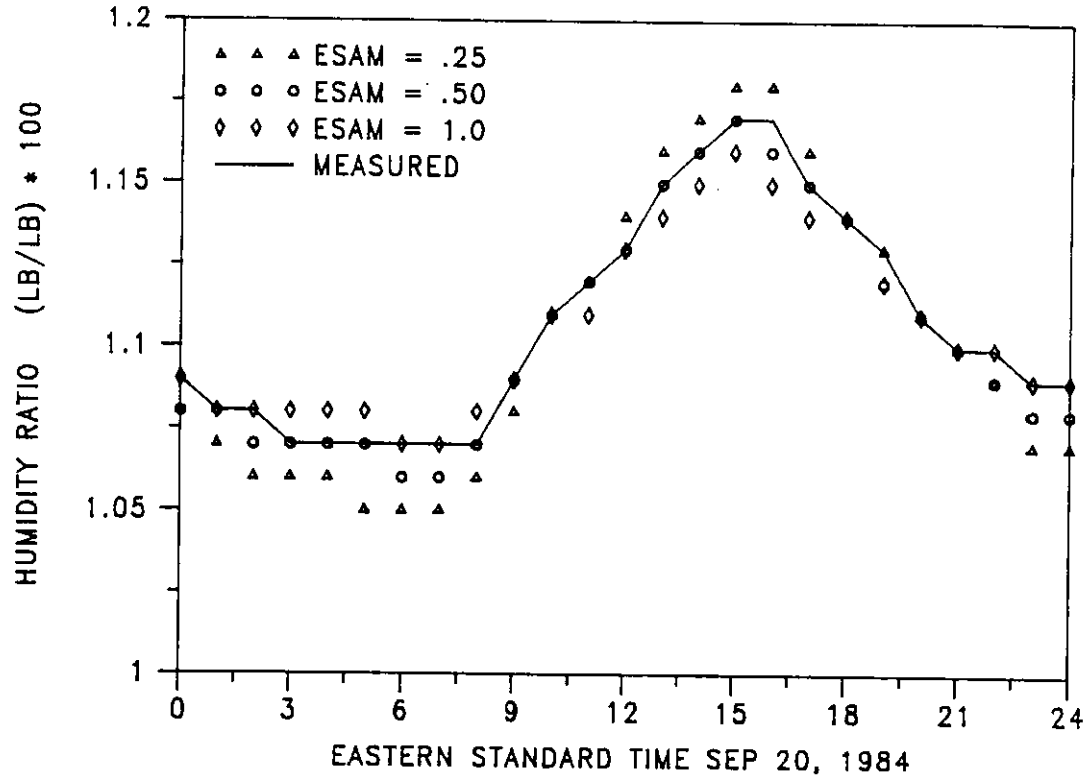

Figure 2-16 Measured and calculated room humidity ratios before vent days.

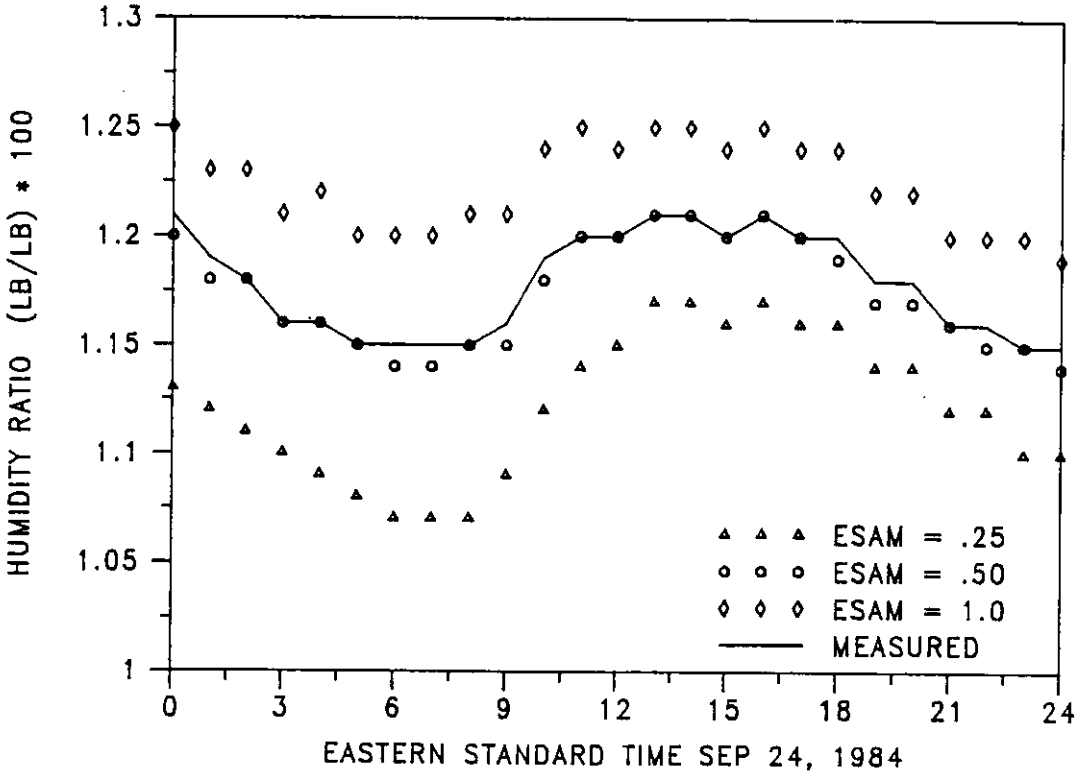

Figure 2-17 Measured and calculated room humidity ratios after vent days.

appear in Figures 2-18 and 2-19. Figure 2-18 shows the annual maximum, minimum and average zone RH as predicted by MADTARP for the **unvented** building. As ESAM increases, the annual RH swing and the annual average decreases. The most significant changes occur at lower ESAMs. As noted in the previous discussion of the townhouse data, the change in average RH is imperceptible at ESAMs of 1.0 or greater. Even the annual maximum and minimum RH rapidly approach their asymptotic limits.

Figure 2-18 shows the variation in building cooling load with increasing ESAM. This figure presents a different picture of the sensitivity of building load to variation in ESAM. For the **unvented** building the difference in predicted building load is insignificant. However, for the **vented** building the cooling load is highly sensitive to ESAM. As yet, insufficient data exist to precisely determine a "typical" ESAM for residences. A value of 0.5 was found to accurately predict the behavior of the monitored townhouses. This value was obviously low for "typical" occupied buildings where much more moisture aborption material exist. Therefore, a conservative value of ESAM = 0.75 was selected for use in this study. The results presented in the remainder of the report should be considered in light of this value and the cooling load sensitivity analysis presented in Figure 2-19.

2.3.4 Interface with TPS

The Machine And Moisture Algorithms (MAMA) are developed in such a way that it is possible to use them with any hourly building load simulator. The relations between MADTARP and MAMA are depicted in Figure 2-1. As indicated, MAMA requires two major input sets. The first input set consists of the material moisture properties that are obtained from MADAM (see Section 2.2). The second input set comes from the thermal performance simulator (TPS). For its moisture algorithms MAMA requires only two input parameters from TPS, the zone

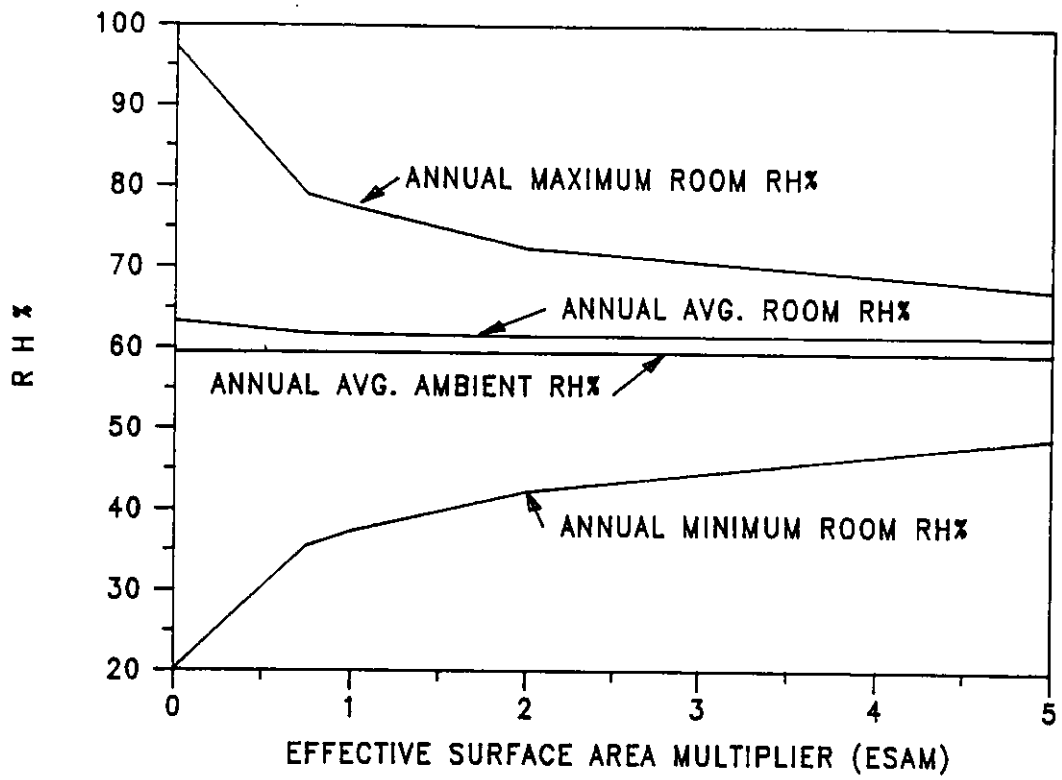

Figure 2-18 Change in room relative humidity with increasing ESAM for unvented passive block home.

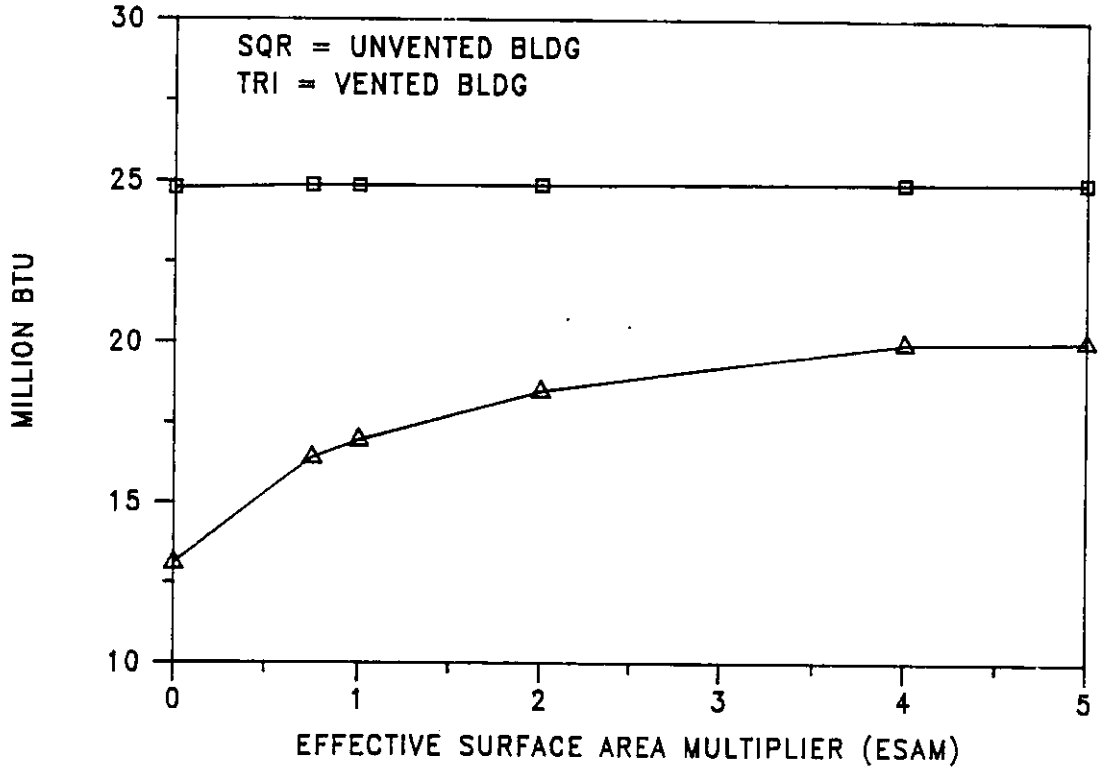

Figure 2-19 Annual cooling load versus ESAM for vented and unvented passive block home.

temperature and the sensible cooling load of the zone. In the current version of MADTARP the zone temperatures and the associated sensible loads are calculated for each hour. Therefore, for every simulated hour a set of zone temperatures and sensible loads have to be supplied to MAMA by TPS. MAMA can perform detailed calculations within a given hour, which means the hour can be discretized into finer time steps. However, TPS can perform only hourly calculations and the hour can not be discretized.

The mathematical relationships between the mechanical systems and TPS have been given in Section 2.3. Currently, the mechanical system affects the results only in terms of zone humidity and latent loads. The sensible load of the zone remains unchanged. Like the moisture algorithms, the mechanical system algorithms require three sets of inputs. The first set consists of the machine performance characteristics. The second set comes from TPS and consists of the temperature and the sensible load of the zone, and the ambient temperature. Finally, the third input set comes from the moisture algorithms and consists of the humidity conditions of the zone and its associated materials. After the zone humidity and sensible load conditions are known, the mechanical system run time and latent load removal by the system can be calculated. Like the moisture algorithms, the mechanical systems algorithms do not alter the results of TPS.

2.4 PASSIVE ANALYSIS AND PERFORMANCE ALGORITHMS (PAPA)

New algorithms were developed to model the performance of passive and hybrid cooling methods. Ventilative, radiative and ground cooling strategies were examined. These strategies were chosen as the most economical for hot, humid climates.

Natural ventilation is totally passive, i.e., it requires no parasitic power or fan control. Ventilation is handled

separately from the other methods (which use PAPA). Details on the ventilation algorithms are presented in Section 3.2.1.

The structure of PAPA and the radiative and ground algorithms are discussed in the following sections.

2.4.1 Structure and Capabilities

The major components of PAPA are shown in Figure 2-20. Presently there are two cooling algorithms, one for ground and one for radiative cooling.

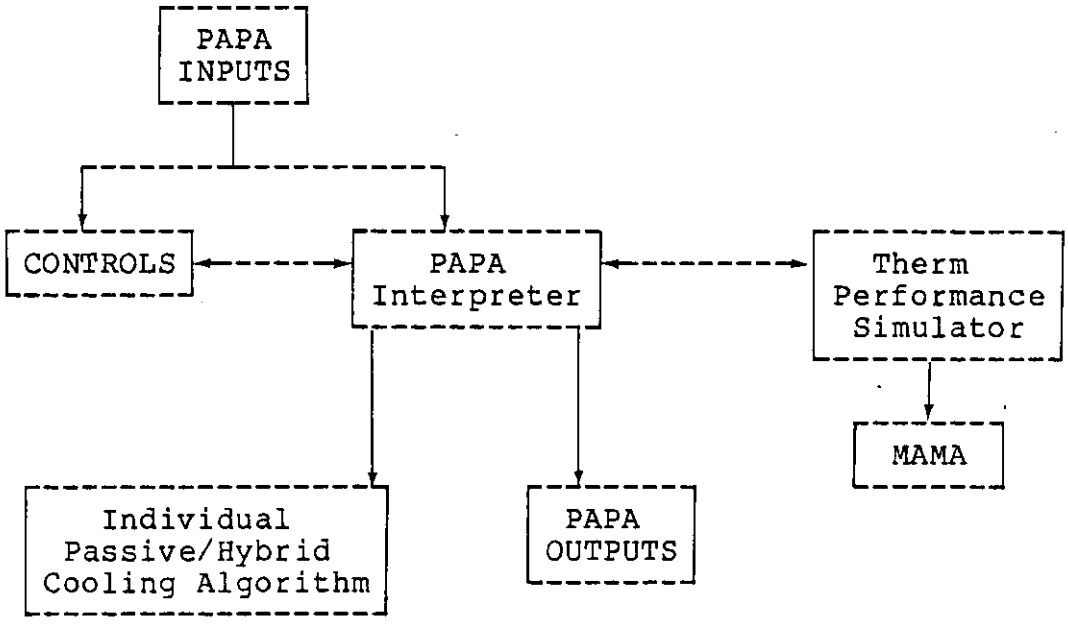

Figure 2-20 Components of Passive Analysis and Performance Algorithms.

Only one passive/hybrid cooling system is allowed for a given run. The PAPA interpreter correlates the user inputs, the control logic and the thermal outputs for each zone, and translates them into inputs for the passive/hybrid cooling algorithms. The passive/hybrid cooling performance characteristics are calculated, then transferred back to the PAPA interpreter which breaks them up into cooling components for each building zone. These cooling components are included in the energy balance for each zone in the MADTARP thermal

performance simulator (TPS), and backup mechanical cooling requirements are calculated by MANA as detailed in Section 2.3.

The user may select which (if any) hybrid cooling option is desired. The user also specifies the control parameters (see Section 2.4.3.1) and the fluid flow parameters (see Section 2.4.3.2) for the system. The user may specify either English or metric units for input or output.

Each passive system has a number of parameters which may be altered. These input parameters make simulating different size systems, component locations, materials and configurations simple. The details of these parameter choices are given in Section 2.4.3.

2.4.2 Theoretical Approach

The components of any passive or hybrid sensible cooling system consist of:

- o A heat dissipator,
- o A distribution system,
- o A heat storage medium.

Passive/hybrid cooling systems require that heat is delivered to storage during times of adverse dissipation conditions and then distributed to the dissipator during times of favorable environmental conditions.

2.4.2.1 Heat Dissipators

A heat dissipator is a component of a passive or hybrid cooling system which is used to transfer heat to the available environmental resource. Table 2-3 lists the typical heat dissipator for each cooling strategy.

In hot, humid climates most cooling sources (natural heat sinks) are weaker than in hot, dry climates. High humidities increase the sky temperature and reduce the daily temperature

Table 2-3

Heat Dissipators for Passive Cooling

Passive cooling strategy	Dissipator Name	Dissipator properties
Ventilation	Vent	Opening to ambient air
Evaporative	Evaporative cooler	Water spray which cools and humidifies air
	Indirect evaporative cooler	Heat exchanger separates building air from evaporatively cooled air
Radiative	Radiator	High thermal emissivity, exposed to night sky
Ground	Earth tube or other system	High conductivity to deep earth

swing. The long summer seasons increase ground temperature and high wet-bulb temperatures limit evaporative cooling potential. Figure 2-21 shows the average July daily cycle of the environmental resources that enable most passive/hybrid cooling in Miami, Florida [Clark, 1981]. Figure 2-22 depicts the same temperatures for Albuquerque, New Mexico, a hot, dry climate [Clark, 1981]. Although the daily high dry-bulb temperature is slightly higher in Albuquerque, passive hybrid cooling is much easier in this dry climate than in humid climates. Table 2-4 indicates the difference in the potential cooling limit for these two climates by passive cooling strategy.

As can be seen from Table 2-4, the only resource that is very powerful in Miami in July is the sky temperature. All other resource temperatures are high and will provide limited passive cooling for a building. However, during milder months and in less severely humid climates, other cooling strategies become more effective, although to a lesser extent than in the dry climates.

Table 2-4

Comparison of Dry and Humid Climate Passive Cooling Resources

Parameter of Interest	Potential Cooling Strategy Effected	Lower Limit Average July Daily Cycle: Miami (°F)	Albuquerque (°F)	Difference (°F)
Wet-bulb	Evaporative	74	61	13
Dewpoint	Evap. & Radiative	72	46	26
Sky	Radiative	61	46	15
Deep ground	Ground coupling	77	62	15

2.4.2.2 Distribution Systems

To maintain comfort in a building, the cooling done at the dissipator must be distributed to the living areas. Depending on the building design, the cooling load and the cooling resource, the amount of forced distribution can vary from low of none to an amount that causes the hybrid system's performance to be no better than that of a conventional cooling system. The distribution system moves heat from the building and/or storage to the dissipator when environmental conditions are favorable. At other times the distribution system may be used to transfer building heat to the storage (thus maintaining comfort).

The same distribution system could be used for the backup cooling system and/or a passive solar heating system.

There are two common types of distribution systems. An air-system type uses the building air as the transfer medium. The air either flows naturally or is forced by a fan. Since the heat capacity of air is very low, the volume of air transferred must be high. Therefore, unless great pressure

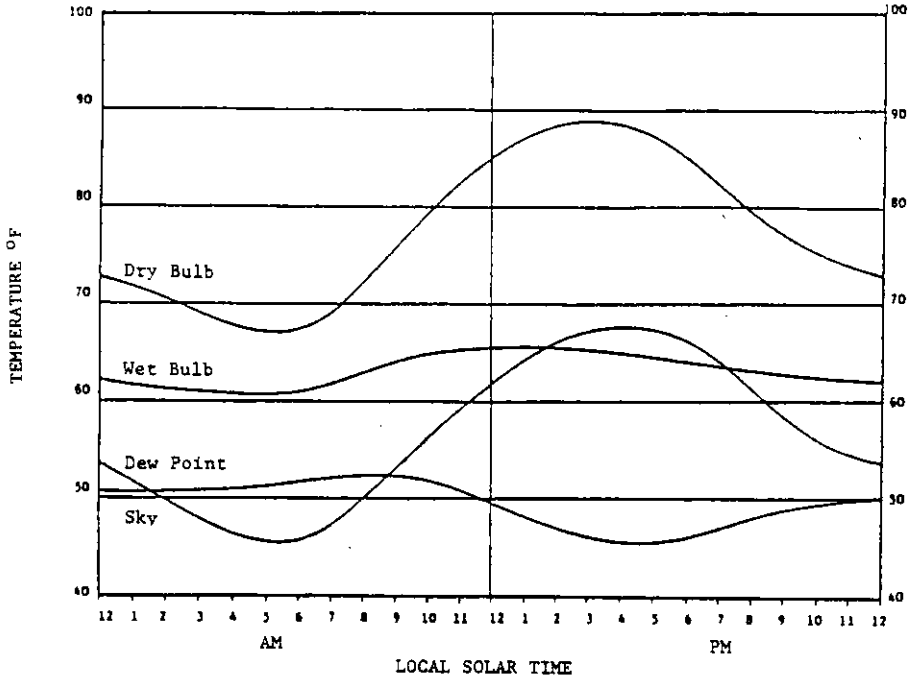

Figure 2-21 Meteorological temperature profiles for average July day. From 12 year average for Albuquerque, NM.

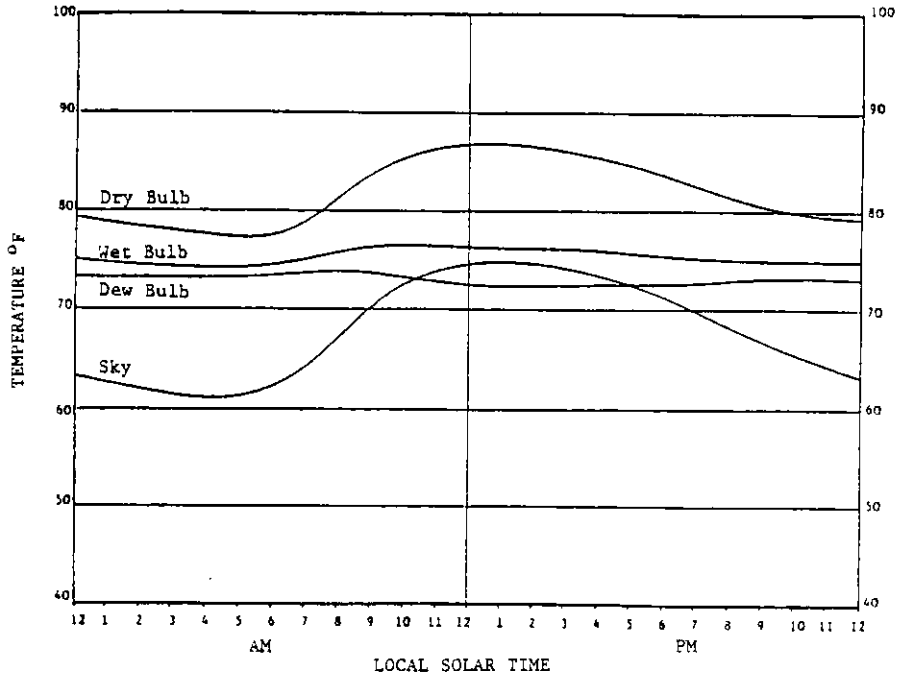

Figure 2-22 Meteorological temperature profiles for average July day. From 12 yer average for Miami, FL.

differences induce natural flow, considerable parasitic fan power is required. The other type of distribution system uses water as the transfer medium and often as the storage medium as well. Efficient pumps have small parasitic power requirements and the heat capacity of water is excellent. It can be used in conjunction with radiative panel backup cooling or heating systems. However, if a conventional forced air system is used, the water cooling distribution system requires a separate network. A heat exchanger to the forced air system is possible, but would give the water-cooled system most of the disadvantages of the air system. The relative initial cost of the water or air distribution system is highly dependent on the heat dissipation and storage methods chosen. Often the efficiency of the water system makes its operating costs less than that of air sytems. Table 2-5 shows the usual components used for air and water distribution systems.

Table 2-5

Comparison of Air and Water Distribution Systems

Fluid	Natural Flow Method	Forced Flow Method	Forced Flow Power Consumption	Capacity to Transfer Heat	Common Storage Component	Compatible Distr. Method
Air	Wind, Pressure or Temp. Driven	Fans	Moderate	Very low	Bldg. mass, Rock beds	Forced Air
Water	Gravity, Thermo-siphon	Pumps	Low	High	Water tanks or tubes	Radiator or fan coil

2.4.2.3 Storage Systems

An important element of any passive hybrid system is the component used to store the heat until the time at which it is distributed to the dissipator to be rejected from the building. Most cooling resources are such that it is

desirable to do all building cooling at night. To do that, heat gain during the day must be stored at comfortable temperatures. At night, natural or forced flow removes the heat from storage and rejects it to the environment through the dissipator.

For effective operation, storage should be very well coupled to the space which is to be cooled. The thermal coupling is usually best if the space-air can freely circulate around the storage and the storage surfaces can freely radiate to other surfaces in the space. An example of such a system is when actual building components -- such as floor or ceiling slabs or/and concrete block walls -- are used as a storage component. However, in some instances remote storage is more practical.

In those cases, the storage is exterior to the space and the distribution system takes heat from the space and transfers it to storage. Typically this is accomplished either by transporting the storage fluid itself to the living space to pick up heat and return to the storage, or by using the space air as the transfer medium and passing it through storage. Examples of remote storage include large well-insulated fluid storage tanks or remote rock beds. In many cases, a combination of remote and integral storage with forced and natural heat flow are used. In the last decade, phase change materials have been developed which have extremely high capacities for heat storage. By using chemicals designed to change phases at specified temperatures, the great majority of the heat is released at specific temperature. Figure 2-23 shows some common passive thermal-storage materials.

2.4.3 Algorithm Development

Descriptions of the control, interpreter, and ground and radiative algorithms are given in this section.

Masonry Walls and Floors

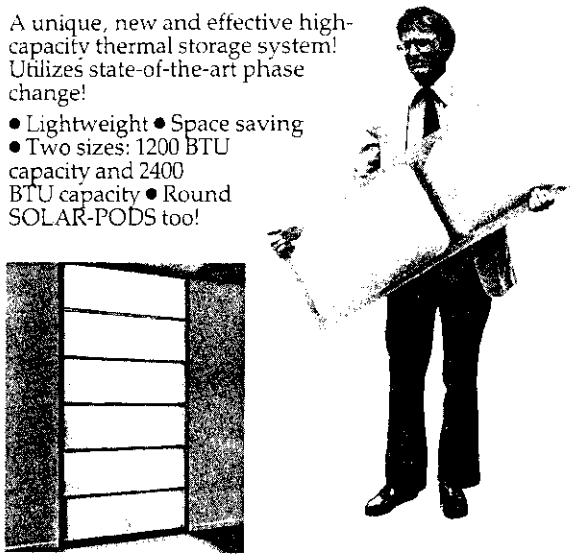

Phase Change Materials

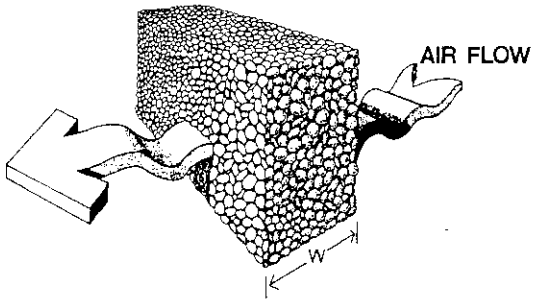

Rock Bins

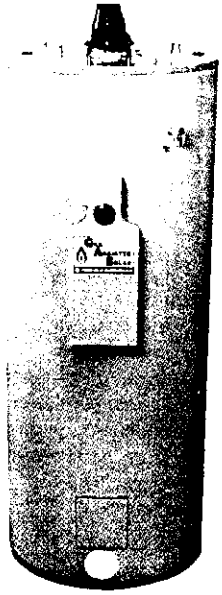

Water Tank

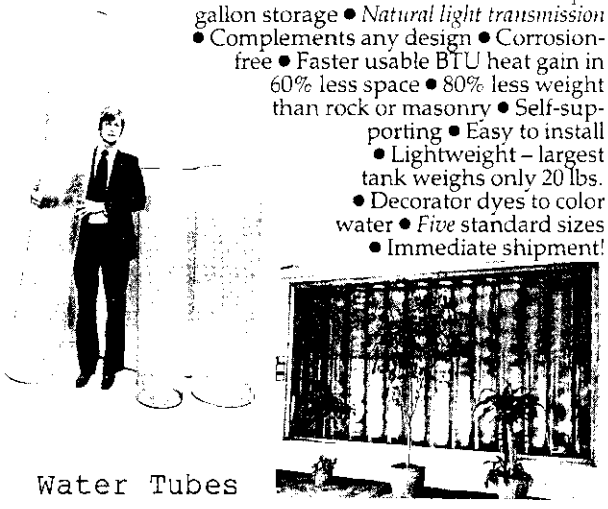

Water Tubes

Figure 2-23 Common passive thermal storage materials.

2.4.3.1 Controls

The purpose of the control algorithms is to maximize the cooling potential of the hybrid system without overcooling the building. Controls should be designed also to prevent use of the hybrid air-conditioning system when it is less efficient than the backup system. Hybrid system efficiencies can vary significantly with climatic conditions, thus tests must be made at each time-step (hour) in the simulation for effective control of the passive/hybrid system.

The user specifies three set-point temperatures -- T_h, T_m, and T_l -- and a temperature difference T_d . Default settings are the cooling set-point for T_h and the heating set-point for T_l. T_m is the average of T_h and T_l. The default for T_d is 1.0°C (1.8°F).

Based on the history of heating and cooling requirements, flags are set which control the setpoint used to turn the hybrid system on or off. The heating flag is set if there is heat required and unset after no heat is required for an entire daily cycle (midnight to midnight). The cooling flag is set if there is cooling required and unset after no cooling is required for an entire daily cycle. The control logic is given in Table 2-6, showing the values used for the ground and radiative cooling runs.

Table 2-6
PAPA Control Logic

Heating Flag Set	Cooling Flag Set	Set point above which hybrid systems turn on (°F) (A/C set-point=78, heater=68)	
		Radiator	Ground
Yes	Yes	73	75.75
Yes	No	76.2	77
No	Yes	69.0	74.5
No	No	no change	no change

Radiative cooling test runs using this logic indicated that the heating load was not increased (compared to a non-hybrid system) nor was the total cooling reduction penalized (compared to lower cooling setpoints).

The entering fluid temperature (see Section 2.2.3.2) is the temperature which is checked against the setpoint.

An additional criterion is made to assure system efficiency. If the system cannot achieve a user-specified coefficient of performance, then the system is shut off for that hour. In this case the current time-step is rerun with the hybrid system off, since the system performance has a cause-and-effect relationship with the building heat balance.

The basecase value for the hybrid system shut-off COP is 2.3. This COP is approximately the rated value for the simulated air conditioner.

2.4.3.2 PAPA Interpreter (including fluid flow)

The interpreter algorithm meshes all the other algorithm outputs for use with the MADTARP thermal processor and MAMA. This algorithm simulates, in a simplified method, the distribution system.

Storage is done by the building components. PAPA uses the thermal processor simulation's internal heat transfer routines to distribute the stored heat to various surfaces. Thus, using the standard building input deck, the user can simulate the effect of various amounts or types of mass. PAPA is presently unable to simulate remote storage as described in Section 2.4.2.3.

For each zone, the user specifies a heat exchanger effectiveness, E_Z, and a surface transfer to total ratio, S_Z.

Each of these values must be between 0 and 1.

$$0 \leq E_Z \leq 1 \qquad (2\text{-}29)$$

$$0 \leq S_Z \leq 1 \qquad (2\text{-}30)$$

Also, the total heat exchanger effectiveness must be 1 or less.

$$E_t = \sum_{z=1}^{N} E_Z \leq 1. \qquad (2\text{-}31)$$

The total heat exchanger effectiveness indicates how much of the cooling done at the dissipator was transferred to the building.

The passive/hybrid cooling which is transferred to each zone is:

$$Q_Z = Q_d * E_Z, \qquad (2\text{-}32)$$

where Qd is the total cooling done at the dissipator.
The portion that goes directly to the zone air is:

$$Qa_Z = Q_Z * (1-S_Z) \qquad (2\text{-}33)$$

And the rest goes to the zone surfaces for storage via the MRT network:

$$Qs_Z = Q_Z * S_Z. \qquad (2\text{-}34)$$

If the system fluid is air, then typically the total heat exchanger effectiveness will equal 1.0, and the surface to total ratios will depend on the distribution system. Air circulated in cinder block cores may have a S_Z of 0.5, whereas a ducted system may have a S_Z of 0. Default value for all hybrid system runs were 1.0 for E_Z and 0 for S_Z.

A water system would typically have a total heat exchanger effectiveness less than 1.0, since the water will be separated from the zone. If the water is simulated as pipes passing through a room a low S_Z may be possible. Most applications would involve water storage and/or radiator distribution in the zone. These options can be approximated in the simulation using a high S_Z and massive building components.

These parameters are also used to calculate the fluid temperature that goes to the dissipator. The starting fluid temperature calculation consists of two components. Some "coolth" may remain in the fluid in the circulation system, if all of it was not transferred to the zones.

$$T_{fs1} = (1-E_t) * T_{f0} \qquad (2\text{-}35)$$

Where T_{f0} is the fluid temperature out of the dissipator. The other component is weighted by each zone heat exchanger effectiveness and the zone's surface to total ratio storage factor:

$$T_{fs2} = \sum_{z=1}^{z=N} E_z * (Tr_z*S_z+Tz_z*(1-S_z)) \qquad (2\text{-}36)$$

where Tr_z and Tz are the zone mean radiant and dry-bulb temperatures, respectively. Thus, the fluid temperature is the sum of these components.

$$T_{fs} = T_{fs1} + T_{fs2} \qquad (2\text{-}37)$$

Note that the passive cooling done is broken up in a similar manner (see Equations 2-32, 2-33 and 2-34).

In air systems, latent cooling may also occur due to condensation on the dissipator. The dew-point temperature of the air is weighted by the heat exchanger effectiveness of each zone times the dew-point of that zone.

$$Tfd = \sum_{z=1}^{z=N} E_z * Td_z \qquad (2\text{-}38)$$

Since this routine is done prior to MAMA, the entering dew-point temperature is based on the previous hour's values. Some error is introduced, but as long as high infiltration or ventilation rates are not concurrent with the PAPA simulated cooling, this error will be small.

The building latent cooling, Q_{ld}, is calculated in the specific passive/hybrid dissipator algorithm (see next sections). The interpreter divides that cooling into values for each zone. If the air were assumed to be very well mixed

when the system was on, then a simple effectiveness weighting is adequate:

$$Q_{lz} = Q_{ld} * E_z \quad (2\text{-}39)$$

However, if the zone air is not well mixed then the moisture levels will be different and the latent cooling may occur only in the most humid zones. The hybrid system may cause mixing which humidifies some zones and dehumidifies other zones. For the present study, only one conditioned zone is simulated, thus Equation 2-39 is adequate.

Typical systems will have just one pump or blower; however, to facilitate certain outputs, the parasitic power is also divided into values for each zone:

$$P_z = E_z * P \quad (2\text{-}40)$$

where P is the user-specified parasitic power for the entire hybrid cooling system.

2.4.3.3 Radiative Cooling

The radiative cooling algorithm is a lumped model of fluid flowing underneath an emissive surface exposed to the night sky. The user may specify the following radiator properties:

- o Length and Width
- o Emissivity
- o Tilt

A wind speed modifier may also be specified to account for radiator configurations which are designed to reduce convective heat transfer.

2.4.3.3.1 The Model

Figure 2-24 depicts the simulated radiator when air is the fluid. When water is the fluid there is no bottom plate. The assumptions for the model are:

- o Radiator is massless and has infinite conductivity
- o Bottom plate is massless
- o There is no heat loss or gain below the bottom plate or to the sides

- For a finite length of fluid in the flow direction,

$$T_f=(T_o+T_i)/2 \qquad (2\text{-}41)$$

In addition to Equation 2-41, the equations which describe the heat transfer are:

$$h_r\ (T_r-T_e)+h_c(T_r-T_a)+h_f(T_r-T_f)+h_i(T_r-T_b)-0 \qquad (2\text{-}42)$$

$$h_f(T_f-T_r)+h_x(T_f-T_b)=(mC_p/A)\ (T_i-T_o) \qquad (2\text{-}43)$$

$$h_i(T_b-T_r)+h_x(T_b-T_f)=0 \qquad (2\text{-}44)$$

Thus, there are four equations and four unknowns (T_f, T_r, T_o, T_b). The solution for the radiator temperature is:

$$T_r=(h_r*T_e+h_c*T_a+V*T_i)/(S-U) \qquad (2\text{-}45)$$

where

$$V=.5*[h_f+Wh_f+h_i*h_x/Z+h_i*h_x*W/(Y*Z) +h_f*h_x^2/(2*a*Y*Z)+h_x^2*h_f*W/(2*a*Y^2*Z)] \qquad (2\text{-}46)$$

$$S=h_r+h_c+h_f+h_i-h_f^2/(2*a*Y) \qquad (2\text{-}47)$$

$$U=(h_i-h_f*h_x/(2*a*Y))*(h_i/Z+h_x*h_f/(2*Z*a*Y)) \qquad (2\text{-}48)$$

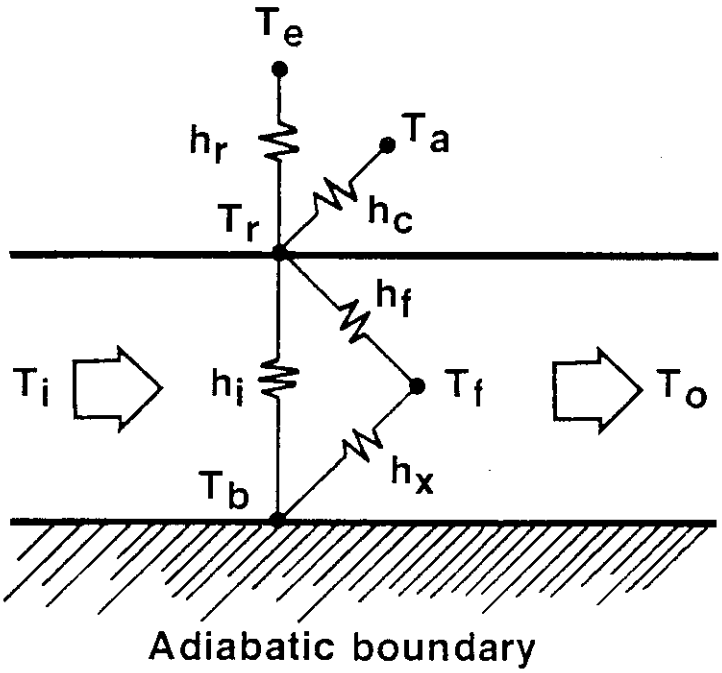

Figure 2-24 Radiator model used in Passive Analysis and Performance Algorithms.

and the following equations apply:

$$a=mC_p/A \qquad (2\text{-}49)$$

$$W=1-h_f/(2*a)-h_x/(2*a) \quad (2\text{-}50)$$

$$Y=1+h_f/(2*a)+h_x/(2*a) \quad (2\text{-}51)$$

$$Z_o=h_x-h_x^2/(2*a+h_f+h_x) \quad (2\text{-}52)$$

$$Z=h_i+Z_o \quad (2\text{-}53)$$

The user specifies the constants h_f, MC_p, and h_x. Therefore, Equations 2-49 through 2-52 are calculated once per run based on user-specified flow parameters. The heat tranfer coefficients h_r, h_c and h_i are a function of T_r. Thus, these variables are calculated for each node, and Tr is calculated using iteration due to the relationship between T_r, h_r, h_c and h_i.

The convective coefficient, h_c, is calculated using the same method as the other outside building surfaces. This method is fully described by Walton [1983]. The environmental temperature seen by the radiator, T_e, is calculated as a function of tilt and sky and ground temperatures. The temperature of the ground surface is assumed equal to the ambient temperature. The view factor of the sky radiation which is reflected from the ground is:

$$G_s = (1-E_g)*(1-\cos(t))/2 \quad (2\text{-}54)$$

where t is the radiator tilt up from horizontal and E_g is the ground emissivity.

The view factor of the ground radiated heat is:

$$G_f = (1-\cos(t))/2 \quad (2\text{-}55)$$

The view factor of the sky is:

$$S_f = (1+\cos(t))/2 \quad (1\text{-}56)$$

The irradiance from the environment is therefore:

$$Q_e = \sigma*S_f*T_s^4 + \sigma*E_g*G_f*T_a^4 + \sigma*G_s*T_s^4 \quad (2\text{-}57)$$

where σ is the Stefan-Boltzman constant.

The environmental temperature is:

$$T_e = \sqrt[4]{Q_e/\sigma} \quad (2\text{-}58)$$

where T_e is in absolute degrees. Note that T_e will equal the sky temperature for a horizontal radiator.

The flux between the radiator surface and this mean radiative environment which it "sees" is:

$$Q_r = E_r * \sigma * (T_r^4 - T_e^4) \qquad (2\text{-}59)$$

so the radiative coefficient is:

$$h_r = Q_r/(T_r - T_e). \qquad (2\text{-}60)$$

The environment temperature is calculated once per hour; however h_r is calculated for each iteration of T_r within each mode.

The radiative flux between the top and bottom plate is:

$$Q_{ri} = E_b * \sigma * (T_r^4 - T_b^4) \qquad (2\text{-}61)$$

where the temperatures are in absolute units (^oK or ^oR). The coefficient is then:

$$h_i = Q_{ri}/(T_r - T_b) \qquad (2\text{-}62)$$

The above calculations are complicated by condensation. If moisture condenses on the top of the radiator (when radiator is cooler than the ambient dew-point temperature) the latent heat of condensation, Q_A, has to be added to the surface:

$$h_r(T_r - T_e) + h_c(T_r - T_a) + h_f((T_r - T_f) + h_i(T_r - T_b) + Q_A = 0 \qquad (2\text{-}63)$$

If, later that night, the radiator is hotter than the dew-point temperature, evaporation can occur. However, so that errors will be on the conservative side, evaporation of the condensed water was not simulated. The authors believe this to be only a minor effect. The new solution, including condensation is:

$$T_r = (h_r T_e + h_c T_a + V T_i + Q_A)/(S - U) \qquad (2\text{-}64)$$

Condensation may also occur if the air flowing in the radiator plenum has a dew-point temperature greater than the radiator surface. In extreme cases, condensation may also occur on the bottom plate of the plenum. The maximum amount of

dehumidification the radiator can do is approximately given by:

$$Q_l = (W_f - W_r) * V_f * D_f \qquad (5\text{-}65)$$

Since moisture adsorption and desorption for the present time step is not modeled until after PAPA is completed, using the house volume as the flow volume could slightly underpredict the dehumidification potential. Therefore, the volume of air used for the Equation, V_f, was set equal to 1.2 times the house volume, or the net flow volume for the hour, whichever was smaller. For the base radiation runs, the flow volume is significantly larger than the house volume.

The sensible heat release by the condensate is added into the next segment's starting air temperature:

$$T_i = T_o + Q / mC_p \qquad (2\text{-}66)$$

Again, evaporation of the condensate was considered unlikely and is not simulated.

The values used for the radiative cooling runs reported herein are:

Emissivity	= .90
Area	= 1625 ft^2
Tilt	= 22.5° from horizontal
Airflow	= 2000 CFM
Flow capacitance (MCp)	= 2.2 kBtu/hr-°F
h_f coefficient	= .50 Btu/hr-ft^2-°F
h_x coefficient	= .50 Btu/hr-ft^2-°F
Fan power	= 225 Watts

2.4.3.3.2 Radiative Model Nomenclature

A - Area of radiator (ft^2)
D_f - Density of air in radiator (lb./ft^3)
E_b - Bottom plate emissivity
E_g - Ground emissivity

E_r - Radiator emissivity

G_f - View factor of the ground

G_s - View factor of ground reflected sky radiation

h_c - Convective heat transfer coefficient (htc) to ambient (Btu/hr-ft^2-^{o}F)

h_f - Convective htc between radiator and air stream (Btu/hr-ft^2-^{o}F)

h_i - Radiative htc between top and bottom surfaces (Btu/hr-ft^2-^{o}F)

h_r - Radiative htc to environment (Btu/hr-ft^2-^{o}F)

h_x - Convective htc between bottom of radiator plenum and air stream (Btu/hr-ftmcp- Air flow capacity (Btu/hr-^{o}F)

Q_A - Heat from ambient condensation (Btu/hr-ft^2)

O_e - Irradiance from environment seen by radiator (Btu/hr-ft^2)

O_l - Latent cooling (Btu/hr-ft^2)

Q_m - Heat of condensation within radiator plenum (Btu/hr-ft^2)

Q_r - Flux between radiator and environment (Btu/hr-ft^2)

O_{ri} -Interior radiative flux between top and bottom plates (Btu/hr-ft^2)

T_a - Ambient dry bulb temperature (^{o}F or ^{o}R)

T_b - Bottom of radiator plenum surface temperature (^{o}F or ^{o}R)

T_e - Mean radiative environmental effective temperature (^{o}F)

T_f - Fluid (air) temperature (^{o}F)

T_i - Entering air temperature (^{o}F)

T_o - Exiting air temperature (^{o}F)

T_r - Radiator temperature (^{o}F or ^{o}R)

T_s - Effective sky temperature (^{o}R)

t - Tilt of radiator

W_f - Absolute humidity level of flowing air (lb H_2O/lb$_{dry\ air}$)

W_r - Absolute humidity at a saturation temperature equal to the radiator temperature (lb H_2O/lb dry air)

V_f - Effective volume of air in radiator (ft^3)

- Stefan-Boltzmann Constant .1712x10^{-8} Btu/hr-ft^2-^{o}R^4

2.4.3.4 Ground Cooling

An earth tube ground cooling model, developed by Benton and Akridge [Abrams 1980], was adapted for the analysis. Their simplified model uses time dependent integral solution to predict the degradation with time of the system, thus accounting for the heating of the soil without a three-dimensional finite difference model. A good agreement was found between the model and a GROCS subroutine for TRNSYS [Abrams 1980]. The details of their model are not repeated here.

Two modifications were made to the model. Dehumidification of the air was modeled if the circulating air dew point was greater than the pipe temperature. Secondly, the system was permitted to cycle on and off based on control criteria. This meant reducing the time variable for the integral solution. Studies [Scott 1965, Hendrick 1980] indicate significant improvement in performance from cycling. Hendrick shows cooling capacity at a 1/3 duty cycle after 20 days to be higher than a 2/3 duty cycle after four days. Based on these results, it appeared reasonable to assume that after some warm-up period (50 hours) every hour the system was off would be equal to having not run the system one- quarter hour previously in terms of the earth cooling potential. Since the rate of degradation decreases with time, the 50 hour minimum assures that the results are conservative estimates of cooling potential.

Parametric analysis by Hendrick leads to the conclusions that a 300-500-foot, 12-18-inch polypropylene pipe buried 12 feet below the surface would be the optimum design regarding costs and efficiency. A 300-foot, 18-inch pipe buried 12 feet was modeled for this study.

Soil moisture level can vary significantly at a given site. Soil type can vary within the same town. Therefore, any

predicted ground cooling potential has a high degree of potential error. A soil diffusivity=0.025 ft^2/hr and soil conductivity=0.75 Btu/hr-ft-^oF were chosen for this study as average soil conditions. Sensitivities to soil conditions and pipe characteristics have been reported previously [Abrams 1980, Hedrick 1980] and are not repeated here.

The ground temperature was calculated using the well-known equation [Labs 1981]:

$$T_{(x,t)} = T_m - A_s e^{-x\sqrt{\frac{\pi}{365\alpha}}} \cos\left[\frac{2\pi}{365}\left(t - t_o - \frac{x}{2}\sqrt{\frac{365}{\pi\alpha}}\right)\right]$$

A 1200 CFM airflow with a flow capacatance of 1.3 kBtu/hr-^oF and an overall heat transfer coefficient of 1.8 Btu/hr-ft^2-^oF and a power draw of 225 Watts was used for the earth tube. A pressure drop of 0.35" H_2O was assumed based on Hendrick's results.

Due to the potential variations of the ground conditions, and unvalidated procedure for accounting for cycling, the results from ground cooling simulation runs should be used with caution. Actual ground cooling potential may be significantly different.

Earth Cooling Nomenclature

$T_{(s,t)}$ - Temperature of soil surface s at time t (F)
$T_{(x,t)}$ - Temperature of soil at depth x at time t (F)
T_m - Mean annual earth temperature (F)
A_s - Amplitude of surface temperature wave (F)
x - Depth below surface (F)
α - Thermal diffusivity of soil (ft^2/day)
t - Time of year (days, where 0 = midnight Dec. 31)
t_o - A phase constant

2.4.4 PAPA and TPS Interface

PAPA is called by TPS if the user specifies a PAPA algorithm. It is called during the first iteration and each subsequent iteration. Figure 2-___ shows where PAPA is called relative to the other algorithms (see Walton [1983] for descriptions of other algorithms).

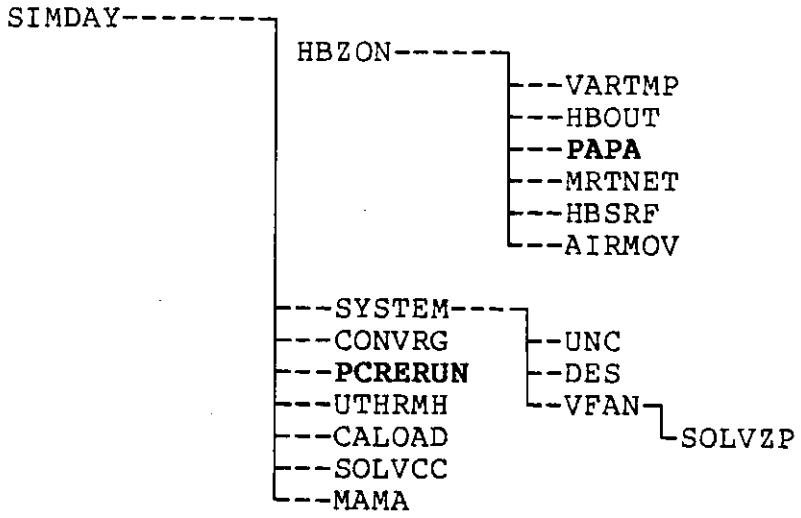

Figure 2-25 Thermal processor algorithm organization.

The interface between PAPA and TPS is partially handled in the PAPA interpreter algorithm (Section 2.4.3.2). The passive/hybrid building cooling parameters are broken into values for each zone. These values are added into the heat balance equations in the MADTARP subroutines MRTNET, AIRMOV, and DES. The cooling component coupled to the building surfaces for storage, qs_z, is added to the heat balance equation through the mean radiant temperature (see Section 3.1.4 and Walton [1983]). In AIRMOV and in UNC and DES where backup cooling is calculated, the hybrid cooling of the zone air, Q_z, is added to the zone air heat balance.

In this manner PAPA results are made a part of the heat balance which must converge. After convergence a test is made

to determine if the hybrid cooling system met the user-specified minimum efficiency criteria (see Section 2.4.3.1). This test is made in PCRERUN (see Section 2.4.4.1). If the criteria are not met, the number of convergence iterations is reset to zero and the simulation is rerun for the time step with the hybrid system off (thus Q_Z and Q_S = 0).

2.5 MECHANICAL SYSTEMS

Two types of mechanical systems are used for the building energy analysis in this report. The "typical" system is discussed in Section 2.3. The other system is referred to as the "ideal" machine. The ideal machine is a hypothetical machine capable of maintaining both a room temperature upper limit and/or a room relative humidity upper limit. Since the ideal machine is hypothetical it has no performance characteristics and no power consumption data are calculated.

2.5.1 Typical System Operating Characteristics

The interface between the mechanical system, its control device (thermostat) and the building load is complex. Mathematical modeling of the typical mechanical system with respect to the internal zone energy balance has already been discussed in Section 2.3. Another determinant of mechanical system performance is the control device. Thermostats, for example, do not really maintain buildings at a "set" upper temperature. Instead they have a built-in hysteresis.

Thermostats will not turn the system on until the sensed temperature is slightly above the set-point, and will not turn the system off until the sensed temperature is slightly below the set-point. Therefore, the cycling rate of a given mechanical system is controlled by a combination of the characteristics of the conditioned zone.

The thermal processor of MADTARP will define the energy

storage (and release) characteristics of the conditioned zone and its associated boundaries, but we must define the control device characteristics before machine run times can be calculated. For the purposes of this analysis a hysteresis of $\pm 0.18^{o}F$ was chosen to characterize the thermostat, and for the ideal machine a hysteresis of 1.0% RH was chosen for the humidistat. Using these characteristics MADTARP is capable of calculating realistic run times for both the cooling and the dehumidification mechanical systems (ideal machine only).

Another system parameter which the control device helps to determine is the cycling rate of the mechanical system. In general this cycling rate (cycles/hour) is controlled by the thermostat anticipator, modified by the thermal and moisture capacitance of the zone (building), and further modified by the hysteresis characteristics of the control device. Cycling rates and transient mechanical system performance were not modeled in this study. For the real machine a machine capacitance and control device hysteresis are specified in the building description and a total machine run-time is calculated for each timestep in accordance with these parameters. The mechanical cooling system is then assumed to begin operation at the beginning of the hour at a zone temperature of the setpoint plus the hysteresis value, and to run continuously until the total hourly load is met. Because of the calculation procedure the zone will be at a temperature equal to the setpoint temperature minus the hysteresis value at the end of the machine run-time. From the end of the run-time to the end of the timestep (one hour in the case of MADTARP) the zone temperature (and moisture level) is allowed to float. The conditions at the end of the current hour are then used as the starting conditions for the following hour's thermal and moisture balance.

Thus, the true performance of a thermostat control device is not fully modeled. In reality, the effective set-point

temperature of the air conditioner will fluctuate over the course of the day due to the self-heating effect of the thermostat anticipator. This will cause the system to operate more (lower effective set-point) at night and less (higher effective set-point) during the day than the model used here predicts. This effect is not modeled in any of the widely used building energy analysis programs. The results of this study indicate that thermostat anticipator effects as well as the transient (start-up) performance of air conditioners may play a significant role in the prediction of moisture transport in buildings. These effects, however, have not been explained in detail in this study.

2.5.2 Ideal Machine

As described in the preceding sections the ideal machine is capable of removing the excessive moisture instantly. It may be considered to have an infinite capacity. Before proceeding, the operating characteristics of the ideal machine need to be described.

The ideal machine can be simulated through the control of a humidistat, and humidistats like thermostats operate with an RH hysteresis (HY_h). Therefore, if the room relative humidity climbs above RH + HY_h the ideal machine starts operating, and brings the room condition to RH - HY_h. In the mathematical simulation of the ideal machine (see Section 2.3.2) the machine is allowed to turn on and off an infinite number of times within the hour. Therefore, when the machine turns on it instantly removes the required amount of moisture from the air and then turns off. The room is then allowed to "float" back up to RH + HY_h. This procedure is performed instantly, hence depending on the magnitute of the latent loads the machine may cycle a large number of times. In the simulation of the ideal machine, MAD also has to be considered for the following reasons.

- o For certain months the room conditions are below the relative humidity setpoint.
- o Simulation of a humidistat creates a dynamic environment in the room through the humidistat hysteresis.

The ideal machine can be simulated in two different ways -- without MAD or with MAD. Simulation without MAD can lead to severe inaccuracies primarily because of the first point given above. This is especially true when the machine operates for only short periods during the day. If the latent loads are very large and the machine has to run for long time periods the error caused by omission of MAD is greatly reduced.

2.5.3 Mechanical System Controls

MADTARP uses different kinds of sophisticated control systems which can be defined by the program users. The control system used by MADTARP can be classified under three major categories, as follows:

- o Passive cooling controls (see Section 2.4)
- o Ventilative controls
- o Thermostat and humidistat controls

The control systems mentioned above can be used independently of each other or they can be used in a combination.

VENTILATIVE CONTROLS: Ventilative controls are used if the building is to be cooled by natural or forced ventilation. Simulation of whole house fans also falls in this category. MADTARP uses different ventilative controls which are:

ENTHALPY CONTROL: If the ambient enthalpy falls between the enthalpy control range the building is allowed to ventilate.

DRY-BULB TEMPERATURE CONTROL: If the ambient dry-bulb falls between the dry-bulb temperature control range the building is allowed to ventilate.

PMV CONTROL: If the zone PMV falls between the PMV control range the building is allowed to ventilate. In PMV control the velocity fields created by ventilation, ceiling or whole house fans also are taken into account.

THERMOSTAT AND HUMIDISTAT CONTROLS: With MADTARP, thermostat and/or humidistat can be modeled. The input requirements for modeling of the thermostat and/or humidistat are the lower and upper hysteresis of the control units. If the zone is to be maintained at a temperature of T_c and a relative humidity of RH_c and the unit responses are within $\pm HY_t$ and $\pm HY_h$ then the mechanical system will be turned on when the zone temperature exceeds

$$T_c + HY_t$$

and the unit will be turned off when the zone temperature drops to

$$T_c - HY_t$$

As with the humidistat, the dehumidifier will be turned on if the zone relative humidity exceeds

$$RH_c + HY_h$$

and it will be turned off at

$$RH_c - HY_h$$

The thermostat and/or the humidistat controls will signal TPS when to turn on and off the mechanical system and the dehumidifier. Therefore, the unit run times can be altered by using different control hysteresis values.

SECTION THREE
BUILDING ENERGY ANALYSIS TECHNIQUES AND ASSUMPTIONS

3.1 TARP PROCEDURES

The MADTARP uses the detailed heat balance techniques of TARP [Walton, 1983] to compute building loads. The TARP may be used to evaluate single "design" days or it may be used with up to one year of weather data for annual performance evaluation. A large number of occupant patterns may be specified with scheduled hourly, daily, and seasonal variations. A full building input language and interpreter allows the building to be specified in great detail both thermally and spatially. Many of the specific heat balance algorithms allow either simple or detailed calculation procedures that are selectable by the user. And a large number of dependent building variables may be selected for output as user-specified reports.

3.1.1 Conductive Heat Transfer

The TARP thermal performance simulator (TPS) uses a heat transfer methodology based on the standard response factor technique developed by Stephenson and Mitalas [1967] and Kusuda [1969] modified for efficiency according to suggestions by Peavy [1978]. These modified response factors are called conduction transfer functions (CTF). The CTF of a particular composite building component describes the dynamic behavior of the particular composite with respect to an imposed triangular temperature pulse on either side of the composite. The exact solution of a series of temperature pulses are solved by Laplace transform (described in detail by Hittle [1981]) and the continuous temperature function for the composite is described as a set of CTF values for the x, y, and z tranform of an imposed pulse. The method is accurate, well documented and validated. Specific implementations of the technique in TARP are covered in detail by Walton [1983].

TPS uses CTF methods to describe envelope heat flows. These functions and algorithms defining the other zone (room) energy balance elements are then iterated to convergence in a zone heat balance. In addition to conductive transfer (described by CTF), separate radiative and convective energy flows are considered in the balance.

3.1.2 Radiative Heat Transfer

Radiative transfer is split between the short-wave solar spectrum and long-wave (far-infrared) spectrum. At the building interior, solar radiation is split into its diffuse and beam components. After accounting for glazing reflectance, absorptance, and transmittance through detailed modeling, diffuse solar radiation is equally apportioned over all interior heat transfer surface areas as a function of their solar absorptance. The beam radiation may either all go the floor as a function of its absorptance (simple method) or be apportioned to the various interior surface areas by geometry as a function of their solar absorptance (detailed method). The analysis reported here was accomplished with the simple beam radiation apportionment method. In either case the amount of radiation (diffuse and beam) not absorbed by the surfaces (1-solar absorptance) is imposed on the zone air and "quick mass" in the zone (see Walton [1983]). Long-wave radiant energy from interior lighting is treated as diffuse solar radiation.

Far-infrared radiation interchange between room surfaces is based on the Mean Radiant Temperature Network (MRTN) methodology of Joseph A. Carroll [1980]. Various surfaces interact with a zone MRT instead of directly with each other, and view factors are modified accordingly to describe the interaction of a surface with other surfaces as well as with itself. Thus, the zone node of the network (the MRT) includes the effect of all surfaces. Coupling the surfaces to the MRT in this way couples it to itself in a way that compensates for

the self weight of the surface in the radiation balance. (For further clarification and detail of the method see Carroll [1980].) The primary disadvantage of the method is that it may give prediction errors for geometries that differ significantly from the hollow cube. For most room geometries, however, it is considered accurate and fast.

Long-wave radiation components may be applied to the zone through user-selectable internal gain parameters (e.g., lights, appliances, etc.). When this is done they are apportioned through the MRTN to the various heat transfer surface areas by area and emissivity of surface.

3.1.3 Convective Heat Transfer

Convective heat transfer occurs on almost all surfaces of a building. TARP models both natural convection at interior heat transfer surfaces and wind-driven (forced) convection at external heat transfer surfaces. The user may select either simplified or detailed natural convection coefficients at interior surfaces. Both the simple and detailed method are directionally dependent with convection upward having the highest coefficients. The detailed natural convection methodology has been used in this study. Convection coefficients are calculated as follows in W/m^2K:

Upward convection	$h_c = 1.52 * \sqrt[3]{T_{air} - T_{surf}}$
Horizontal convection	$h_c = 1.31 * \sqrt[3]{T_{air} - T_{surf}}$
Downward convection	$h_c = 0.76 * \sqrt[3]{T_{air} - T_{surf}}$

Convective transfer from surfaces is further modified by surface roughness factors. For forced convection at external surfaces the transfer rate at leeward surfaces is assumed to be half of the rate at windward surfaces. Wind speeds reported at airports or from weather tapes may be modified by terrain factors to account for lower building site wind speeds. The terrain factor used in this analysis resulted in

the weather tape wind speed data input being multiplied by 0.67 to account for suburban terrains.

The reader is referred to Walton [1983] for detailed explanations of TARP's heat transfer methodologies and user input requirements.

3.1.4 MAD and TARP

The MAD algorithms discussed in Section 2 of this report interact with TARP through the TARP thermal processor. The MAD algorithm uses the results from the TARP thermal processor to determine the MAD potential of the building interior. This MAD rate is then used in the calculation of the machine performance and room air humidity conditions. Thus, in MADTARP the moisture transfer and heat transfer equations are not fully coupled. The consequential heat of sorption associated with MAD is not accounted for in the TARP thermal processor.

Because of this the sensible building loads predicted by the TARP thermal processor will be somewhat inaccurate. This inaccuracy is potentially significant in some cases. For instance, in the ventilative cooling analysis the thermal heat of sorption will add or remove heat depending on the operating mode of the building. During ventilation periods the building interior will be warmed by the adsorption process. Some of this added heat is removed by the ventilation air.

During the day when the building is under air conditioning, the desorption process acts to cool the surfaces from which it occurs. The net result of the effect will be to reduce the sensible building load slightly during the day. This results in slightly less air conditioner run times and slightly higher room humidities.

Therefore, the error in sensible load prediction leads to a

slight underprediction of the room humidity conditions and moisture removal requirements for ventilative cooling strategies.

The magnitude of the sensible load error for the closed building cases is insignificant. In the vented buildings it will not have nearly the same magnitude as the diurnal MAD cycle. During the adsorption cycle much of the heat of sorption will be stored along with the moisture in the building materials. This has the net result of overpredicting temperature reductions and net thermal energy removal in the building materials due to ventilation.

During air conditioning cycles the interior surface temperatures are cooled by the desorption process, resulting in increasd envelope temperature differences and causing slightly more inward heat flow. Thus, the magnitude of the sensible load error is affected by the thermal capacity of the building. Therefore, the sensible load reductions predicted in vented massive buildings are more accurate than those for light frame buildings. Without explicit coupling of the TARP thermal processor and the MAD algorithms the degree of this error is uncertain.

3.2 OTHER MADTARP MODIFICATIONS AND APPLICATIONS

3.2.1 Infiltration and Ventilation Algorithms

An equation for the mass flow of infiltration air can be developed from measured values in similar structures [Coblenz, 1963]. The MADTARP assumes a correlation of the form.

$$FI = (A_0 + A_1 * T_Z - T_a + A_2 * V + A_3 * V^2) \qquad (3\text{-}1)$$

This correlation accounts for the stack effects in the temperature difference term and wind effects in the two velocity terms. In Equation 3-1, T_z, T_a and V denote room and ambient temperatures and 10m site velocity, respectively. The

constants used in Equation 3-1 can be defined by the program user.

Constants A_0 through A_3 have been changed from their default values for these runs. The new values are derived according to the following constraints:

FI = 0.67 when $T_z - T_a = 15^oF$ and V = 0 mph

FI = 1.0 when $T_z - T_a = 15^oF$ and V = 7.5 mph

and

FI = 1.67 when $T_z - T_a = 40^oF$ and V = 15 mph

The last two sets of constraints represent typical summer and winter design conditions respectively. At these prescribed conditions, basecase air change rates are 0.75 ACH for summer and 1.25 ACH for winter. For the energy conserving residences the associated rates are 0.5 ACH for summer and 0.835 ACH for winter.

Velocity values in Equation 3-1 as used to derive these constants are assumed to be 10-meter site wind velocities. If airport 10-meter wind speed data are used as input (as is the case with MADTARP) the wind speed data must be adjusted for terrain conditions. MADTARP was modified to use a wind speed terrain modifier of 0.67, representing suburban conditions, for the analysis reported in this study [Walton 1985].

Equation 3-1 represents a modifier for a user-defined base infiltration rate. Its results is multiplied by the user-specified base infiltration rate in order to account for the variations of temperature difference between the interior and exterior of the building and the effects of site wind velocity.

With MADTARP ventilation is treated in two different ways.

- o user-specified ventilation rates
- o calculated ventilation rates (only for the base case)

Users may specify a fixed or variable ventilation rate schedules.

If the room and ambient conditions meet the ventilation control requirements (See Section 2.5.3), the building is allowed to ventilate at the user-defined design condition ventilation rate as modified by Equation 3-1.

If desired, MADTARP can calculate an estimated ventilation rate with respect to building configurations and ambient conditions. This calculation has been performed only for the basecase house. The calculations are based on a user-defined library of ventilation rates as a function of pressure coefficients at each aperture surface. Pressure coefficients are derived from wind speed and direction inputs (hourly weather tapes) and ventilation through each aperture is calculated.

The building ventilation load is then given by Equation 3-2.

$$VL = m\ C_p\ (T_a - T_z) \qquad (3\text{-}2)$$

where

m	is the mass of dry air comming into the building by ventilation
C_p	is the specific heat of air
T_a	is the ambient temperature
T_z	is the zone temperature.

3.2.2 Sky Temperature Algorithms

The procedure used by Walton [1983] for predicting the effective sky temperature has been revised. The most major change was using opaque sky cover as opposed to plain sky cover. Sky temperature has been correlated to opaque sky cover and dew-point temperature by Clark and Blanpied [1982]. The cloud correction factor (ratio of cloudy sky horizontal

irradiance to clear-sky irradiance) is:

$$CC=1.00+.0074n+.0028n^2-7.84*10^{-5}n^3-.00076n_t*T_{dew} \quad (3\text{-}3)$$

where n is tenths of opaque sky cover and T_{dew} is the ambient dew point in ^oC.

The clear sky emissivity equation used in conjunction with the cloud correction factor was developed by Berdahl and Fromberg [1981]:

$$E_{s(clear)} = .741 + .0062(1/^oC) * T_{dew} (^oC) \quad (3\text{-}4)$$

The cloudy sky emissivity is therefore:

$$E_s = E_{s(clear)} * CC \quad (3\text{-}5)$$

The sky temperature is:

$$T_s = T_a * {}^4 E_s \quad (3\text{-}6)$$

Where T_s and T_a are the sky and ambient dry-bulb temperatures, respectively, in ^ok.

3.2.3 Slab Conduction Modeling

Simulation of heat transfer between the ground and adjoining surfaces is one of the building areas that requires significant research. Research is being conducted by various groups, but no conclusive validated simulation procedure has been developed and accepted. Most studies have focused on either peak heat transfer or simple steady-state solutions. Detailed transient solutions require large finite element programs. Research results have also often applied only to one specific system or building. Moreover, research on ground/building interaction in summer and in hot, humid climates is almost non-existant. Further complications occur because soil properties can vary significantly with building location, even in the same city. A fully validated method to use with a detailed hourly simulation does not exist, and the experimental work involved to validate a method was beyond the scope of this project. Nevertheless, a reasonable method of simulating slab heat transfer was developed from National Bureau of Standard (NBS) studies.

3.2.3.1 Modeling Approaches

TARP does not have a ground model. TARP does not easily permit one to model slab perimeters differently than slab bottoms. However, TARP does permit monthly ground temperatures to be entered for a given climate. The ground temperature for any date is linearly interpolated from these average (or mid-month) ground temperatures. These temperatures can then be used in conjunction with an "other side coefficient (OSC)" to specify the temperature on the other side of a surface (floor for example).

FSEC has used this approach to model the ground/slab heat transfer. However, determining the appropriate ground temperatures for each city and for insulated and uninsulated perimeters required some research.

3.2.3.2 Uninsulated Perimeter

Kusuda, et al., [1982] developed a simple procedure for estimating the effective earth temperatures at a given depth below an uninsulated slab-on-grade building. The procedure was derived from extensive Lachenbruch type calculations [Lachenbruch, 1975], and the temperature, at a depth z, is:

$$T_z = T_m + (T_r - T_m) f_1 + B\, f_2 + (C - B)\, f_3$$

where

T_m = annual deep earth temperature, ^oF

T_r = annual building temperature, ^oF

B = amplitude of the annual cycle of the monthly normal temperature, ^oF

C = amplitude of the house temperature cycle, ^oF

f_1 = annual average temperature function

$$\exp\left(-(z/a)^{0.8} \times (3.312 - 3.324(b/a) + 1.476(b/a)^2)\right)$$

a = half length of a rectangular slab, ft

b = half width of a rectangular slab, ft

f_2 = annual cycle of undisturbed earth temperature, which is a function of day of the year, depth and soil diffusivity

f_3 = annual cyclic temperature effect upon the sub-slab temperature, which is a function of depth, a,b, day of year and soil diffusivity.

This method was used to determine the effective temperature one foot below the slab, using the parameters given in Table 3-1.

Table 3-1

Input Parameters Used for Slab Model

Soil Properties:
Moisture content - moderate
Thermal diffusivity = .025 ft^2/hr = .6 ft^2/day

Building Geometry
half length = a = 15 ft half width = b = 25 ft

City Specific Properties

City	Annual deep Earth Temp., (T_m) oF	Ambient Amplitude, (B) oF	Annual Av. Building Temp., (T_r) oF	Amplitude of House Temp., Cycle, (C) oF
Atlanta, GA	64	17.8	73	5
Baltimore, MD	57	21.6	73	5
Charleston, SC	67	15.9	73	5
Dallas, TX	69	20.2	73	5
Houston, TX	76	15.7	74	4
Miami, FL	77	7.9	77	2
New Orleans, LA	70	14.5	74	4
Orlando, FL	74	10.8	75	4
St. Louis, MD	58	23.7	73	5

Insulated Perimeter

A recent study by Kusuda [1984] has yielded some results for uninsulated and insulated slab perimeters. The results were based on experiments conducted in the Washington, DC area where heat loss during winter was the prime concern.

The results (see Figure 3-1) indicate that the heat loss

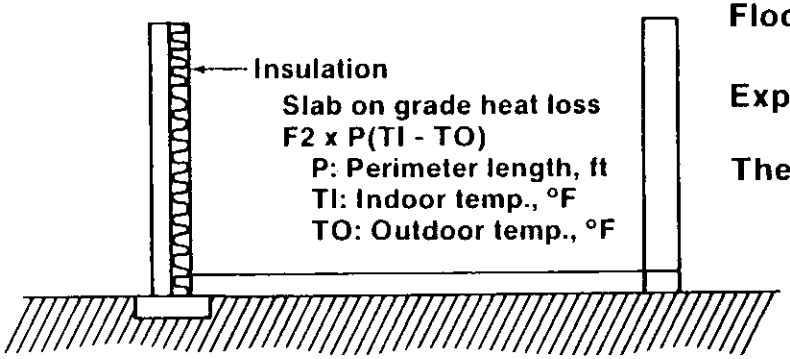

Slab on grade heat loss factor F2, Btu/hr x ft x °F
Location: Washington, D.C.
Floor dimension: Length: 30 ft
Width: 27.9 ft
Exposed wall height: 7.00 ft
Overall U value: 0.09 Btu/hr x ft² x °F
Thermal insulation:
R value: 8.8 hr x ft² x °F/Btu

Soil thermal conductivity
Btu-in/hr x ft² x °F
6.25 (41-53)
9.38 (54-66)

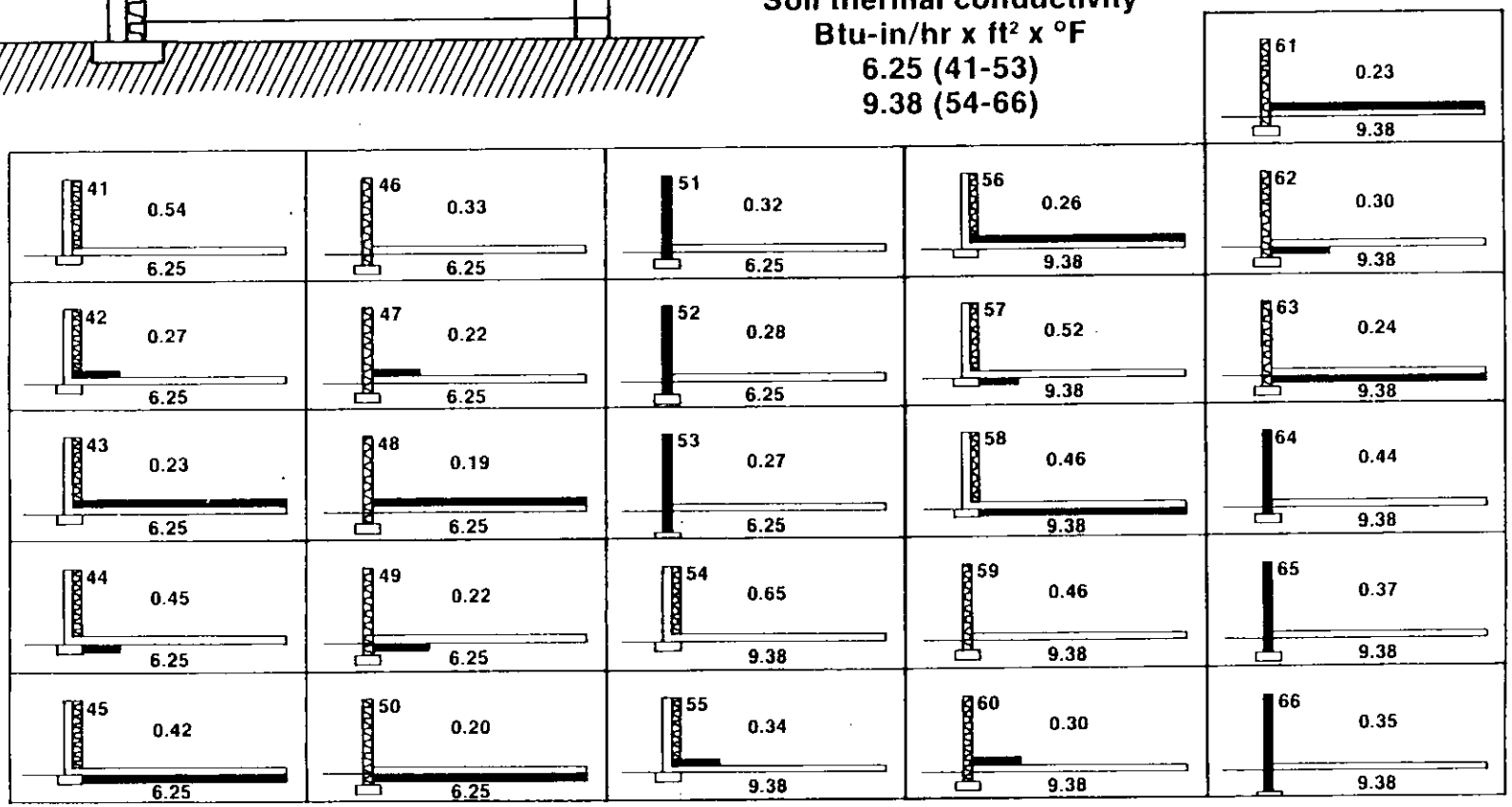

Figure 3-1 Slab-on-grade basement heat loss factor, Washington, D.C.

factor (F_2) is about halved for slab-on grade construction with perimeter insulation. The slab heat loss is given by:

$$Q_S = -F_2 * P * (T_i - T_o)$$

where

P is the perimeter length in feet,
T_i is the indoor air temperature, ^oF
T_o is the outside air temperature, ^oF
F_2 is the heat loss factor Btu/hr-ft-^oF.

Kusuda, et al.,[1984] determined that there was some climatic sensitivity to the results as shown in Figure 3-2. However, the ratio of the uninsulated slab perimeter (system 41) versus the insulated perimeter (system 53) remains about 2:1 for all climates.

These results are good for the heating season. However, what happens during the cooling season? The major differences are that during the heating season the perimeter is exposed to an average ambient temperature much lower than the deep ground temperature and very much lower than the building. In summer, the average ambient temperature may be about the same as the building. Thus, heat transfer in winter is primarily through the perimeter, whereas in summer it tends to be more vertically into the earth. Figure 3-3 shows this effect [Kusuda 1983].

Kusuda's [1982] method was used to predict the average monthly temperatures beneath the uninsulated slab. To simulate the effect of perimeter insulation when desired, the winter values were modified. The difference between the uninsulated winter month ground temperature and the annual average ground temperature for that city was cut in half to approximate the

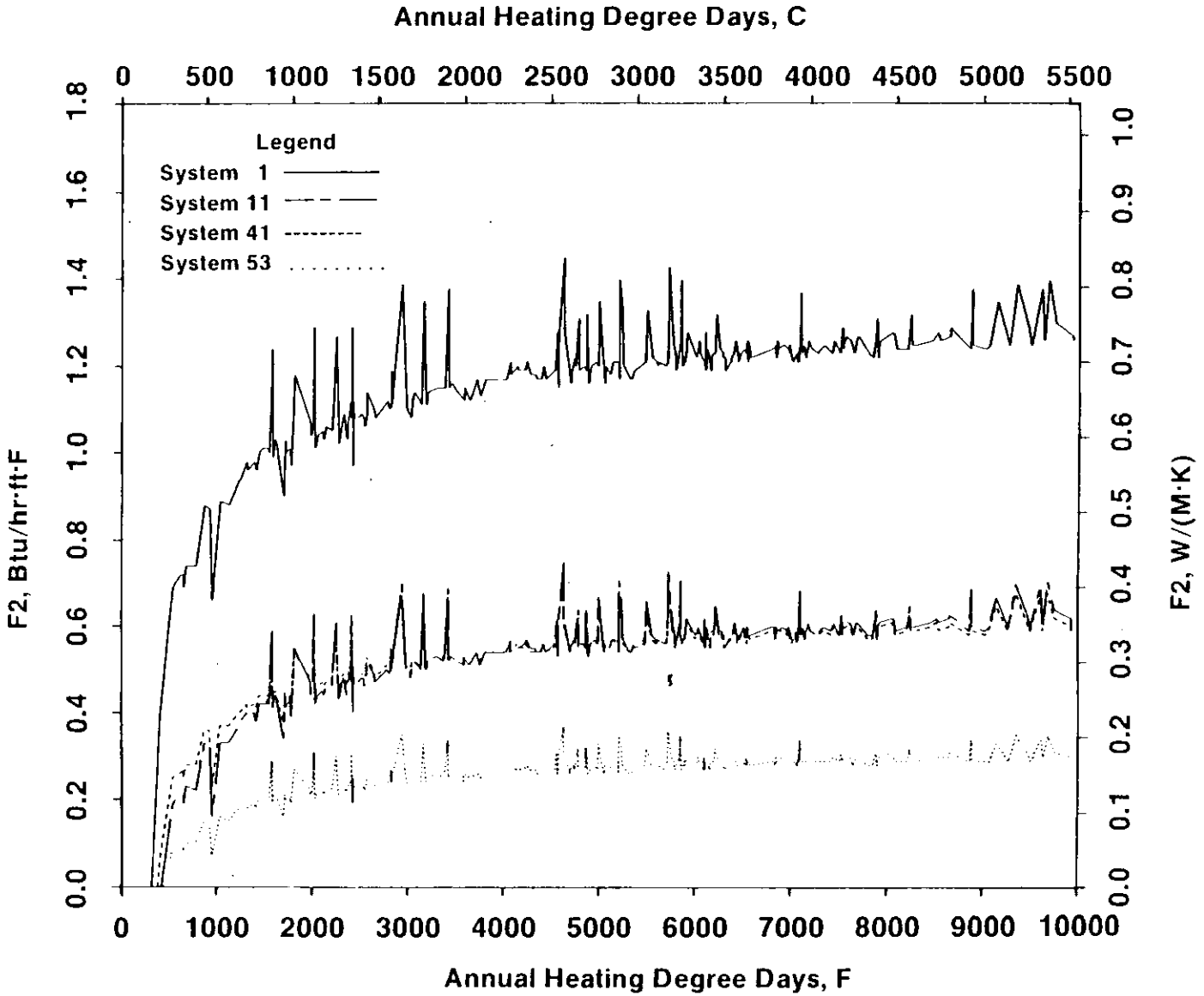

Figure 3-2 Climatic sensitivity of the basement heat loss factor, F_2.

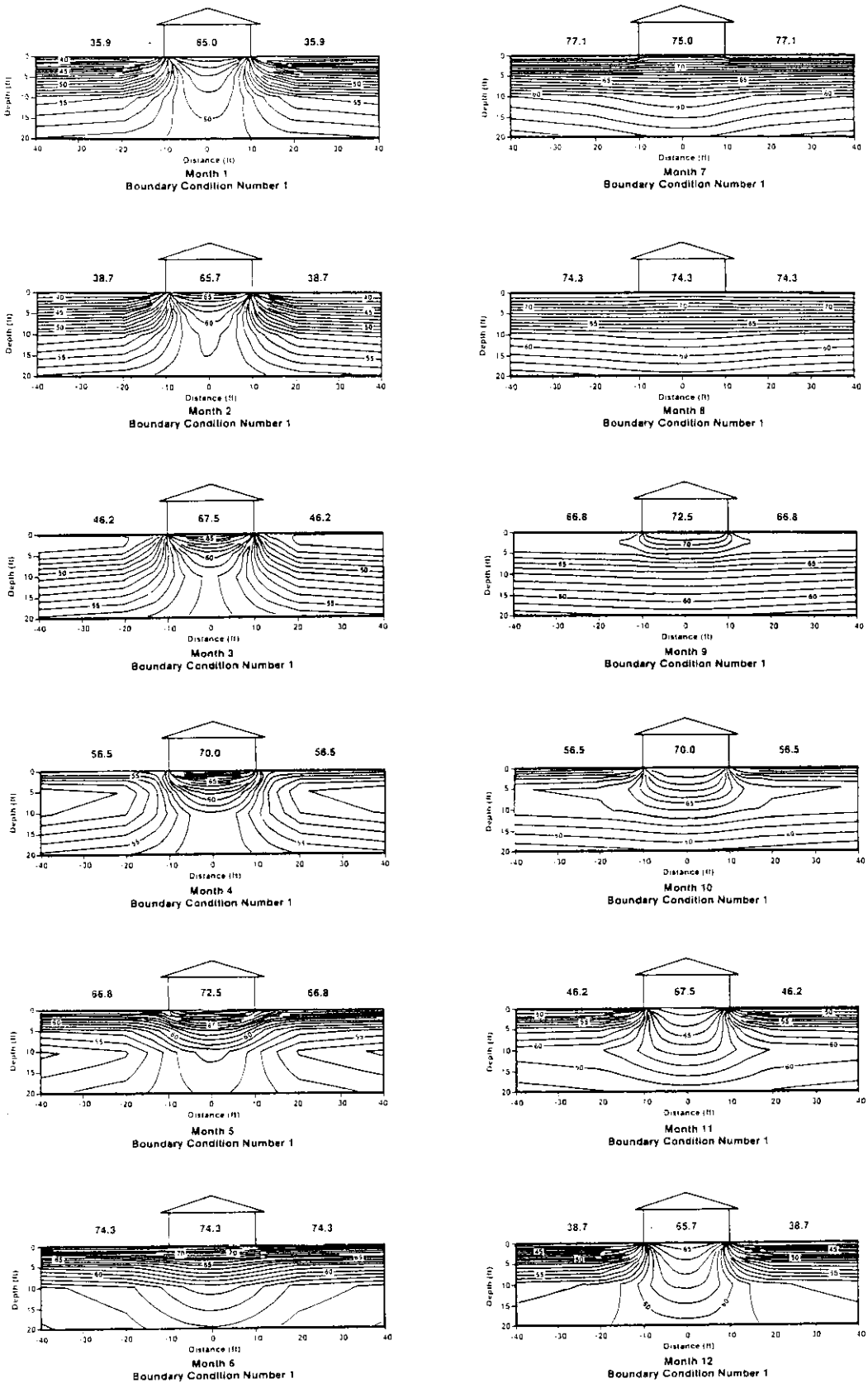

Figure 3-3 Monthly earth temperature profile under a house with slab-on-grade floor.

effect of perimeter insulation. Thus:

$$T_{WI(M)} = T_A - (T_A - T_{WU(I)})/2$$

where

T_A = Mean annual ground temperature under the building

$T_{WI(M)}$ = The insulated perimeter temperature for winter month M

$T_{WU(M)}$ = The uninsulated perimeter temperature for winter month M.

The benefit of perimeter insulation in climates with short and mild heating seasons is limited. In climates with moderate heating seasons, perimeter insulation is helpful and is becoming more widespread in use. Therefore, all cities with heating degree days greater than 2000 (base 65°F) were simulated as having perimeter insulation. Those cities with less than 2000 degree days were simulated without perimeter insulation. This strategy is based solely on climate, thus it did not vary by building type. Table 3-2 shows which type of slab model was used for each city.

Table 3-2

Type of slab model used for each city

Uninsulated	Insulated
Houston	Atlanta
Miami	Baltimore
Orlando	Charleston
New Orleans	Dallas
	St. Louis

The monthly one-foot-deep ground temperatures used for the simulation are given in Table 3-3.

3.3 ENVIRONMENTAL DATABASE

3.3.1 SOLMET Database

Solar and meteorological data were collected at 26 sites from 1952 to 1964 and compiled. The solar data for the 26 cities were used with computer models to develop a database of 209 cities. These SOLMET data are available on computer tapes and are the basis for almost all environmental data inputs for U.S. cities used in detailed hourly thermal simulations.

The hourly SOLMET data are not assumed to be perfect; however, the errors present in the data and methods for obtaining the data have been discussed adequately in other sources (SOLMET, 1979). Also, no suitable alternative is available. Since much of the assessment consists of comparisons, the resulting relative difference of the various buildings and machines should be representative of the region despite the limitations of the weather data.

It is impractical to use twelve years of data to analyze one climate. Therefore, standard or typical years of data have been created for each city using January data that are average or typical, based on certain criteria from the 12 years of data. The process is repeated each month. The major difference between methods is the criteria used.

3.3.2 Development of TCY (Typical Cooling Year) Tapes

Typical Cooling Year (TCY) tapes were selected as the most practical for the purpose of performing a cooling analysis. The TCY data were available for the cities chosen for the study and the Trinity University weighting criteria for choosing typical months included ambient moisture parameters as well as temperature and solar. The reasons for creating the tapes and the criteria have previously been outlined [Vieira, 1983].

Table 3-3

Ground Temperatures (^{o}F) 1 ft Under Building for Nine Selected Cities

City	I–U	Jan	Feb	Mar	Apr	May	Jun	Jul	Aug	Sep	Oct	Nov	Dec
Atlanta, GA	I	69.3	68.8	68.9	69.7	70.9	73.7	75.8	76.9	76.6	75.1	72.6	70.4
Baltimore, MD	I	68.3	67.7	67.9	68.7	69.9	72.8	75.0	76.2	75.9	74.3	71.7	69.5
Charleston, SC	I	69.8	69.3	69.4	70.2	71.4	74.0	76.1	77.2	76.9	75.4	72.9	70.9
Dallas, TX	I	69.9	69.4	69.5	70.3	71.5	74.3	76.5	77.7	77.4	75.8	73.3	71.1
Houston, TX	U	71.0	70.1	70.3	71.6	73.5	75.7	77.5	78.4	78.2	76.9	74.9	72.8
Miami, FL	U	75.3	74.9	75.0	75.6	76.6	77.7	78.6	79.1	79.0	78.3	77.3	76.2
New Orleans, LA	U	70.2	69.4	69.6	70.8	72.8	74.9	76.7	77.6	77.3	76.1	74.1	72.0
Orlando, FL	U	71.7	71.0	71.2	72.4	74.3	76.3	77.9	78.8	78.5	77.3	75.4	73.4
St. Louis, MO	I	68.4	67.8	67.9	68.9	70.0	72.9	75.2	76.5	76.2	74.6	71.9	69.6

I — Insulated
U — Uninsulated

Table 3-4

Selected Climate Types

Climate	Cities Selected
Hot, humid	Charleston, SC. Houston, TX Miami, FL New Orleans, LA Orlando, FL
Borderline	Atlanta, GA Dallas, TX
Humid, but not overheated	Baltimore, MD St. Loius, MO

3.3.3 Climates

One of the first tasks of this project was to determine cities representative of various humid climates.

3.3.3.1 Definitions

Three types of climates were defined for this study:

- Hot, humid
- Borderline hot, humid
- Humid but not overheated.

Humid climates were defined as having average August relative humidities of 60% or greater. Dry climates were defined as having relative humidities of 50% or less. Hot climates were defined as the average contour between 400 Langleys of annual solar radiation and 60 days of high dry-bulb temperature over 90°F. These climates are shown in Figure 3-4.

3.3.3.2 City Selection

Two cities were chosen to represent the borderline and humid but not overheated climate types. However, five cities were chosen for the hot, humid climate since this study focuses on conservation techniques which will be most economical in the hot, humid region. The cities selected for each climate type are given in Table 3-4. These nine cities are shown in Figure 3-4. Other long term average meteorological data for the nine cities are shown in Table 3-5.

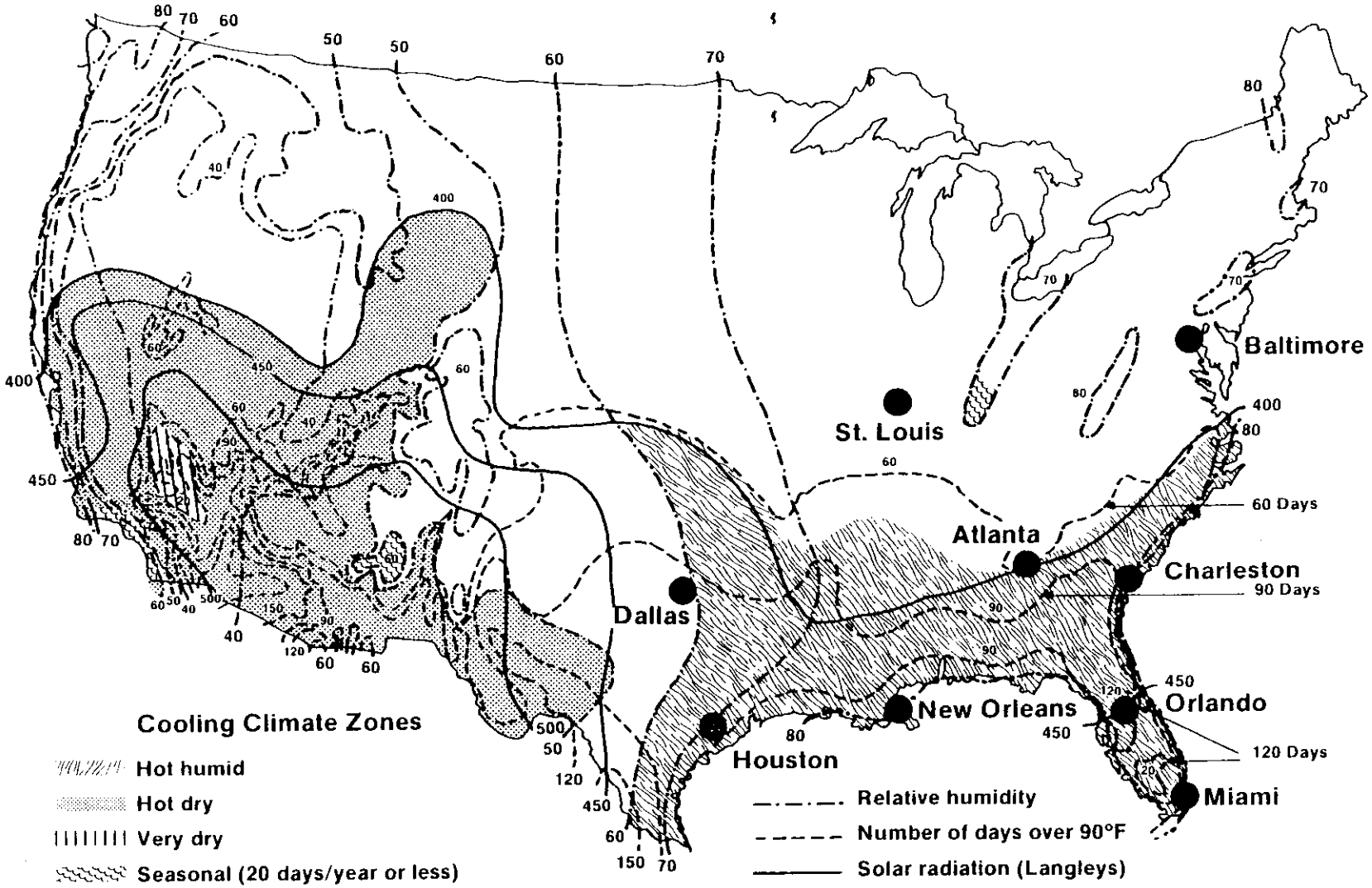

Figure 3-4 U.S. major cooling climate zones showing overlay of nine selected cities for analysis.

Table 3-5 Long term average meteorological parameters for nine selected cities.

SUGGESTED ABBREVIATION	CITY, STATE	STATION CODE	LATITUDE	LONGITUDE	MONTHLY GLOBAL RAD. Btu/ft^2	K_T	T_{mean} ^oF	HDD Base 65^oF	CDD Base 65^oF
ATL	Atlanta, GA	13874	$33^o39'N$	$84^o26'W$	1345	.495	60.8	3094	1588
BAL	Baltimore, MD	93721	$39^o11'N$	$76^o40'W$	1215	.476	55.0	4729	1107
CHS	Charleston, SC	13880	$32^o54'N$	$80^o02'W$	1345	.491	64.7	2146	2077
DAL	Dallas, TX	13960	$32^o51'N$	$96^o51'W$	1468	.536	66.2	2290	2754
HOU	Houston, TX	12918	$29^o59'N$	$95^o22'W$	1351	.480	68.9	1433	2889
MIA	Miami, FL	12839	$25^o48'N$	$80^o16'W$	1473	.506	75.5	205	4037
NOL	New Orleans, LA	12916	$29^o59'N$	$90^o15'W$	1437	.511	68.3	1463	2705
ORL	Orlando, FL	12841	$28^o33'N$	$81^o20'W$	1487	.522	71.8	733	3226
STL	St. Louis, MO	13994	$38^o45'N$	$90^o23'W$	1327	.517	55.9	4748	1474

Knapp, C.L., T.L. Stoffel, S.D. Whitaker, Insolation Data Manual, SERI, (1980)

3.4 BUILDING DATABASE

3.4.1 Building Selection

A total of six building types have been described for analysis using MADTARP. Two types of construction (wood frame and concrete block) are considered. A "basecase" building is described for each building type. The basecase buildings are considered to be typical of recent construction practices in the southeast. The basecases have been evaluated against the GRI residential database developed by Applied Management Sciences (AMS) and found in good agreement with type C housing [DeLima, 1984] for the extreme southeastern sector of the U.S.

Four additional buildings have been described in order to evaluate energy conserving and passively designed residences. Three of these are concrete block residences and one is wood frame.

A mnemonic code has been developed to identify each housing type for ease of information storage and retrieval. The two-digit mnemonic codes for each of the residence types is given at the start of each description. It, coupled with additional mnemonics identifying other aspects of the analysis, will often be used to refer to a specific analysis or result. The building type will always be the first two letters of any such code. A summary of the building types is given in Table 3-6 followed by detailed descriptions for each building.

Table 3-6

Summary of Building Types

Characteristics	Frame Base (FB)	Frame Conserve (FC)	Block Base (BB)	Block Internal Insulation (BI)	Block External Insulation (BE)	Block Passive (BP)
Windows	A=224 SF SC=.45 EWN SC=0.87 S +2' overhang	A=140 SF on N/S only SC=.87S .2N +2' overhang	FB	FC	FC	FC
Roof/Attic	5/12 pitch a = 0.8 R-19 clg.	FB + attic radiant barrier	FB	FC	FC	FC
Walls	R-11 in 16 inch centers a = .75 e = .9	R-19 for all walls + a=.1 & e=.5 on EWN walls (simulates RB)	8x16x8 CB with R2.7 inside insul.	R-11 on inside of CB insulation	Block + ext. insulation R-11 on S & R-6 on EWN a=.1 & e=.5N E,W,N	External walls=BE all internal partitions 8' block block walls
Infiltration @ design	0.75 ach	0.5	FB	FC	FC	FC
Sensible internal loads Btu/day	50,807	44,620	FB	FC	FC	FC
Duct Location	Attic	Cond	Attic	Cond	Cond	Cond

3.4.2 Detailed Building Descriptions

Each of the six residences has an identical floor plan. This plan is shown in Figure 3-5. It consists of an open living plan that is quite popular in concept with a qreatroom separating the master bedroom and kitchen areas from the children bedrooms. The residence is oriented as shown by the north arrow in Figure 3-21 for all computer runs unless otherwise specified in the report.

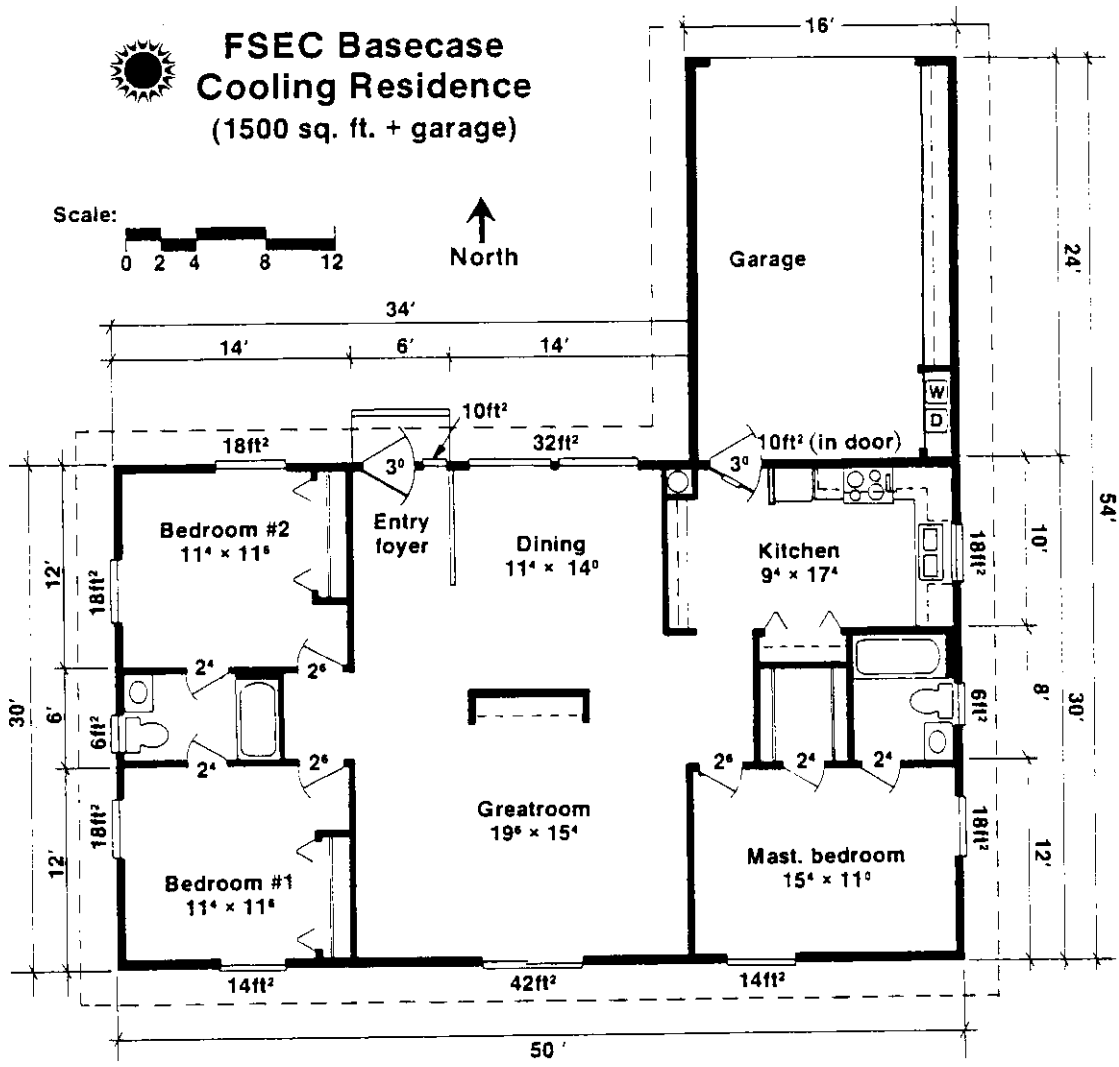

Figure 3-5 Floor plan for residences used in MADTARP building analysis model.

FB - Frame Basecase Residence

BUILDING CHARACTERISTICS

Residence Type:

- o Single story slab on grade
- o "L" shaped ranch style with attached carport
- o Open living plan

Aspect Ratio: (excluding carport) = 1.0:1.6 (30x50')

major axis: east-west

Window glass:

- Area = 224 ft^2 (15% gross floor area) proportioned such that the ratio of window area to exterior wall area (including unglazed portion of doors) remains constant on each building face.
- Shading coefficient (SC)
  - South glass SC = 0.87
  - All other glass SC = 0.45
- Double glazed with good weather seals
- Glass areas by orientation:
  - North = 70 ft^2 (net wall = 330 ft^2):ratio = .2121
  - South = 70 ft^2 (net wall = 330 ft^2):ratio = .2121
  - East = 42 ft^2 (net wall = 198 ft^2):ratio = .2121
  - West = 42 ft^2 (net wall = 198 ft^2):ratio = .2121

Roof:

- Type: hipped
- Construction: (from exterior) shingles on 30# felt on 1/2" plywood on trusses @ 24" o.c.
- Slope = 5:12(22.6°) on trusses @ 24" o.c.
- Solar adsorptance ( ) = 0.80
- Emissivity ( ) = 0.90
- Roof overhang = 2' on all sides

Walls:

- Type: 2 x 4 wood frame at 16" o.c.
- Construction: (from interior) 1/2" gypsum drywall on 4 mil continuous polyethelene vapor barrier on studs with R-11 batt infill on 7/16" Masonite exterior siding
- Solar adsorptance ( ) = 0.75
- Emissivity ( ) = 0.90
- Net exterior wall area by orientation (excluding doors and windows)
  - North = 288 ft^2 (gross = 400 ft2)

South = 330 ft^2 (gross = 400 ft2)
East = 198 ft^2 (gross = 240 ft2)
West = 198 ft^2 (gross = 240 ft2)

- Internal partitions: wood 2x4 frame with no insulation

Doors:

- Two each: 3'-0"x6'-8" on north side-one entry, one carport/garage (garage door has 10 ft2 glazing)
- Type: insulated metal with magnetic weather seals

Floors:

- Construction: 4" structural slab on grade, monolithic with 10 x16" thickened edge at perimeter
- 1-1/2" perimeter insulation installed horizontally @ 10" below finished grade where indicated by climate considerations.

Ceiling:

- Type: 8 ft height in all main spaces, 7 ft height (dropped) in hallways and baths only.
- Construction: from interior 1/2" gypsum drywall on 4 mil polyethelene on trusses @ 24" o.c. with R-19 mineral fiber ceiling insulation

LOAD CHARACTERISTICS

Infiltration:

- Average rate = 0.75 ACH = 18 AC/day
- Scheduled rates:

12 pm - 7 am	= 0.6 ACH =	4.2 AC/day
7 am - 9 am	= 1.2 ACH =	2.4 AC/day
9 am - 3 pm	= 0.6 ACH =	3.6 AC/day
3 pm - 7 pm	= 1.2 ACH =	4.8 AC/day
7 pm -12 pm	= 0.6 ACH =	3.0 AC/day
	TOTAL =	18.0 AC/day

Internal Building Loads:

Internally generated heat sources account for about 20% of the sensible cooling load in a conventionally built residence. In residential building designs that incorporate well-insulated envelopes and shaded windows, the internally generated sensible load can be as much as 50% of the total sensible cooling load. At reasonable infiltration rates (0.5 to 0.75 ACH) the latent heat gain generated by people, washing, plants, and food preparation is also a significant fraction of the total latent load (approximately 1/3 to 1/2 in most humid cities).

In the basecase residence, the total (sensible and latent) internally generated load is 75,844 BTU/day. The breakdown of the loads is shown in Table 3-7. The lighting and occupancy load is typical for an average single-family detached house [NBSIR 80-2184]. The sensible load due to appliances was derived from average household ownership and predicted energy use of appliances [U.S. DOE, 1980]. The breakdown of the latent loads results from research in home humidity control [Hite, 1948]. The fraction of the heat generated by people is divided into latent and sensible fractions in the MADTARP based on temperature [Walton, 1983]. At 78°F the occupant heat released is roughly 52% latent and 48% sensible.

Hourly Profiles:

A breakdown of the hourly profiles is shown in Table 3-8. The total hourly profiles for appliances, lighting and occupants were obtained from the recommendation of a study by the National Bureau of Standards [NBSIR 80-2184]. Since MADTARP cannot schedule occupant activity levels, the schedule for occupancy was modified somewhat to account for lower metabolic rates at night and higher levels during the day and evening. The latent load hourly profile was chosen based on the occupant profile and the data given in Table 3-7. The values used were based on averages, and no adjustment was made based on season.

Table 3-7

BASECASE RESIDENCE INTERNAL DAILY LOADS

SENSIBLE LOADS

Source		BTU/day
Occupants	at 78oF	16,600
Appliances		25,935
Lighting		8,272
Total sensible		50,807

LATENT LOADS
(family of four)

Source	lb	BTU
Food preparation		
Breakfast	.34	357
Lunch	.51	535.5
Dinner	1.17	1,228.5
Dishes		
Breakfast	.20	210
Lunch	.15	157.5
Dinner	.65	682.5
Mopping (twice/wk)	1.29	1,354.5
Plants (total of 7)	.93	976.5
Showers (3/day)	1.50	1,575
Subtotal		7,077
People at 78oF	17.05	17,960
Total latent	23.79	25,037.

TOTAL DAILY INTERNAL GAINS 75,844

Table 3-8

FOUR ZONE INTERNAL LOAD SCHEDULE*

	OCCUPANCY					APPLIANCES					LIGHTING					LATENT				
hr	z^1	z^2	z^3	z^4	TOT	z^1	z^2	z^3	z^4	TOT	z^1	z^2	z^3	z^4	TOT	z^1	z^2	z^3	z^4	TOT
1	–	–	.35	.50	.85	–	.25	–	–	.25	–	–	–	–	–	.03	–	–	–	.03
2	–	–	.35	.50	.85	–	.25	–	–	.25	–	–	–	–	–	.03	–	–	–	.03
3	–	–	.35	.50	.85	–	.25	–	–	.25	–	–	–	–	–	.03	–	–	–	.03
4	–	–	.35	.50	.85	–	.25	–	–	.25	–	–	–	–	–	.03	–	–	–	.03
5	–	–	.35	.50	.85	–	.25	–	–	.25	–	–	–	–	–	.03	–	–	–	.03
6	–	–	.40	.60	1.00	–	.25	–	–	.25	–	–	–	–	–	.03	–	–	–	.03
7	–	.40	.30	.30	1.00	–	.25	.05	.03	.33	–	.40	.30	.30	1.00	.03	–	–	.38	.41
8	.30	.40	–	.30	1.00	–	.36	–	.10	.46	.30	.40	–	.30	1.00	.03	.26	–	–	.29
9	.30	.10	–	.10	.50	.10	.53	–	–	.63	–	.02	–	–	.02	.03	.15	–	–	.18
10	.30	.10	–	.10	.50	.10	.78	–	–	.88	–	.02	–	–	.02	.03	.97	–	–	1.00
11	.30	.20	–	–	.50	.10	.25	–	–	.35	–	.02	–	–	.02	.03	–	–	–	.03
12	–	.50	–	–	.50	–	.88	–	–	.88	–	.02	–	–	.02	.03	.38	–	–	.41
13	.30	.20	–	–	.50	.10	.32	–	–	.42	–	.02	–	–	.02	.03	.11	–	–	.14
14	.30	.10	–	.10	.50	–	.25	–	–	.25	–	.02	–	–	.02	.03	–	–	–	.03
15	.30	.10	–	.10	.50	–	.25	–	–	.25	–	.02	–	–	.02	.03	–	–	–	.03
16	.40	.15	.20	.10	.85	.10	.38	.10	–	.58	–	.02	–	–	.02	.03	–	–	–	.03
17	.40	.30	.20	–	.90	.10	.38	.10	–	.58	–	.02	–	–	.02	.03	.22	–	–	.25
18	.50	.30	.20	–	1.00	.10	.60	.10	–	1.0	–	.02	–	–	.02	.47	.22	–	–	.69
19	.50	.30	.20	–	1.00	.30	.52	.10	–	.92	–	.02	–	–	.02	.03	.49	–	–	.52
20	.50	.30	.20	–	1.00	.20	.38	.10	–	.68	.25	.15	.10	–	.50	.03	–	–	–	.03
21	.50	.30	.20	–	1.00	.20	.28	.10	.10	.68	.25	.15	.10	–	.50	.03	–	.38	–	.41
22	.50	–	.20	.30	1.00	.20	.28	.10	.10	.68	.50	–	.20	.30	1.00	.03	–	.19	.19	.41
23	–	–	.35	.50	.85	–	.28	.10	.13	.51	–	–	–	–	–	.03	–	–	–	.03
24	–	–	.35	.50	.85	–	.23	–	–	.23	–	–	–	–	–	.03	–	–	–	.03
	5.4	3.75	4.55	5.5	19.2	1.80	8.70	.85	.46	11.81	1.30	1.35	.70	.90	4.25	1.16	2.8	.57	.57	5.10

Peak Cap	1800 BTU/hr lat. + sens.	2196 BTU/hr sensible	1945 BTU/hr sensible	1396 BTU/hr latent
Daily	34,560 BTU/day	25,938 Btu/day	8272 BTU/day	7120 BTU/day

z^1 = Living/Dining z^2 = Kitchen z^3 = Children's Bedroom z^4 = Master Bedroom

*Values given times peak capacity = Zone load for hour

Although multizone building decks have been run, most analysis was accomplished with single zone decks. For these runs the hourly profiles given in the totals column of Table 3-7 are used.

Details of how the different loads are treated in the MADTARP are given by Walton [1983], and are not repeated here.

In addition to the frame basecase residence, five other buildings have been described for MADTARP analysis. The building plan and many of the schedules remain the same for these buildings and only the differences are described here.

BB - Block Basecase Residence

BUILDING CHARACTERISTICS

Exterior walls:

- Type: 8x16x8" standard concrete masonry units
  Conductivity (k) = 0.53 Btu/ft^2 ^oF
  Density ( ) = 38 lb/ft^3
  Specific heat (c) = 0.20 Btu/lb ^oF
- Construction: (from interior) 1/2" gypsum drywall on 4 mil continuous polyethylene vapor barrier on 1x2" furring @ 16" o.c. with R-2.7 mineral fiber infill on concrete block on 5/8" stucco.

All other building and load characteristics for BB are identical to FB.

FC - Frame Energy Conserving Residence

BUILDING CHARACTERISTICS

Window Glass:

- Area = 140 ft^2 (10% gross floor area)
  no windows on east and west building face.

- Shading Coefficient (SC)
  - South glass SC = 0.87
  - North glass SC = 0.20
- Glass areas by orientation:
  - North = 70 ft^2
  - South = 70 ft^2
- All glass has R-2 movable night insulation in place from 6 pm to 6 am from 21 Oct. - 12 Mar.

Roof:

- Construction: (from exterior) shingles on 30# felt on 1/2" plywood on trusses @ 24" o.c with radiant barrier 3-1/2" below plywood roof decking
  - Radiant barrier emissivity ( )
    - upper face = 0.9
    - lower face = 0.05

Walls:

- Type: 2x6" wood frame @ 16" o.c. with R-19 fiber infill insulation.
- Solar Absorptance ( )
  - South walls = 0.75
  - All other walls = 0.1 (to simulate exterior radiant barrier construction)
- Emissivity ( )
  - South walls = 0.9
  - All other walls = 0.5 (to simulate exterior radiant barrier construction)
- Net exterior wall area by orientation
  - North = 288 ft^2 (gross = 400 ft^2)
  - South = 330 ft^2 (gross = 400 ft^2)
  - East = 240 ft^2 (gross = 240 ft^2)
  - West = 240 ft^2 (gross = 240 ft^2)

LOAD CHARACTERISTICS

Infiltration:

- Average rate = 0.5 ACH = 12 AC/day

- Scheduled rates:

12 pm - 7 am	= 0.4 ACH	=	2.8 AC/day
7 am - 9 am	= 0.8 ACH	=	1.6 AC/day
9 am - 3 pm	= 0.4 ACH	=	2.4 AC/day
3 pm - 7 pm	= 0.8 ACH	=	3.2 AC/day
7 pm - 12 pm	= 0.4 ACH	=	2.0 AC/day
	TOTAL	=	12.0 AC/day

Internal Building Loads:

- Internal lighting loads were reduced by 75% from 8272 Btu/day to 2067 Btu/day to account for increased efficacy of fluorescent lighting to the same luminance level.

All other building and load characteristics for FC are identical to FB.

BI - Block Energy Conserving Residence: Interior Insulation

BUILDING CHARACTERISTICS

Exterior Walls:

- Type: 8x16x8" standard concrete masonry units (same as BB)
- Construction: (from interior) 1/2" gypsum on 4 mil continuous polyethelyne on 2x2" furring with R-11 rigid insulation infill on concrete block with 5/8" exterior stucco.

All other building and loads characteristics identical to FC.

BE - Block Energy Conserving Residence: Exterior Insulation

BUILDING CHARACTERISTICS

Exterior Walls:

- Type: 8x16x8 standard concrete masonry units (same as BB)

- Construction:
  - South wall: (from interior) 1/8" plaster on concrete block on 2x2 furring @ 16" o.c. with R-11 rigid infill on 7/16" Masonite siding.
  - All other walls: (from interior) 1/8 plaster on concrete block on 1x2" furring @ 16" o.c. with R-6 rigid infill on 7/16" Masonite siding.
- Solar Absorptance ( )
  - South wall = 0.75
  - All other walls = 0.1 (to simulate exterior radiant barrier wall system)
- Emissivity ( )
  - South wall = 0.9
  - All other walls = 0.5 (to simulate exterior radiant barrier wall system)

All other building and load characteristics identical to BI.

BP - Block Passive Residence

BUILDING CHARACTERISTICS

- **Internal Partitions:**
  - 8x16x8" standard concrete masonry units with 1/8" plaster on each face.

All other building and load characteristics identical to BE.

SECTION FOUR
BUILDING ENERGY ANALYSIS RESULTS

The results of this study represent the first known set of annual building energy analysis computer simulations that attempt to accurately predict the combined thermal and moisture performance of residential buildings. As such, there is no historical database against which the results can be directly compared. Only limited measured building performance data exist for use in model validation. Where measured performance data were available they were used to validate new sections of the code.

Detailed hourly building energy analysis computer codes are voluminous and complex, but every effort has been made to assure that the individual components of the MADTARP code produce reasonable and accurate results. Wherever inaccurate or unreasonable performance prediction potentials existed, an effort was made either to improve on the existing analysis code or to develop completely new algorithms. The reasoning for and the theoretical approach to these changes have been discussed in Sections 2 and 3.

Some of these improvements make only a small difference in results but others offer significant improvements in MADTARP's predictive capability. Moisture absorption and desorption, for instance, have turned out to be much more significant and important than previously suspected.

4.1 INTRODUCTION

With any analysis technique the underlying assumptions control the results of the analysis. The specific assumptions and analytical techniques that control the performance of individual algorithms used in the code are given in Sections 2 and 3, but the more general, overall objectives and assumptions of a particular study contribute greatly to its outcome.

4.1.1 Lifestyle Influences

It is a relatively well-known fact that a building's occupancy pattern plays a major role in its ultimate energy use. This is particularly true in this study where cooling loads are emphasized. Figure 4-1 presents a pie-chart that describes the Orlando, FL load distributions for the basecase building used in this study. A full 29 % of the building cooling load is a direct result of its occupancy patterns (internal loads). A different set of internal loading assumptions would drastically alter the magnitude and distribution of these building loads. No attempt has been made to parametrically analyze the sensitivity of this factor on the results of this study.

The response of the building occupants is important in other ways as well. Different occupants have different comfort criteria. This will affect their thermostat settings and their building ventilation patterns in a significant manner. Parametric analysis of thermostat settings and two generic ventilation strategies (temperature controlled venting and enthalpy controlled venting) have been examined in a number of climates to study this effect.

The occupancy patterns of a building are particularly important to the moisture loads on buildings. The effect is dramatic in the ventilation analysis where large discrepancies exist in cooling load as a function of the two generic ventilation strategies. Similarly, strategies that have not been examined, such as daytime set-up of thermostats when building occupants are not home during the day, may have significant building load consequences with respect to moisture loads.

4.1.2 Human Comfort Constraints

Human comfort has been the subject of many detailed studies.

It remains, however, a somewhat nebulous and subjective phenomenon that exhibits large variations among individuals. Comfort, therefore, is an individual **perception.** Some of the comfort criteria used in this study are based on the detailed work of P.O. Fanger [1970]. There are major areas of disagreement between the work of Fanger and established industry comfort standards (ASHRAE Standard 55-1981) with respect to allowable room humidity conditions. Figure 4-2 is a graphic depiction of the two comfort zones.

By contract requirement this study addresses potential moisture loads primarily with respect to the ASHRAE comfort standard (room moisture limit=58% RH @ 78°F). A limited number of more relaxed "mold and mildew" prevention runs (room

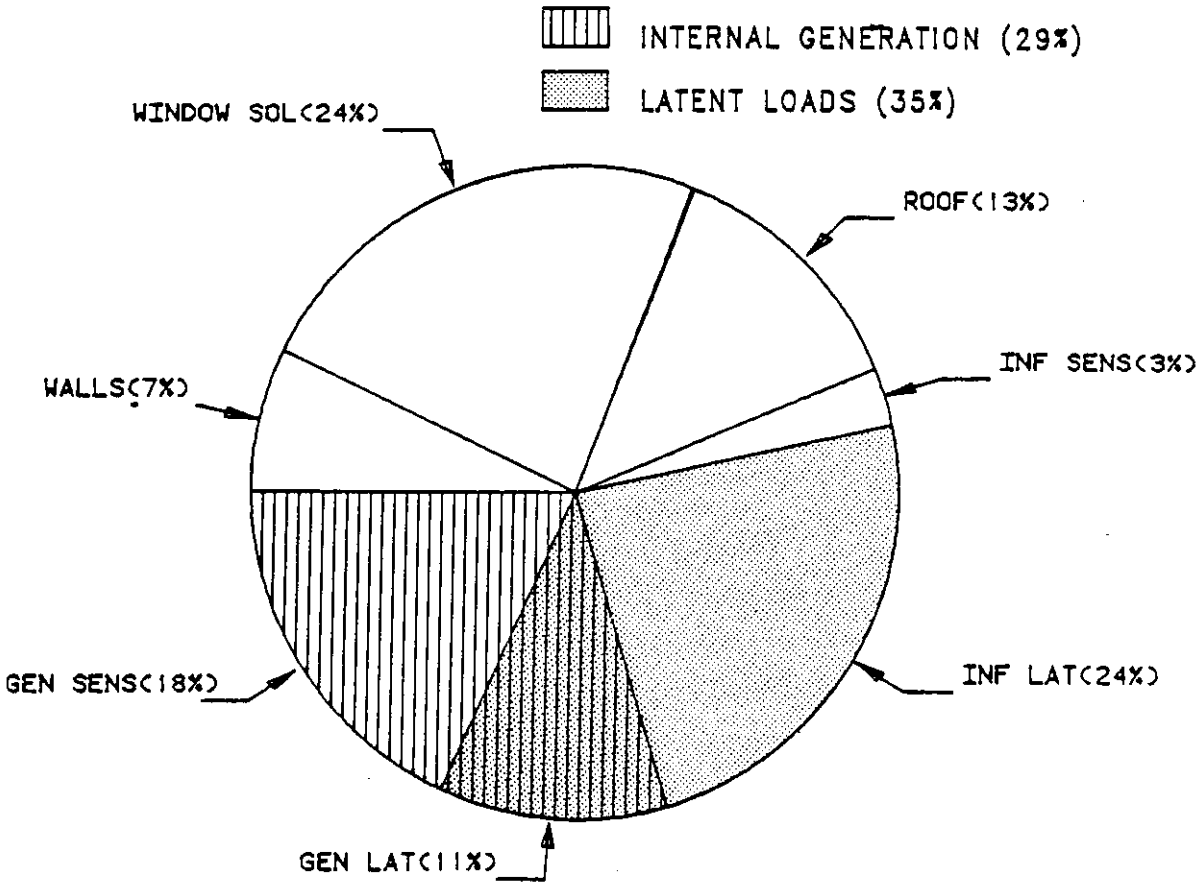

Figure 4-1 Air conditioning load sources for frame basecase residence in Orlando, FL.

moisture limit=68% RH @ 78°F) have been accomplished for comparative purposes. The latter value lies outside of the ASHRAE zone but is well within the human comfort requirements of the Fanger zone.

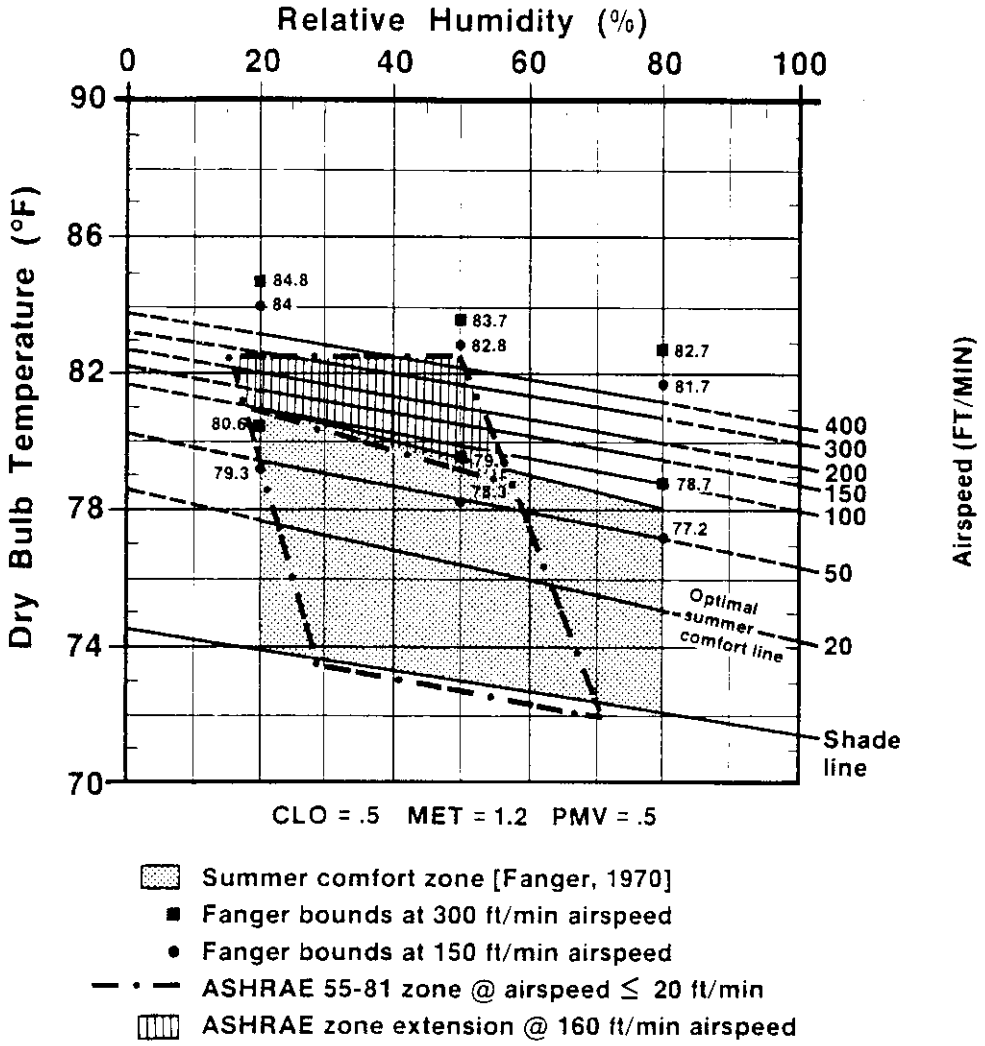

Figure 4-2 Comparison of ASHRAE Standard 55-1981 and Fanger comfort zones at equivalent levels of comfort prediction.

4.2 INFLUENCE OF MAD ON BUILDING ENERGY PREDICTION

The results of the analysis conducted during this study indicate that modeling of moisture absorption and desorption (MAD) by building materials is of significant importance to building load prediction. If MAD is not modeled the predicted energy savings of certain cooling strategies (e.g., temperature controlled venting) may be significantly in error. It becomes obvious as the results are examined that typical buildings have a large, often overriding, moisture storage capacity that should not be overlooked in predictive energy analysis techniques.

At this point, it should again be noted, that the thermal and mass transfer are not interactive in MADTARP. There will be some degree of sensible load redistribution over the course of the day because of this. During periods when room RH is rising, temperature will also incrase somewhat due to the heat of adsorption. During periods when the room RH is falling, there will be an evaporative cooling effect caused by moisture desorption. These effects have not been modeled by MADTARP.

As discussed in Section 3.1.4, this phenomenon does not significantly affect the closed building analyses. However, the current results may overestimate the daytime sensible cooling load in the vented buildings. In realty, the building will have slightly higher room humidities and slightly lower temperatures. The sensible heat fraction (SHF) of the air conditioner will drop somewhat and the latent fraction of the building load will increase. Thus, for the reported ventilation results the sensible building loads may be overestimated, but the latent loads and room moisture conditions are predicted somewhat conservatively.

The extent of the uncertainty is likely to be small, but its magnitude is unknown at the present time. It should also be

noted that, to our knowledge, MADTARP is the first building energy analysis program to attempt a detailed analysis of moisture and thermal interactions.

4.2.1 Measured and Simulated Building Performance

An assessment of the reasonableness of MADTARP's building performance predictions has been made using measured data from monitored townhouses in Cocoa, FL (see Section 2.2.3). Figure 4-3 shows the predicted room relative humidities for the basecase residence in Orlando, FL for the vented and unvented MAD and NOMAD (**no** moisture absorption and desorption) cases. The difference in the predictions for MAD and NOMAD is quite pronounced. First, for both vented and unvented runs the MAD analysis shows far less swing over the daily cycle. Second, and more important, in the MAD ventilation run there is a

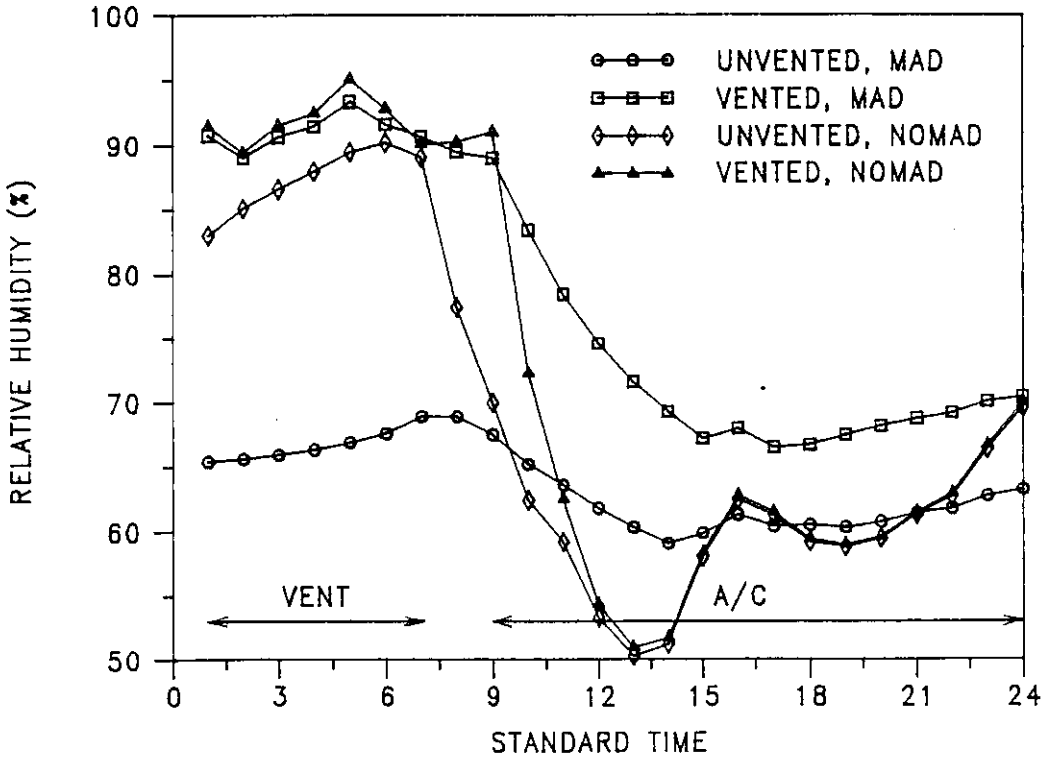

Figure 4-3 Room relative humidity for vented and unvented MAD and NOMAD basecase residences in Orlando, FL on July 20.

significant residual humidity penalty predicted as a result of ventilation. The room RH does not return to the unvented condition after the a/c begins to run as it does in the NOMAD case. This results in an underprediction of the cooling load for the NOMAD case.

Figure 4-3 gives data for only one isolated day. In order to ascertain the consistency of this trend the hourly average values of the room and ambient humidity conditions for the entire month of June were examined. Figure 4-4 is a plot of these humidity parameters for the unvented MAD and NOMAD cases. It is important to note that a strong relationship exists between the ambient dewpoint temperature and the room RH for the NOMAD case. This indicates that room RH is a strong function of infiltration. For the MAD case, however,

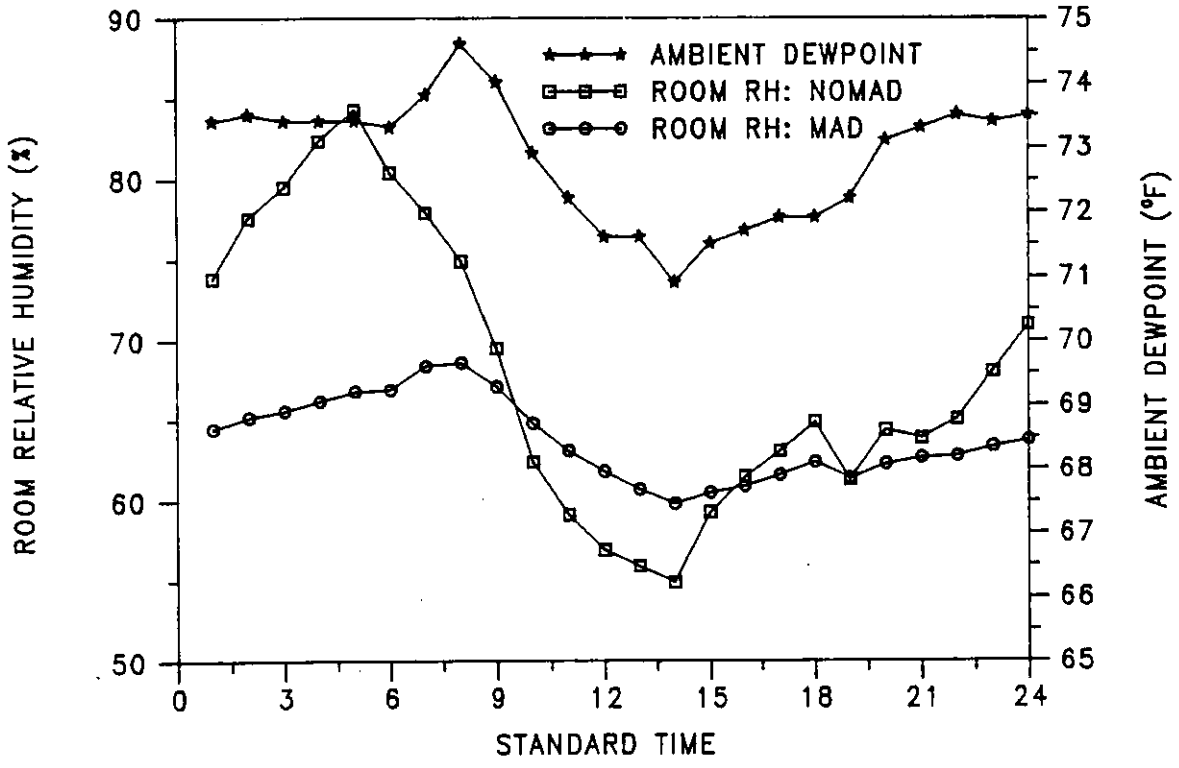

Figure 4-4 July hourly average room and ambient humidity conditions for unvented MAD and NOMAD basecase in Orlando, FL.

room RH is only a weak function of the ambient dewpoint temperature, indicating that infiltration has a much weaker effect than MAD on room RH.

Figure 4-5 shows measured data-sets for an unvented and vented day at the townhouses. The same trends that are observed in the MAD runs are seen in the measured data. This strongly supports the use of an accurate MAD algorithm for building energy analysis prediction, particularly when building ventilation studies are contemplated.

4.2.2 Comparison of MAD and NOMAD

Previous computer analyses of building loads and cooling strategies have not considered MAD. In order to provide a comparative baseline for MAD a number of computer runs have been made with MAD surface areas set to zero. These runs have been made for the three major building types (FB, FC and BP), for two of the control strategies (T and V) and for four major cities (ORL, ATL, HOU and MIA). Results from these runs illustrate the significance of MAD in building energy analysis. **In all cases** the NOMAD runs **underpredicted** the cooling load. The degree of underprediction is highly dependent on control strategy. Figure 4-6 presents the NOMAD cooling load underprediction for the vented and unvented basecase buildings as a percentage of the predicted MAD cooling load in the four major cities. For the unvented building the underprediction of cooling load for the NOMAD case ranges from 2.5% to 5% percent. This represents the best case condition. The worst case condition is represented by the temperature-controlled ventilated building where the underprediction for NOMAD ranges from 10% to 20% percent. It should be noted that these results are conservative and that if the effective MAD surface area is raised, the percentage of underprediction in cooling load will also rise (see Figure 2-17 and ESAM discussion in Section 2.3.3).

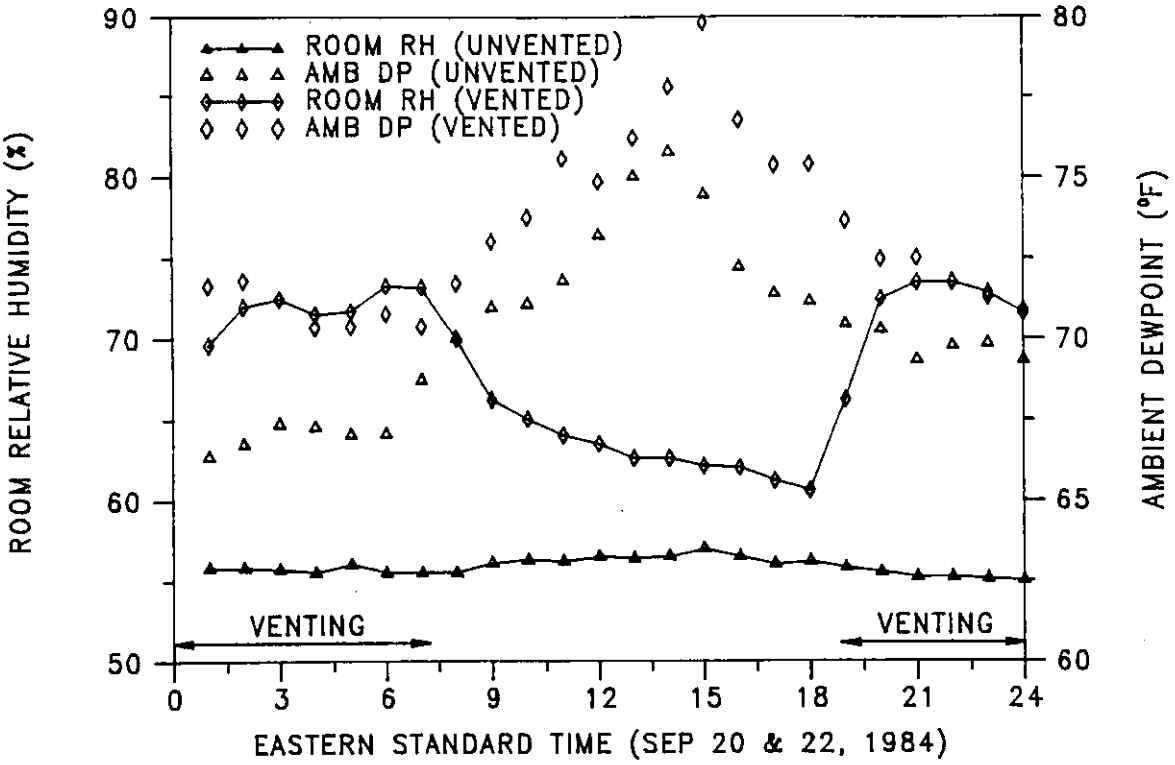

Figure 4-5 Measured ambient dew point and room RH for townhouse in Cocoa, FL on vented and unvented days.

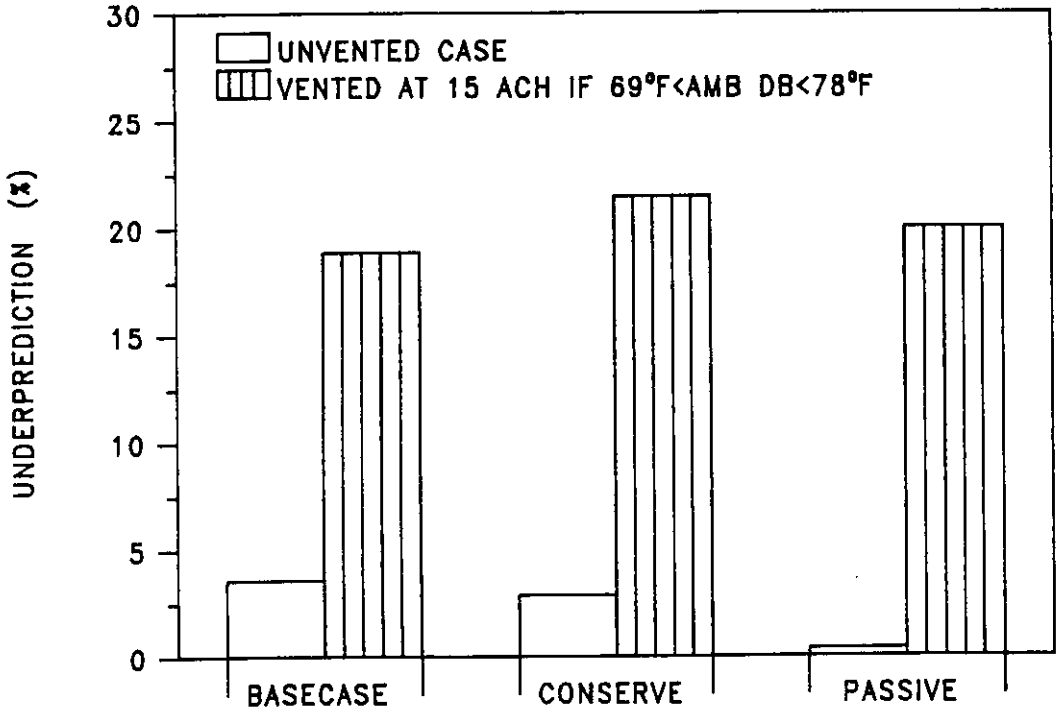

Figure 4-6 Unprediction of cooling load for FB buildings when MAD not considered.

In Orlando, FL this underprediction represents a significant error in the predicted cooling load savings that are achievable through temperature-controlled natural ventilation. Figure 4-7 presents the percent savings in cooling load achievable through temperature-controlled natural ventilation in the three building types for both the MAD and NOMAD cases. The NOMAD cases (labeled "without MAD") significantly overpredict the achievable savings. The basecase residence savings are overpredicted by 125% ! All previous predictions of natural ventilation energy savings potential have been based on this NOMAD predictive technique. The predominant evidence from this study indicates that the energy savings potential of temperature-controlled natural ventilation as a passive cooling technique has been overpredicted by recent building analysis studies [e.g., see Kamerud, et al., 1984]. Figure 4-8 illustrates the potential percent error in ventilation cooling savings prediction when MAD is not included in the predictive model.

It is interesting to note that the percent error decreases with an increase in the thermal performance of the building. This is true for all four of the major climates. The reason for this is not immediately apparent but it is caused by a decrease in the run-time of the air-conditioner and a resulting higher room RH (see Section 4.3.2, specifically Figure 4-12). Thus, for the most efficient buildings the loads are better predicted for the NOMAD case but the resulting room RH is more poorly predicted.

Based on the results of this study it appears that surface moisture absorption/desorption is a critical parameter in the prediction of cooling loads. Both building load and machine performance characteristics can be significantly altered through MAD, and how we approach the design of energy conserving building systems and cooling equipment is altered by the effects of moisture capacitance in buildings. These

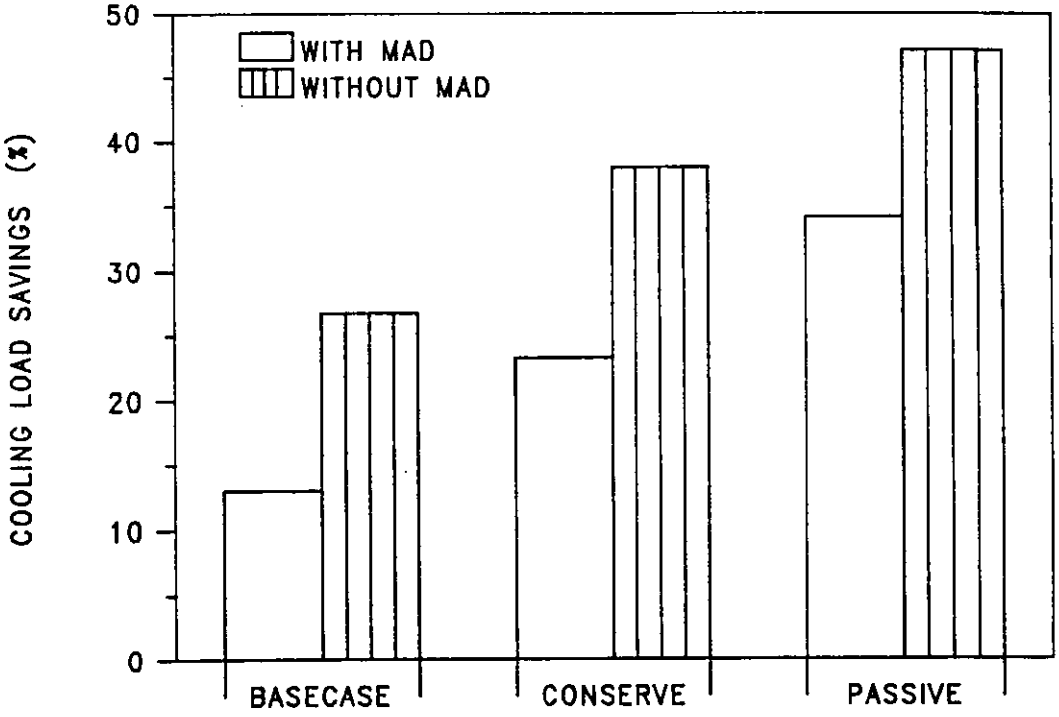

Figure 4-7 Comparison of predicted ventilation savings in Orlando, FL with and without MAD by building type. Vented if 69°F < ambient dry-bulb < 78°F.

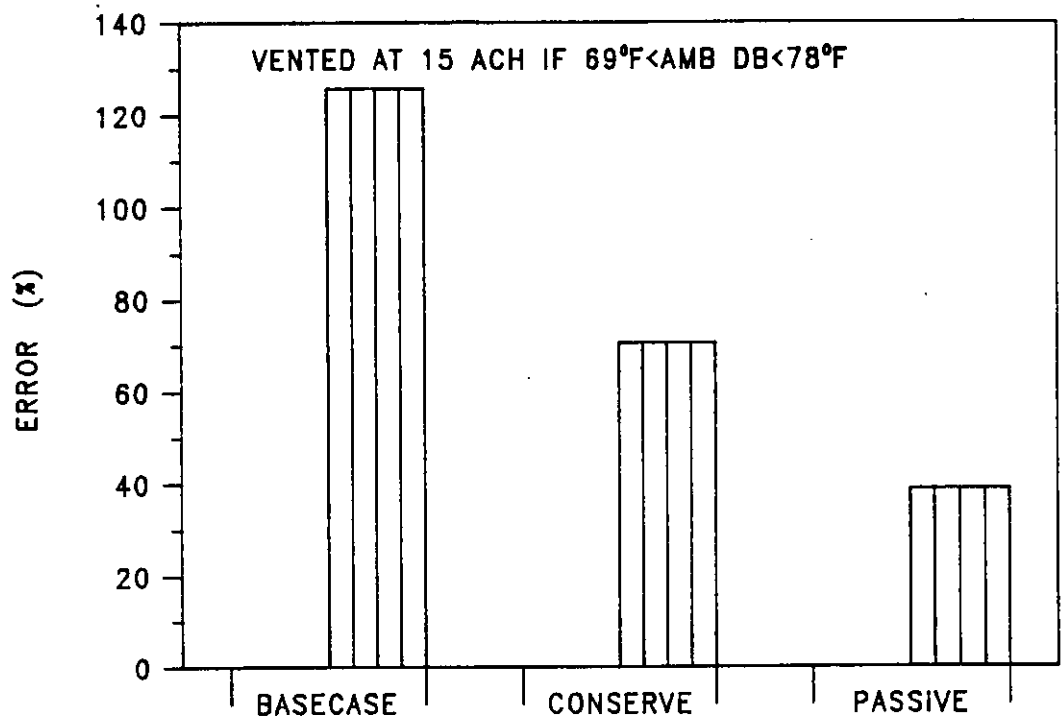

Figure 4-8 Error in predicted cooling savings for ventilation by building type in Orlando, FL. Vented if 69°F < ambient dry-bulb < 78°F.

results are conservative (i.e., they probably err on the side of more traditional cooling load analysis techniques), but the effects are significant, even at conservative analysis levels. We do not know the absolute error of the results from this analysis but there is sufficient evidence to assure us that the use of MAD analysis significantly increases the accuracy of cooling load predictions.

4.3 THERMAL MODELING OF RADIANT BARRIER SYSTEMS

A Radiant Barrier System (RBS) comprises a low emissivity surface (aluminum foil) and an adjacent airspace. Together these two components almost completely eliminate the transfer of energy by far-infrared radiation (4-40 m). RBSs have been researched during this study and through previous research work at FSEC [Fairey, 1983; Fairey, et al., 1983; and Chandra, et al. 1984].

Findings of the work have comfirmed that:

- A major portion of the ceiling heat transfer on summer days is driven by the radiant interchange between the hot roof deck and the cooler attic floor. Over 90% of the net downward heat flow from the hot roof across the attic air space to the attic floor will occur by far-infrared radiation.
- The primary driving force of downward ceiling heat transfer in typical buildings is solar radiation. On a cooling season basis, the absence of sunshine would cause attics to lose more energy through radiation to the sky than they gain, even in midsummer (see Section 4.4).
- Traditional attic insulation materials (mineral fiber, etc.) have high emissivities (>0.9) and absorb almost all radiation emitted by hot roof decks. This radiation is absorbed both at and below the upper surface of the insulation, greatly increasing the upper surface

temperature of the insulation material and thus the heat transfer through the insulation and into the room.

- Without an attic RBS the attic air temperature will always be less than the insulation or attic floor temperature when heat transfer is down. Thus, even under peak summer conditions convective heat transfer in attics will be upward from the hot insulation or attic floor to the attic air.
- For summer design day conditions the daily heat flow down and through the ceiling of a typical residence may be reduced by over 40% by using an attic RBS.
- Attic RBSs are a very effective means of reducing heat transfer in attic spaces in both summer and winter.

4.3.1 Modeling Approaches

The modeling of an RBS cannot be accurately accomplished by assigning it an R-value or U-value. Traditional insulation materials have been approached in this manner but an RBS responds through optical phenomena and simply does not fit the thermal conductance paradigm of simplified building envelope analysis techniques.

One method of modeling RBSs is to model them as complete building zones (e.g., an air volume that is bounded by either interzone solid partitions or partitions that separate the zone from the ambient environment). This technique will not work well with models that perform load calculations based on room weighting factors like DOE.2. For models like MADTARP, TARP, BLAST that perform a detailed zone energy balance that account separately for radiation and convection the radiant barrier zone method will be more accurate. In the final analysis, the results will depend on the accuracy of the zone balance model that is used. The zone modeling approach has been used for roof RBS analysis in this study.

If each external building surface (e.g., each wall

orientation, etc.) is modeled as a complete building zone, modeling complexity increases dramatically. In order to alleviate this problem, simplified methods of evaluating the thermal performance of RBS have been investigated at FSEC. The most promising of the methods investigated to date involves manipulation of the exterior solar absorptance and emissivity values for the envelope.

Experimental data obtained at the FSEC Passive Cooling Laboratory (PCL) strongly indicate that the effect of an RBS at the outer layer of the building envelope (exterior RBS) will be the significant reduction of the sol-air effect on that surface. This effect can be simulated through a reduction of external surface solar absorptance (alpha) and far-infrared emissivity (epsilon) values. When detailed finite difference modeling techniques are used, this method gives good agreement with the measured data at alpha values of 0.1 to 0.2. However, emissivity values must also be reduced to account for the reduced nocturnal radiation effects of such systems. Far-infrared emissivity values of 0.5 have been used to account for this phenomenon. For the wall RBS modeled in this report the alpha and emissivity modeling method was used.

4.3.2 Comparison of Simulated Results and FSEC Experiments

A number of experimental full-scale tests have been conducted in the FSEC PCL over the past three years. The tests are conducted on a side-by-side basis with "traditional" insulation or construction practices being the "standard" (or control) against which alternatives are measured. Both roof/attic/ceiling and wall components of buildings have been examined.

The intent of the research has been to provide the necessary, carefully-measured performance data to assure that the phenomena being observed in the experiments can be accurately

and faithfully reproduced by building energy analysis programs like MADTARP. When this is accomplished the performance of an RBS may be "predicted" with some confidence for a wide variety of climates and applications through computer models.

Experimental data on roof radiant barrier performance is available from both full-scale and hot box tests [Fairey, 1983]. Results from these tests show a 42-44% reduction in summer design day ceiling heat flux over standard R-19 batt insulation when attic RBSs are used.

To evaluate RBS performance on a seasonal basis, MADTARP building input decks that employ a separate roof RBS building zone were created. The roof RBS zone was composed of the roof of the building with a 4-inch airspace directly beneath it followed by a single-sided radiant barrier with a thermal resistance (R-value) of 0.002, an upward emissivity of 0.9 and a downward emissivity of 0.05. This roof RBS zone adjoined the attic zone of the building.

The roof RBS input deck was then used in design day MADTARP runs for two thermostat setpoints ($78^{o}F$ and $81^{o}F$) at two radiant barrier zone air change rates (0.25 and 1.0 ACH). Very low air change rates were used because test data were obtained in unvented attic spaces and hot boxes. The heat flux through the ceilings for the various runs was examined to determine the modeling capability of the roof radiant barrier zone as compared to the measured data. Table 4-1 presents a summary of the ceiling fluxes for the eight runs.

The ceiling flux reductions given in Table 4-1 compare favorably (erring on the conservative side) with the measured flux reductions in both full-scale attics (42%) and in hot box tests (44%) under design day conditions. Thus it is felt that analysis of attic RBS can be effectively modeled with a

separate roof radiant barrier building zone using the MADTARP code.

TABLE 4-1

Comparison of Ceiling Heat Fluxes for Design Day MADTARP Analysis in Orlando, FL - Attic Radiant Barrier Zone versus Standard R-19 Ceiling

MADTARP RUN	@ ach = .25		@ ach = 1.0	
	Ceiling flux Btu/ft2 -day	Flux Reduction WRT Base	Ceiling flux Btu/ft2 -day	Flux Reduction WRT Base
Base (R-19) : T_{stat} = 78°F*	27.15	---	25.94	---
Attic RB Zone: T_{stat} = 78°F	17.56	35.3%	15.69	39.5%
Base (R-19) : T_{stat} = 81°F*	24.06	---	22.78	---
Attic RB Zone: T_{stat} = 81°F	14.75	38.7%	12.98	43.0%

A series of annual MADTARP runs were performed using the basecase, roof RBS zone, and R-30 ceiling insulation input decks. The R-30 deck was added to the analysis for comparison purposes so as to arrive at energy conservation parameters for increased traditional insulation materials.

For annual runs the roof RBS zone air change rates were increased to a value which would be appropriate for a poorly vented (soffit vents only) roof system. Due to the small volume of the airspace these air change rates appear high (10 ACH); however, the same flows would produce an air change rate of only 1.2 ACH if applied to the entire attic space volume.

MADTARP runs have been made for seven climates using these building input decks. Considering both heating and cooling,

the roof RBS zone case outperformed R-30 ceiling insulation in all southern cities. In Baltimore, the performance difference was still in favor of RBS in terms of annual energy consumption (savings of 532 kWh vs 497 kWh). In Chicago, R-30 ceiling insulation did outperform RBS on the basis of total kWh savings, but even in Chicago RBS performed very well in summer saving, 211 kWh, where R-30 saved only 94 kWh.

In terms of the winter performance of a roof RBS ceiling, heat flux measurements in the PCL roofs show a net daily increase in heat loss for RBS over standard attics. Flux results from three consecutive cold days in December 1984 indicate a greater net outward ceiling heat flux for the RBS as compared to R-19 ceilings. Table 4-2 presents a summary of the ambient conditions and ceiling flux data for the three days. On day 4344 the two constructions had very similar total heat losses. On day 4345 there is also a small difference, but on day 4346 the radiant barrier had a 16% greater net heat loss. Figures 4-9a and 4-9b give the hourly ceiling heat flux and ambient conditions for day 4346. From the flux histories one can see that the RBS is reducing nighttime heat loss but increasing the daytime heat loss as compared to the standard. The increase in daytime heat loss is caused by the elimination of the normal sol-air effect at the roof with respect to heat transfer across the attic.

There is good evidence to indicate that the model is predicting heating energy use correctly. However, the data given in Table 4-2 and Figure 4-9a need a more subtle interpretation to understand how this occurs. If heating load is the parameter of real interest, when will that load occur? The greatest part of that load should occur during the evening when the RBS is retarding heat loss, not during the day when heat gain is retarded.

Figure 4-10 is a comparison of the predicted net monthly heat

Table 4-2

Ambient Conditions and Ceiling Flux Summaries
from PCL Experimental Database

	Minimum	Maximum	Average	Summation
DAY 4344 (Dec.9,'84)				
Ambient drybulb (°F)	45.27	66.85	54.57	
Horiz. radiation (Btu/hr ft2)	-1.80	205.80	53.76	
Wind velocity (mph)	0.26	9.83	5.33	
Base case:				
MRT	44.20	82.42	58.10	
Ceiling inside surf	61.19	71.55	66.08	
Flux Btu/hr ft2	-1.10	0.07	-0.45	-42.75
Rad. barrier case:				
MRT	48.48	71.72	58.08	
Ceiling inside surf	63.47	71.26	67.04	
Flux	-1.03	-0.16	-0.46	-43.83
DAY 4345 (Dec.10,'84)				
Ambient drybulb	47.96	72.07	59.43	
Horiz. radiation	-1.50	201.60	49.48	
Wind velocity	1.22	8.15	4.63	
Base case:				
MRT	46.74	86.25	62.22	
Ceiling inside surf	62.58	73.48	68.12	
Flux	-0.94	0.23	-0.36	-34.08
Rad. barrier case:				
MRT	50.79	74.98	61.46	
Ceiling inside surf	64.27	72.66	68.41	
Flux	-1.11	0.06	-0.38	-35.66
DAY 4346 (Dec.11,'84)				
Ambient drybulb	55.16	75.63	63.61	
Horiz. radiation	-1.30	197.20	41.56	
Wind Velocity	0.24	9.01	4.54	
Base case:				
MRT	54.12	90.98	67.80	
Ceiling inside surf	68.18	76.57	72.21	
Flux	-0.73	0.27	-0.25	-23.39
Rad. barrier case:				
MRT	56.91	78.84	66.48	
Ceiling inside surf	67.83	75.64	71.61	
Flux	-0.67	-0.07	-0.29	-27.26

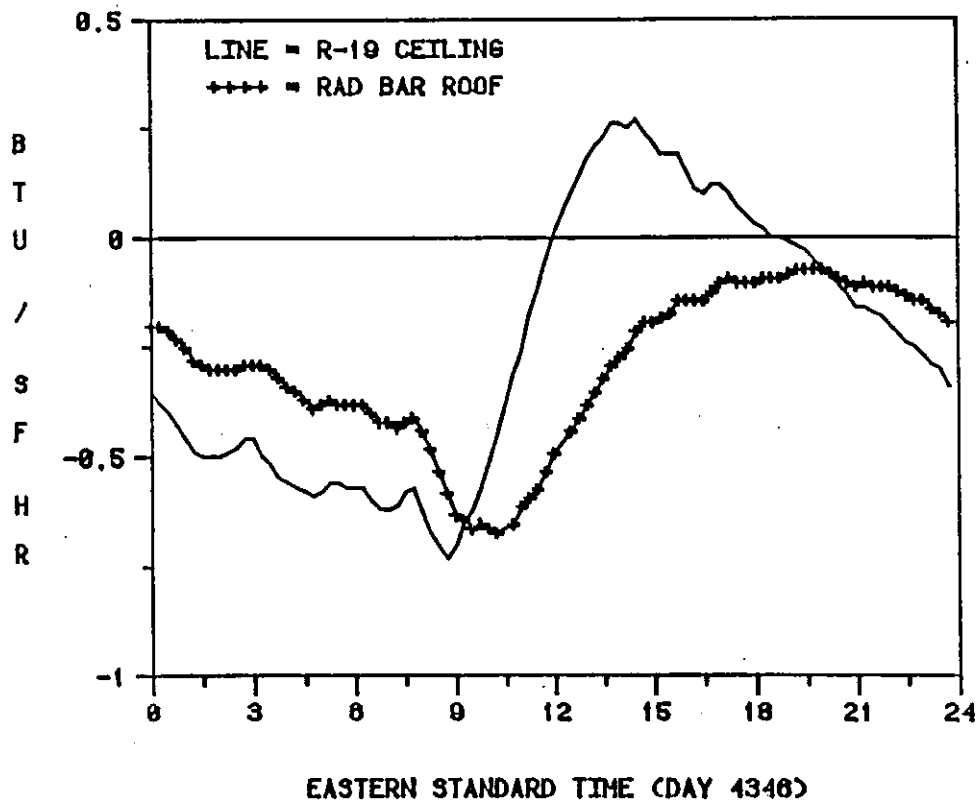

Figure 4-9a Measured ceiling heat flux for R-19 and R-19 plus radiant barrier system attics.

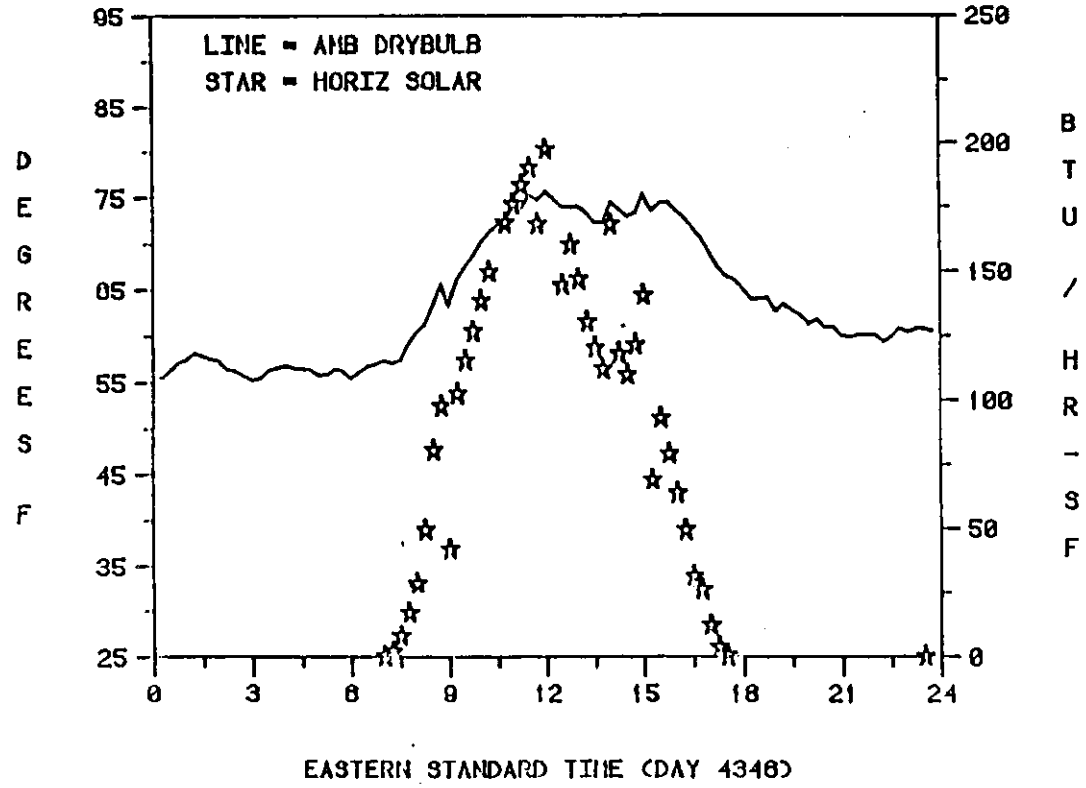

Figure 4-9b Measured ambient temperatures and solar radiation.

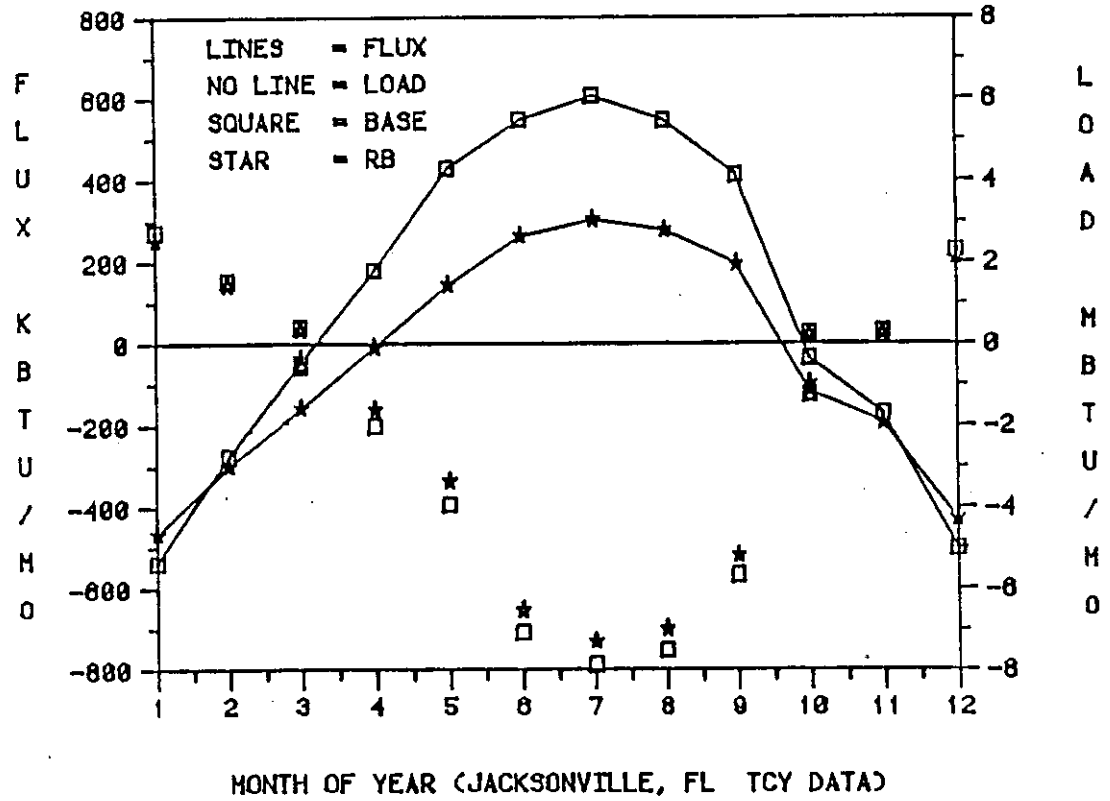

Figure 4-10 Ceiling heat flux and building loads as predicted by MADTARP in Jacksonville, FL.

flow at the ceilings and the total building loads for the basecase and the RBS roof zone. The relationship between net ceiling heat fluxes and the associated heating and cooling loads is interesting. First, looking at the ceiling fluxes during the winter, the months of January and December show a greater heat loss for the R-19 ceiling (standard) than the roof RBS case. As expected, heating loads for these months are lower for the RBS case.

However, the months of February, March, October and November show a different phenomenon. The ceiling heat loss for the R-19 case is the lower of the two but its associated building load is the higher! This appears to be contradictory. The explanation, although not immediately obvious, is simple: The radiant barrier case is providing additional thermal protection for the roof when it is most needed -- at night.

During the day when the radiant barrier performs poorly there is little or no heating requirement during these months.

To substantiate this theory the hourly values for ceiling heat fluxes and heating loads were examined during February and March. Results from four days in February (Feb. 2 through 5) were taken from the data set and plotted in Figures 4-11 through 4-15. Figure 4-11 gives results for the entire period and Figures 4-12 through 4-15 are subsets of this data. The TCY weather conditions in Jacksonville, FL on February 2 (Figure 4-11) are similar to the weather conditions on day 4346 (see Figures 4-9a and b) at FSEC. Comparison of Figures 4-9a and 4-12 show very similar trends for predicted versus measured heat flux. If the flux values of Figure 9 are divided by the ceiling area of the modeled house (1500 ft^2) even the heat flux magnitudes are very similar. The daily minimum and maximum ambient conditions were close for the days (50.0°F to

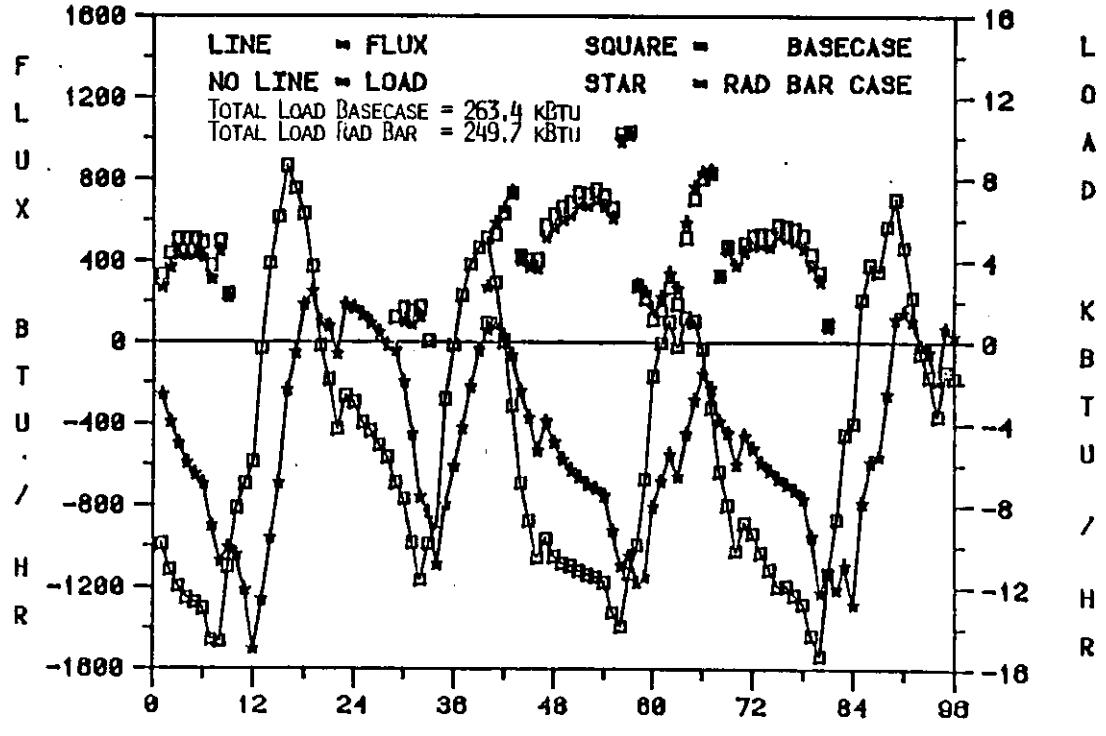

Figure 4-11 Comparison of ceiling fluxes and building heating loads.

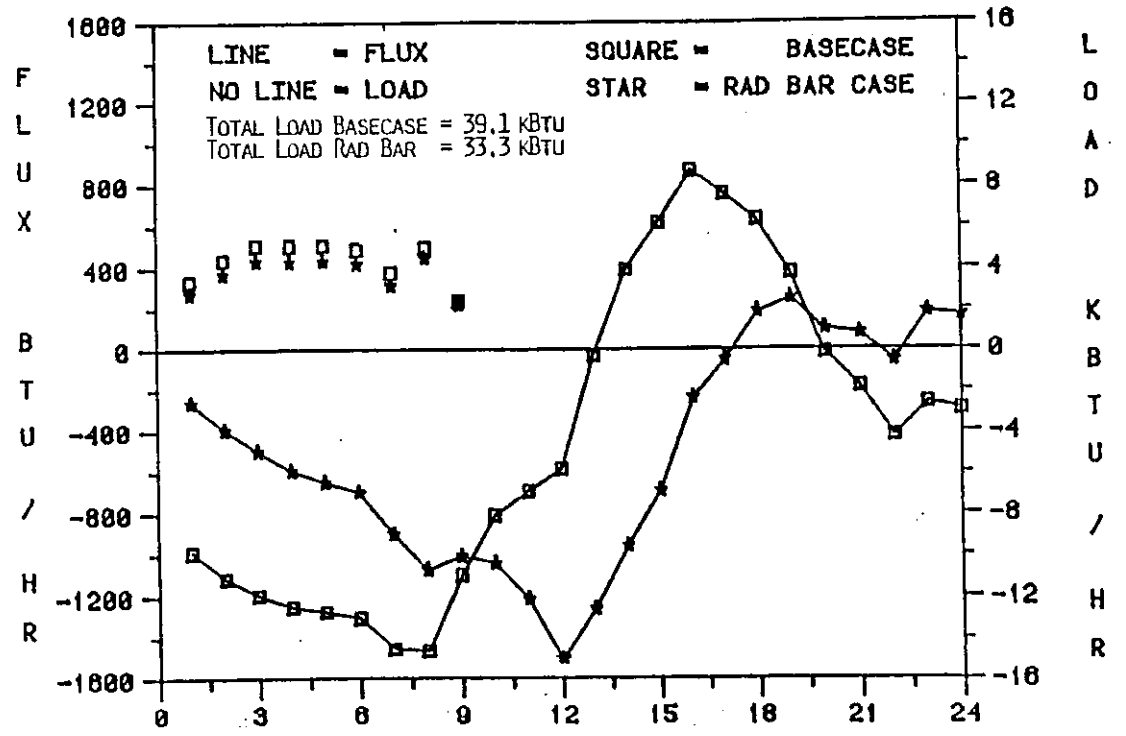

Figure 4-12 Comparison of ceiling fluxes and building heating loads.

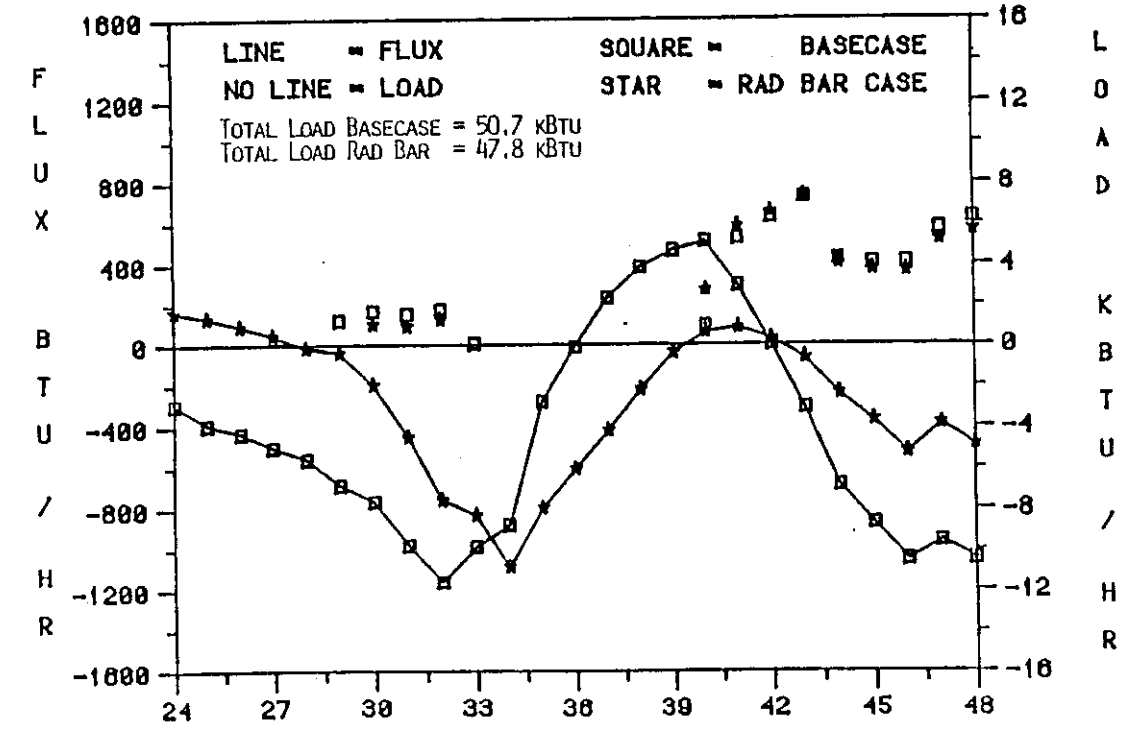

Figure 4-13 Comparison of ceiling fluxes and building heating loads.

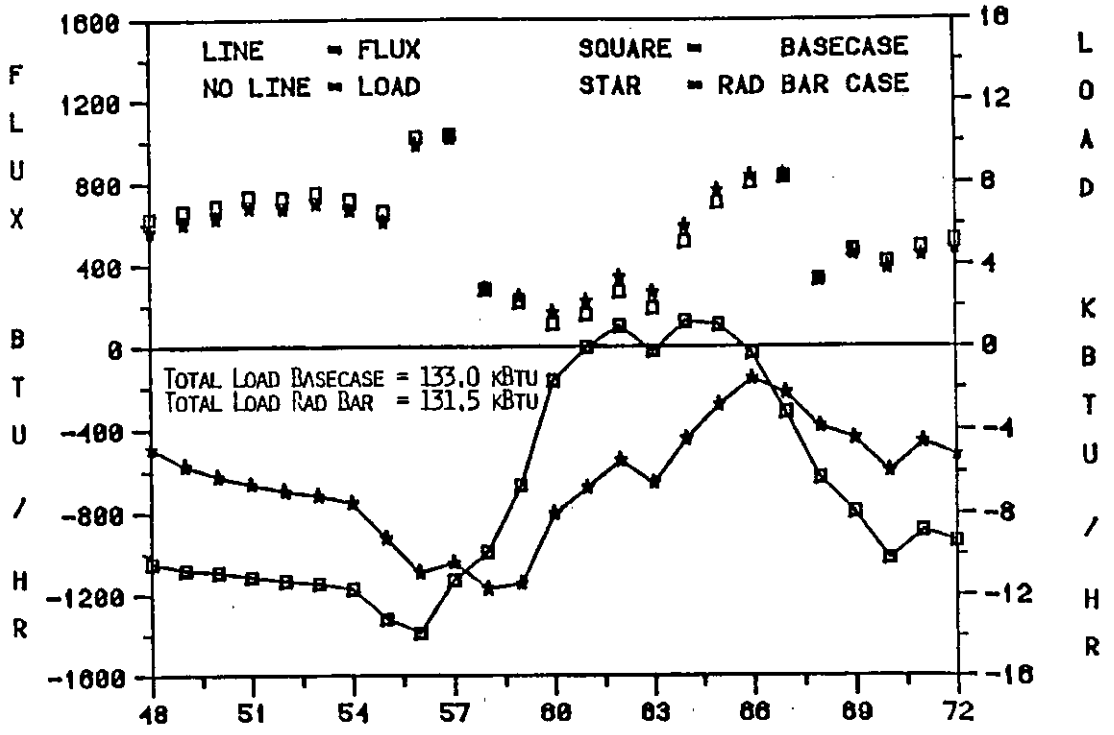

Figure 4-14 Comparison of ceiling fluxes and building heating loads.

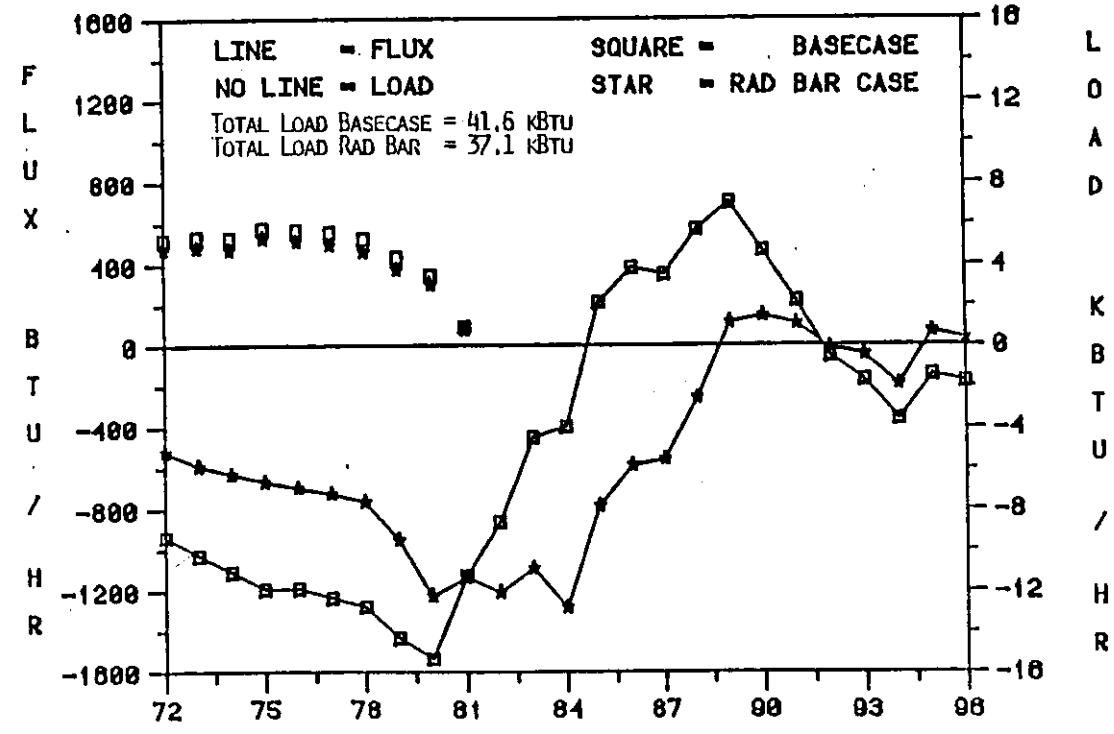

Figure 4-15 Comparison of ceiling fluxes and building heating loads.

73.9°F and 180 Btu/hr-ft^2 peak radiation for the model and 48.5°F to 72.0°F and 202 Btu/hr-ft^2 peak radiation for the measured data). It is reasonable to assume that heating loads would occur only early in the mornings on such days, and that the model is predicting reality.

Thus, the data, both measured and simulated, indicate that there is an excellent match between heating load schedules and the beneficial performance of RBSs. The relatively poor performance of RBSs during the day in winter is more than compensated for by their beneficial night performance when heating loads are highest. Even on February 4 (Figure 4-14) when heating loads existed for each hour of the day, the RBS case overcame its poorer daytime performance through its superior night efficacy (net daily heating load of 133.0 kBtu versus 131.5 kBtu). The total net heating loads for the four-day period were 263.4 kBtu for the R-19 ceiling versus 249.7 kBtu for the RBS case -- a net savings of 5.2% for the RBS over the standard heating load.

As a final check the output data files from February and March were processed to give monthly average hourly data. These data are plotted in Figures 4-16 and 4-17 and show that the predominant loads do in fact occur during times of superior RBS performance. In March there are no daytime loads and in February they are quite low with respect to the night loads.

To assure that this was not a Jacksonville peculiarity, monthly ceiling flux results from each of the cities were checked for consistency. Referring to Figure 4-10 one can see that the ceiling flux lines for the basecase and radiant barrier case cross between January and February and between November and December in Jacksonville. Examination of the other cities for this phenomenon showed this happening in each city. Of greatest interest was the point at which the crossing occurred. For all the cities analyzed, the crossing

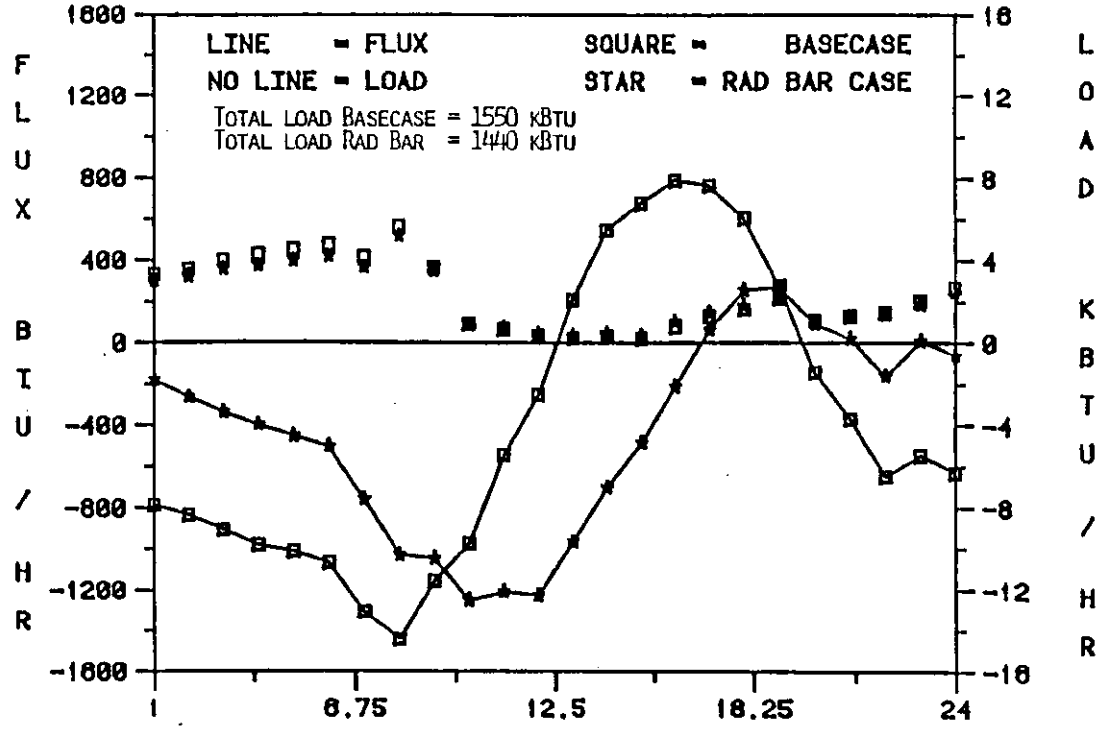

Figure 4-16 Ceiling fluxes versus heating loads for Jacksonville TCY data.

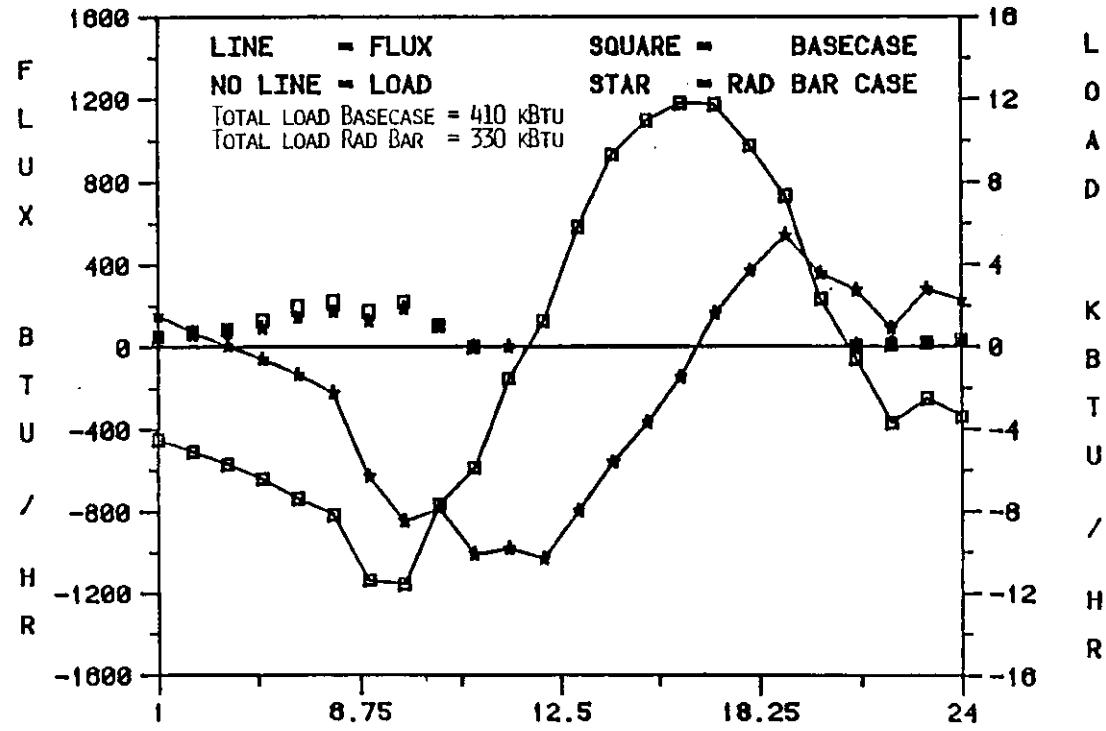

Figure 4-17 Ceiling fluxes versus heating loads for Jacksonville TCY data.

point occured during the month that the monthly average daily horizontal radiation dropped below 1000 Btu/day. The months changed from city to city but the radiation level of the cutoff remained very stable. This indicates that the roof radiant barrier system performance will be well matched to the building load in almost any climate.

4.3.3 Energy and Cost Savings

Table 4-3 presents a comparison of the results for the roof RBS zone and the R-30 ceiling insulation with respect to the basecase residence. Costing figures are based on local area prices. There is a wide variance in the prices of radiant barrier products, depending on the product chosen. Pricing of installed RBS for this cost analysis is based on a raw product cost to the installer of $\$0.07/ft^2$ and a total installed cost of $\$0.20/ft^2$. For R-30 ceilings only the cost differential between blown R-19 and R-30 fiber insulation was considered. This cost also proved to be $\$0.20/ft^2$ installed. The difference in the installed cost of the two systems is based on the fact that blown fiber insulation is at the attic floor (1500 ft^2) and the radiant barrier is at the roof undersurface (1600 ft^2 assuming a 5-in-12 roof pitch). This results in a total installed cost of $300.00 for the blown fiber insulation and $320.00 for the radiant barrier system.

The radiant barrier system performs admirably in all climates that were examined. Only in Chicago did the R-30 insulation save more total annual energy than the radiant barrier system plus R-19 ceiling insulation.

4.4 BUILDING LOAD SOURCES

During analysis the sources of the heating and cooling loads were carefully traced. MADTARP was modified to sum the mass and heat fluxes from each energy transfer source in three different catagories: 1) during heating periods, 2) during cooling periods and, 3) during neutral periods when no heating

Table 4-3

Comparison of savings from addition of attic radiant barrier system versus addition of R-11 insulation to a standard R-19 attic system.

City	kWh Savings						Annual Cost Savings @ $.085/kWh		Simple Paypack in years		Return on Invst 15 yr Life 5% Fuel Infl. Rate	
	Cooling		Heating		Annual							
	R-30	RBS + R-19	R-30	RBS + R-19	R-30	RBS + R-19	R-30	RBS + R-19	R-30 @300.00	RBS @320.00	R-30	RBS + R-19
Miami, FL (heat COP=1)	272.4	537.7	29.3	38.1	301.7	575.8	$25.64	$48.94	11.7	6.5	8%	17%
Orlando, FL (heat COP=1)	243.7	491.0	128.9	137.7	372.6	628.7	$31.67	$53.44	9.5	6.0	11%	19%
Jacksonville, FL (heat COP=2)	217.1	426.9	99.6	99.6	316.7	526.5	$26.92	$44.75	11.1	7.2	8%	16%
Houston, TX (heat COP=2)	202.1	389.1	121.6	95.2	323.7	484.3	$27.51	$41.17	10.9	7.8	9%	14%
Atlanta, GA (heat COP=2)	155.3	341.8	224.2	162.6	379.5	504.4	$32.25	$42.87	9.3	7.4	11%	15%
Baltimore, MD (heat COP=2)	124.8	282.8	372.1	249.1	496.9	531.9	$42.24	$45.21	7.1	7.1	16%	16%
Chicago, IL (heat COP=2)	94.1	211.2	474.7	278.4	568.8	489.6	$48.34	$41.61	6.2	7.7	18%	14%

or cooling was required. The thermal as well as radiative (solar) fluxes were tracked by building surface, then grouped by surface type and orientation.

Pie-charts representing the sources of the direct heating and cooling loads have been developed for some major cities from this data. For some analyses an attempt was made to split the thermal fluxes traveling through the opaque building surfaces into their solar induced and air temperature induced components. This was done by reducing the external solar absorptance values by 10% and re-running the analysis. The difference in performance represents a 10% reduction in the solar driving force. When multiplied by 10 the result is assumed to be the full solar induced load for that component. Small errors may be expected in the results from this type of analysis. Due to the detailed room balance performed by MADTARP, a change in the performance of one building component affects the response of the other room components. This is why a small reduction of only 10% was used rather than complete elimination of the solar loading.

4.4.1 Basecase Building Analysis

A full description of the basecase residence (FB) is given in Section 3.4. It is not repeated here.

Both heating and cooling load sources have been analyzed but emphasis was placed on cooling load. Heating loads are not presented here. Figure 4-18 presents the annual and peak month (July) air conditioning load sources in Orlando, FL. the total loads as a function of building floor area are also given.

The most significant load sources are infiltration and internal generation (27% and 28% respectively). Infiltration at the summer design condition (15^{o}T and 7.5 mph site 10m wind speed) was set at 0.75 ACH. The average during the month

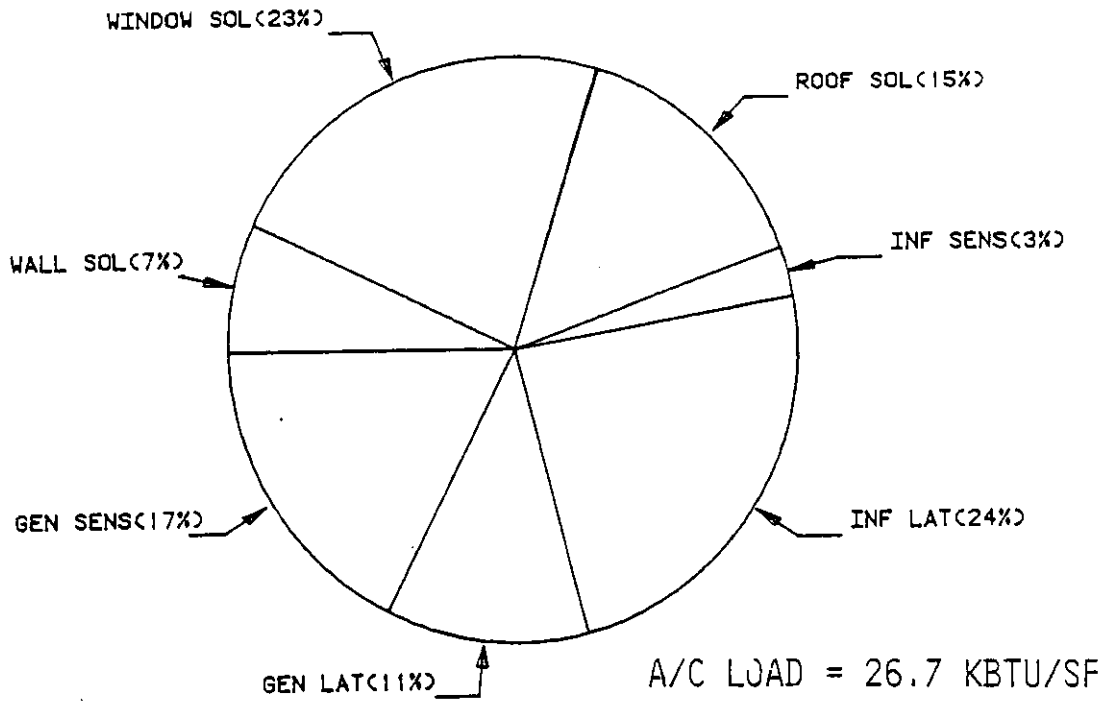

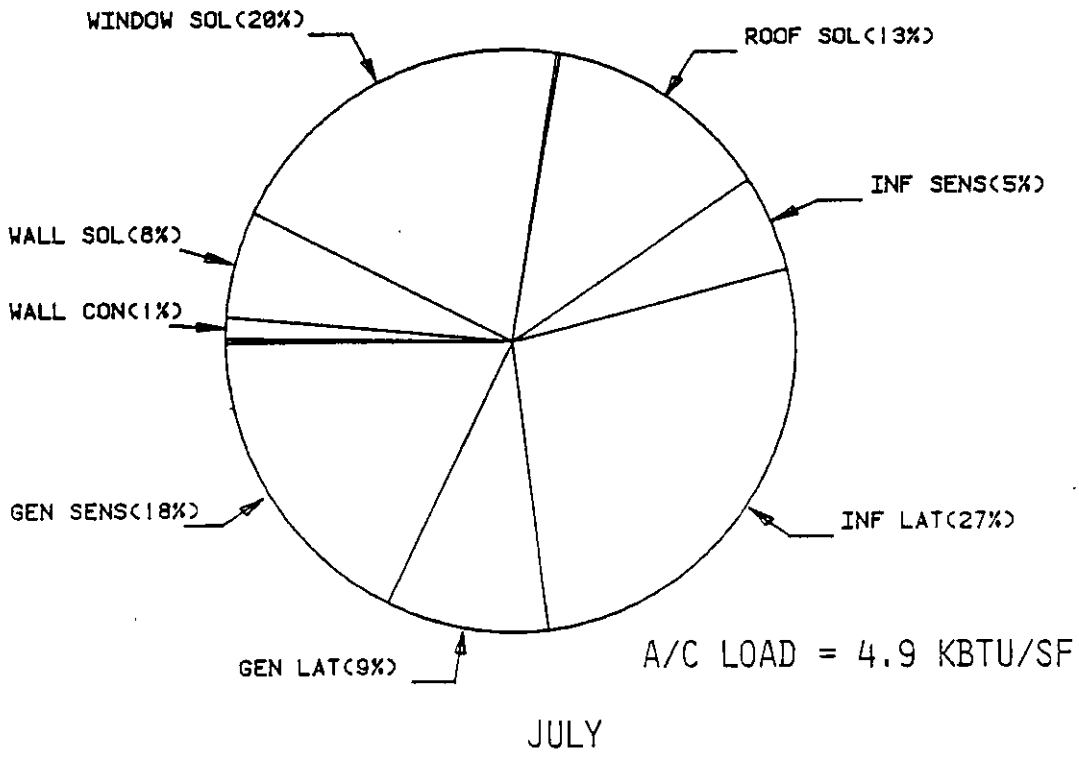

Figure 4-18 Annual and peak month air conditioner load sources for frame basecase house in Orlando, FL at T_{stat}=78°F.

of July after modification due to wind speed and temperature is only 0.59 in Orlando. Since a minimum air-change rate of 0.4-0.5 is recommended to maintain satisfactory indoor air quality, only minor savings in cooling energy can be expected through further reductions in the infiltration level.

The next most significant load source is the solar load through windows (23%). The basecase window shading coefficient assumed (except on the south) was 0.42 with additional shading provided by two-foot roof overhangs. A window shading coefficient of 0.2 is readily possible through external shades or large overhangs and would result in a/c kWh savings of about 6%.

The internally generated load accounts for a significant portion of the cooling load (28%). Control of internal loads is highly user-dependent. Through the use of very efficient refrigerators, microwave ovens and less indoor cooking, significant reductions in internal load (say 25%) may be possible. This 25% reduction would result in about 5% to 8% savings in cooling energy. Internal loads may not be radically reduced since they come almost exclusively from occupancy of the building.

The roof and wall solar loadings are the next major contributors to the cooling loads. To understand the interaction of solar and conductive loading through roofs and walls, Figure 4-19 has been prepared, showing heat balance diagrams for the cooling season. The diagrams show that the a/c removed only 83% of the building heat gains. Even in Orlando, the net conduction through floor, roof and walls (in the absence of solar radiation) is actually a net benefit during a/c operation! Thus, the heat gains through the roof of the building are almost exclusively driven by solar radiation, and in the absence of the solar flux the roof would account for 3% of the building cooling. The 3% difference

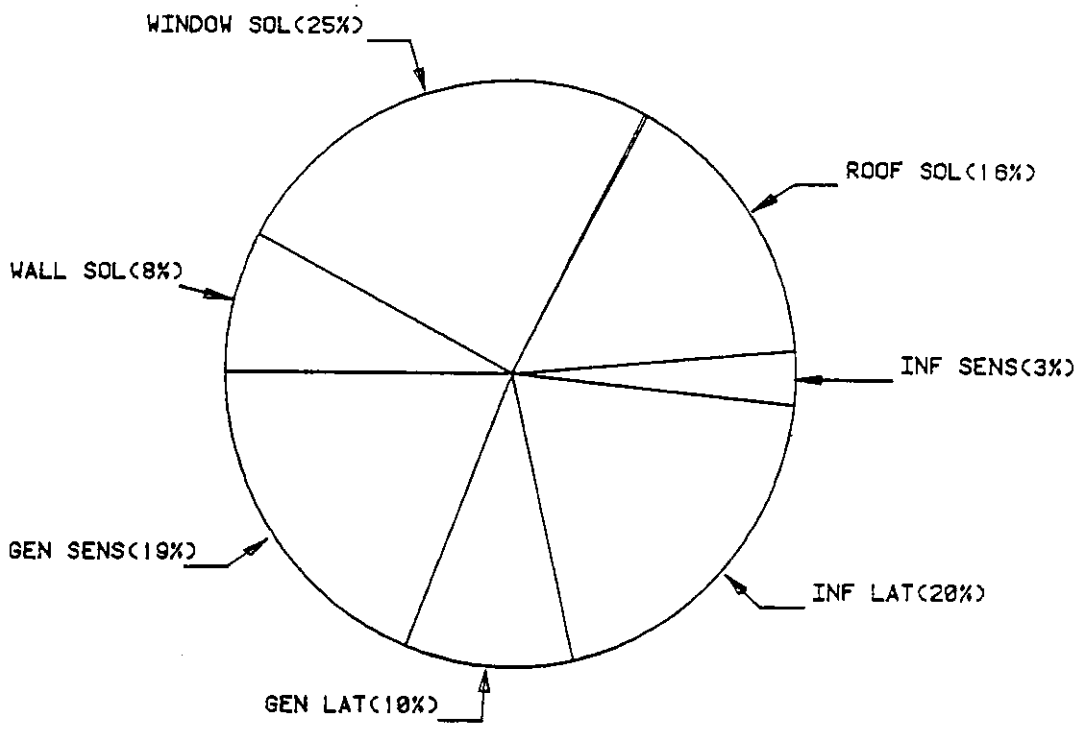

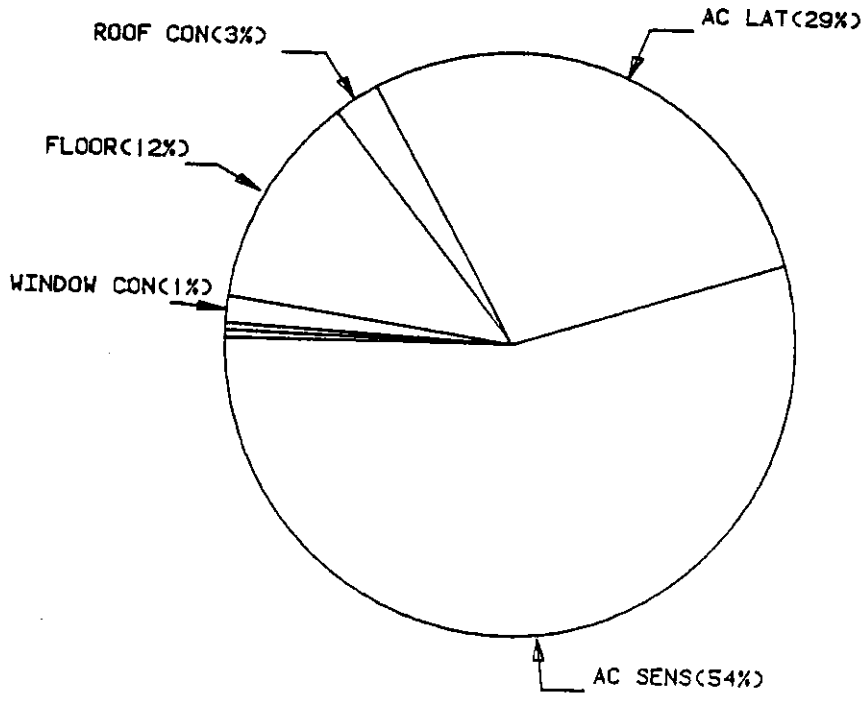

Figure 4-19 Cooling season energy balance (3.21 kBtu/ft^2) for Orlando, FL at T_{stat}=78^{o}F.

represents the net roof convective losses to air and radiative losses to the night sky (Figure 4-19 bottom). Similar calculations were performed for the walls. One could say that were it not for the sun, the roofs and walls of the building should not be insulated to save cooling energy. Night sky radiation reduces the roof and wall surface temperatures below the ambient air and often the house setpoint. This phenomenon occurs for all months in the case of the roof load. Wall conduction, however, is a positive load in July in Orlando (see Figure 4-18).

The loading through the wall is small and thus extra wall insulation may not save significant cooling energy. Light-colored walls, shade trees, or wall radiant barrier systems are more cost effective than increased wall insulation for cooling.

The traditional advice for roofs has been to use light-colored roofs. Light-colored roofs have some aesthetic drawbacks (less curb appeal) and, moreover, are hard to maintain. Many darken due to mold, mildew, rain streaks, etc. A much more cost effective strategy for both new and retrofit construction (for pitched roof attics) is to use radiant barrier systems. For the basecase house in Orlando, attic radiant barriers save 8% to 10% of the cooling energy requirment. (See Section 4.3 for a full discussion of radiant barrier systems.)

Figure 4-20 gives the a/c load pie-charts for the four main climates of Atlanta, Houston, Miami and Orlando. Roof and wall solar loads are not given for these runs but the same phenomena occur here as in Orlando. From the infiltration loads Houston appears to be the most humid climate and Atlanta the driest. However, the basic distribution of cooling load sources appear to be similar across all climate regions in the souteast.

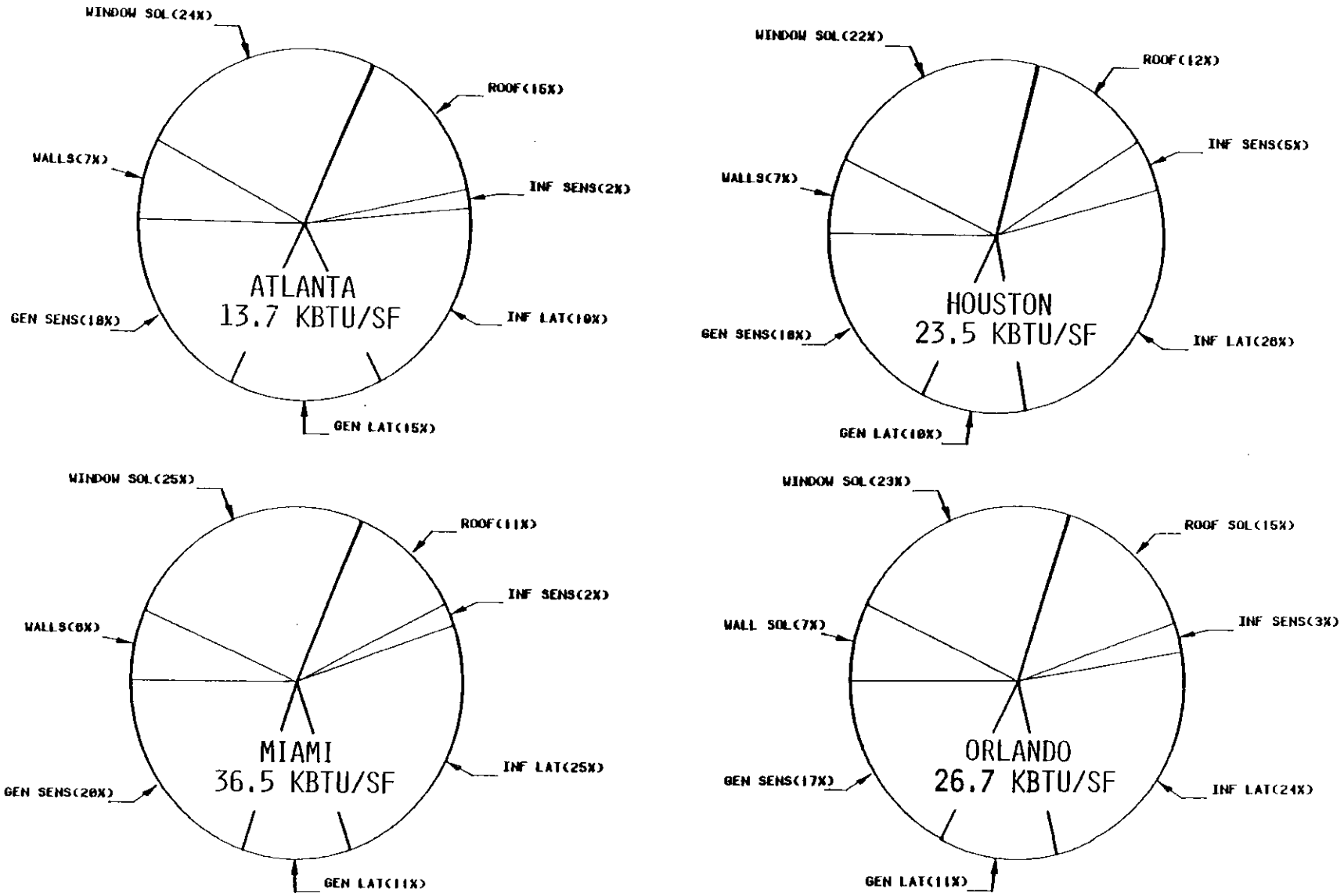

Figure 4-20 Comparison of air conditioner load sources in four different climates for frame basecase house at $T_{stat}=78^{o}F$.

4.4.2 Comparison of Energy Conservation Techniques

A number of energy conservation strategies have been considered through parametric analysis using the basecase residence. Temperature setpoint variation (a measure of ceiling fan performance) has been studied in four climates on an annual basis and radiant barrier performance is reported for seven climates in Section 4.3.

Figure 4-21 gives the general results of the Orlando analysis. Of considerable interest is the attendant rise in room RH that is observed with increasing thermal energy savings where infiltration levels are not reduced. The fact that the air conditioner runs less results in less moisture removal from the building. Thus the thermal technique gains a load benefit from the reduced moisture load at the a/c. This of course results in an increase in the monthly average room RH. At RH levels of 68% or greater this can constitute a mold and mildew problem in buildings [Humphries, 1972]. More recently Sterling, et al. [1985] have studied the effect of RH on a number of health and human habitation parameters. Their results are given by Figure 4-22.

Figure 4-21 clearly shows that RH levels increase as the building thermal integrity increases, until the infiltration rate is reduced. Conservation strategies which increase room RH levels past about 68% constitute a serious potential problem with respect to health and habitability in residences. Such practices must consider the need for additional dehumidification capacity with respect to the thermal cooling capacity of the mechanical system.

Nonetheless it is apparent from Figure 4-21 that significant cooling energy may be saved through the judicial use of energy conservation strategies. Window shading and radiant barrier systems appear to be cost- and energy-effective methods of controlling heat gain into buildings. Additional traditional

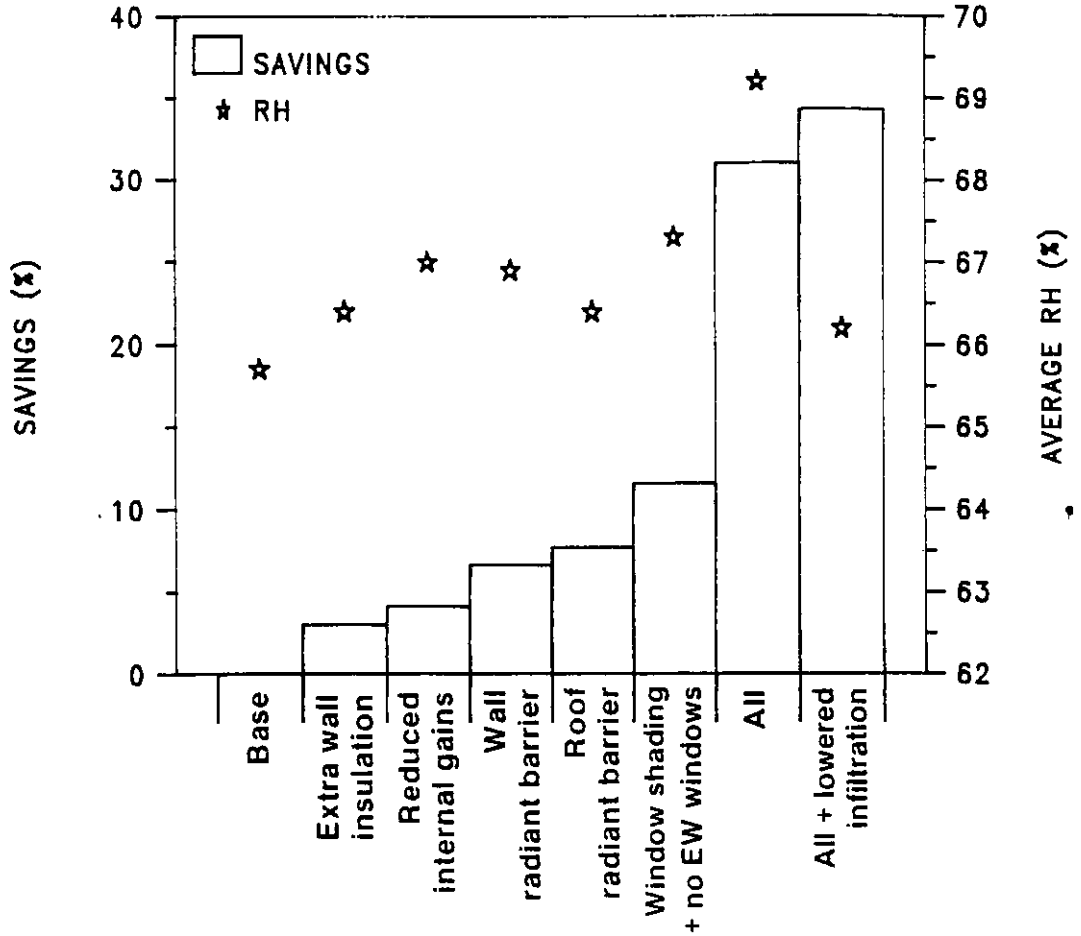

Figure 4-21 Comparison of predicted savings from energy conservation measures.

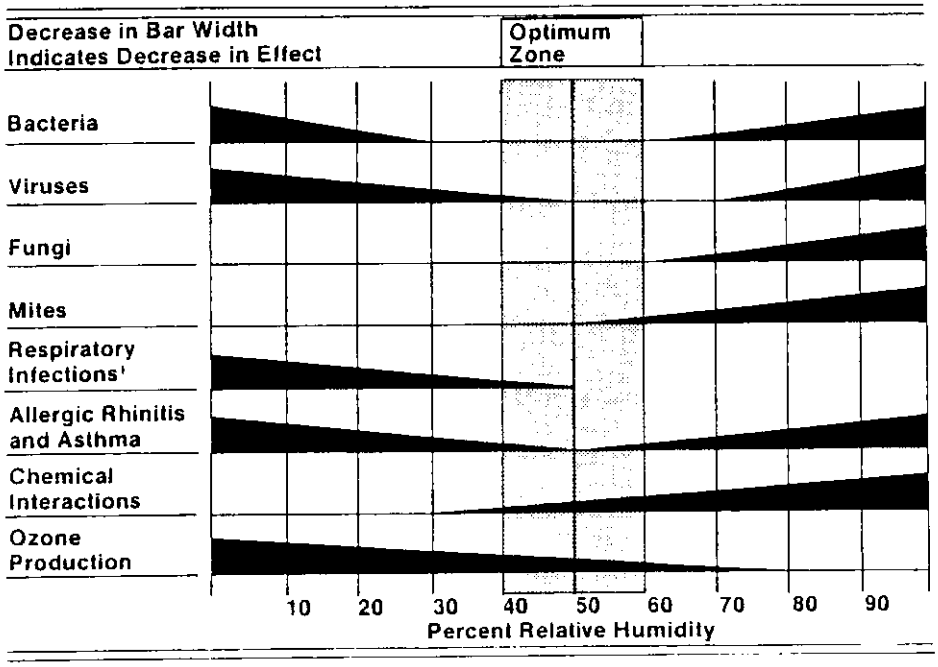

' INSUFFICIENT DATA ABOVE 50% PERCENT R.H.

SOURCE: Sterling [1984] ASHRAE Transactions V. 90, Part 2.

Figure 4-22 Effect of room relative humidity on selected human health parameters.

insulation does not appear to be as effective as radiant barrier systems in reducing cooling loads. Unless additional dehumidification potential is available, thermal conservation strategies will increase room RH levels.

The use of ceiling fans as a conservation measure departs slightly from the previous parametric analysis because energy savings result from an increase in allowable room temperature rather than a modification to the building envelope. This is important for two reasons:

- Increasing the thermostat does not result in an appreciable increase in RH because the room air temperature rises along with the amount of moisture (lb/lb) in the room air.
- There is a parasitic power requirement for the use of ceiling fans.

Table 4-4 details the load sources for the four major climates for various thermostat setpoints. At the bottom of the table the worst month RH and the average RH for May-October are listed. Table 4-4 points out the dramatic cooling load reductions possible by increasing the thermostat setpoint. It also shows that as the setpoint is increased the operating SEER of the a/c improves slightly.

As the thermostat increases, the sources of the cooling load remain about the same except for infiltration and the latent loads from internal generation. These loads are very climate- and setpoint-dependent. As the setpoint increases the difference between the internal and external driving forces (both humidity ratio and temperature) decreases; therefore cooling energy requirements also decrease, but without a significant RH penalty.

Table 4-4

Air Conditioning Loads and Load Source Percentages at Different Indoor Thermostat Set Points

FRAME BASECASE HOUSE

	ATLANTA				HOUSTON				MIAMI				ORLANDO			
SET POINT °F	76	78	80	82	76	78	80	82	76	78	80	82	76	78	80	82
TOTAL LOADS																
Load [kBtu/sf/yr]	17.7	13.7	10.3	7.4	29.3	23.5	18.6	14.2	45.2	36.5	28.7	21.5	33.5	26.7	20.9	15.8
A/C [kWh/sf/yr]	2.1	1.6	1.2	0.8	3.5	2.8	2.2	1.7	5.3	4.2	3.2	2.4	4.0	3.1	2.4	1.8
Seasonal A/C EER	8.6	8.7	8.8	8.9	8.4	8.4	8.5	8.6	8.6	8.7	8.9	8.9	8.5	8.6	8.7	8.7
LATENT LOADS																
Infiltration [%]	20.5	18.9	19.8	10.6	26.9	26.4	26.0	24.2	25.3	24.8	24.6	23.4	24.4	23.8	23.1	20.8
Generation [%]	11.5	14.9	16.8	28.3	8.3	10.1	12.6	16.3	8.6	10.6	13.2	16.9	9.2	11.4	14.5	19.3
TOTAL LATENT [%]	32.0	33.8	36.6	38.9	35.2	36.5	38.6	40.5	33.9	35.4	37.8	40.3	33.6	35.2	37.6	40.1
SENSIBLE LOADS																
Window Solar [%]	24.1	23.8	22.8	21.8	21.3	21.8	22.1	22.1	23.8	24.7	25.1	25.3	23.5	23.8	23.8	23.1
Generation [%]	19.9	18.1	16.8	16.0	18.9	17.9	16.4	14.6	20.6	19.8	18.4	15.9	19.3	18.2	16.1	14.7
Roof [%]	14.1	15.0	15.4	15.7	11.6	11.9	12.4	13.1	10.9	11.2	11.7	12.2	12.2	12.7	13.3	13.9
Walls and Doors [%]	7.5	7.6	7.4	7.3	7.3	7.1	7.0	7.0	7.0	6.7	6.3	6.2	7.4	7.3	7.2	7.2
Infiltration [%]	2.4	1.7	1.0	0.3	5.7	4.7	3.6	2.6	3.8	2.1	0.6	0.0	3.9	2.9	2.0	1.0
MONTHLY INDOOR RH																
May-Oct Indoor RH [%]	58.1	58.4	58.5	58.8	62.7	62.9	62.8	63.0	63.2	63.3	63.1	63.4	62.6	63.0	62.9	63.2
Worst Month RH [%]	62.3	63.1	63.4	63.9	64.8	65.2	65.2	65.5	63.9	63.8	63.8	64.2	64.9	65.7	66.0	66.5
Worst Month for RH	<—— AUGUST ——>				<—— JUNE ——>				<— JULY —>				<— OCT. —>			
													<—— SEPTEMBER ——>			

Figure 4-23 shows the cooling load savings (accounting for parasitic fan power) that are achievable at equivalent comfort conditions as air motion is increased. Ceiling or other fans can easily produce 150 ft/min air motion. This leads to a comfort zone shift of about 4°F. Thus, a nominal thermostat setting of 78°F can be moved up to 82°F in the presence of air circulation fans without sacrificing comfort.

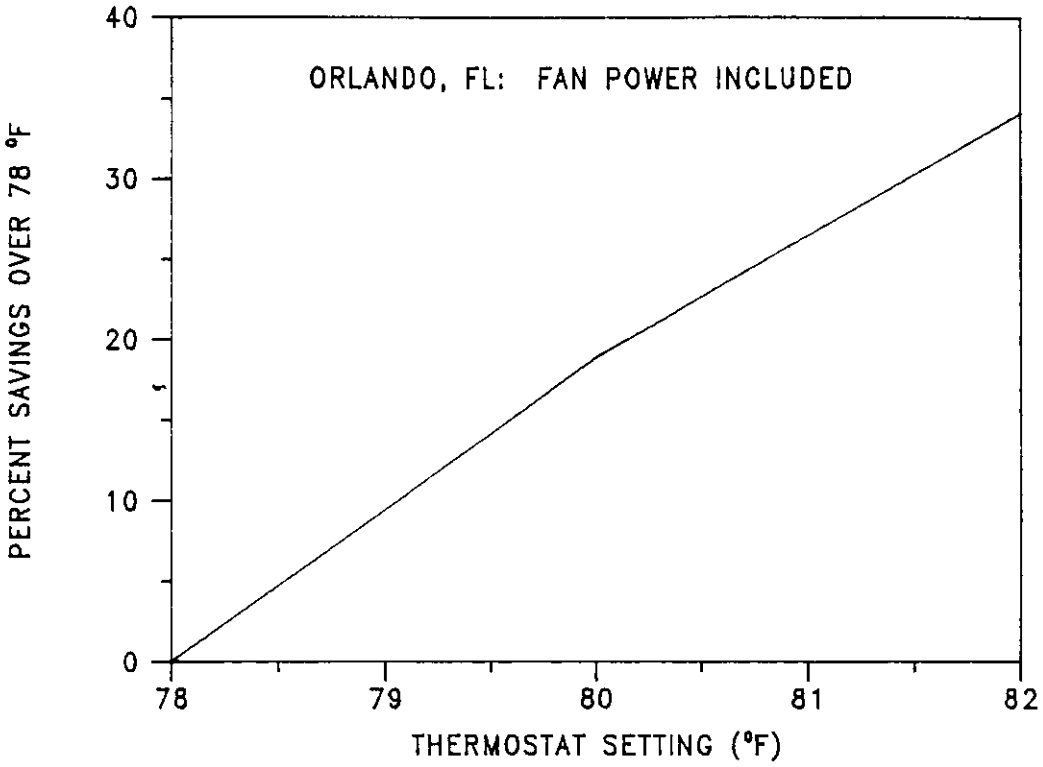

Figure 4-23 Ceiling fan cooling energy savings possible in Orlando, FL for basecase residence.

The percent savings in cooling load as the thermostat is increased can be calculated from values given in Table 4-5. However, fans consume power (see Table 4-5).

To estimate the cooling energy savings given by Figure 4-23 we estimate a 24 hour load of 50 watts continuous power to maintain the house at 80F (a 2°F setup) and 100 watts continuous to maintain the house at 82°F. The fan kWh consumption was subtracted from the predicted a/c kWh savings to arrive at Figure 4-23 for Orlando, FL. One can conclude

that in Orlando ceiling fans would save about 7% to 8% cooling energy per degree setup of the house thermostat, and a significant savings of 32% is possible from a thermostat setup from 78° to 82°F with no appreciable increase in room RH liability or sacrifice in comfort.

Table 4-5

Power Consumption (watts) of Fans
(FSEC test Results)

	Fan Speed Setting		
	High	Medium	Low
1. Ceiling fan, 48"	75	40	15
2. Oscillating portable fan, 12"	42	34	27
3. Box fan, 20"	160	104	74

Major conservation opportunities exist for window shading devices and attic radiant barriers and the use of ceiling fans. Combined, they can save upwards of 50% of the cooling costs and can be very cost effective. Note that these are not heating solutions like air infiltration reductions or more insulation. As a matter of fact, low summer windspeeds and moderate house to ambient temperature differentials result in basecase normal infiltration levels that are relatively low (0.6 ACH). Significant air infiltration reduction measures may be counterproductive from an indoor air quality standpoint.

More traditional insulation is also not necessarily a cost-effective summer solution. As for attics, attic radiant barriers are clearly superior to additional attic insulation (see Section 4.3). Walls are a low percentage source of cooling loads and the floor slab actually promotes cooling in all climates including Miami.

4.4.3 Passive and Energy Conserving Load Distributions

A mnemonic code has been established to maintain a reasonable

method of referencing the results of the analysis. Table 4-6 gives a synopsis of the code. A specific "basic building code" may be addressed by a minimum of four characters. The first two characters, the building type, are discussed in detail in Section 3.5, mechanical systems are discussed in Section 2.5, and control strategies are discussed in Section 4.4.3. Thus, the basecase building for this study is FBTT (frame, basecase, typical system, traditional control strategy).

The basic building code may be followed by a "parametric extension" of up to three characters representing some sets of parametric analysis that have been or may be accomplished. The maximum number of characters does not exceed seven. Much of the following report will refer to a specific analysis result according to this code.

Cooling load distributions for the passive and energy conserving residences have also been examined. The BP building was shown to have the lowest cooling load with respect to cooling season performance. For closed buildings, there is only a small difference in the cooling performance of the FC (frame energy-conserving) and BP residences regardless of climate. However, when passive or hybrid cooling strategies (eg, natural ventilation, night sky radiation or ground cooling) are implemented the BP building has greater reductions in cooling load than the FC building.

Cooling load distributions for the FBTT, FCTT, BPTT and BPTR residences are shown in figures 4-24 through 4-27. The most dramatic shift in load distribution is seen in the internal building generation. This load is shifted from 28% of a/c cooling load in FBTT (Figure 4-24) to 44% of the cooling a/c load in both the FCTT and BPTT residences (Figures 4-25 and 4-26, respectively). The percentage drops slightly (41%) when

Table 4-6

KEY TO BUILDING DESCRIPTION MNEMONICS

BASIC BUILDING CODE:

Construction type:
- F = frame
- B = block

Building type:
- B = basecase ("typical")
- C = energy conserving (frame only)
- I = interior insulation (energy conserving block)
- E = exterior insulation (energy conserving block)
- P = block-passive, mass partition walls

Mechanical system type:
- T = typical (SEER = 8.0 SHF = .76 @ ARI)
- I = ideal (set = 68/78^{O}F & 58% RH)
- M = mildew control (ideal @ 68% RH)
- N = no moisture ABDES

Strategy:
- T = traditional closed building (T_{set} = 68/78^{O}F)
- V = ventilation with temp. control
- E = enthalpy ventilation
- S = super enthalpy ventilation
- R = night sky radiant cooling
- G = ground tube cooling

PARAMETRIC EXTENSION:

Parametric Code
- E = ESAM variation
- A = ACH variation for venting
- H = h_c variation
- C = Convergence checks
- Z = Combination ACH & h_c

Two Digits USER Code (User maintained)

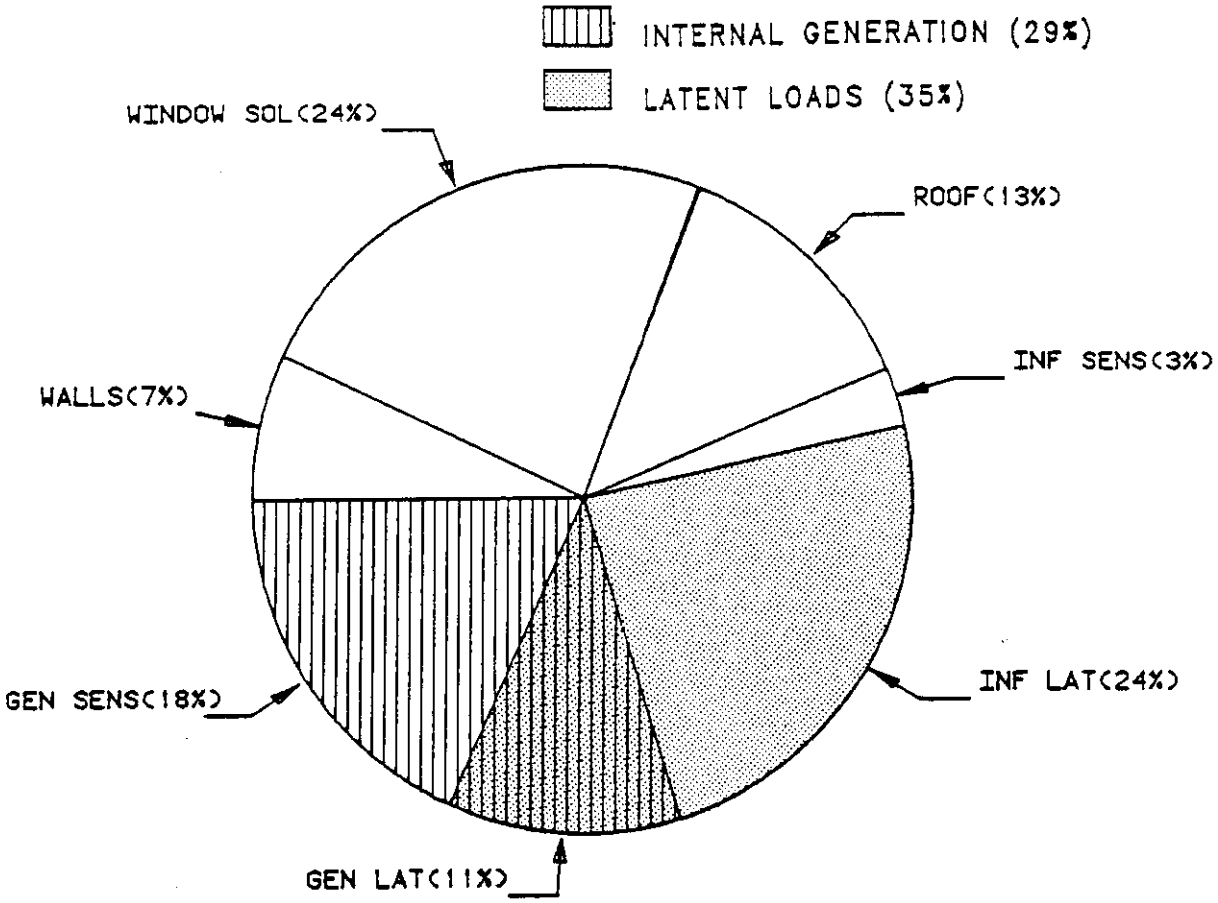

a) Air-conditioner load sources (26.7 kBtu/ft^2)

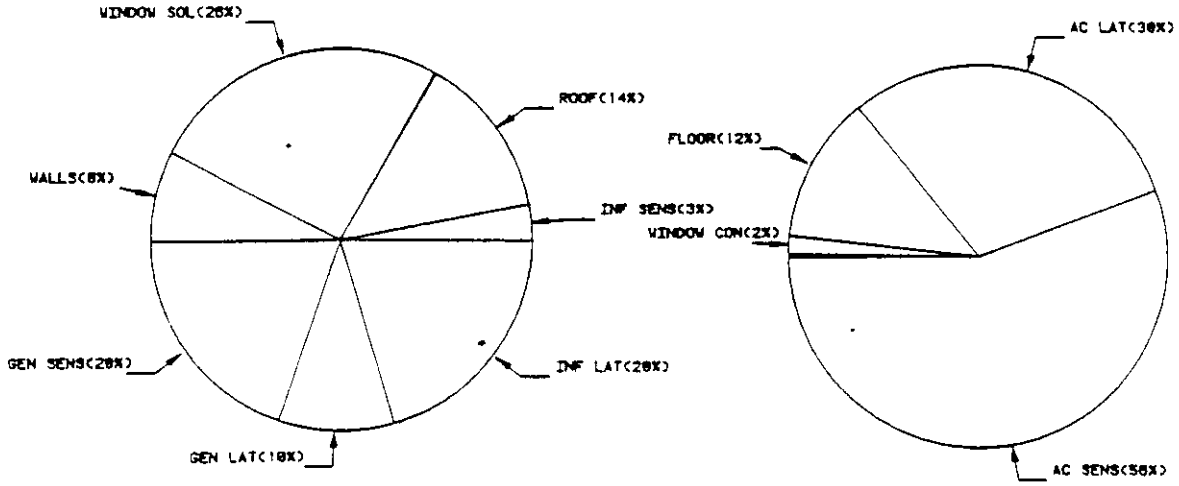

b) Heat gain sources

c) Heat removal means

Energy Balance (31.1 kBtu/ft^2)

Figure 4-24 Annual load sources and energy balance for 1500 ft^2 frame basecase house in Orlando, FL at $T_{stat}=78^{o}F$.

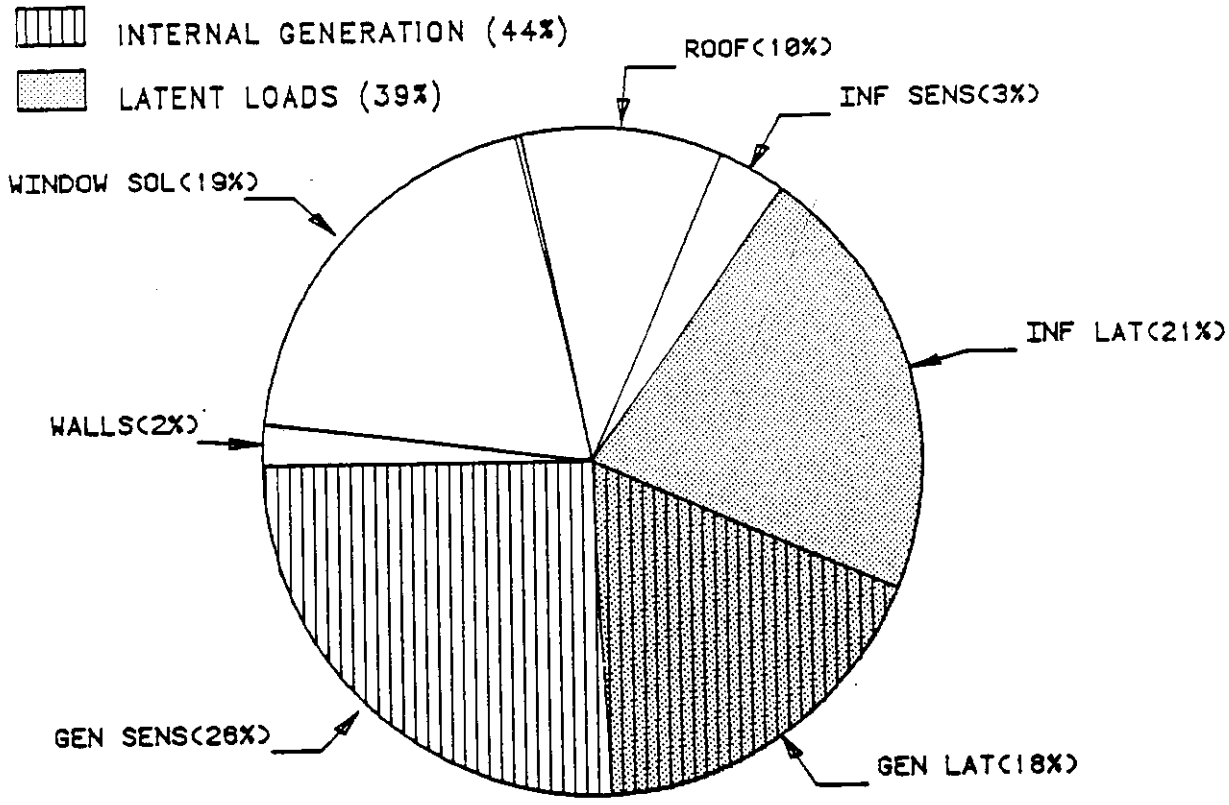

a) Air-conditioning load sources (17.6 kBtu/ft^2)

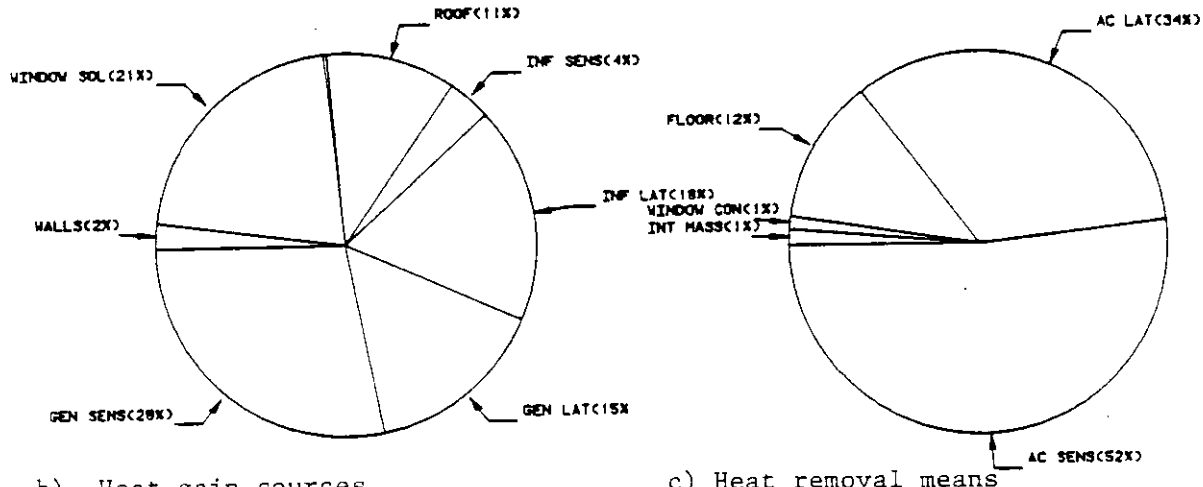

b) Heat gain sources

c) Heat removal means

Energy Balance (20.5 kBtu/ft^2)

Figure 4-25 Annual load sources and energy balance for 1500 ft^2 frame energy conserving house in Orlando, FL at $T_{stat}=78^{o}F$.

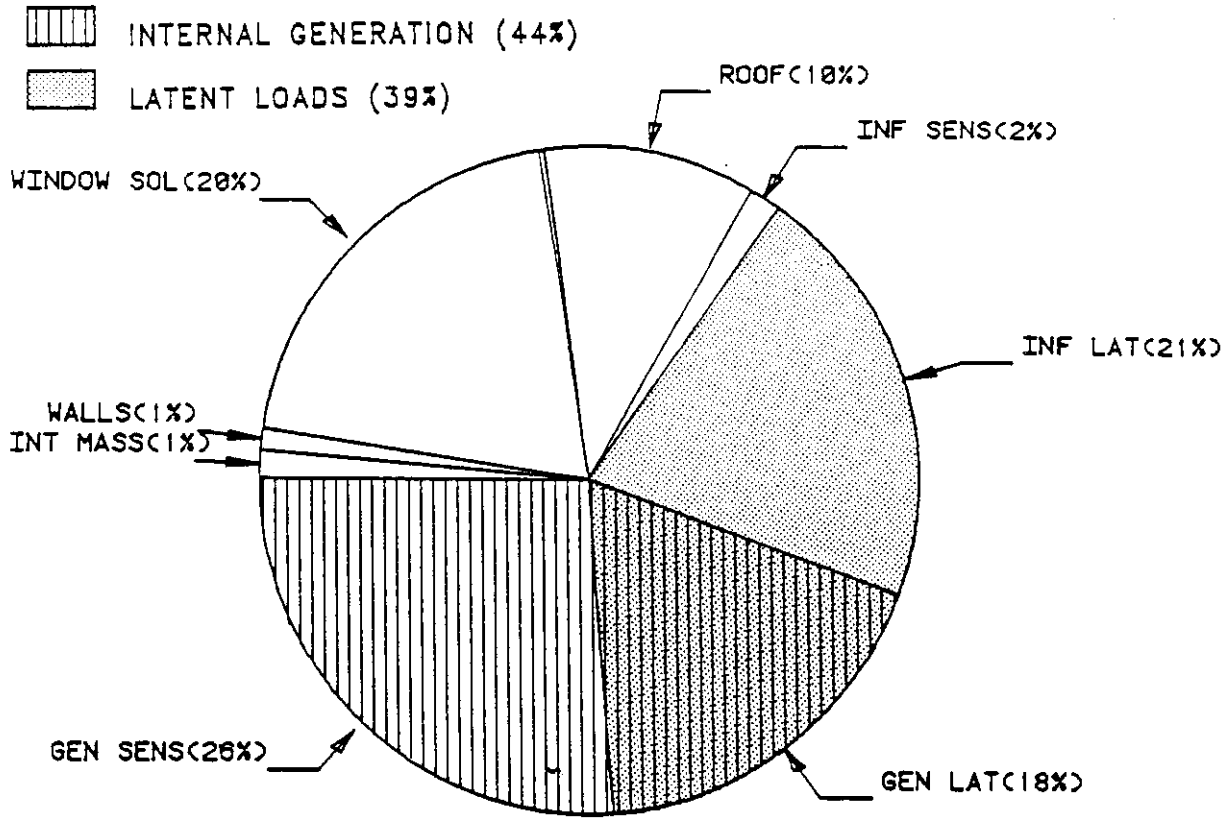

a) Air-conditioner load sources (16.6 kBtu/ft^2)

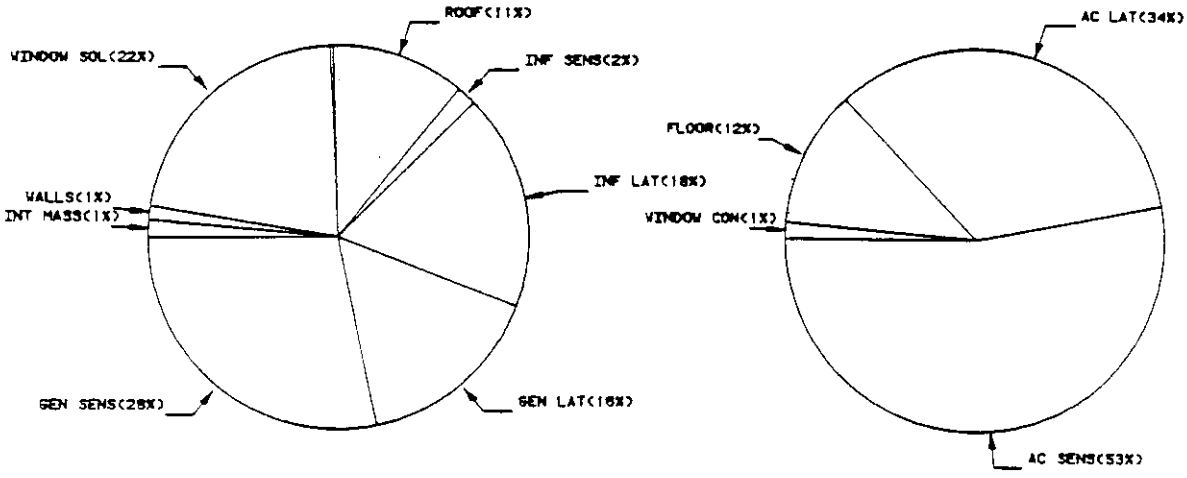

b) Heat gain sources

c) Heat removal means

Energy Balance (19.0 kBtu/ft^2)

Figure 4-26 Annual load sources and energy balance for 1500 ft^2 block-passive house in Orlando, FL at T_{stat}=78^{o}F.

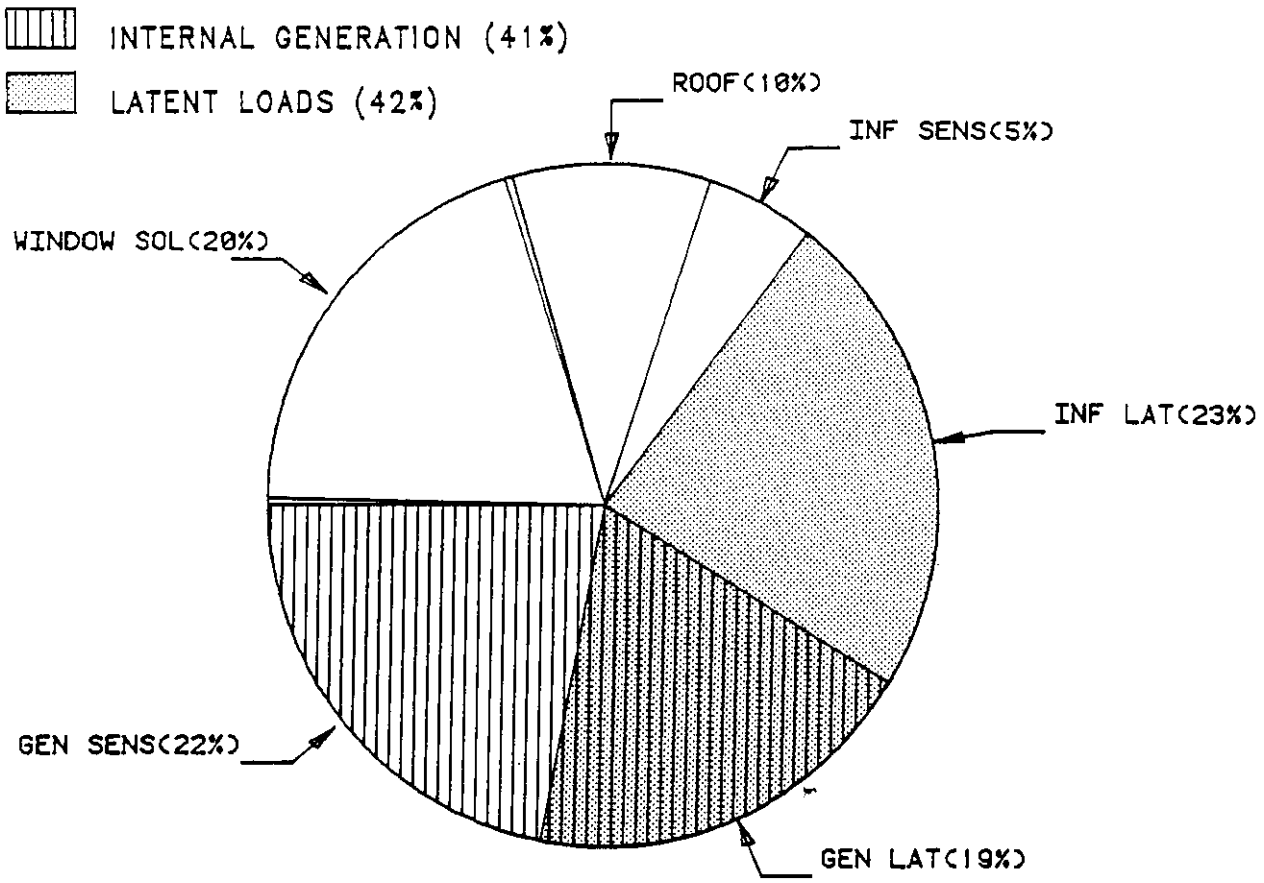

a) Air-conditioner load sources (12.2 kBtu/ft^2)

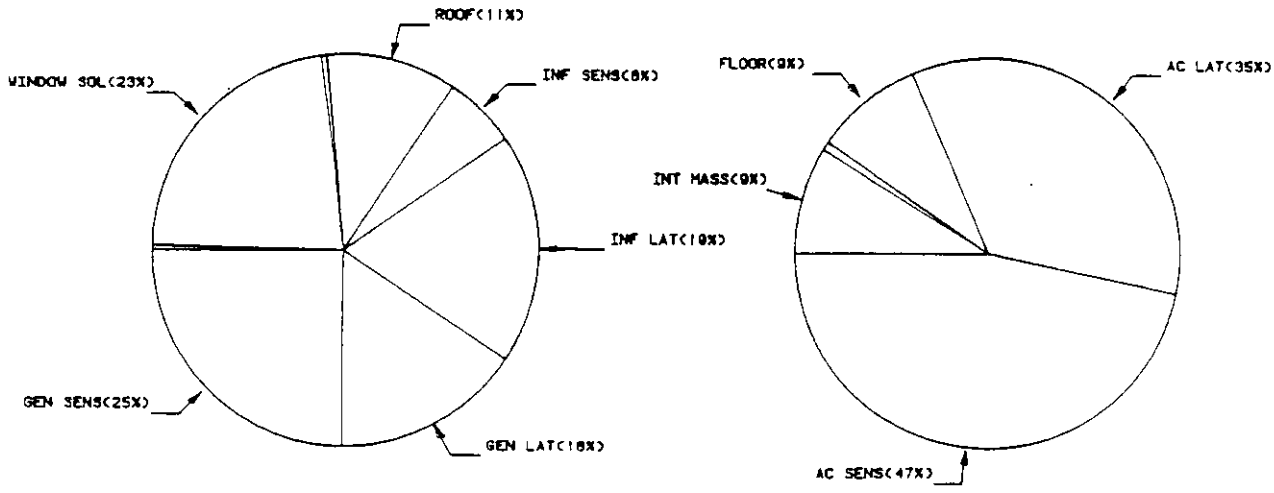

b) Heat gain sources c) Heat removal means

Energy Balance (14.9 kBtu/ft^2)

Figure 4-27 Annual load sources and energy balance for 1500 ft^2 block-passive-radiation cooling house in Orlando, FL at T_{stat}=78^{o}F).

the sky radiation cooling option (BPTR) is selected (Figure 4-27). Accordingly, the envelope and infiltration loads have been reduced from 74% to 56% of the a/c load for the FCTT and BPTT residences, and to 59% for BPTR.

Another shift in load distribution is in latent load. The total latent load (INF+GEN) on the air conditioner changes from 35% for FBTT to 39% for FCTT and BPTT, and moves to 42% when the night sky radiative cooling option is included. If the BP residence is cooled by temperature-controlled natural ventilation, the total latent load becomes 51% of the a/c load. One should note that these load precentages are calculated with a typical air conditioner. Thus, the latent load percentages are slightly misleading because RH varies with control strategy. If a room RH setpoint were maintained the latent load fraction would increase dramatically in the radiator and ventilation runs.

Note that when night sky radiative cooling is being used, the internal building mass is shown in Figures 4-25c and 4-26c to be contributing 9% of the cooling required by the residence **while** the a/c is operating. Window conduction remains a benefit of roughly equal contribution (1% to 2%) for all building types. Roof and wall loads drop from about 15% and 7% of the a/c load to about 10% and 2% respectively for the energy conserving and passive runs.

4.5 COMPARATIVE ANALYSIS

Six different building types have been compared. Three of these (FB, FC, BP) have been examined in nine different climates. These three have been examined in terms of at least two machine types (typical and ideal). Four cooling strategies have been examined: traditional closed building (T), temperature-controlled natural ventilation (V), hybrid night sky radiation cooling (R), and hybrid earth-tube cooling (G). The full set of yearly output reports for the analysis

may be found in Appendix A (GRI copy only). Tables 4-7 give a summary of the annual heating and cooling loads for the full run set.

4.5.1 Building Types

All six building types have been analyzed for Orlando, Florida. The frame basecase residence (FB) and the block basecase residence (BB) are typical of present hot, humid climate construction practices. A number of energy conservation measures have been added to create a frame energy conserving residence (FC) and three different block energy conserving residences (BI, BE and BP). Each residence is fully described in Section 3.4 and summarized in Table 4-7.

To understand the effects of the conservation strategies that were used in the energy conserving buildings, a separate set of parametric annual analyses was performed. Proceeding from the basecase building [FBTT] to the energy conserving building [FCTT], each of the conservation strategies was examined separately and in various combinations. Figure 4-28 gives the results of this analysis. The most interesting phenomenon seen in the analysis is the tendency for the peak month (September) room relative humidity to rise with increases in building thermal efficiency. When all conservation strategies except lowered infiltration are employed (T11), the average September room RH climbs to over 69%. When only reduced infiltration is examained (T12), the peak month RH can be reduced from its basecase value of 65.7% to 63%.

It is also interesting to note the difference in the summer and winter performance of the individual strategies. Three cooling strategies (wall radiant barriers [T02], increased window shading [T04], and decreased internal generation [T10]) produce an increase in the winter heating load (shown as negative heating savings). The individual strategy savings do not necessarily produce additive savings when used in

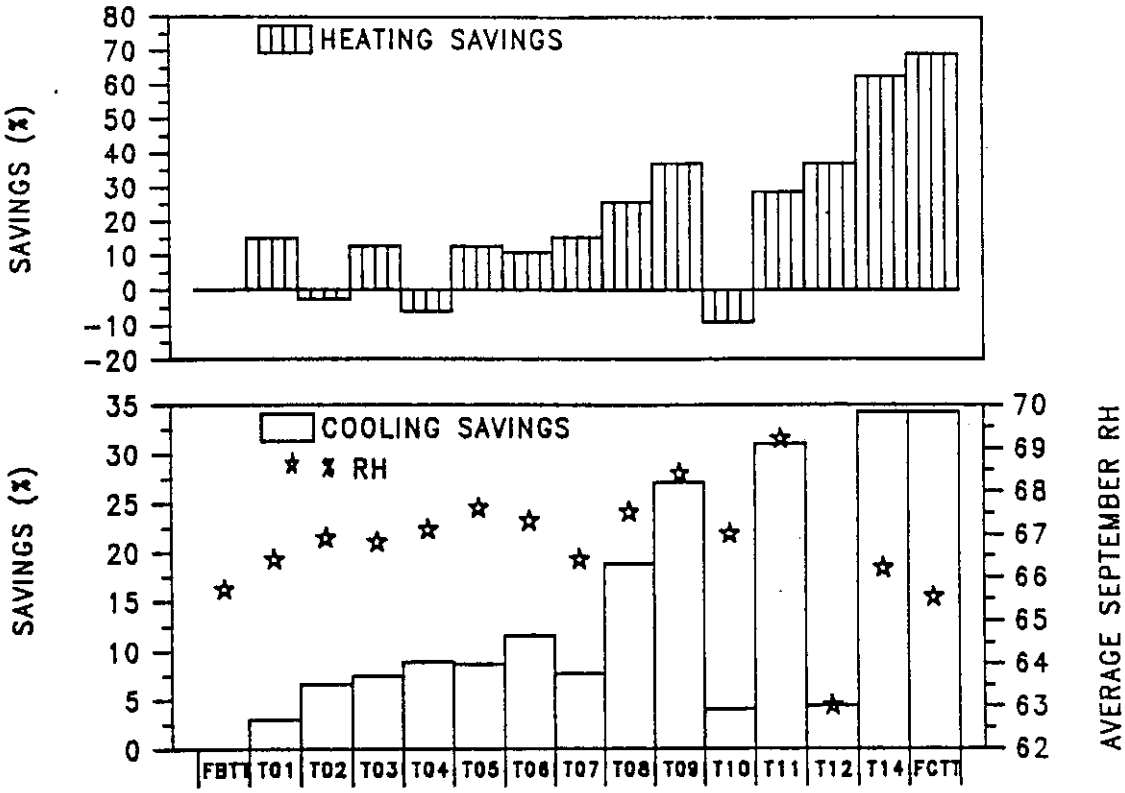

PREDICTED ANNUAL COOLING AND HEATING LOAD SAVINGS
AS PERCENT OF BASE CASE (FBTT) FOR ORLANDO, FLORIDA
FBTT COOLING LOAD = 40.09 MBTU HEATING LOAD = 2.29 MBTU

Nomenclature for Parametric Runs

RUN	DESCRIPTION
FBTT	Frame Base Case Residence
T01	Increased Wall Insulation (from R-11 to R-19)[WI]
T02	Wall Radiant Barriers [WR]
T03	WI + WR
T04	Increased window shading coefficient [SC]
T05	Eliminated East & West Windows (reduce total glass by 84 ft^2)[EW]
T06	SC + EW
T07	Roof Radiant Barrier [RR]
T08	SC + EW + RR
T09	WI + WR + SC + EW + RR
T10	Decreased Internal Load [GEN]
T11	WI + WR + SC + EW + RR + GEN
T12	Decreased Infiltration [INF]
T14	WI + WR + SC + EW + RR + GEN + INF
FCTT	WI + WR+ SC + EW + RR + GEN + INF + Winter Night Insulation

Figure 4-28 Predicted annual cooling and heating load savings as percent of basecase (FBTT) in Orlando, FL (FBTT cooling load = 40.09 MBtu heating load = 2.29 MBtu).

combination. For instance, increasing the window shading coefficient [T04] and eliminating the east and west windows [T05] produce similar summer savings; however, when used in combination the individual savings are not additive. This phenomena also holds for the combination of increased wall insulation [T01] and wall radiant barrier systems [T02] where the increased wall insulation appears to primarily affect the winter savings with no appreciable effect on summer savings. In general, the conservation strategies produced greater heating load savings than cooling load savings. Because of the discrepancy between the total heating and cooling season loads, however, the total cooling season savings for FCTT (13,600 kBtu) are significantly greater than its heating season savings (160 kBtu).

The heating and cooling loads for each building type with the typical machine and traditional cooling strategy (TT) are compared in Figures 4-29 for Orlando. The energy conserving buildings save over 30% of the cooling load and 60% of the heating load of the basecase residence. The block base (BBTT) performance is not as good as the frame base (FBTT), causing about a 10% increase in cooling load. However, the exterior insulated energy conserving block building (BETT) out-performed the frame energy conserving building (FCTT). The passive building, which incorporates the most mass, has the best performance. Overall, there is little difference between energy conserving building types for typical non-vented residences.

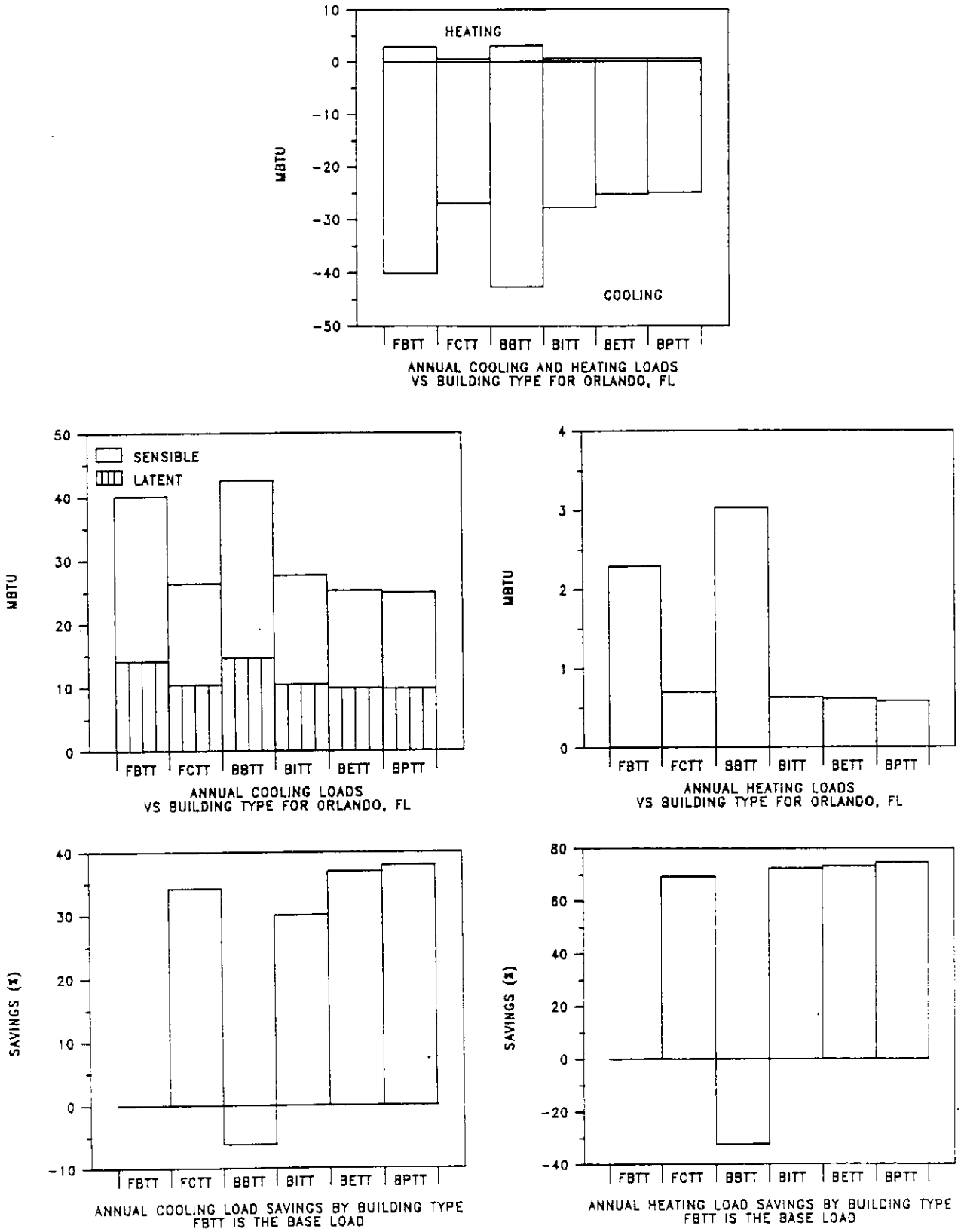

Figure 4-29 Cooling load comparison for six building types in Orlando, FL.

Table 4-7.a

Cooling and Heating Loads for **Atlanta, GA** as Predicted by MADTARP Using TCY Weather Data

Conditioned Bldgs:

FBTT	20.49/6.91(16.38)
NT	19.52/5.94
IT	22.71/9.13
MT	18.26/4.69
FCTT	12.27/4.75(8.96)
NT	11.88/4.36
IT	13.97/6.45
MT	10.85/3.34
BPTT	11.21/4.46(10.26)
NT	11.06/4.32
IT	13.20/6.46
MT	10.04/3.30
BETT	
NT	
IT	
MT	
BITT	
NT	
IT	
MT	
BBTT	
NT	
IT	
MT	

Temp. Vent. Bldgs:

FBTV	16.20/6.76(16.45)
NV	13.43/3.98
IV	21.74/12.30
MV	15.70/6.26
FCTV	8.08/3.91(8.98)
NV	6.52/2.35
IV	15.72/11.55
MV	10.30/6.13
BPTV	5.51/2.75(10.28)
NV	4.58/1.82
IV	14.14/11.38
MV	8.68/5.92
BETV	
ITV	
BTV	

Ground Coupled Bldgs:

BPTG	.20/.12(10.26)
NG	
IG	7.79/7.73
MG	4.62/4.56

Radiator Coupled Bldgs:

BPTR	5.69/2.61(10.29)
NR	
IR	11.04/7.94
MR	6.71/4.32

Enthalpy Vent. Bldgs:

FBTS	16.05/6.10(16.69)
NS	
IS	
MS	
FCTS	9.33/3.94(9.13)
NS	
IS	
MS	
BPTS	8.12/3.46(10.47)
NS	
IS	
MS	

Other bldgs:

FBTE	17.78/6.45(16.64)
FCTE	10.63/4.43(9.09)
BPTE	9.29/3.85(10.45)
FBTV	C01

Parametric Bldgs:

FBTT	76	26.54/8.49
	80	14.46/5.62
	82	11.10/4.32
	WA	
	RA	
BPTT	E01	
	E02	
	E05	
BPTV	E01	
	E02	
	E05	
	E04	
BPTV	A07	
	A30	
	A60	
FBTE	80	12.91/5.13
	82	
TS	80	11.56/4.81
	82	7.42/3.48

Parametric Code:
76
80 = Set points
82

*The first number given is the total cooling load in MBtu. It is followed by a slash (/) and the latent cooling load in MBtu. In parenthesis ( ) is the heating load for the base building in each category of runs.

Table 4-7.b

Cooling and Heating Loads for **Baltimore, MD** as Predicted by MADTARP Using TCY Weather Data

Conditioned Bldgs:

FBTT	15.73/5.12(32.84)
MT	
IT	17.28/6.67
MT	
FCTT	8.98/3.39(19.56)
MT	
IT	10.39/4.81
MT	
BPTT	7.99/3.14(22.52)
MT	
IT	9.61/4.76
MT	
BETT	
MT	
IT	
MT	
BITT	
MT	
IT	
MT	
BBTT	
MT	
IT	
MT	

Temp. Vent. Bldgs:

FBTV	12.20/4.87(32.92)
MV	
IV	16.44/9.12
MV	
FCTV	6.06/2.84(19.58)
MV	
IV	11.67/8.45
MV	
BPTV	4.17/2.08(22.53)
MV	
IV	10.36/8.28
MV	
BETV	
ITV	
BTV	

Ground Coupled Bldgs:

BPTG	0.0/0.0(22.53)
NG	
IG	
MG	

Radiator Coupled Bldgs:

BPTR	4.09/1.84
NR	
IR	8.06/5.78
MR	

Enthalpy Vent. Bldgs:

FBTS	
NS	
IS	
MS	
FCTS	
NS	
IS	
MS	
BPTS	
NS	
IS	
MS	

Other bldgs:

FBTE	
FCTE	
BPTE	
FBTV	C01

Parametric Bldgs:

FBTT	76	
	80	
	82	
	WA	
	RA	
BPTT	E01	
	E02	
	E05	
BPTV	E01	
	E02	
	E05	
	E04	
BPTV	A07	
	A30	
	A60	
FBTE	80	
	82	
TS	80	
	82	

Parametric Code:

*The first number given is the total cooling load in MBtu. It is followed by a slash (/) and the latent cooling load in MBtu. In parenthesis ( ) is the heating load for the base building in each category of runs.

Table 4-7.c

Cooling and Heating Loads for **Charleston, SC** as Predicted by MADTARP Using TCY Weather Data

Conditioned Bldgs:

FBTT 27,28/10,23(10,11)
NT
IT 32,41/15,36
MT

FCTT 17,10/7,14(4,83)
NT
IT 20,86/10,89
MT

BPTT 16,30/6,93(5,38)
NT
IT 20,33/10,96
MT

BETT
NT
IT
MT

BITT
NT
IT
MT

BBTT
NT
IT
MT

Temp. Vent. Bldgs:

FBTV 23,80/10,81(10,21)
NV
IV 34,20/21,22
MV

FCTV 13,00/6,74(4,88)
NV
IV 25,46/19,21
MV

BPTV 10,05/5,39(5,42)
NV
IV 23,63/18,98
MV

BETV
ITV
BTV

Ground Coupled Bldgs:

BPTG 3,40/1,97(5,38)
NG
IG
MG

Radiator Coupled Bldgs:

BPTR 11,92/5,43
NR
IR 18,77
MR

Enthalpy Vent. Bldgs:

FBTS 24,57/9,92(10,60)
NS
IS
MS

FCTS
NS
IS
MS

BPTS
NS
IS
MS

Other bldgs:

FBTE 25,72/10,00(10,55)
FCTE
BPTE

FBTV C01

Parametric Bldgs:

FBTT 76
80
82
WA
RA

BPTT E01
E02
E05
BPTV E01
E02
E05
E04
BPTV A07
A30
A60

FBTE 80 19,70/8,34(10,59)
82 14,28/6,55(10,60)
TS 80 18,40/8,10(10,61)
82 13,21/6,40(10,61)

Parametric Code:
76
80 = Set points
82

*The first number given is the total cooling load in MBtu. It is followed by a slash (/) and the latent cooling load in MBtu. In parenthesis ( ) is the heating load for the base building in each category of runs.

Table 4-7.d

Cooling and Heating Loads for **Dallas, TX** as Predicted by MADTARP Using TCY Weather Data

Conditioned Bldgs:		**Temp. Vent. Bldgs:**		**Enthalpy Vent. Bldgs:**		**Parametric Bldgs:**	
FBTT	33.89/9.95(11.41)	FBTV	31.05/10.22(11.51)	FBTS		FBTT 76	
NT		NV		NS		80	
IT	35.35/11.41	IV	34.24/13.41	IS		82	
MT		MV		MS		WA	
FCTT	21.20/6.96(5.81)	FCTV	18.69/6.97(5.86)	FCTS		RA	
NT		NV		NS			
IT	22.47/8.23	IV	23.68/11.96	IS		BPTT E01	
MT		MV		MS		E02	
BPTT	20.58/6.78(6.48)	BPTV	17.39/6.47(6.55)	BPTS		E05	
NT		NV		NS		BPTV E01	
IT	22.03/8.23	IV	22.74/11.82	IS		E02	
MT		MV		MS		E05	
BETT		BETV		**Other bldgs:**		E04	
NT		ITV		FBTE		BPTV A07	
IT		BTV		FCTE		A30	
MT				BPTE		A60	
BITT		**Ground Coupled Bldgs:**					
NT		BPTG	10.95/4.04(6.51)	FBTV C01		FBTE 80	
IT		NG				82	
MT		IG		**Parametric Code:**		TS 80	
BBTT		MG				82	
NT		**Radiator Coupled Bldgs:**					
IT		BPTR	13.59/5.03				
MT		NR					
		IR	18.25/9.70				
		MR					

*The first number given is the total cooling load in MBtu. It is followed by a slash (/) and the latent cooling load in MBtu. In parenthesis ( ) is the heating load for the base building in each category of runs.

Table 4-7.h

Cooling and Heating Loads for **Houston, TX** as Predicted by MADTARP Using TCY Weather Data

Conditioned Bldgs:		**Temp. Vent. Bldgs:**		**Enthalpy Vent. Bldgs:**		**Parametric Bldgs:**		
FBTT	35,30/12,90(7,12)	FBTV	32,12/13,99(7,22)	FBTS	31,86/12,11(7,65)	FBTT	76	44,01/15,49
NT	34,36/11,96	NV	27,42/9,28	NS			80	27,91/10,77
IT	41,38/18,97	IV	43,49/25,36	IS			82	21,35/8,66
MT	34,21/11,81	MV	33,62/15,49	MS			WA	
							RA	
FCTT	23,10/9,13(3,32)	FCTV	19,56/9,52(3,37)	FCTS				
NT	22,83/8,85	NV	16,29/6,24	NS		BPTT	E01	
IT	27,42/13,44	IV	32,69/22,65	IS			E02	
MT	22,26/8,29	MV	24,08/14,04	MS			E05	
						BPTV	E01	
BPTT	22,54/8,96(3,63)	BPTV	17,24/8,52(3,68)	BPTS			E02	
NT	22,52/8,94	NV	14,63/5,90	NS			E05	
IT	27,19/13,61	IV	31,20/22,48	IS			E04	
MT	21,97/8,39	MV	22,53/13,80	MS		BPTV	A07	
							A30	
BETT		BETV		**Other bldgs:**			A60	
NT		ITV		FBTE	33,44/12,57(748)			
IT		BTV		FCTE		FBTE	80	
MT				BPTE			82	
		Ground Coupled Bldgs:				TS	80	
BITT		BPTG	20,99/8,37(3,63)	FBTV	C01		82	
NT		NG						
IT		IG	26,30/13,68					
MT		MG	21,08/ 8,46					
		Radiator Coupled Bldgs:						
BBTT		BPTR	17,08/7,29(3,67)					
NT		NR						
IT		IR	24,83/15,02					
MT		MR	17,14/ 9,38					

Parametric Code:
76
80 = Set points
82

*The first number given is the total cooling load in MBtu. It is followed by a slash (/) and the latent cooling load in MBtu. In parenthesis ( ) is the heating load for the base building in each category of runs.

Table 4-7.m

Cooling and Heating Loads for **Miami, FL** as Predicted by MADTARP Using TCY Weather Data

Conditioned Bldgs:		**Temp. Vent. Bldgs:**		**Enthalpy Vent. Bldgs:**		**Parametric Bldgs:**		
FBTT	54.76/19.41(0.29)	FBTV	46.25/18.96(0.31)	FBTS	48.55/18.17(0.40)	FBTT	76	67.82/23.01
NT	53.6218.27	NV	41.44/14.15	NS			80	43.03/16.28
IT	58.45/23.10	IV	56.71/29.42	IS			82	32.21/12.98
MT	50.02/14.67	MV	45.35/18.06	MS			WA	
							RA	
FCTT	37.65/14.28(0.03)	FCTV	29.50/13.18(0.03)	FCTS				
NT	37.31/13.93	NV	26.26/9.94	NS		BPTT	E01	
IT	40.81/17.44	IV	42.11/25.79	IS			E02	
MT	34.73/11.36	MV	32.36/16.05	MS			E05	
						BPTV	E01	
BPTT	36.61/14.04(0.00)	BPTV	26.43/11.85(0.01)	BPTS			E02	
NT	36.63/14.06	NV	24.05/9.47	NS			E05	
IT	39.97/17.40	IV	40.06/25.48	IS			E04	
MT	33.89/11.32	MV	30.30/15.72	MS		BPTV	A07	
							A30	
BETT		BETV		**Other bldgs:**			A60	
NT		ITV		FBTE	51.08/18.74(0.37)			
IT		BTV		FCTE		FBTE	80	
MT				BPTE			82	
		Ground Coupled Bldgs:				TS	80	
BITT		BPTG	36.57/14.03(.00)	FBTV	C01		82	
NT		NG						
IT		IG	39.94/17.40	**Parametric Code:**				
MT		MG	33.86/11.32	76				
		Radiator Coupled Bldgs:		80 = Set points				
BBTT		BPTR	23.86/10.37(0.02)	82				
NT		NR						
IT		IR	32.46/18.95					
MT		MR	23.99/13.07					

*The first number given is the total cooling load in MBtu. It is followed by a slash (/) and the latent cooling load in MBtu. In parenthesis ( ) is the heating load for the base building in each category of runs.

Table 4-7.n

Cooling and Heating Loads for **New Orleans, LA** as Predicted by MADTARP Using TCY Weather Data

Conditioned Bldgs:

FBTT	32.55/12.19(5.12)
NT	
IT	37.65/17.29
MT	
FCTT	20.46/8.44(2.11)
NT	
IT	24.61/12.59
MT	
BPTT	19.72/8.21(2.25)
NT	
IT	24.23/12.72
MT	
BETT	
NT	
IT	
MT	
BITT	
NT	
IT	
MT	
BBTT	
NT	
IT	
MT	

Temp. Vent. Bldgs:

FBTV	28.93/13.14(5.22)
NV	
IV	40.45/24.66
MV	
FCTV	16.63/8.55(2.14)
NV	
IV	30.27/22.18
MV	
BPTV	14.14/7.45(2.27)
NV	
IV	28.69/22.00
MV	
BETV	
ITV	
BTV	

Ground Coupled Bldgs:

BPTG	10.44/4.91(2.26)
NG	
IG	
MG	

Radiator Coupled Bldgs:

BPTR	15.66/6.92(2.31)
NR	
IR	22.44/13.68
MR	

Enthalpy Vent. Bldgs:

FBTS	
NS	
IS	
MS	
FCTS	
NS	
IS	
MS	
BPTS	
NS	
IS	
MS	

Other bldgs:

FBTE	
FCTE	
BPTE	
FBTV	C01

Parametric Bldgs:

FBTT	76	
	80	
	82	
	WA	
	RA	
BPTT	E01	
	E02	
	E05	
BPTV	E01	
	E02	
	E05	
	E04	
BPTV	A07	
	A30	
	A60	
FBTE	80	
	82	
TS	80	
	82	

Parametric Code:

*The first number given is the total cooling load in MBtu. It is followed by a slash (/) and the latent cooling load in MBtu. In parenthesis ( ) is the heating load for the base building in each category of runs.

Table 4-7.o

Cooling and Heating Loads for **Orlando, FL** as Predicted by MADTARP Using TCY Weather Data

Conditioned Bldgs:		**Temp. Vent. Bldgs:**		**Enthalpy Vent. Bldgs:**		**Parametric Bldgs:**		
FBTT	40.09/14.11(2.29)	FBTV	34.87/15.43(2.36)	FBTS	35.83/13.36(2.53)	FBTT	76	50.32/16.90
NT	38.65/12.67	NV	28.31/8.87	NS			80	31.35/11.79
IT	44.27/18.28	IV	46.48/27.03	IS			82	23.75/9.50
MT	37.30/11.31	MV	36.06/16.62	MS			WA	39.62/14.02
							RA	39.16/13.92
FCTT	26.36/10.38(0.70)	FCTV	20.21/10.17(0.72)	FCTS	23.13/9.34(0.80)			
NT	25.60/9.61	NV	15.87/5.83	NS		BPTT	E01	24.86/9.71
IT	29.46/13.48	IV	34.90/24.86	IS			E02	24.87/9.72
MT	24.38/8.40	MV	25.71/15.67	MS			E05	24.98/9.84
						BPTV	E01	16.98/9.05
BPTT	24.87/9.72(0.58)	BPTV	16.37/8.48(0.61)	BPTS	21.95/8.88(0.69)		E02	18.46/10.57
NT	24.78/9.63	NV	13.09/5.20	NS			E05	
IT	28.64/13.50	IV	32.38/24.50	IS			E04	19.96/12.07
MT	23.51/8.37	MV	23.14/15.25	MS		BPTV	A07	17.48/8.68
							A30	15.63/8.32
BETT	25.24/9.82(0.61)	BETV	18.32/9.36(0.80)	**Other bldgs:**			A60	15.24/8.24
NT		ITV	21.31/10.58(0.65)	FBTE	37.34/13.60(2.48)			
IT		BTV	35.69/15.36(3.09)	FCTE	24.54/9.90(0.76)	FBTE	80	29.08/11.36
MT				BPTE	23.28/9.26(0.65)		82	
		Ground Coupled Bldgs:				TS	80	27.79/11.16
BITT	27.67/10.43(0.63)	BPTG	21.44/8.52(0.58)	FBTV	C01 34.83/15.43(2.35)		82	20.51/8.89
NT		NG						
IT		IG	26.61/13.69	**Parametric Code:**				
MT		MG	21.47/ 8.55	E01: ESAM = 1.0				C01: Convergence
		Radiator Coupled Bldgs:		02: = 2.0				= 0.01,0.001,
BBTT	42.56/14.63(3.03)	BPTR	18.27/7.78(0.63)	05: = 5.0				0.034,15
NT		NR		A07: ACH = 7.5				76
IT		IR	25.38/14.88	30: = 30				80 = Set points
MT		MR	18.13/ 9.63	60: = 60				82

*The first number given is the total cooling load in MBtu. It is followed by a slash (/) and the latent cooling load in MBtu. In paranthesis ( ) is the heating load for the base building in each category of runs.

Table 4-7.s

Cooling and Heating Loads for **St. Louis, MO** as Predicted by MADTARP Using TCY Weather Data

Conditioned Bldgs:

FBTT	16.64/4.92(34.79)
NT	
IT	17.09/5.36
MT	
FCTT	9.54/3.33(20.97)
NT	
IT	10.12/3.91
MT	
BPTT	8.54/3.10(24.17)
NT	
IT	9.30/3.86
MT	
BETT	
NT	
IT	
MT	
BITT	
NT	
IT	
MT	
BBTT	
NT	
IT	
MT	

Temp. Vent. Bldgs:

FBTV	12.70/4.59(34.87)
NV	
IV	15.25/7.14
MV	
FCTV	6.23/2.65(20.99)
NV	
IV	10.31/6.73
MV	
BPTV	4.40/1.98(24.19)
NV	
IV	8.99/6.56
MV	
BETV	
ITV	
BTV	

Ground Coupled Bldgs:

BPTG	0.01/.00(24.18)
NG	
IG	
MG	

Radiator Coupled Bldgs:

BPTR	3.68/24.19
NR	
IR	7.06/4.99
MR	

Enthalpy Vent. Bldgs:

FBTS	
NS	
IS	
MS	
FCTS	
NS	
IS	
MS	
BPTS	
NS	
IS	
MS	

Other bldgs:

FBTE	
FCTE	
BPTE	
FBTV	C01

Parametric Bldgs:

FBTT	76	
	80	
	82	
	WA	
	RA	
BPTT	E01	
	E02	
	E05	
BPTV	E01	
	E02	
	E05	
	E04	
BPTV	A07	
	A30	
	A60	
FBTE	80	
	82	
TS	80	
	82	

Parametric Code:

*The first number given is the total cooling load in MBtu. It is followed by a slash (/) and the latent cooling load in MBtu. In paranthesis ( ) is the heating load for the base building in each category of runs.

4.5.2 Climate Effects

One of the major differences in the climates is the length of the seasons. Cities in the hot, humid climates have short heating seasons and long cooling seasons, whereas the opposite is true for the moderate climate cities. The long seasons lead to significant differences in the annual cooling and heating loads as shown in Figures 4-30 and 4-31 for the basecase residence. Miami has the highest cooling load at 54.8 MBtu. Orlando, Houston, Dallas and New Orleans have 32 to 40 MBtu loads. Charleston is a little less at 27.3 MBtu. Atlanta, St. Louis and Baltimore each have loads less than 21 MBtu. The order presented in this histogram, decreasing annual cooling load, will be maintained for other figures in this section. Comparisons are easier to make by having the order consistent.

St. Louis and Baltimore have basecase heating loads of over 30 MBtu, but all other cities have mild heating loads -- less than 20 MBtu as shown in Figure 4-31.

Various comparisons of the heating and cooling loads for each city are given in Figures 4-32 through 4-34. The cooling load in Miami is larger than the combined heating and cooling load in any other city as shown in Figure 4-32. The variation in the total load is relatively small (<20 MBtu). Figure 4-33 shows the heating and cooling loads for each city with the cooling load represented as negative. The algebraic sum of the heating (positive) and cooling (negative) loads, Figure 4.34, shows that all the cities but St. Louis and Baltimore are cooling-load dominated.

Despite the heating load being less, the cost to heat the residence using electric resistance heat (COP=1.0) can be more than the cost for cooling using the typical basecase air conditioner. Figure 4-35 shows the electric use and cost of conditioning the residence at 10c/kWh. At a heating COP=1.0

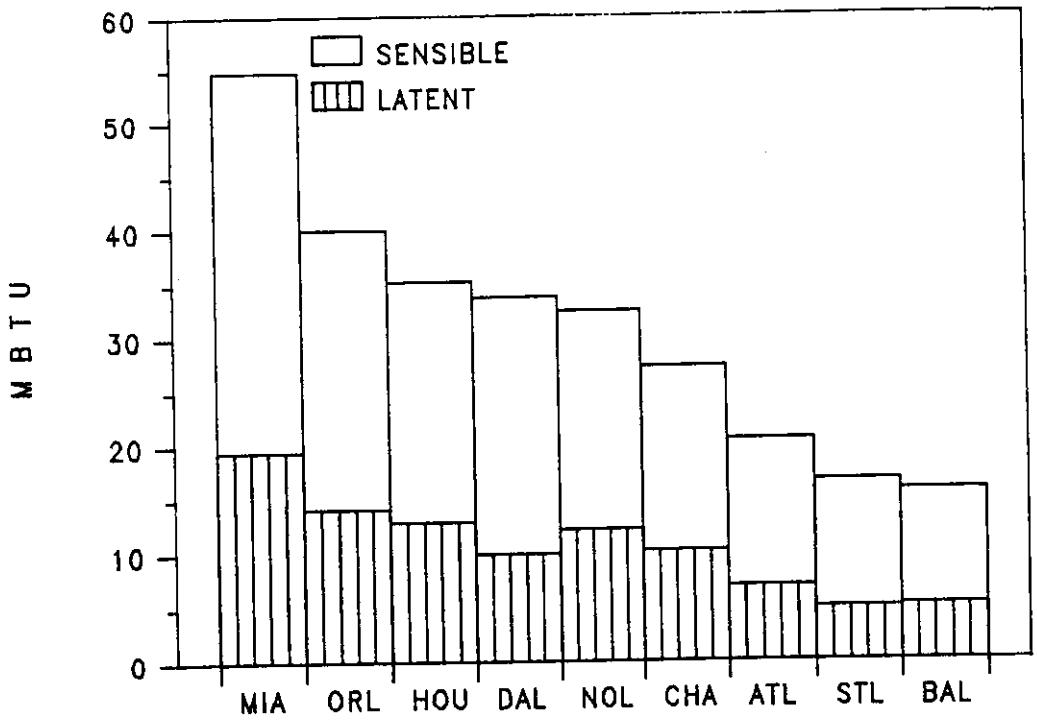

Figure 4-30 Annual cooling load for basecase frame residence in nine climates at $T_{stat}=78^{o}F$.

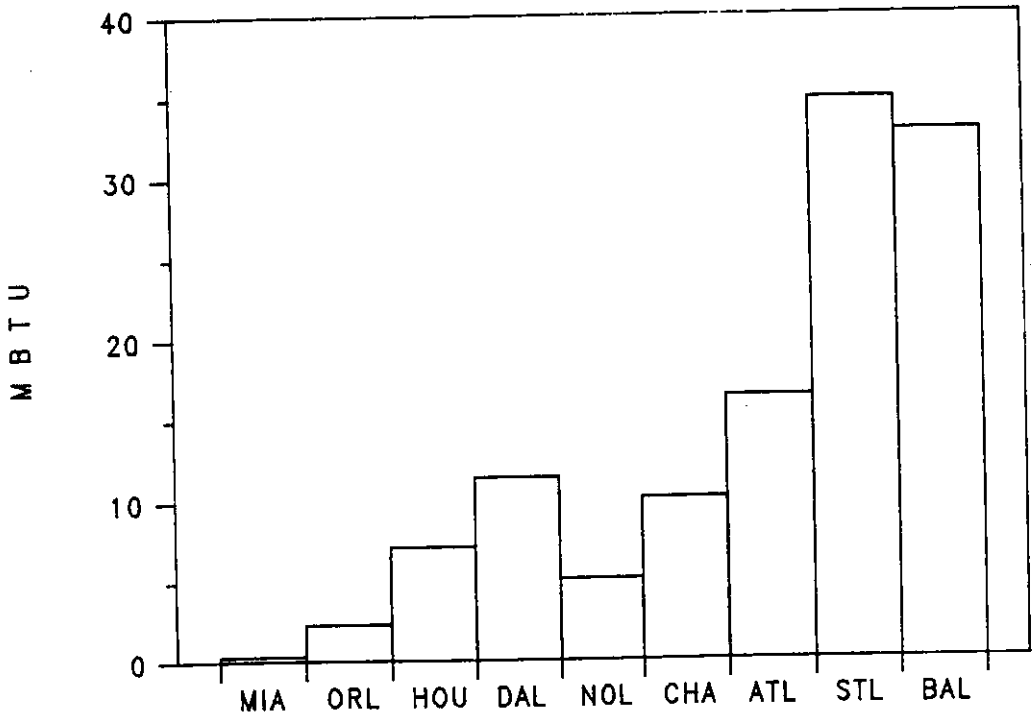

Figure 4-31 Annual heating load for basecase frame residence in nine climates at $T_{stat}=68^{o}F$.

the heating costs is more than $200/year (200 MWh) for all cities but Miami, Orlando, New Orleans and Houston. The cooling electric use ranges from 200 to 600 MWh (or $200-$600 at $0.10/kWh). Figure 4-36 indicates the total annual electric use if a heatpump or other high performance heater with a seasonal COP=2.0 is used. In this case cooling is a much larger part of the total electric usage and cost. The cost of the conditioning would also apply to high efficiency heaters with alternative energy sources with lower COPs (0.8-1.0) and fuel cost equivalents of 40% to 50% that of electricity at $0.10/kWh (for example, 90% efficient gas furnace with gas costs at $13.15/MBtu).

The order of cities changes significantly when comparing peak month or peak hour cooling loads, as shown in Figures 4-37 and 4-38. Miami, where surrounding water bodies prohibit excessively high maximum daily temperatures, has the lowest peak hour load of the nine cities.

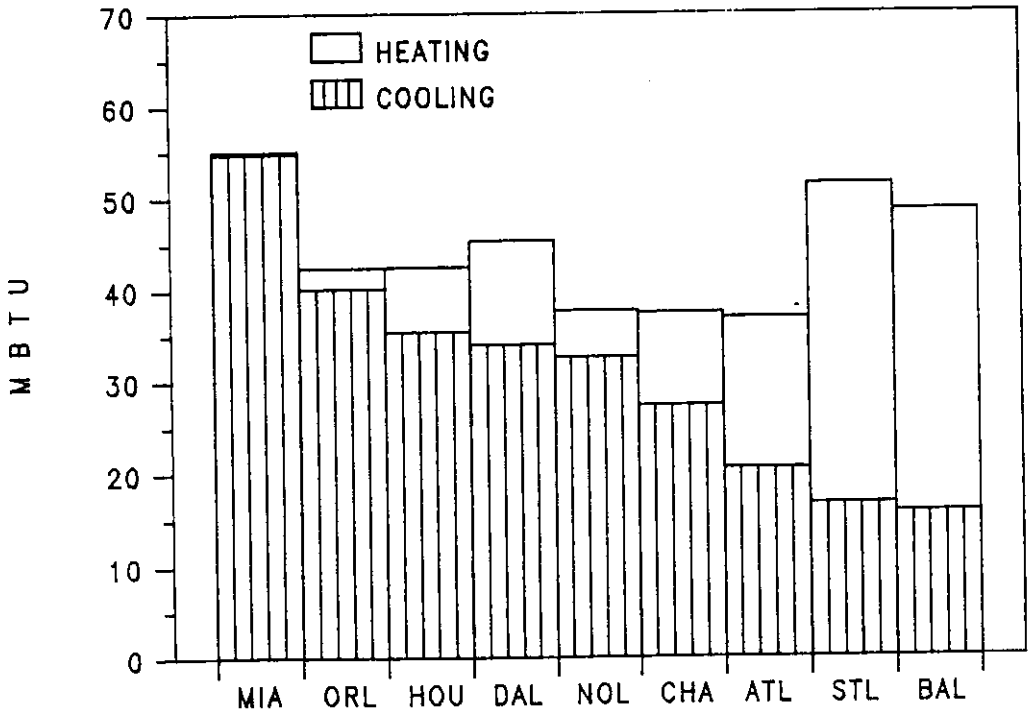

Figure 4-32 Annual cooling and total loads for basecase frame residence in nine climates at T_{stat}=68°F and 78°F.

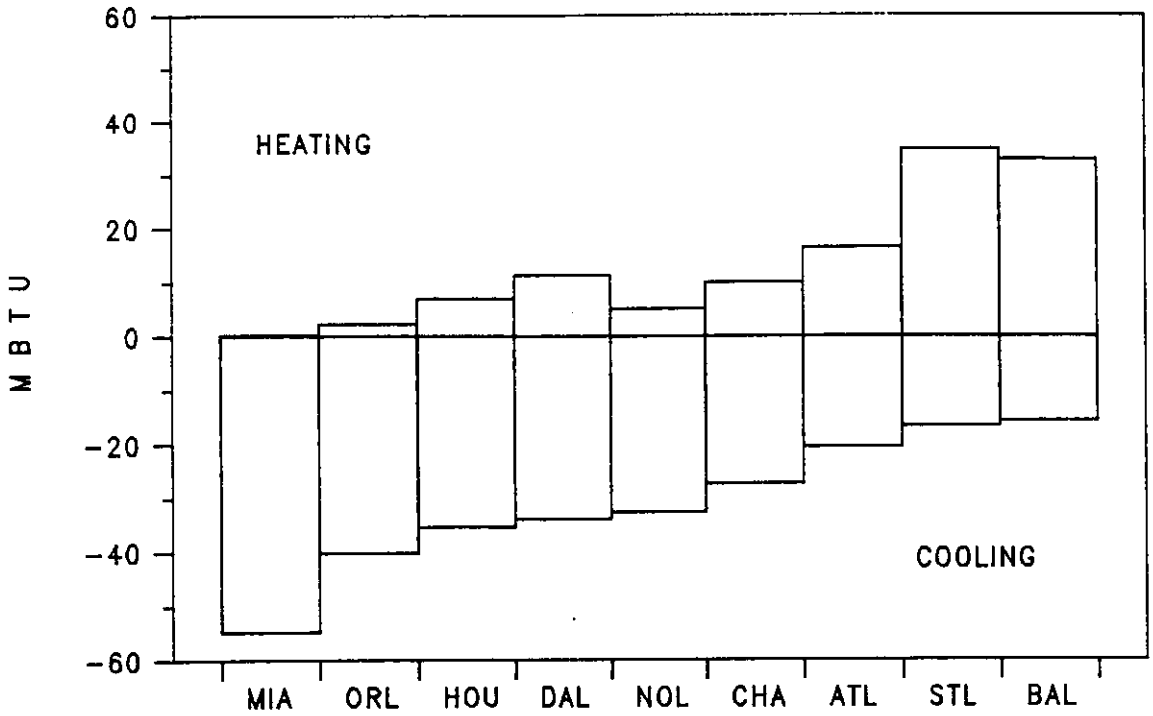

Figure 4-33 Annual cooling and heating loads for basecase frame residence in nine climates at T_{stat}=68°F and 78°F.

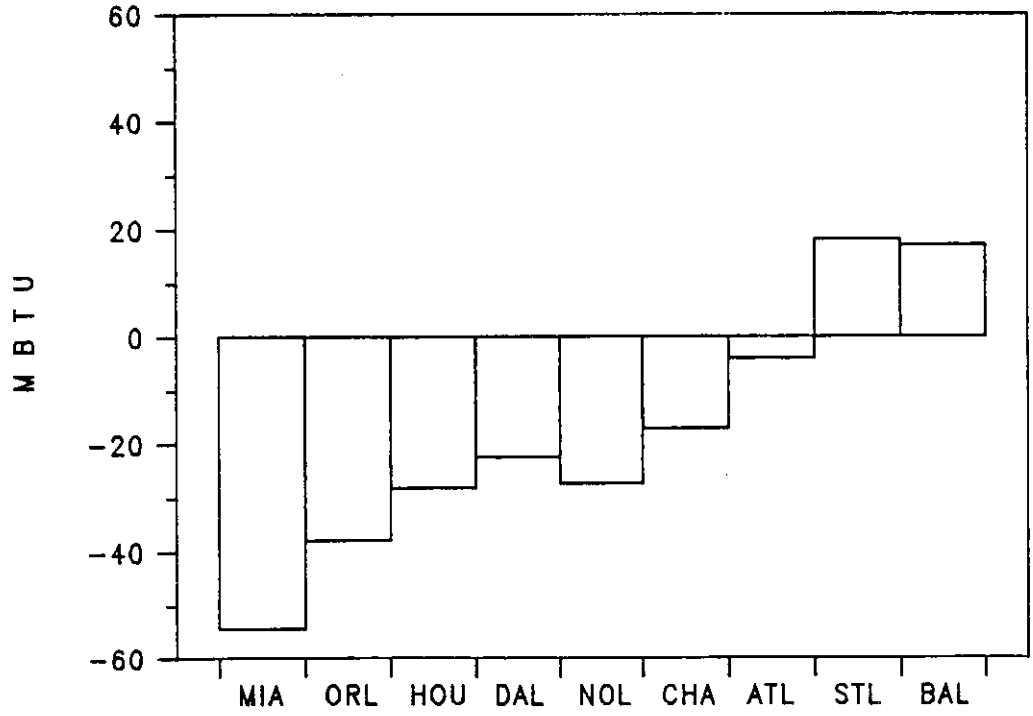

Figure 4-34 Sum of annual loads for basecase frame residence in nine climates at T_{stat}=68°F and 78°F.

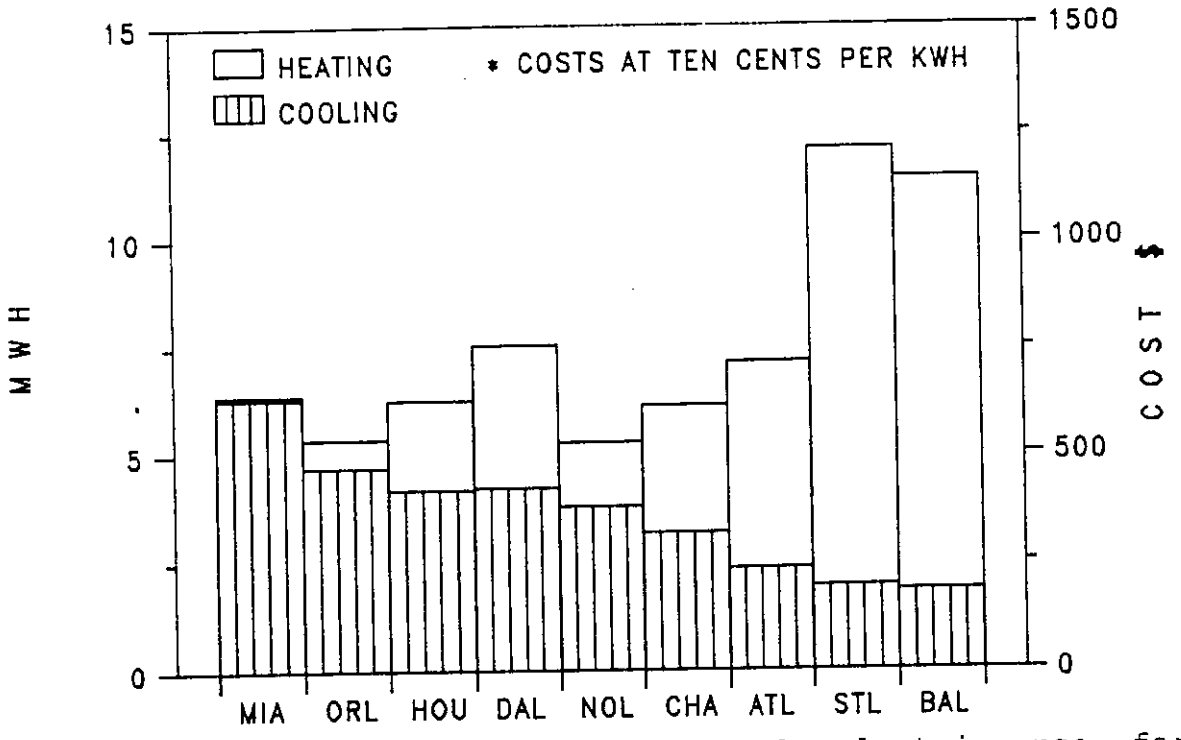

Figure 4-35 Annual cooling and total electric use for basecase frame residence in nine climates $T_{stat}=68^{o}F$ and $78^{o}F$ (heating COP=1.0).

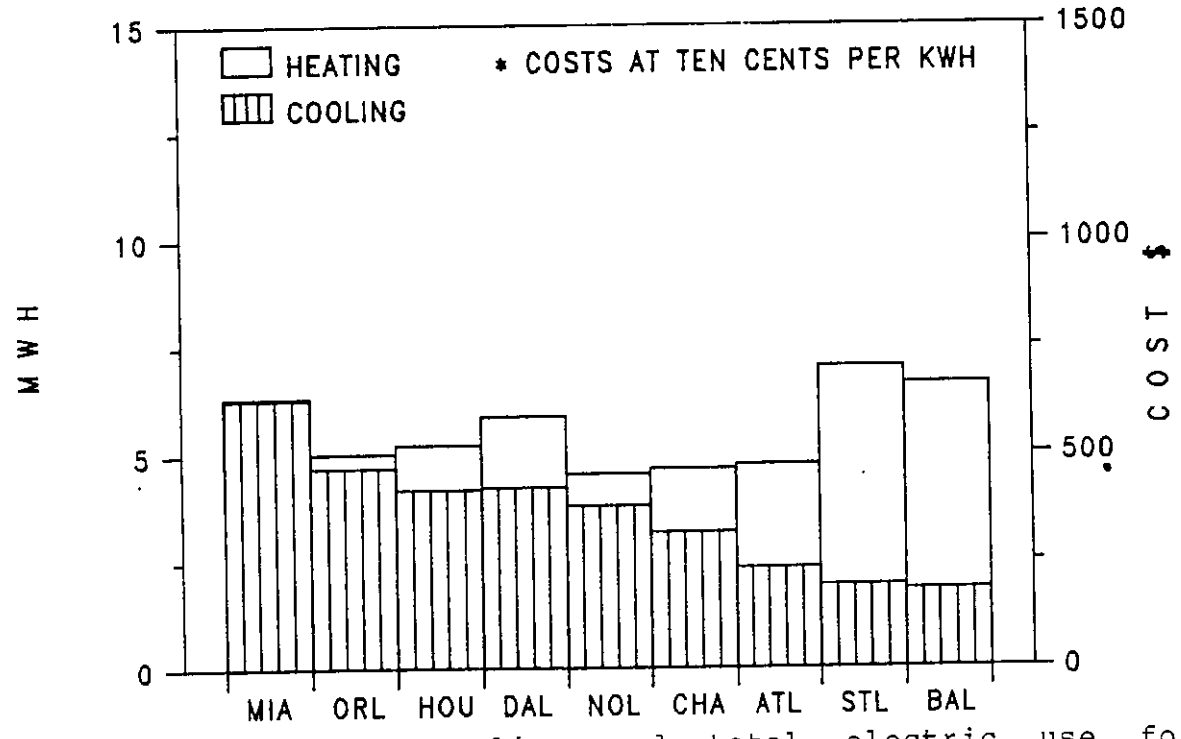

Figure 4-36 Annual cooling and total electric use for basecase frame residence in nine climates $T_{stat}=68^{F}$ and $78^{o}F$ (heating COP=2.0).

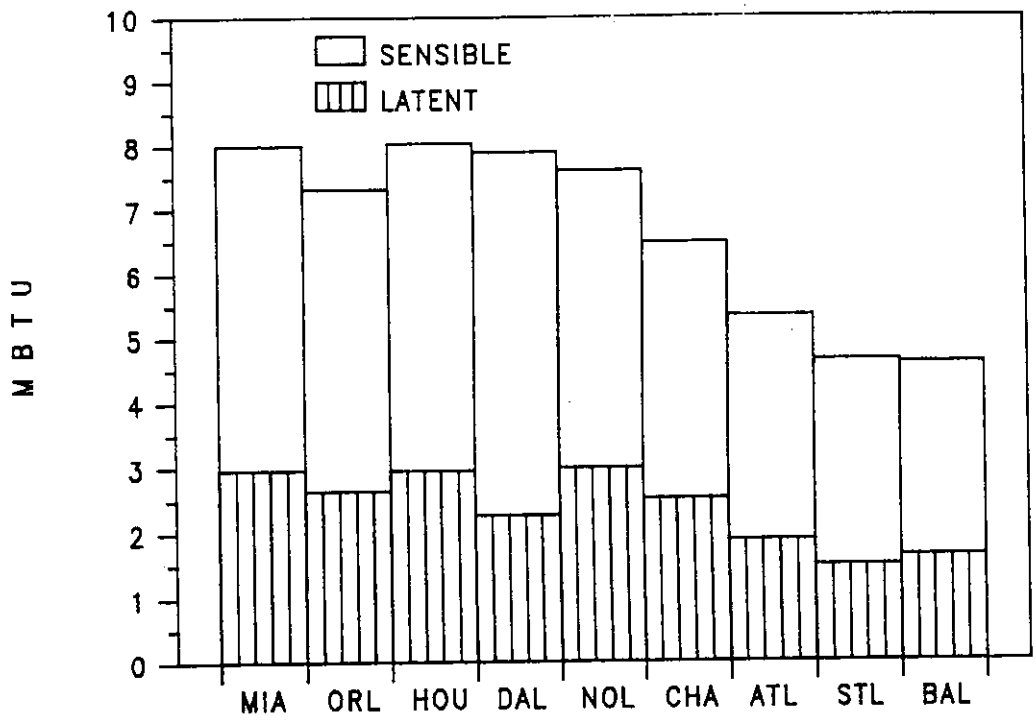

Figure 4-37 Peak month cooling load for basecase frame residence at $T_{stat}=78^{o}F$.

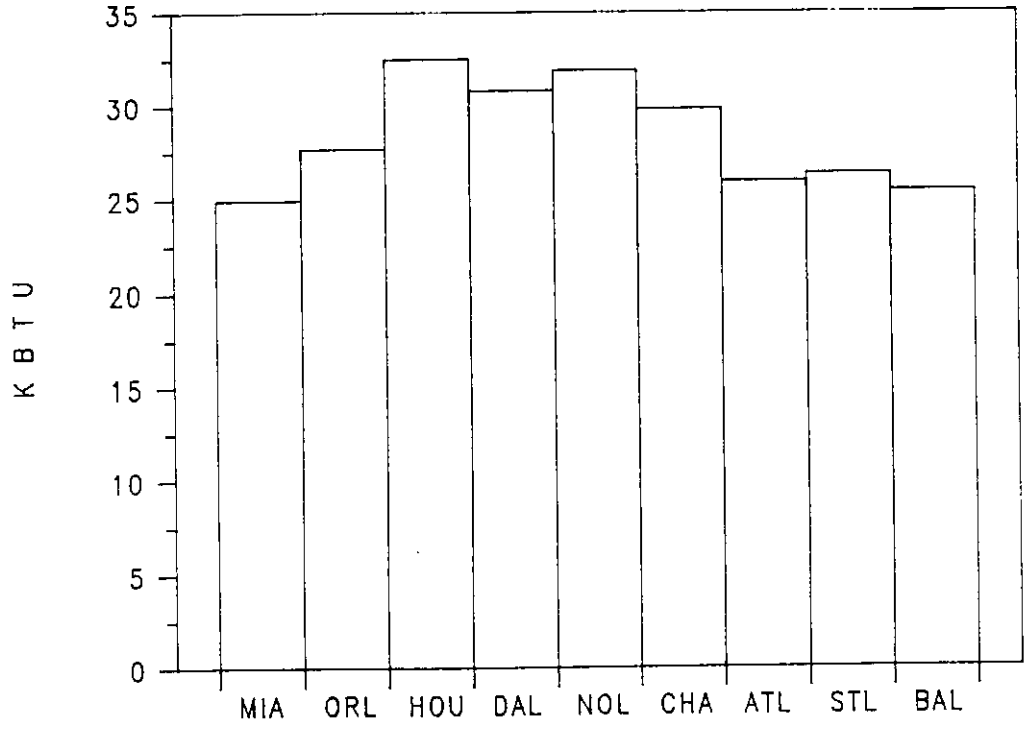

Figure 4-38 Peak hour cooling load for basecase frame residence at $T_{stat}=78^{o}F$.

A new way of presenting the total cooling load as a function of climatic variables is shown in Figures 4-39 through 4-42 for the four climates of Atlanta, Houston, Miami and Orlando. These again are from MADTARP runs of the unvented basecase house. The top graph in each figure is the percentage of the cumulative annual cooling load as a function of outdoor air temperature. The bottom graph shows the percentage of the cumulative cooling load with respect to the enthalpy of the outdoor air. From these graphs one can answer various climate-related questions like "What percentage of the total cooling load occurs below an air temperature of, say, 80°F?" The answer for Atlanta for a house maintained at 78°F is about 47%. One can also determine that cooling loads for the unvented house maintained at 78°F begin at about 68°F outdoor air temperature. From these graphs one can also get a feel for the severity of the climate in terms of heat and humidity (enthalpy). While the drybulb reaches above 93°F in all climates, the outdoor enthalpy rarely exeeds 40 Btu/lb in Atlanta, but in Houston a full 25% of the cooling load occurs above an enthalpy of 40 Btu/lb.

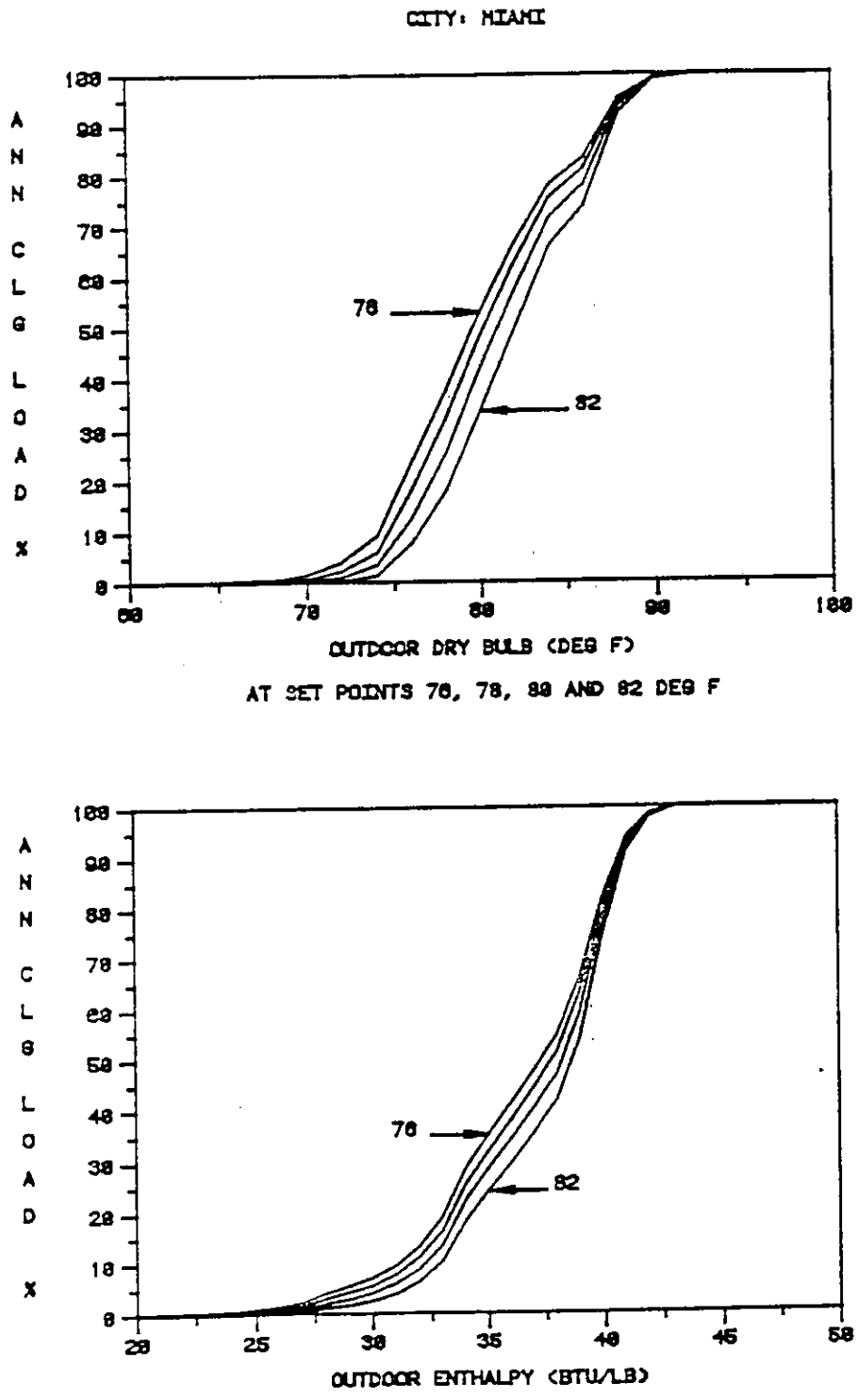

Figure 4-39 Cumulative cooling load for Miami, FL as a function of ambient dry-bulb temperature (top) and ambient enthalpy (bottom).

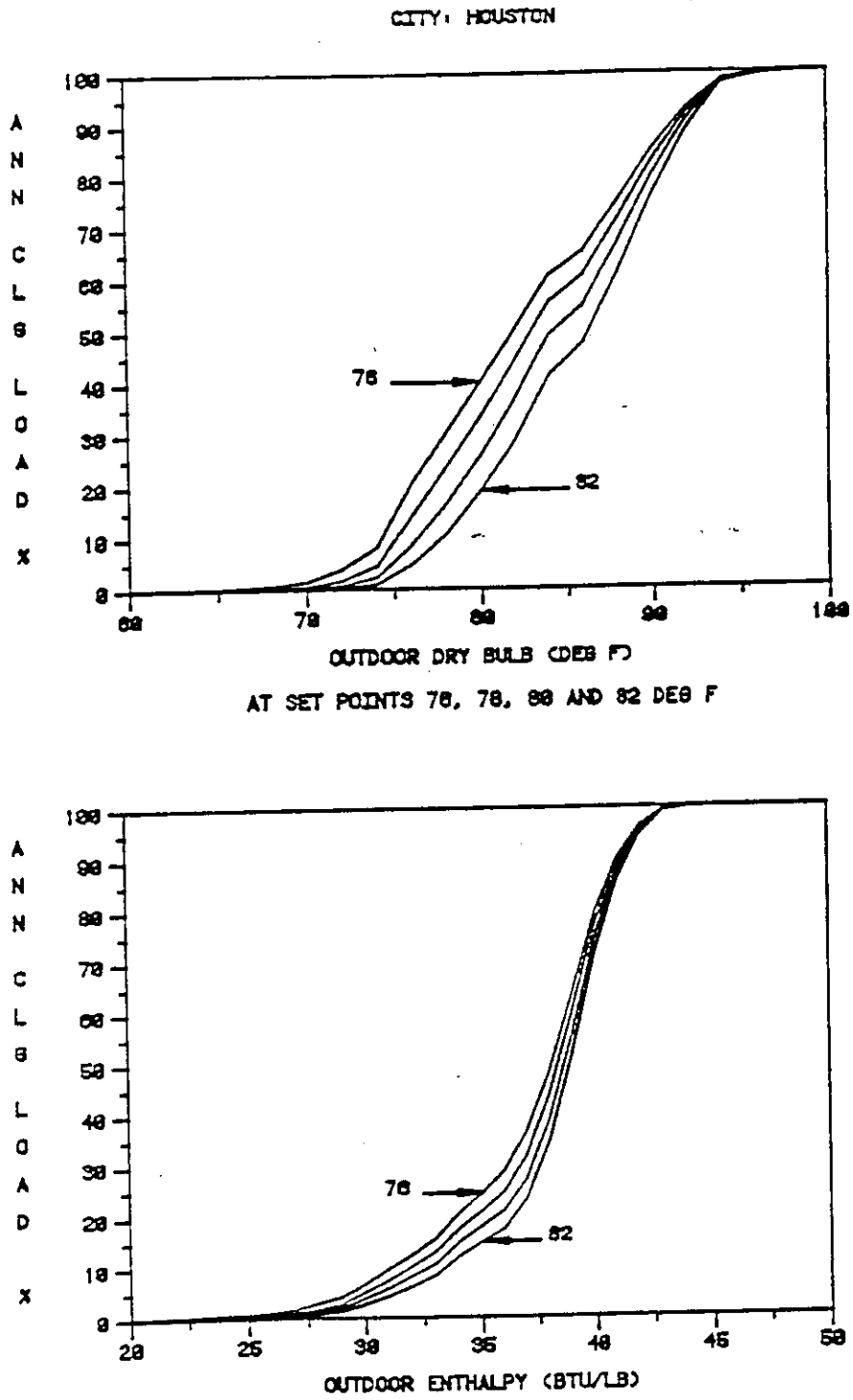

Figure 4-40 Cumulative cooling load for Houston, TX as a function of ambient dry-bulb temperature (top) and ambient enthalpy (bottom).

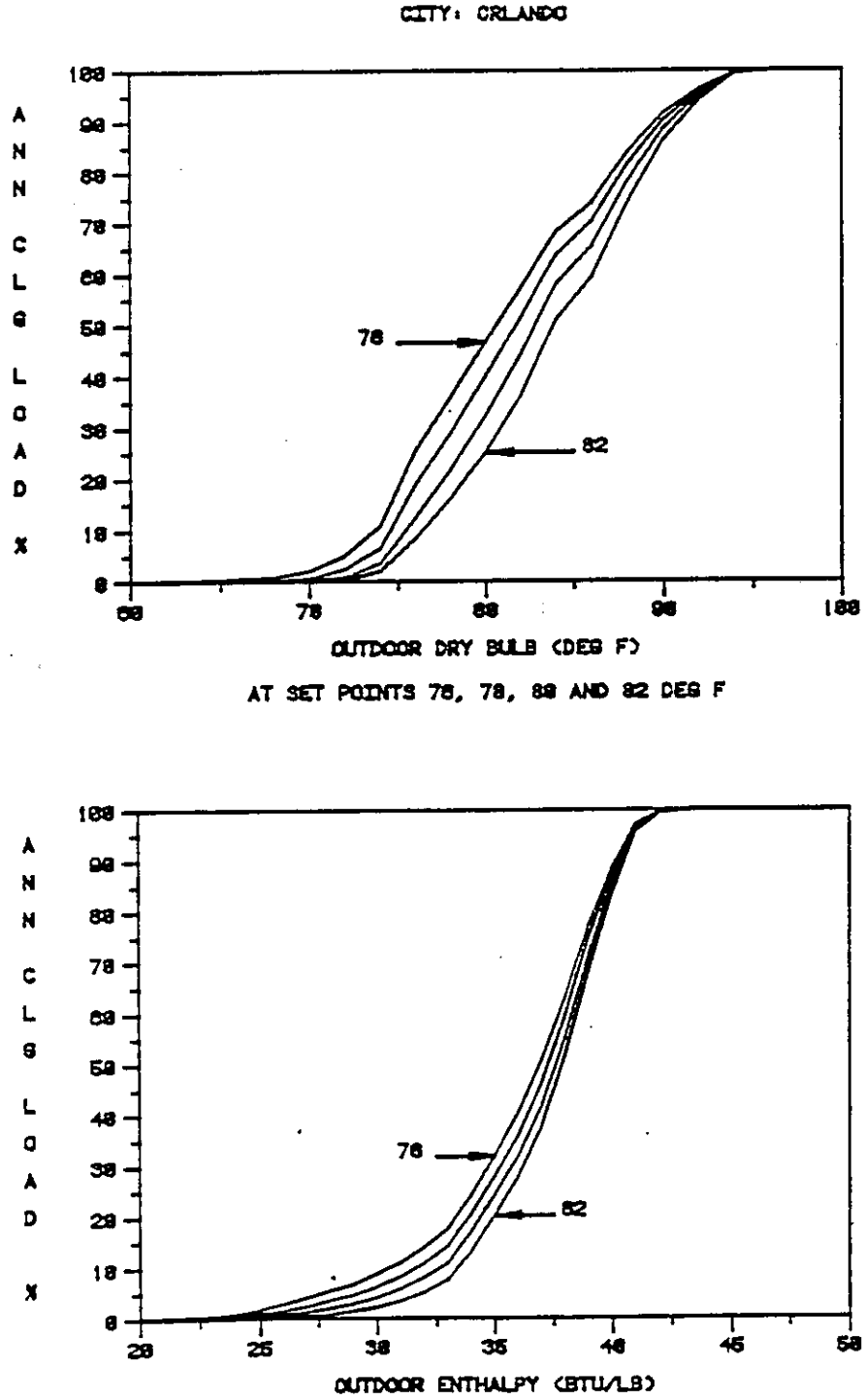

Figure 4-41 Cumulative cooling load for Orlando, FL as a function of ambient dry-bulb temperature (top) and ambient enthalpy (bottom).

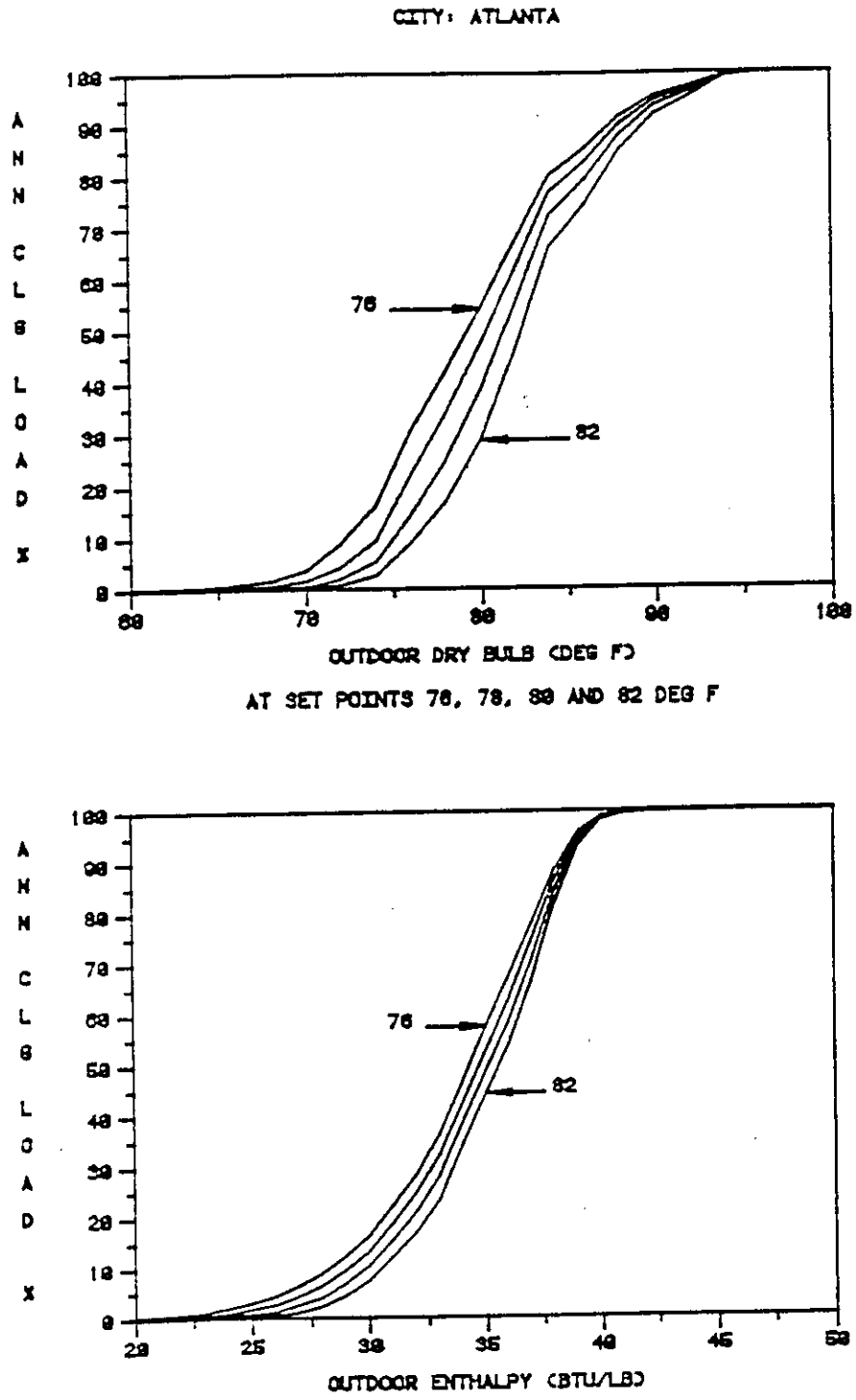

Figure 4-42 Cumulative cooling load for Atlanta, GA as a function of ambient dry-bulb temperature (top) and ambient enthalpy (bottom).

4.5.3 Natural Cooling Strategies

Three specific natural cooling strategies have been investigated: passive natural ventilation cooling, hybrid night sky cooling, and hybrid earth-tube cooling. Ventilative cooling is assumed to require no external parasitic power; for night sky radiation and earth-tube cooling, parasitic power is required to move the cooling fluid (room air).

Because these analyses are for natural cooling strategies, the BP building was the primary building of comparison for each. Without the capacitance effect of the additional thermal mass contained in the BP building, cooling strategies that require daily cycling of the building conditions may be largely non-productive. For ventilation cooling, however, most of the building types were analyzed.

The cooling of building inhabitants by airflow across the skin results in higher permissible thermostat settings, as discussed in Section 4.4.2 under conservation strategies. Natural ventilation as discussed here is a building cooling rather than a people-cooling strategy. The combination effects of higher thermostat settings and ceiling fans for people-cooling coupled with natural ventilation for building cooling have not been studied here. There is ample reason to believe, however, that such combinations will result in significant cooling energy savings. This consideration is also true of the hybrid strategies investigated where similar performance improvements may be expected with higher thermostat settings.

Table 4-8 presents a detailed comparison of the results in four cities. One can see that each of the three strategies is highly climate-dependent and that both night sky radiation cooling and earth-tube cooling have significant parasitic power requirements.

Table 4-8

Comparison of Passive/Hybrid Cooling Strategies

		A/C DISSIPATION				PASSIVE/HYBRID DISSIPATION				POWER CONSUMPTION			SAVINGS		PEAK AVG
CITY	RUN	Sen MBtu	Lat MBtu	Total MBtu	SHF	Sen MBtu	Lat MBtu	Total MBtu	SHF	A/C kWh	Hybrid kWh	Total kWh	A/C LOAD %	Power %	Month RH %
ATL	BPTT	6.7	4.5	11.2	.60	—	—	—	-	1187	—	1187	—	—	65.0
	BPTV	2.8	2.8	5.5	.50	N/A	N/A	N/A	N/A	600	0	600	50.9	49.4	80.9
	BPTG	0.1	0.1	0.2	.39	11.1	0.5	11.6	.96	23	634	657	98.2	45.5	87.9
	BPTR	3.1	2.6	5.7	.54	8.7	0.8	9.4	.92	619	308	927	49.0	22.1	71.8
CHA	BPTT	9.4	6.9	16.3	.58	—	—	—	-	1744	—	1744	—	—	69.5
	BPTV	4.7	5.4	10.1	.46	N/A	N/A	N/A	N/A	1094	0	1094	38.0	37.3	84.7
	BPTG	1.4	2.0	3.4	.42	10.3	0.6	10.9	.94	367	724	1091	79.1	37.4	89.4
	BPTR	6.5	5.4	11.9	.55	6.1	0.9	7.0	.87	1295	254	1549	27.0	11.2	75.6
MIA	BPTT	22.6	14.0	36.6	.62	—	—	—	-	3916	—	3916	—	—	65.0
	BPTV	14.6	11.9	26.4	.55	N/A	N/A	N/A	N/A	2868	0	2868	27.9	27.8	75.8
	BPTG	22.6	14.0	36.6	.62	0	0	0	0	3916	0	3916	0	0	65.0
	BPTR	13.5	10.4	23.9	.57	15.4	0.9	16.3	.95	2586	607	3193	34.7	18.5	72.2
ORL	BPTT	15.2	9.7	24.9	.61	—	—	—	-	2679	—	2679	—	—	66.2
	BPTV	7.9	8.5	16.4	.48	N/A	N/A	N/A	N/A	1790	0	1790	34.1	33.2	85.1
	BPTG	12.9	8.5	21.4	.60	2.7	0	2.7	1.00	2314	298	2612	14.1	2.5	74.4
	BPTR	10.5	7.8	18.3	.57	9.9	0.9	10.8	.92	1994	403	2397	26.5	10.5	71.0

The results compare only the simple cooling stategies modelled. Increased cooling potential and savings could be achieved using alternative radiative (and evaporative) cooling strategies (e.g., trickle roof or roof ponds). The modelled radiator was chosen as a low-first cost system which could be compatible with a GRDD system.

Full scale experimental results of the ground and radiatively cooled buildings are not available. Therefore, the results of the cooling strategies are not validated.

4.5.3.1 Natural Ventilation Cooling

The mass effects of a building is especially important when it is vented. Night venting can cool the mass, and the cooled

mass can then reduce the daytime cooling load. Figure 4-43 shows the annual cooling loads for non-vented and vented buildings in Orlando, Florida. Although significant energy savings occur, the highest monthly average relative humidity rises from 65% to 85%. The RH in the base buildings is slightly lower than in the energy conserving buildings. Much of the ventilation savings is being paid for with increased room RH.

Figures 4-44a and b show the savings due to ventilation for each building type. Not only do the block buildings have a greater percentage savings (Fig. 4-44a and 4-21a) but each block building saves more net energy (in MBtu's) than the comparable frame buildings (Fig. 4-44b). The percentage savings range from 13% to 34%. These results indicate that mass is very helpful if passive cooling techniques are used. Since the percent savings increases from BITV to BETV to BPTV, it appears that a limit to the amount of mass which is useful was not achieved in these simulated buildings. This is

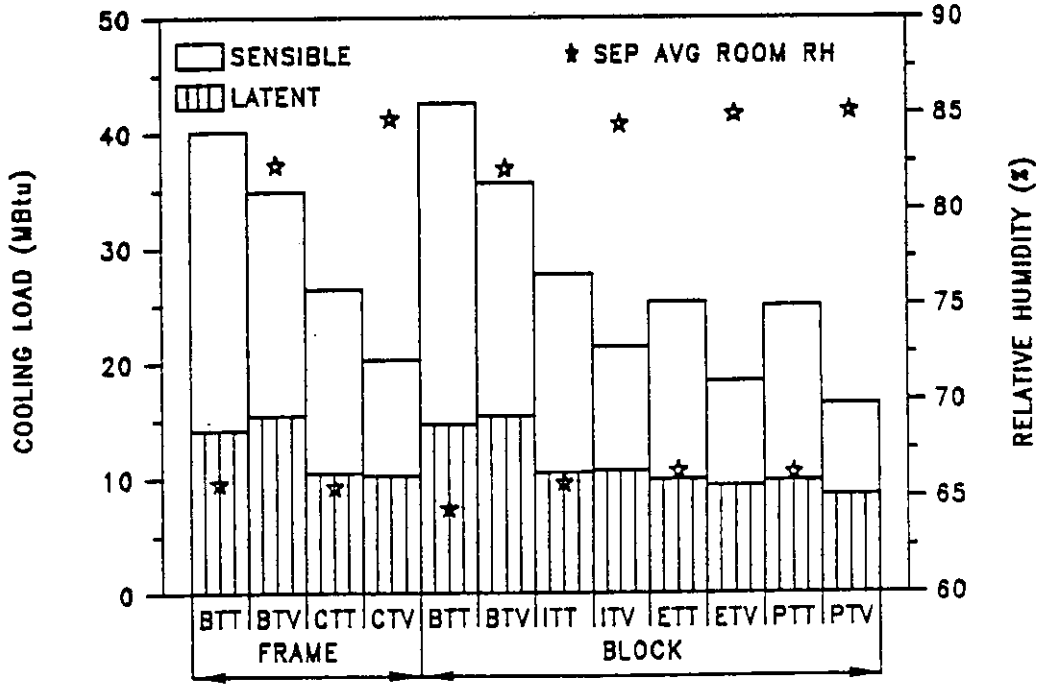

Figure 4-43 Annual cooling loads for vented and unvented buildings in Orlando, FL. Vented at 15 ACH if $69^{o}F$ < ambient dry-bulb < $78^{o}F$.

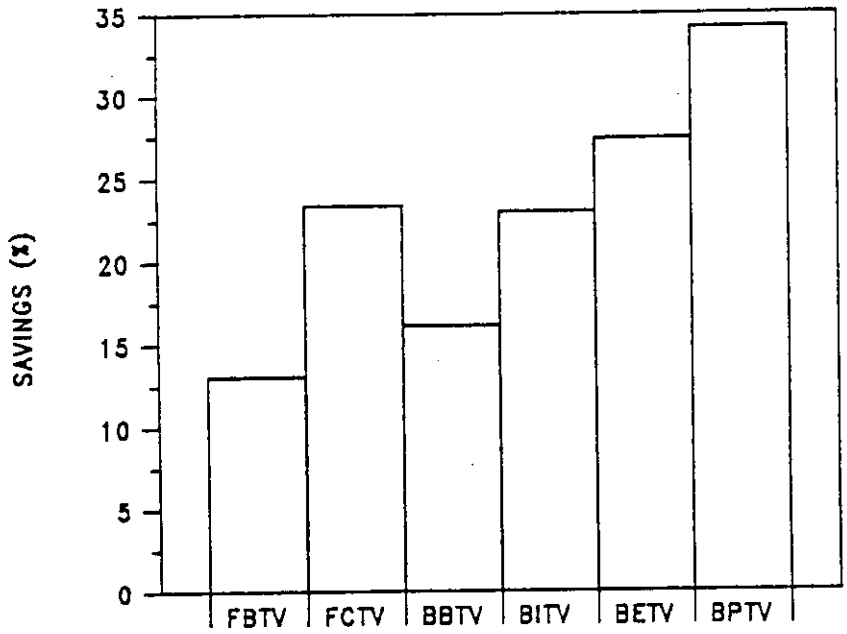

Figure 4-44a Annual cooling load savings for venting by building type (base load is the same building type without venting). Vented at 15 ACH if 69°F < ambient dry-bulb < 78°F in Orlando, FL.

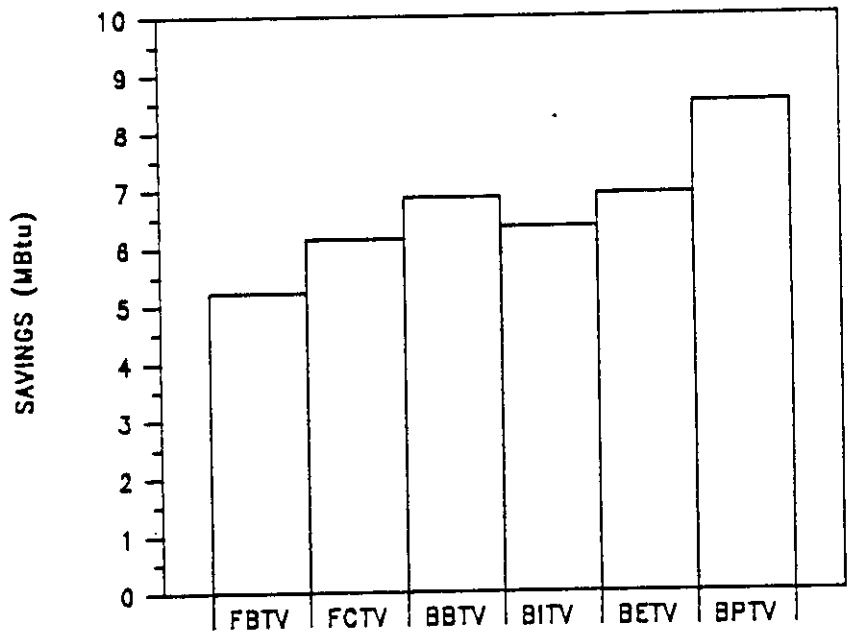

Figure 4-44b Annual cooling load reduction by venting by building type (base load is the same building type without venting). Vented at 15 ACH if 69°F < ambient dry-bulb < 78°F in Orlando, FL.

perhaps because total heat transfer surface area was increased along with the total mass capacity. The interior partition mass walls in the BP building increased savings by about 1.5 MBtu relative to the BE deck.

Figures 4-45 presents a comparison of the potential cooling savings and peak month RH for natural ventilation cooling in each of the nine climates studied. For natural ventilation there are no parasitic power requirements; therefore, the raw loads savings shown in Figure 4-45b represents actual savings. Miami appears to have the most to gain by ventilative cooling even though its percent savings is lower than many other climates.

4.5.3.2 Hybrid Night-Sky Radiation Cooling

Night-sky radiation cooling is similar to ventilative cooling in that it uses a highly cyclical heat sink. All building cooling must be accomplished at night and stored for the following day. Therefore, as indicated in Table 4-8, the sum of night-sky radiation cooling dissipation and the backup a/c cooling dissipation is always significantly greater than the base (BPTT) a/c cooling dissipation. Night-sky radiation is further reduced in effectiveness by its parasitic power requirements. However, on the good side, night-sky radiation does not generate as high indoor RH as ventilative cooling does. BPTR's high humidity levels are due to the fact that very little moisture is removed by the a/c rather than the ventilation moisture carry-over that is seen in the vented buildings.

Figure 4-46 compares night-sky radiation cooling load electric power savings for the nine climates studied. Note that peak month room RH levels are lower than for the ventilation cooling savings in Figure 4-45. Note that electrical savings are low compared to natural ventilation but load savings are generally higher or about the same. A significant increase in

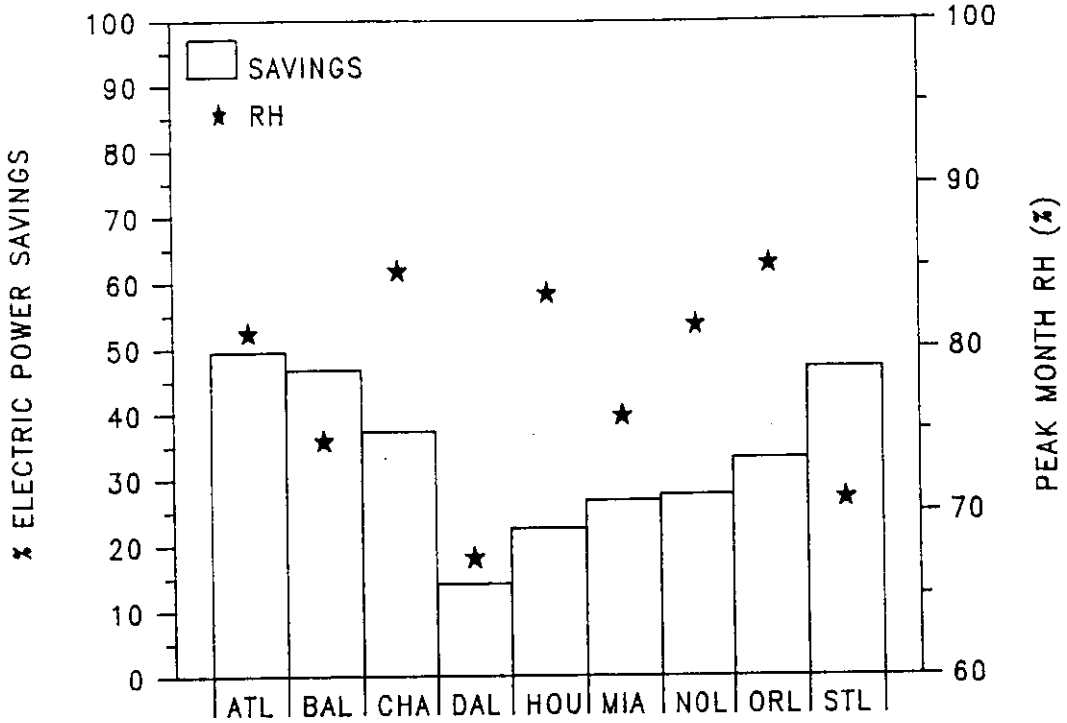

Figure 4-45a Effective savings of natural ventilation in nine cities. Vented at 15 ACH in 69°F ambient dry-bulb < 78°F.

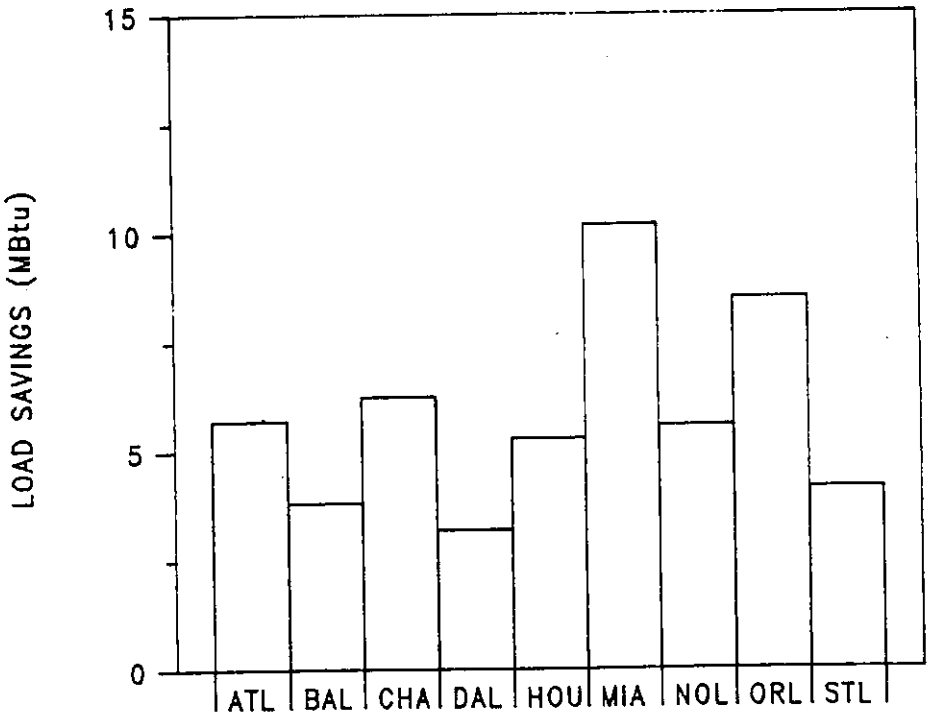

Figure 4-45b Raw load savings achieved by natural ventilation in nine cities. Vented at 15 ACH if 69°F < ambient dry-bulb < 78°F.

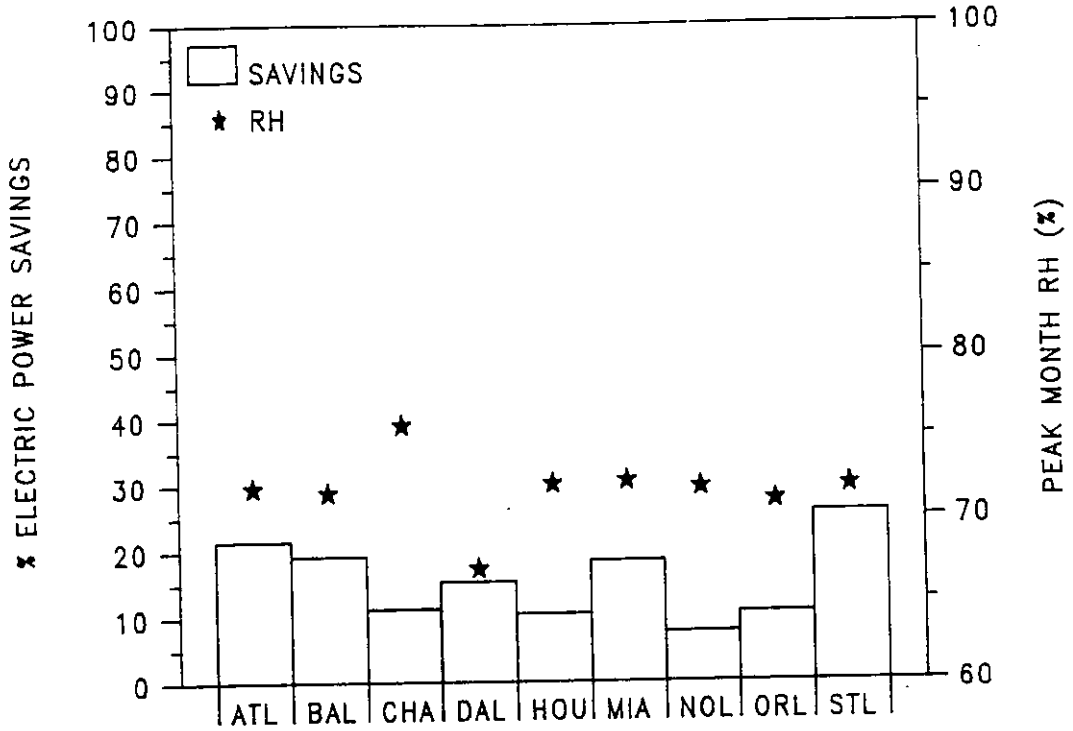

Figure 4-46a Effective savings of hybrid night sky radiation cooling in nine cities accounting for parasitic power requirements.

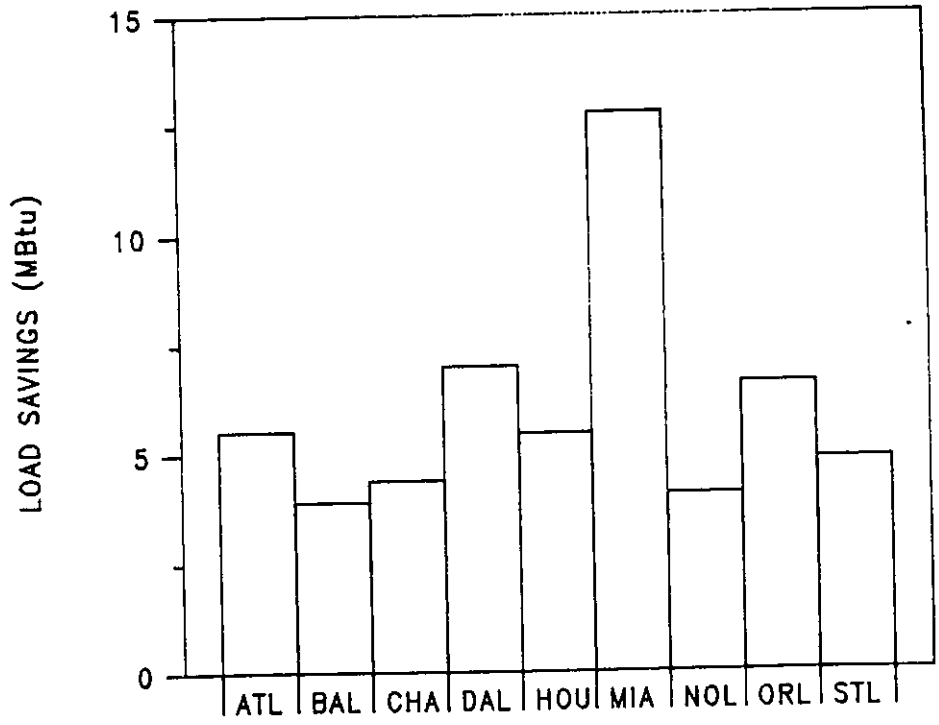

Figure 4-46b Raw load savings achieved by night sky radiation in nine cities not accounting for parasitic power requirements.

load savings is seen in Dallas where humidity is relatively low. In fact, in Dallas hybrid night sky radiation cooling shows greater electrical savings than does natural ventilation cooling.

4.5.3.3 Hybrid Earth-Tube Cooling

Since earth-tube cooling potential is primarily determined by the deep-ground temperature of the earth, the daily cycle of the heat sink resource is very small compared to the previous cooling strategies. Thus, ground cooling can be used at any time of the day that cooling is required if the ground is cool enough. Earth-tube cooling, therefore, does not suffer the large requirement for building thermal storage which the previous strategies do. In Table 4-8 one can see a relatively large difference between the base load and the sum of the a/c and hybrid dissipation loads for night sky radiation cooling. This difference is significantly reduced for earth-tube cooling. Earth-tube cooling, however, is much more climate-dependent than night-sky radiation or natural ventilation cooling. In Miami, for example, there is no earth-tube cooling potential at all, while in the northern climates earth-tube cooling can effectively eliminate backup air conditioning requirements. This is slightly misleading, however, because surely dehumidification would be an absolute requirement for such cooling strategies as evidenced by the very high peak-month room humidities.

Figure 4-47 gives the potential cooling-load electric power savings and peak-month average room RH for earth-tube cooling in each of the nine climates.

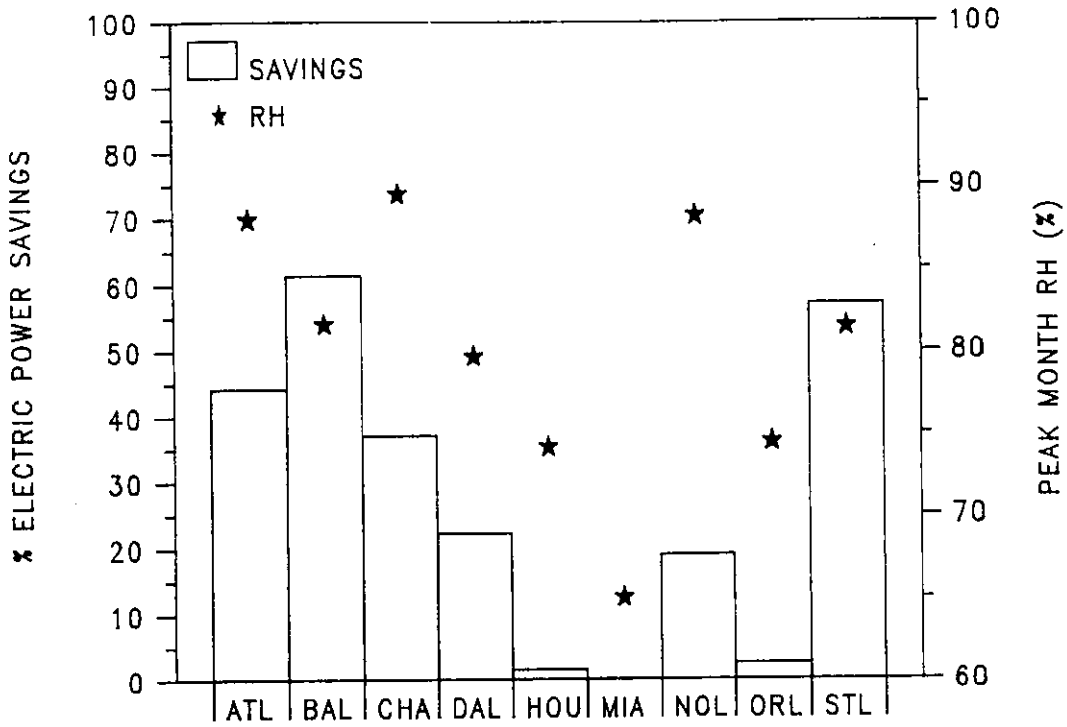

Figure 4-47a Effective savings of hybrid earth-tube cooling in nine cities accounting for parasitic power requirements.

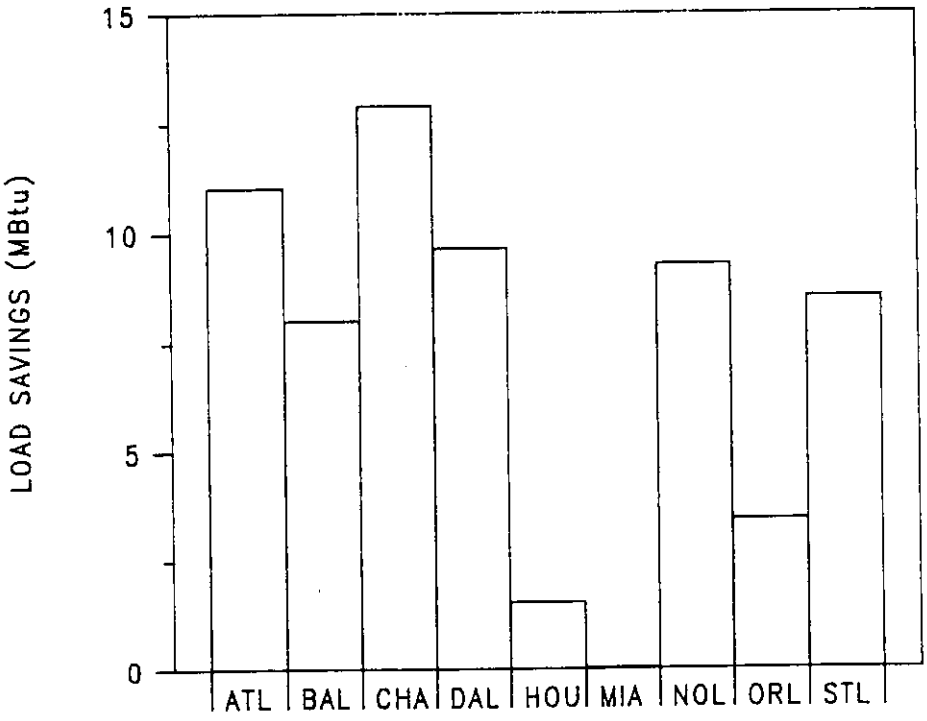

Figure 4-47b Raw load savings achieved by hybrid earth-tube cooling in nine cities not accounting for parasitic power requirements.

SECTION FIVE
ECONOMIC ANALYSIS RESULTS

As discussed previously, building loads were simulated using two mechanical systems: a "typical" and an "ideal" machine. It is important to emphasize again that the ideal machine, as the name suggests, is a hypothetical air conditioner and does not exist in reality. The ideal machine is capable of maintaining set conditions of both indoor dry-bulb and relative humidity, while the typical or real machine responds only to changes in indoor dry-bulb. This, however, does not mean that set conditions of relative indoor humidity cannot be maintained in a building. The real machine in conjunction with an appropriate choice of reheat, vapor compression dehumidifier (VCD) or gas regenerated desiccant dehumidifier (GRDD) can be used to maintain indoor RH as well. The indoor humidity resulting from the use of a typical machine is dictated by the characteristics of both the machine and envelope. It is therefore obvious that when set conditions of dry-bulb and relative humidity are to be maintained, the typical machine alone will not always meet the RH expectations.

Among the alternatives available to combat that problem, only the use of the VCD and GRDD is considered here. This section examines the relative economics of using the two systems in conjunction with a typical air conditioner when it is desirable to maintain an upper limit on RH as well as an upper limit on temperature.

5.1 ANALYSIS PROCEDURE AND ASSUMPTION

The economic analysis primarily involves the determination of the simple payback in years and the associated return on investment when the GRDD plus a/c system saves on operating costs relative to the VCD plus a/c. For this purpose, the inputs required are the initial costs of the two systems and their annual operating costs.

At the outset, it would appear feasible that the above inputs can be easily generated from the hourly MADTARP analysis output file. However, closer examination reveals that simulating the VCD or GRDD in MADTARP is the only true way to obtain accurate and reliable estimates of capacities and costs. Attempting to predict them from the hourly MADTARP output file would result in uncertainties, and estimates may be somewhat inaccurate. The following will serve to clarify this argument.

Let us consider a case where indoor conditions of 78°F and 58% RH must be maintained. The building loads at this setpoint can be simulated by MADTARP using an ideal machine, and the hourly output can be obtained. In attempting to derive the economics of the VCD or GRDD systems from the hourly file, the following three possibilities, one of which may occur at any given hour, must be considered.

Condition 1:	sensible load = 0	DB $\leq$ 78°F
	latent load > 0	RH = 58%

It would seem that only dehumidification is required. However, the sensible heat added to the space by the VCD or GRDD must be considered. If the indoor dry-bulb due to this heat addition exceeds 78°F, the a/c must be turned on. But, purely from the data available in the output file it is impossible to predict the ensuing room conditions and the time when the indoor temperature is about to exceed 78°F. On the other hand, to run the a/c to remove all the sensible heat added by the dehumidifier even when the indoor temperature is less than 78°F would be superfluous and defeat the economics. This case poses a major problem in the analysis.

Condition 2:	sensible load > 0	DB = 78°F
	latent load > 0	RH = 58%

In this case, depending on the sensible heat fraction (SHF) of the air conditioner at the indoor and outdoor conditions, the a/c will remove the sensible load, including the heat added by the dehumidifier, and, and for the VCD option, a portion of the latent load. If, in removing the sensible load, the latent load removed by the a/c is more than the latent load, the room RH will fall. There is no way of predicting the resulting indoor RH from the MADTARP output files. If less than all of the latent load is removed by the a/c, apportioning the latent load between the VCD and a/c makes the analysis possible.

Condition 3:	sensible load	> 0	DB = 78°F
	latent load	= 0	RH < 58%

If the house relative humidity level was very low (much less than 58%) the a/c may operate under dry coil conditions to remove the sensible load. Dry coil conditions did not present any analysis problems because there was not a latent load. However, at higher relative humidity levels (but less than 58% for this case) the SHF of the air conditioner may be less than 1.0. Therefore, some latent load might be removed, causing a drop in humidity level which would not be reflected in the analysis.

In the present analysis the machine capacities and operating costs were generated by comparing the hourly MADTARP outputs of the typical and the ideal runs. The analysis was carried out for an indoor setpoint of 78°F and two RH setpoints for the ideal runs (58 and 68%). In the VCD plus a/c system, it was assumed that the VCD removed the difference in latent loads between the typical and ideal runs for any given hour; whereas in the case of the GRDD plus a/c system, the dehumidifier removed all the latent load and the a/c removed only sensible loads. In both cases the sensible heat added by

the dehumidifier was added to the corresponding sensible loads reported in the MADTARP analysis. The regenerative heating in the case of the VCD was 2400 Btu/lb H_2O removed and 295 Btu/lb H_2O removed in the case of the GRDD. These values were taken from the data developed by Marciniak, et al., [1985] under separate contract with GRI. The capacities of the a/c in both systems were based on the peak hourly cooling loads; the capacity of the VCD and GRDD were based on peak daily loads. The costs of the systems were estimated using formulae and data given in Marciniak [1985].

Following this procedure, the operating costs of each system were calculated for each city.

The difference in the initial costs of the two systems was chosen to represent the initial investment and the difference in the operating costs represented the savings. From this, the simple paybck (SPB) in years was calculated as follows:

$$SPB = \frac{\text{Initial Investment}}{\text{Savings/Year}} = \frac{\text{GRDD-VCD initial cost}}{\text{VCD-GRDD annual operating costs}} \qquad (5\text{-}1)$$

Also, to indicate economic viability, the return on investment (ROI) was calculated. The ROI is the discount rate at which the initial investment equals the present worth of lifetime savings. The formula used is:

$$\text{Present worth} = \begin{cases} S^* \frac{1}{(d-i)} \left(1-\left(\frac{1+i}{1+d}\right)^N\right) & \text{if } id \\ S^* N(1+i) & \text{if } i=d \end{cases} \qquad (5\text{-}2)$$

where

d - discount rate = ROI when present worth is equal to the initial investment

i - inflation rate of fuel displaced

N - life in years

S - initial savings per year

If the ROI calculated is greater than the market discount rate, then the system may be considered economically viable as a long-term investment.

A life-time of 10 years and a fuel inflation rate of 2.5% were used throughout the analysis.

5.2 ECONOMIC RESULTS

Economic analysis of the GRDD system versus the VCD system was carried out for four building types in nine cities. Further, the analysis was carried out using a two-tier utility pricing system, one with geographically dependent gas and electricity costs and the other with uniform utility prices based on average prices in all cities (7.77 cent/kWh for electricity and 62.4 cent/therm for gas). This was done to demonstrate the influence, if any, of location as well as utility costs on the economics. The electricity and gas prices were obtained from Kosar [1985]. Figure 5-1 compares the gas and

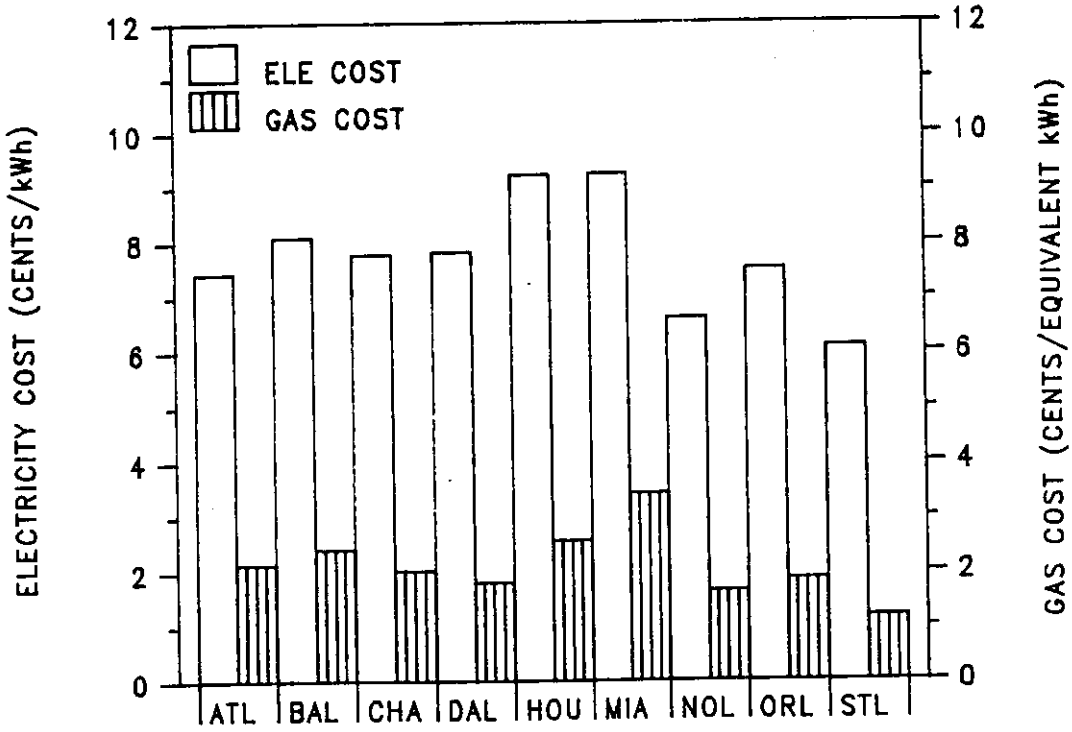

Figure 5-1 Comparison of utility prices in different cities expressed in equivalent units to show differences.

electricity prices in the nine cities. Note that a pseudo-equivalent unit for gas price (kWh_e) was used to show differences in utility costs. The equivalent gas price in all cities is less than half of the electricity cost. This, perhaps, is the single most important factor contributing to the economic viability of GRDD systems.

5.2.1 Results Based on Actual Costs

Figure 5-2 compares the initial costs of the two systems in nine cities for four building configurations. The initial costs in the frame basecase buildings are higher than in other buildings in all locations. The graph also highlights the separate air conditioner and dehumidifier costs for each system. A large portion of the initial cost is that of the a/c in the VCD system. For the GRDD system the a/c cost is reduced somewhat but GRDD cost is substantially increased, making net system costs higher for the GRDD system.

The reason for the different system a/c requirements is that in the VCD system the a/c removes all the sensible load as well as a portion of the latent load, while in the GRDD system the a/c removes only the sensible load. Also, the amount of sensible heat added to the space by the VCD system is almost eight times that for the GRDD system, for every pound of moisture removed [Marciniak 1985].

In all city and building type combinations, except Charleston for the frame basecase house, the initial investment on the GRDD system is higher than the VCD system. The difference in initial system costs is shown in Figure 5-3. The extra investment requirement of the GRDD system varies anywhere from a few dollars in Houston for the block passive radiator building to about $400 in St. Louis for the basecase and energy conserving buildings. This extra investment is not substantial, and a user can be expected to willingly spend this extra amount if he can obtain a reasonable return on his

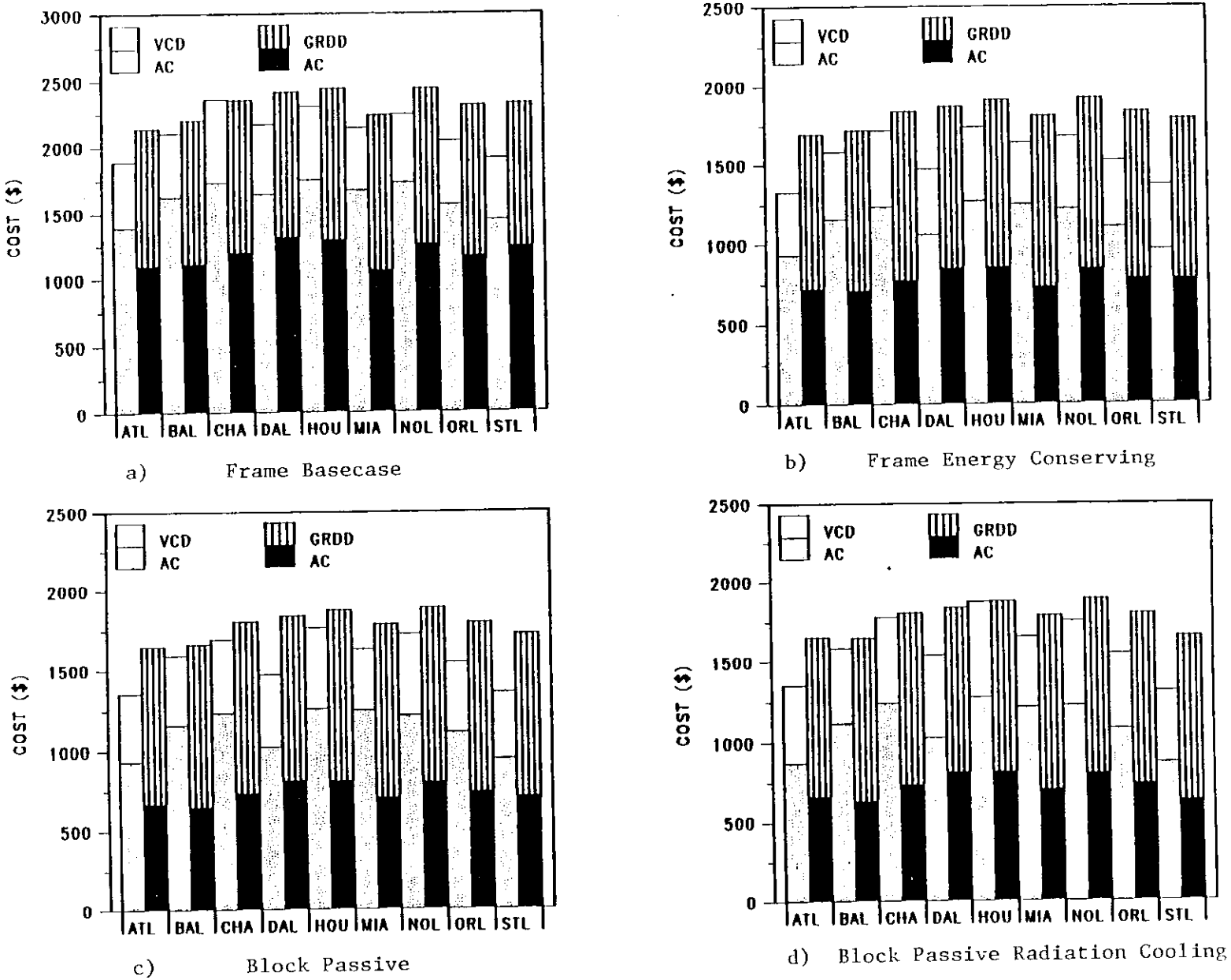

Figure 5-2 Initial costs of GRDD and VCD systems (78°F and 58% RH)

investment (and particularly if he proposes to install a dehumidifier anyway).

Figures 5-4 and 5-5 compare the annual operating costs of the two systems in each city for geographically dependent utility costs and uniform utility prices, respectively. Figure 5-6 compares the annual operating cost savings of the GRDD system over the VCD system. The savings are considerable, especially in humid climates such as Miami, Houston and Orlando. The higher annual savings are obtained where the latent load to be removed is highest (e.g., the frame basecase house or the block passive-radiator building). In fact, the operating cost of only the a/c in the VCD system is almost equal to the total operating cost (dehumidifier plus a/c) in the GRDD system. The high a/c-VCD operating costs are primarily due to the intensive amount of sensible heat added by the dehumidifier in the VCD system. Assuming uniform utility prices in all cities does not alter these trends. Notable operating cost differences are obtained in Miami and Houston only.

Figure 5-7 compares the simple payback of the initial cost difference of the two systems for the four building types in all cities. All four building types in all cities but St. Louis show paybacks of less than three and a half years. The payback of the frame base house in Charleston and the block passive-radiator house in Houston is immediate because the initial system cost difference is negative. The returns on investment for each city and building types are shown in Figure 5-8. Barring the block passive-radiator building in Charleston, the return on investment ranges from 13% to 350%. The extremely high return on investment in Charleston for the block passive-radiator building is attributed to an extremely low required investment differential ($25) and a relatively high annual savings($300). The return on investment for the Charleston basecase building and the Houston block passive-radiator building cannot be calculated because the

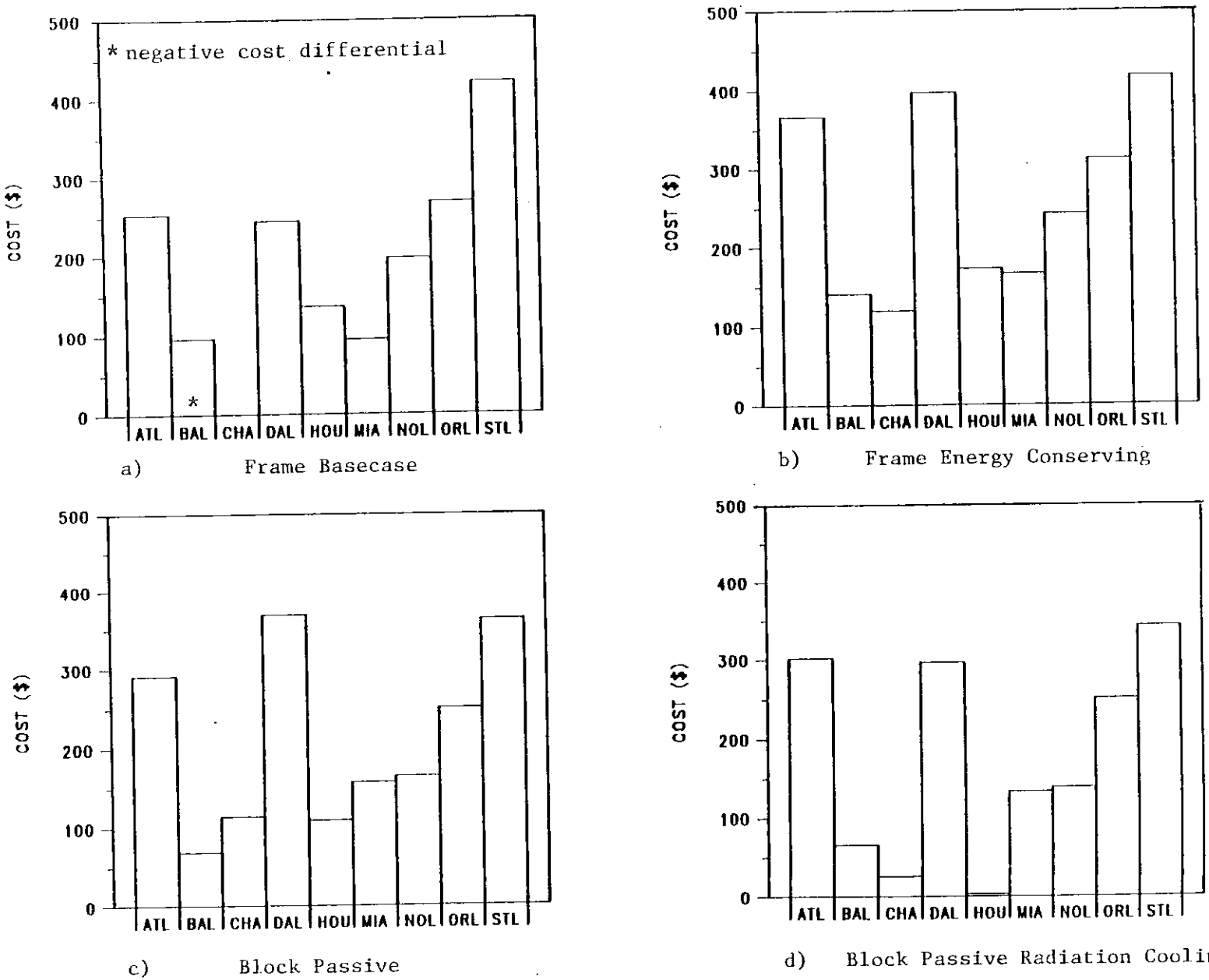

Figure 5-3 Difference in required initial investment (GRDD cost - VCD cost) for room conditions of 78°F and 58% RH.

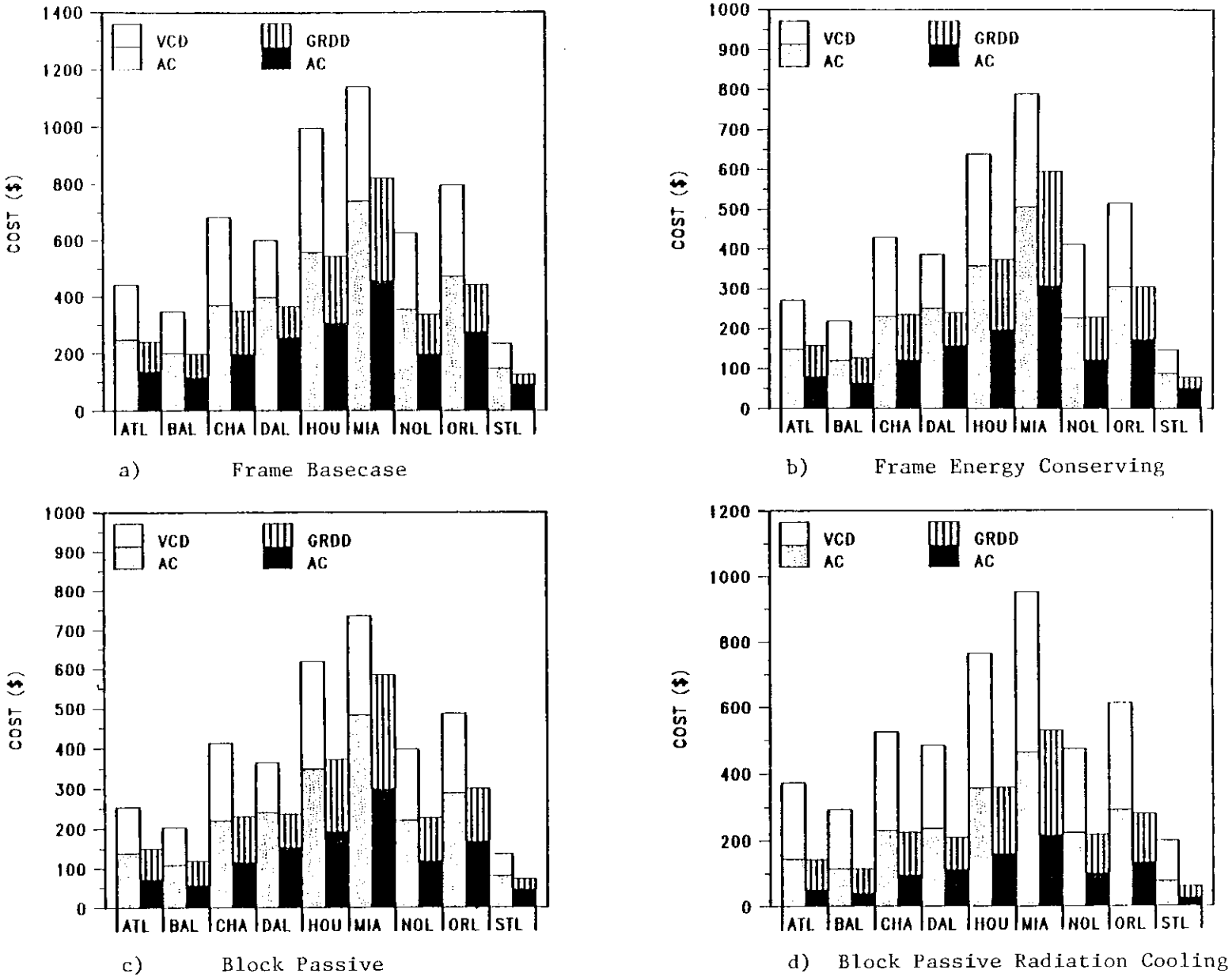

Figure 5-4 Annual operating costs of GRDD and VCD systems with geographically dependent utility costs in all cities for room conditions of 78°F and 58% RH.

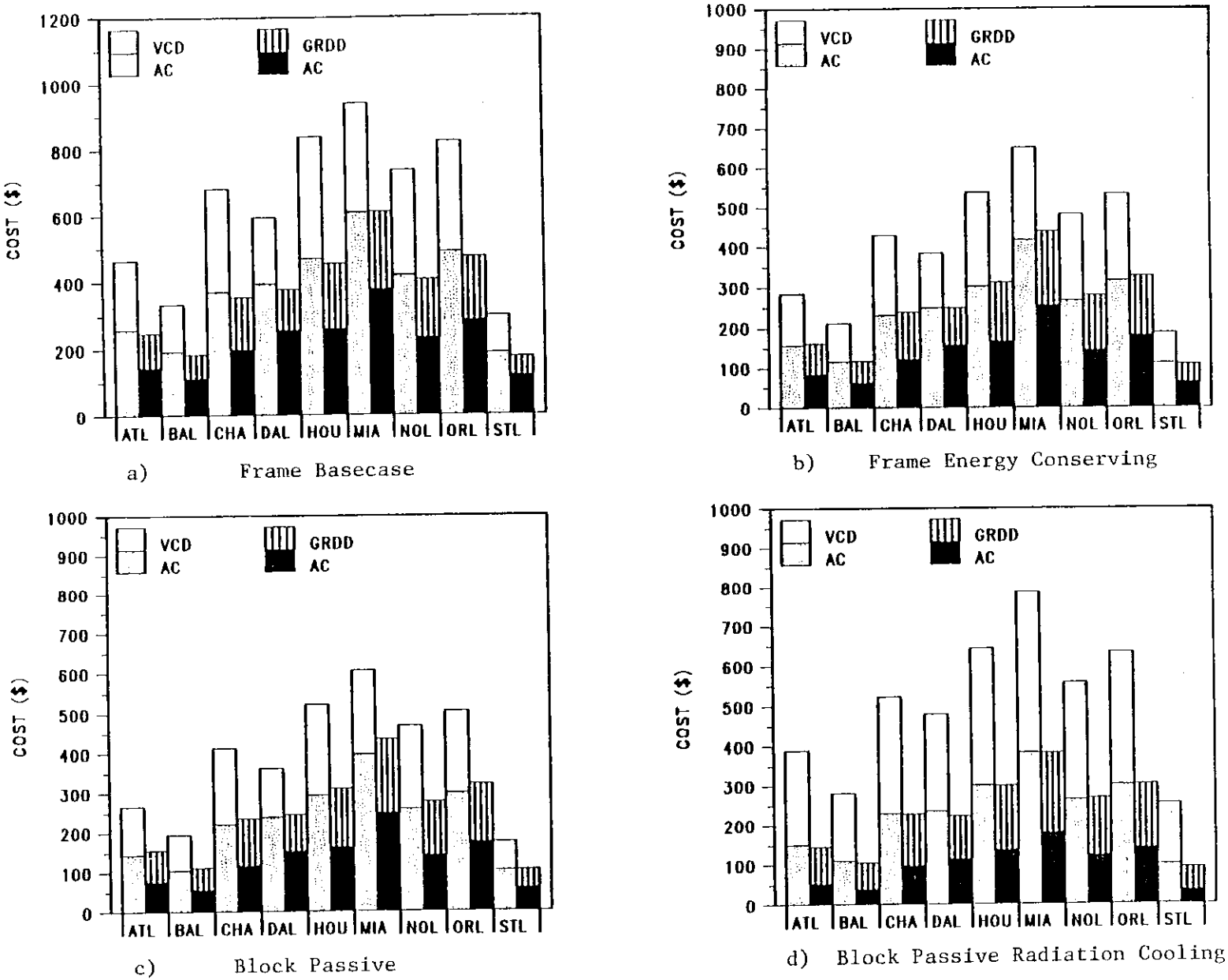

Figure 5-5 Annual operating costs of GRDD and VCD systems with uniform utility costs in all cities for room conditions of 78°F and 58% RH.

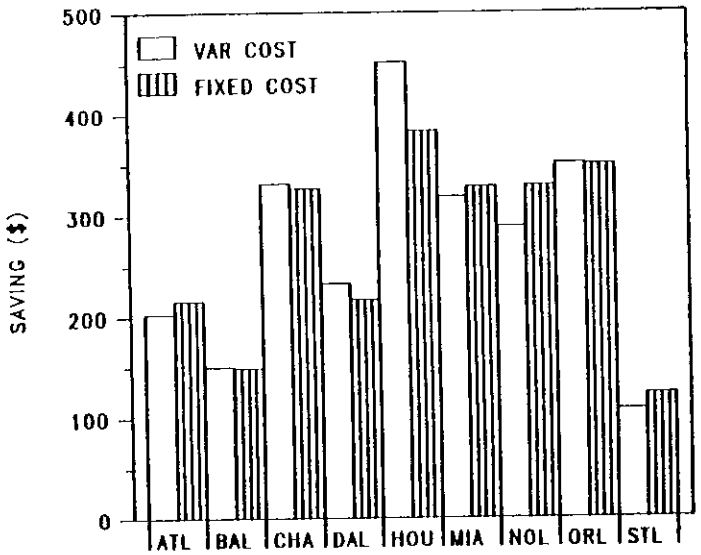

a) Frame Basecase

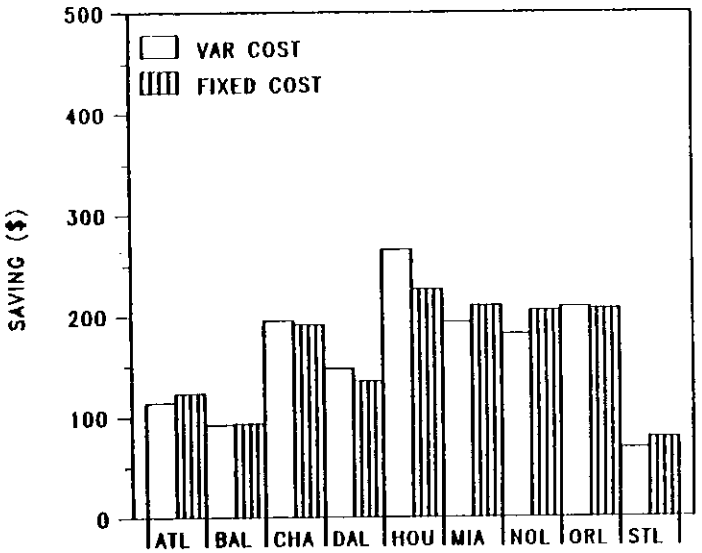

b) Frame Energy Conserving

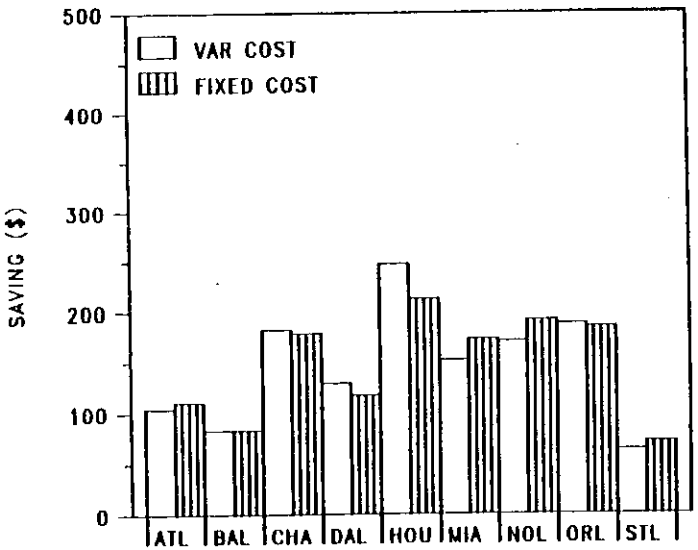

c) Block Passive

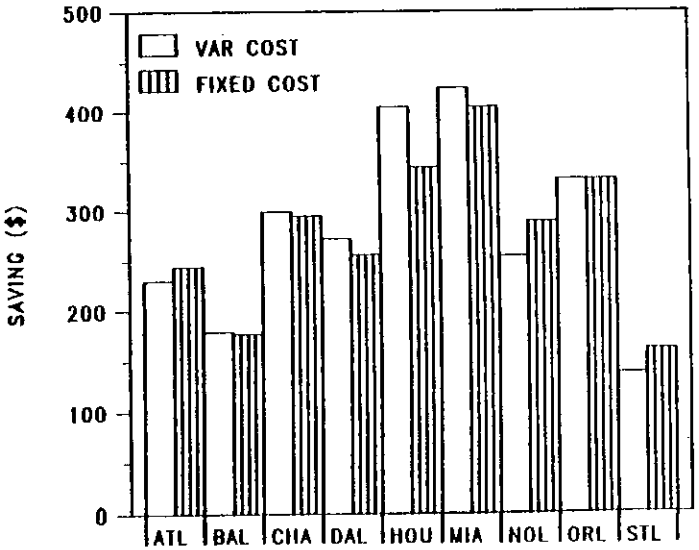

d) Block Passive Radiation Cooling

Figure 5-6 Annual operating cost savings for GRDD system as compared to VCD system for room conditions of 78^{O}F and 58% RH.

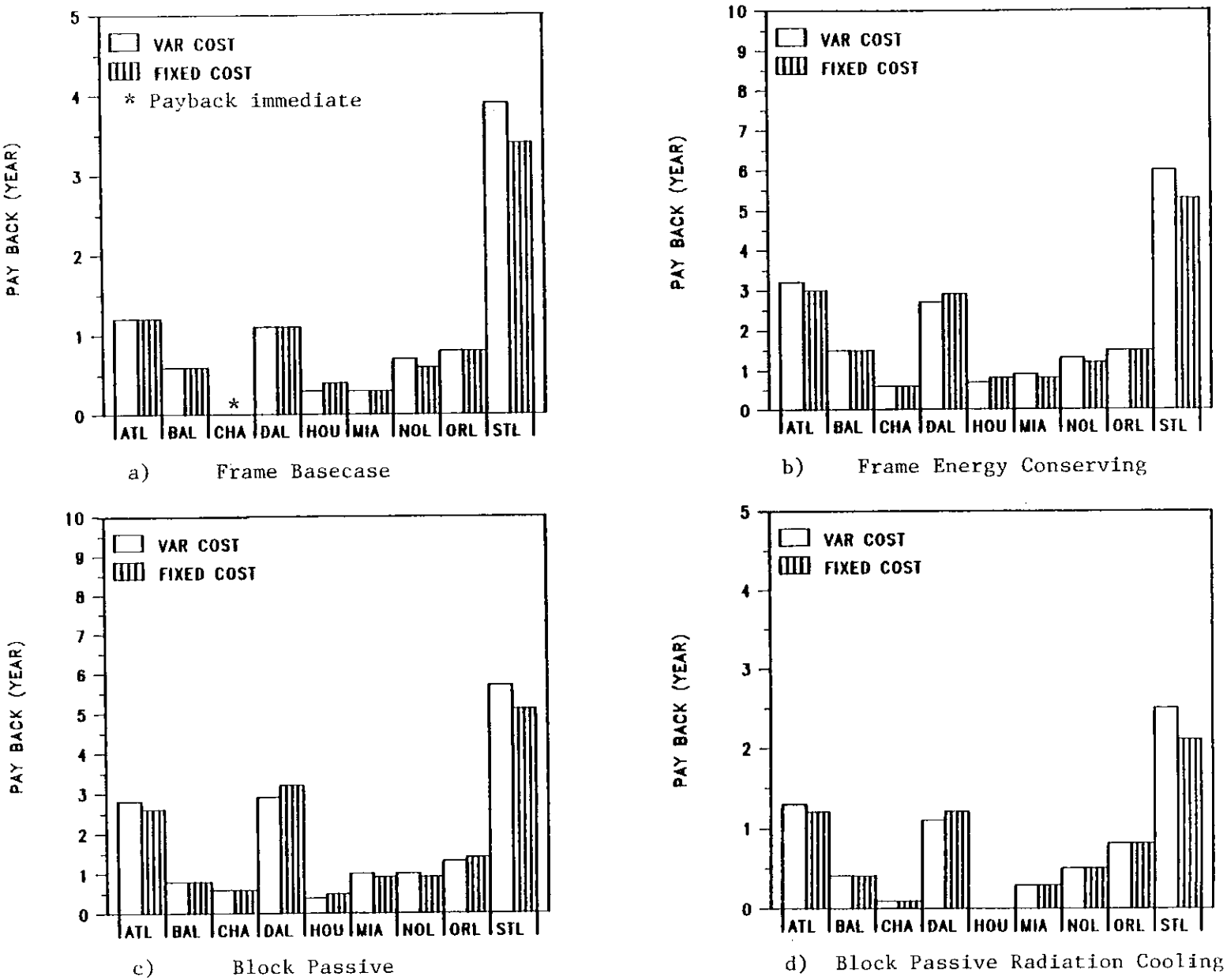

Figure 5-7 Simple payback period for initial system cost difference of GRDD system as compared to VCD system for room conditions of 78°F and 58% RH.

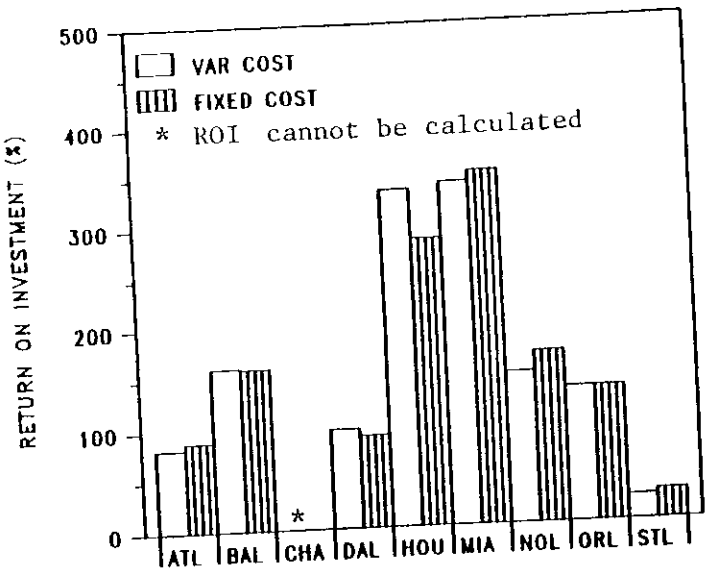

a) Frame Basecase

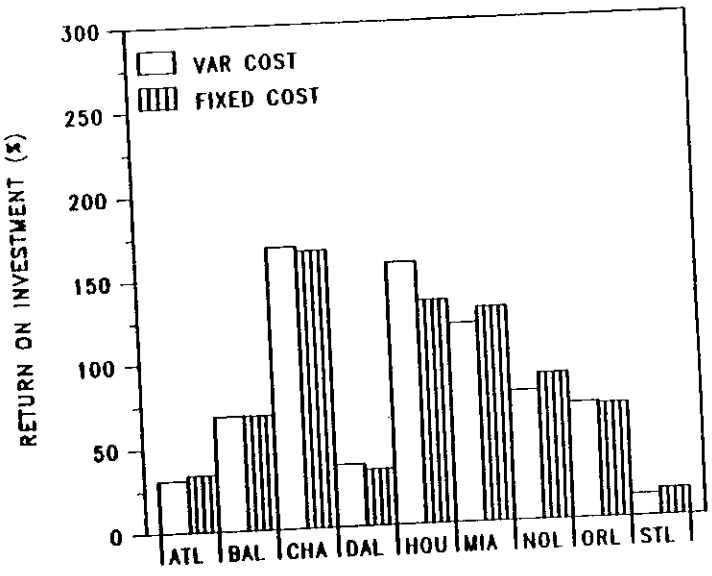

b) Frame Energy Conserving

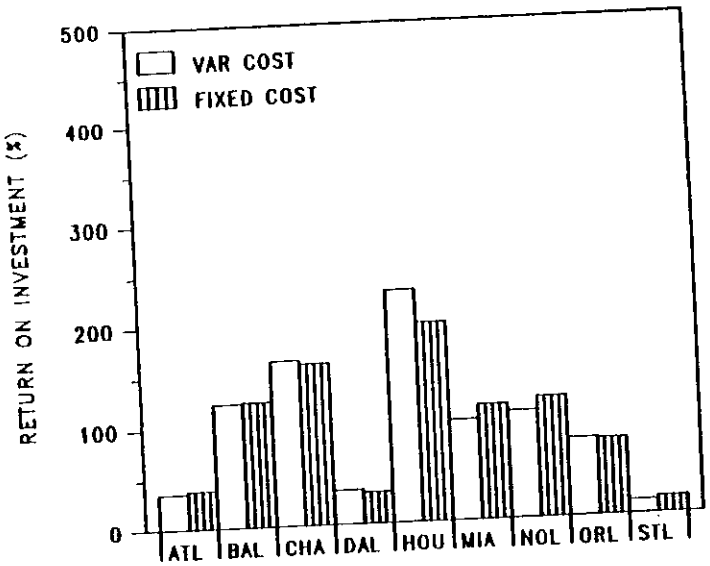

c) Block Passive

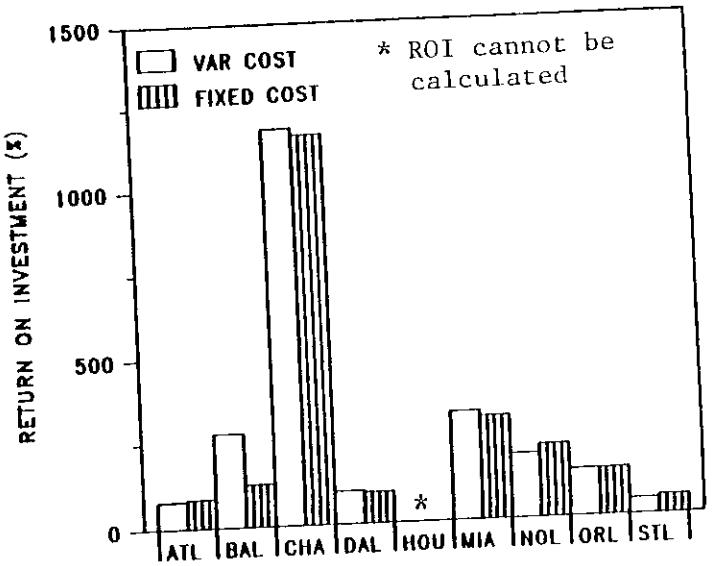

d) Block Passive Radiation Cooling

Figure 5-8 Return on initial investment of GRDD system as compared to VCD system for room conditions of 78°F and 58% RH.

initial investment differential is negative (see Equation 5-1).

5.2.2 Results Based on Required ROI and Payback

In view of the fact that the GRDD costs are difficult to estimate accurately, an alternative approach to the economics was also studied. In this approach maximum allowable investment for a desired ROI or payback is calculated based on operating cost savings potentials.

Figures 5-9 and 5-10 give the maximum allowable initial investment differential for ROIs of 10%, 15% and 20% for geographically dependent and uniform utility prices, respectively. In all cases except in St. Louis for the frame conserving and block passive building, the estimated investment cost for the GRDD system is always less than the maximum allowable, even for 20% ROIs and regardless of the utility pricing scheme used.

Similarly, Figures 5-11 and 5-12 show the maximum allowable investment differential between the two systems based on paybacks of 3, 5 and 7 years for geographically dependent and uniform utility prices, respectively. In most cases, for desired paybacks of 3 years the estimated cost differential is less than the maximum allowable differential.

5.3 OTHER MARKETING AND ECONOMIC CONSIDERATIONS

The results of the economic analysis are clear. Given the choice between a VCD or GRDD dehumidification and air conditioning system, almost any potential user should choose the GRDD system. However, from a market potential perspective these results may be quite misleading.

The analysis assumes an upper RH limit of 58% for the conditioned room. This represents the upper limiting

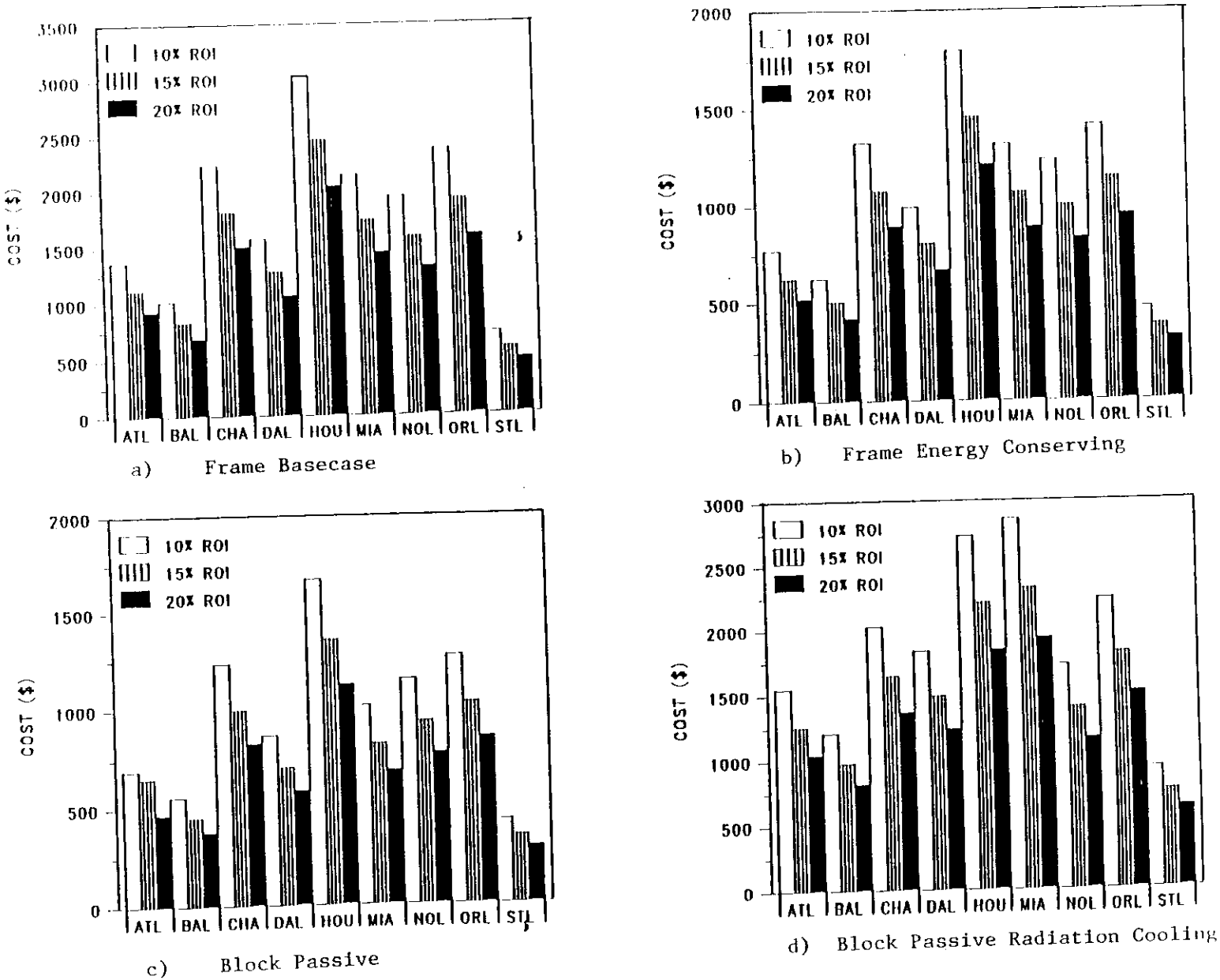

Figure 5-9 Maximum allowable initial investment differential for various ROI assuming a ten year life and geographically dependent utility prices for room conditions of 78°F and 58% RH.

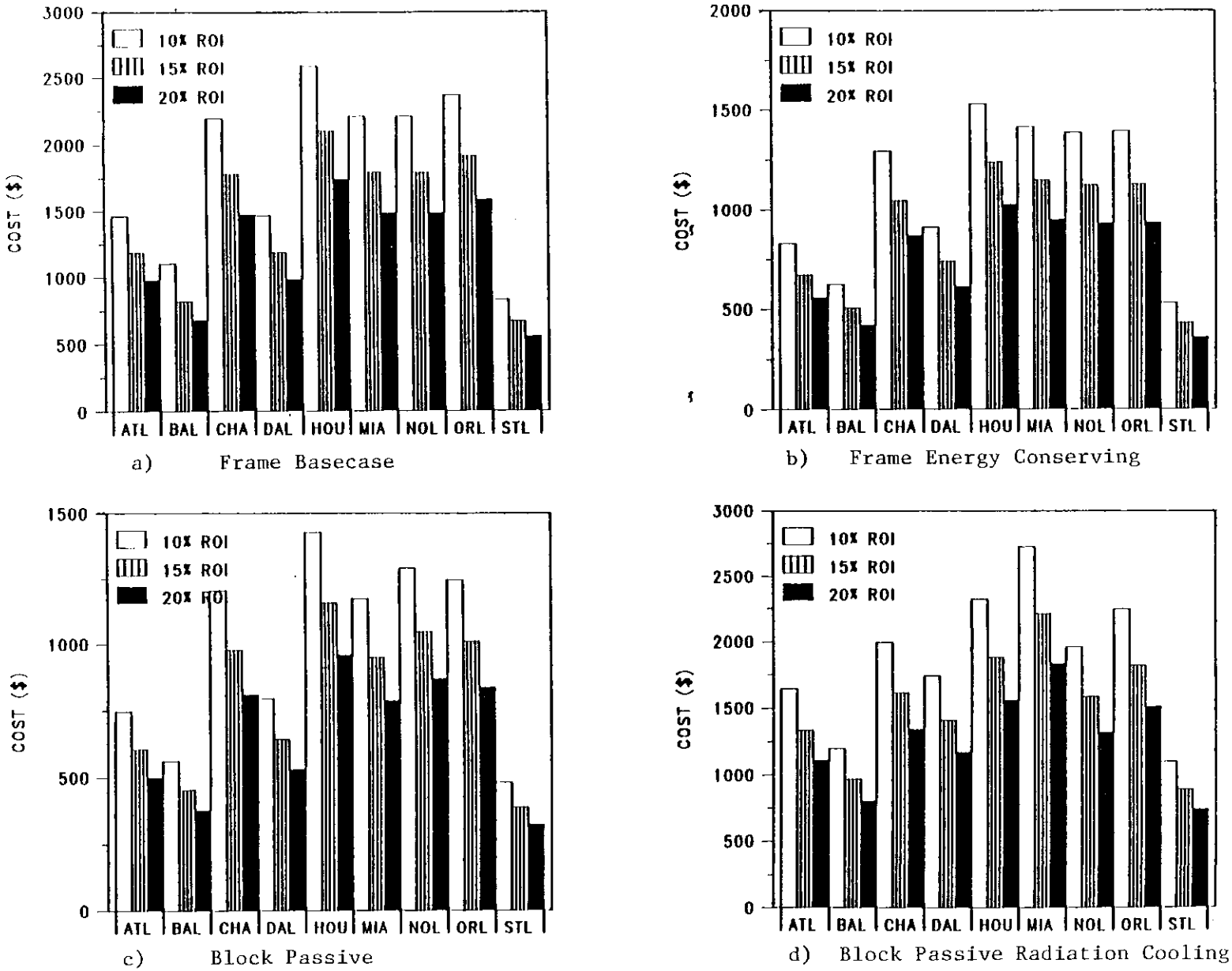

Figure 5-10 Maximum allowable initial investment differential for various ROI assuming a ten year life and uniform utility costs in all cities for room conditions of 78°F and 58% RH.

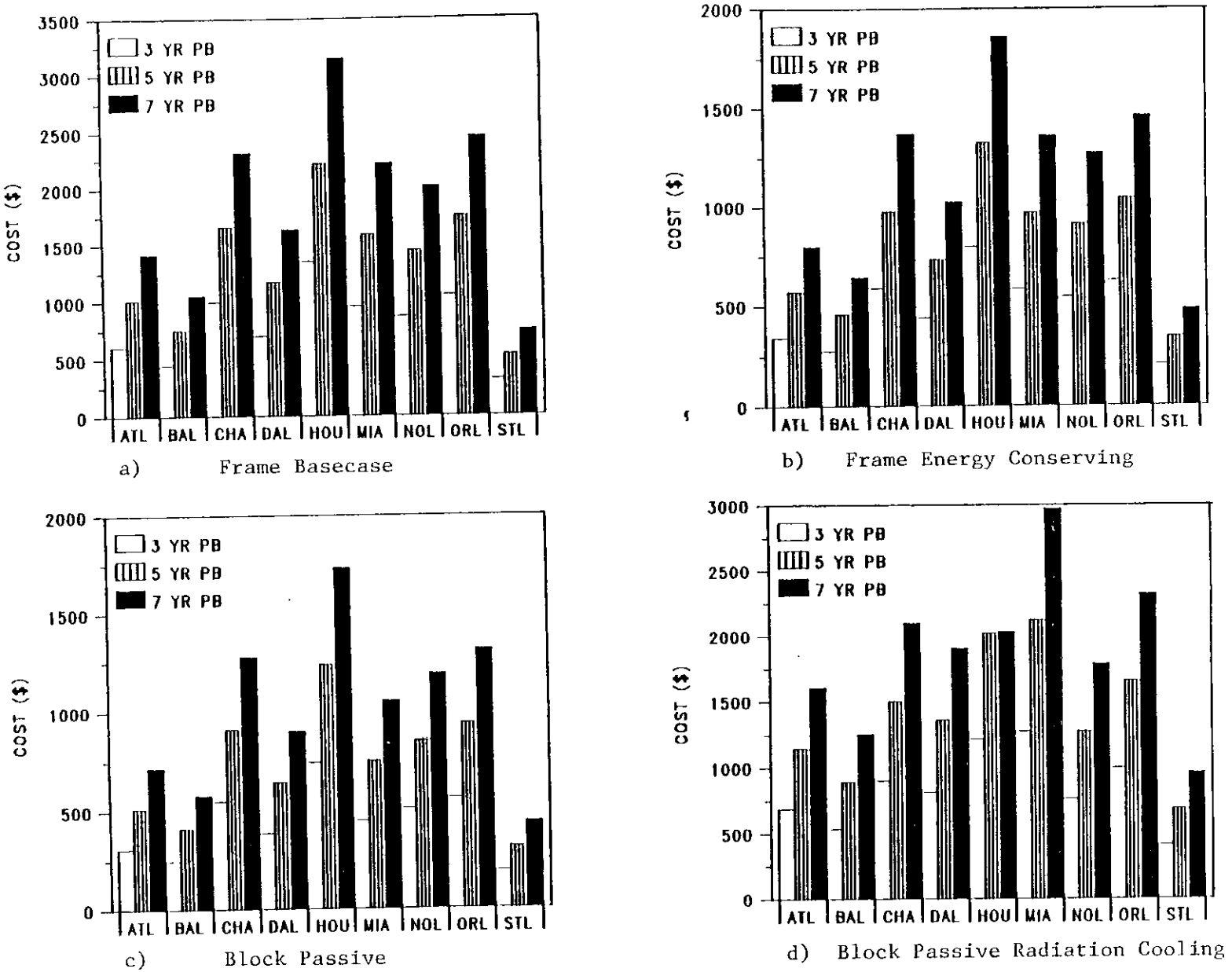

Figure 5-11 Maximum allowable initial investment differential for various simple paybacks assuming a ten year life and geographically dependent utility prices for room conditions of 78°F and 58% RH.

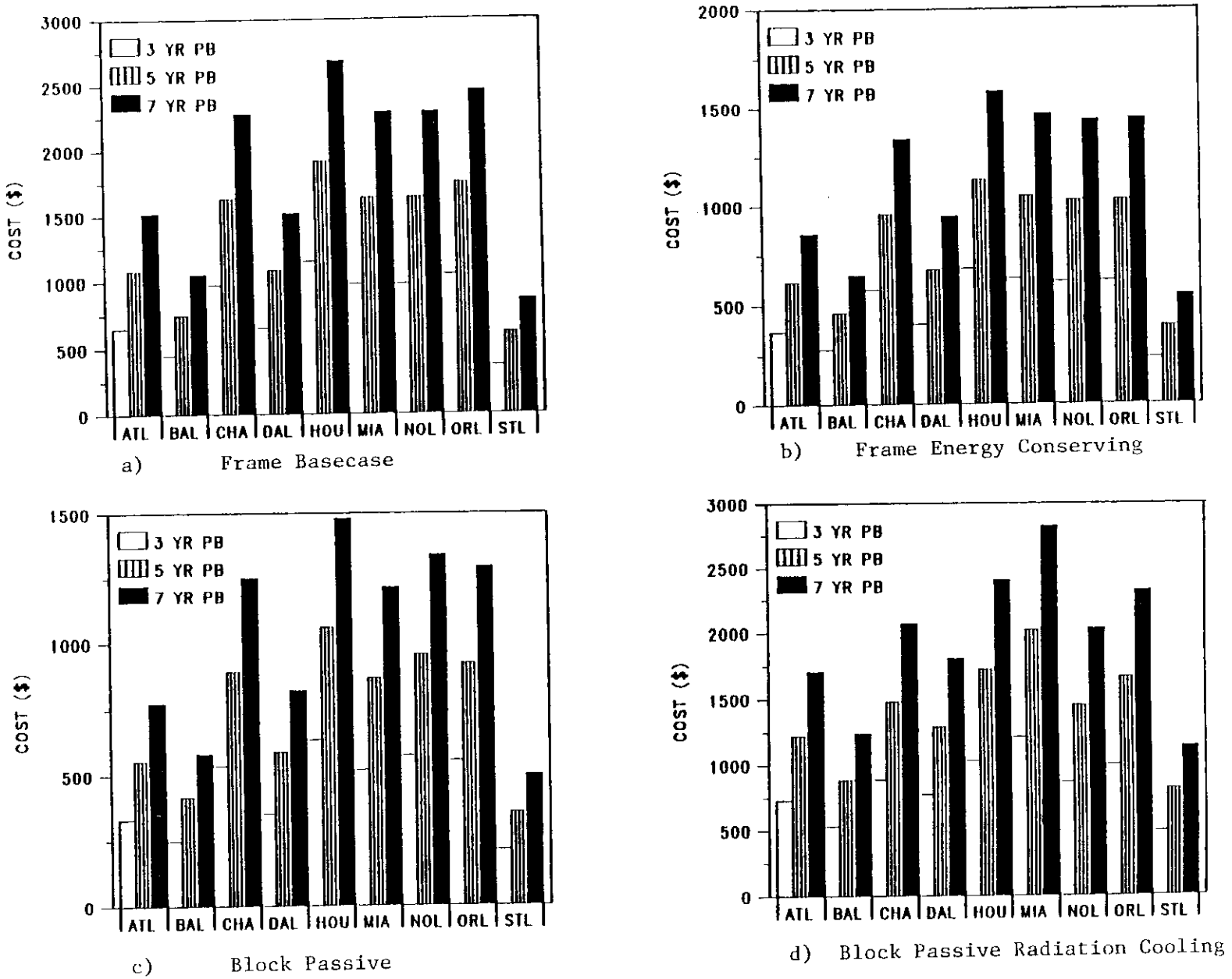

Figure 5-12 Maximum allowable initial investment differential for various simple paybacks assuming a ten year life and uniform utility costs in all cities for room conditions of 78°F and 58% RH.

condition of the ASHRAE Standard 55-1981 for human comfort at a room temperature of 78°F. There is absolutely no firm evidence to indicate that homeowners or building occupants will seek extra dehumidification capacity if room relative humidities exceed this limit.

According to the Association of Home Appliance Manufacturers, 591,000 electric dehumidification units were shipped in 1984. There is no specific knowledge of the total dehumidification capacity this number of units represents. However, information obtained from Sears Roebuck, Inc. (which hold 40% of the total market) indicates that the largest majority of their sales of such equipment is in the 30-40 pint per day range. Furthermore, Sears estimates that only 10% of their sales are in the southeastern Gulf Coast sector of the U.S.[1]. This estimate indicates that no more than 60,000 electric dehumidification units with a total capacity of 245,000 pints are sold for summer dehumidification. It further indicates that southern home residents may not be overly concerned with room humidity levels which exceed 58% RH.

In order to examine the degree to which the 58% room RH limit has affected the results of this economic analysis, four climates (Miami, Houston, Orlando and Atlanta) have been evaluated for the basecase and energy conserving frame residences at room humidity upper limits of 68% RH. The 68% RH limit was chosen because current research ([Humphries, 1972] and [Sterling, 1985]) indicates that this may be an upper threshold for the growth of mold and mildew in enclosed spaces. This is substantiated in part by the sales figures for dehumidifiers. Marketing analysts for Sears and other companies assume (and probably correctly) that upward of 90%

---

1. Phone conversation between P. Fairey and Assistant National Marketing manager for Plumbing at Sears headquarters in Chicago.

of the dehumidifier sales in the U.S. are to relieve summer basement moisture problems in the relatively cool climates of the northeastern U.S. Without such dehumidification equipment there is ample reason to believe that mold, mildew and rust would constitute significant problems for the homeowner under circumstances where cold basement walls contact relatively humid basement air.

The results of this analysis indicate that similar problems would occur in the humid southeast as well. For passively cooled buildings the problem could be extensive. Figure 5-13 shows that for each of the four major climates a shift in room RH patterns occurs for passively cooled buildings. The extent of the shift depends heavily on the degree of cooling done by the hybrid/passive system.

The results of the economic analysis are given in Figure 5-14. They show a marked increase in simple payback periods for the 68% RH limit. Nonetheless, for certain climates and building strategies a significant incentive still exists for the use of dehumidification equipment. Although payback periods climb to as high as seven years in Miami for the energy conserving residence, they are as low as nine months in Houston for the basecase residences. Payback periods of less than three years are obtained for appropriate passive cooling methods (e.g., radiator in Miami, earth-tube in Atlanta). This is indicative of the fact that gas-fired dehumidification may be a cost-effective solution to the high humidity problems faced by passive residences in the hot, humid southeast.

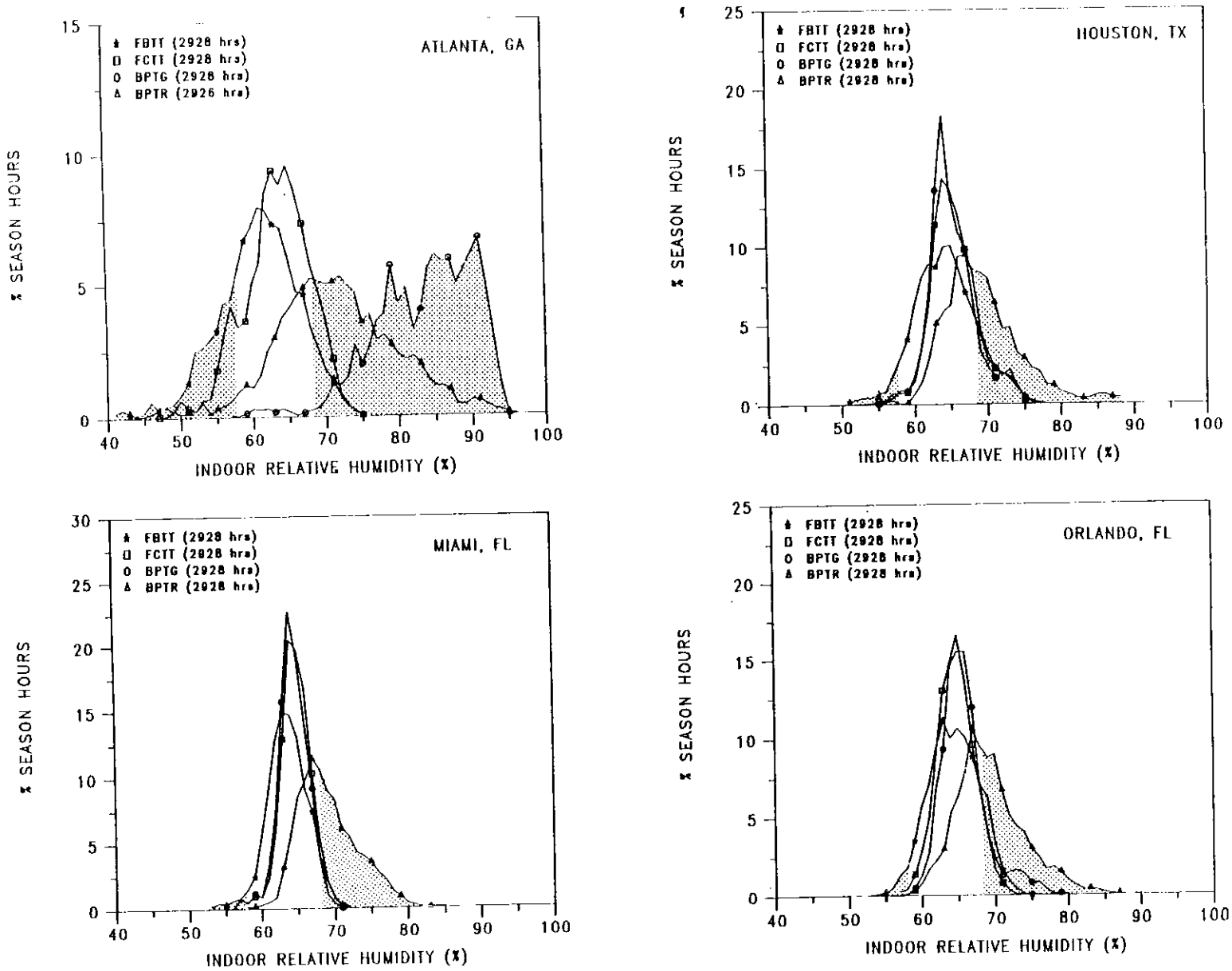

Figure 5-13 Effects of control strategy on resultant room relative humidity for four building types in four cities.

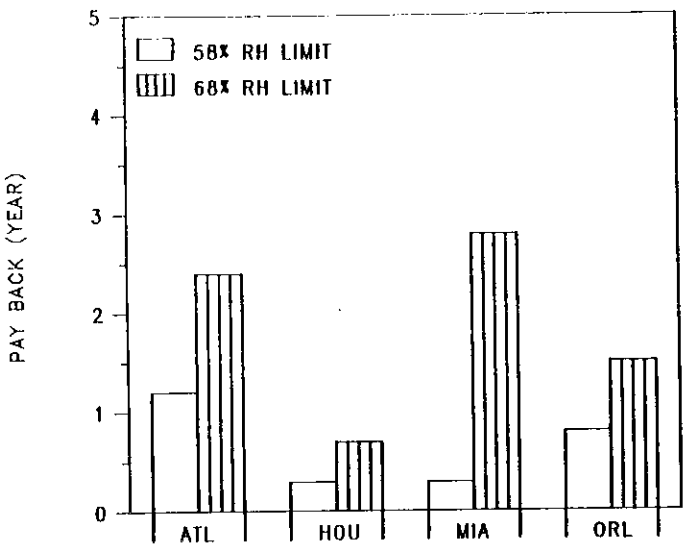

a) Frame base

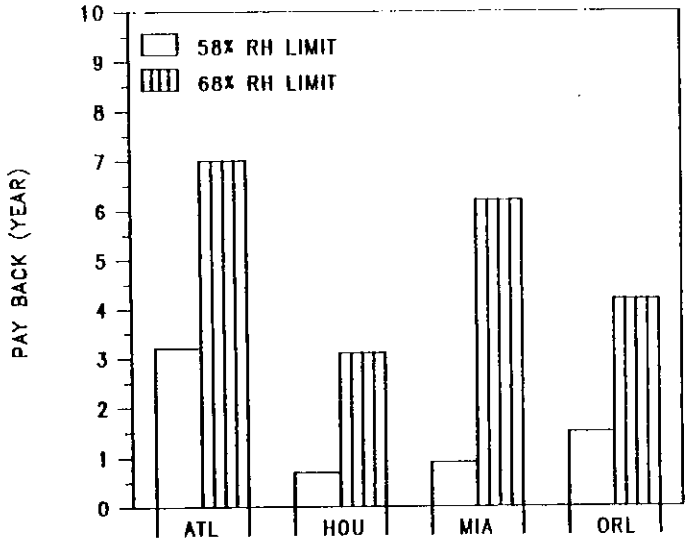

b) Frame Energy Conserving

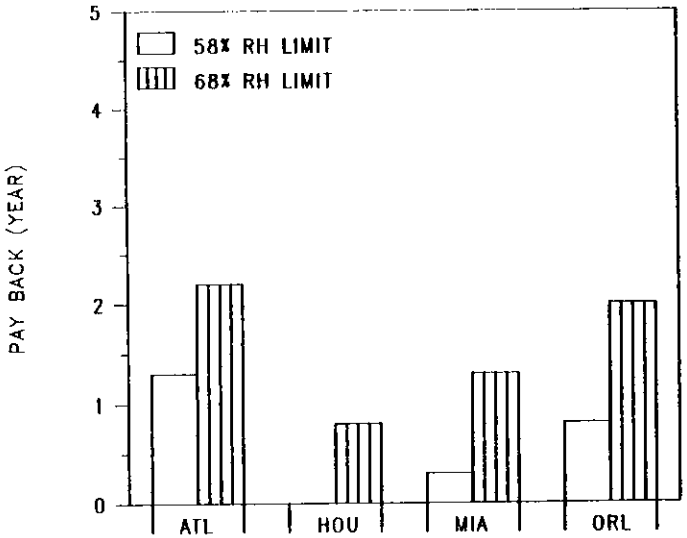

c) Block Passive-Radiation Cooling

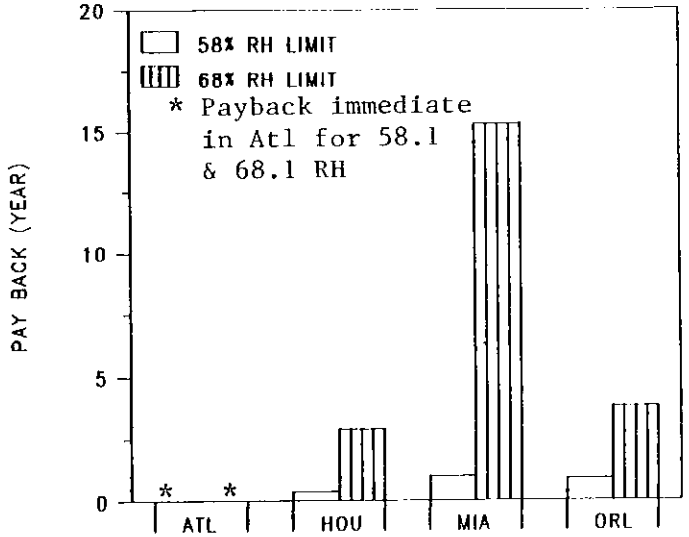

d) Block Passive Hybrid Earth-Tube Cooling

Figure 5-14 Comparison of simple payback periods for four building types in four climates at maximum room relative humidities of 58% and 68%.

SECTION SIX

REFERENCES

Abrams, D.W., C.C. Benton and J.M. Akridge, "Simulated and Measured Performance of Earth Cooling Tubes," Proceedings of 5th National Passive Conference, 1980.

ASHRAE, "Thermal Environmental Conditions for Human Occupancy," Standard 55-1981.

ASHRAE, ASHRAE Handbook-1981 Fundamentals, Atlanta: American Society of Heating and Air Conditioning Engineers, Inc., 1981.

Berdahl, P., and R. Fromberg, "An Empirical Method for Estimating the Thermal Radiance of Clear Skies," Lawrence Berkeley Laboratories, Report LBL-12720, 1981.

Carroll, J.A., "An MRT Method of Computing Radiant Energy Exchange in Rooms," Proceedings of the 2nd Systems Simulation and Economics Analysis Conference, 1980.

Chandra, S., P. Fairey and M. Houston, "Analysis of Residential Passive Design Techniques for the Florida Model Energy Code," Final Report to University of Central Florida, FSEC-CR-113-84, December 1984.

Clark, G. and M. Blanpied, "Radiative and Alternative Dehumidification Strategies for Humid Climates," Proceedings of the International PLEA Technical Conference, Bermuda, 1982.

Clark, G., "Passive Hybrid Comfort Cooling by Thermal Radiation," Proceedings of the Passive Cooling, ASES, Miami Beach, FL, 1981.

Cole, R.J. and N.S. Sturrock, "The Convective Heat Exchange at the External Surface of Buildings," Building and Environment, Vol. 12, (1977), p.212.

DeLima, H., J. Bluestein, and Chin, "Selection and Modeling of Residential Buildings," Presentation to FSEC Staff, June 1984.

Fairey, P., "Effects of Infrared Radiation Barriers on the Effective Thermal Resistance of Building Envelopes," Proceedings of the ASHRAE/DOE Conference on Thermal Performance of the Exterior Envelopes of Buildings II, Las Vegas, NV, December 1982.

Fairey, P.W., and A.A. Keresteciogl u, "Dynamic Modeling of Combined Thermal and Moisture Transport in Buildings: Effects on Cooling Loads and Space Conditions," presented at ASHRAE meeting in Honolulu, June 1985.

Fairey, P., G. Ventre, M. Houston, M. Khattar, and M. Girgis, "The Thermal Performance of Selected Building Envelope Components in Warm, Humid Climates," Proceedings of the 1983 ASME Solar Division Conference, Orlando, FL, April 1983.

Fanger, P.O. Thermal Comfort -- Analysis and Applications in Environmental Engineering., New York: McGraw-Hill, 1970.

Hendrick, Peter L., "Performance Evaluation of a Terrestrial Heat Exchanger," Proceedings of 5th National Passive Conference, 1980.

Hite, S.C., and J.L. Bray, "Research in Home Humidity Control," Purdue University, Lafayette, IN, June 1984.

Hittle, D.C., "Calculating Building Heating and Cooling Loads Using the Frequency Response of Multilayered Slabs," CERL Technical Manuscript E-169 (Construction Engineering Research laboratory, 1981), pp. 20-70.

Humphreys, W.E. "Condensation and Remedial Measures," Condensation in Buildings, London, England: Applied Science Publishers Ltd., 1972.

Goblenz, C.W. and P.R. Achenbach, "Field Measurements of Ten Electrically-Heated Houses," ASHRAE Transactions (ASHRAE, 1963), pp. 358-365.

Kammerud, R., et al., "Ventilation Cooling of Residential Buildings," ASHRAE Transactions, Vol. 89, Pt. II, 1983.

Keresteciogl u, A. "The Detailed Mathematical Prediction of Simultaneous Heat and Mass Transfer in Cavities, Ph.D. Dissertation, Florida Institute of Technology, Melbourne, FL, in publication.

Knapp, C.L., T.L. Stoffel and S.D. Whitaker, Insolation Data Manual, SERI, 1980.

Kosar, D., Letter and attachments to P. Fairey, January 10, 1985.

Kusuda, T., "Indoor Humidity Calculations," ASHRAE Transactions, Vol. 89, 1983.

Kusuda, T., NBSLD, the Computer Program for Heating and Cooling Loads in Buildings, National Bureau of Standards, (1976)

Kusuda, T., "Thermal Response Factors for Multilayer Structures of Various Heat Conduction Systems," ASHRAE Transactions, Vol. 75 (ASHRAE, 1969), p. 246.

Kusuda, T., and J.W. Bean, "Design Heat Loss Factors for Basement and Slab Floors," Proceedings of 4th ASTM Conference on Thermal Insulation, Materials and Systems, Dallas, TX, 1984.

Kusuda, T., M. Mizuno and J.W. Bean, "Seasonal Heat Loss Calculation for Slab-on-Grade Floors," NBSIR 81-2420, 1982.

Kusuda, T., O. Piet and J.W. Bean, "Annual Variation of Temperature Field and Heat Transfer Under Heated Ground Surfaces (Slab-on-Grade Floor Heat Loss Calculation)," NBS Building Science Series 156, 1983.

Labs, Kenneth, Regional Analysis of Ground and Above-Ground Climate," ORNL/Sub-81/40451/1, 1981.

Lachenbruch, A.H., "Three Dimensional Heat Conduction in Permafrost Beneath Heated Buildings," Geological survey bulletin 1052-B U.S. Government Printing Office, Washington, DC, 1957.

Loxsom, Fred, "Trinity's Typical Cooling Year," Trinity University, San Antonio, TX, 1980.

Luikov, A.V, Heat and Mass Transfer in Capillary Porous Bodies, Oxford, England: Pergamon Press, 1966.

Luikov, A.V., "System of Differential Equations of Heat and Mass Transfer in Capillary-porous Bodies," Int. J. Heat Mass Transfer, Vol. 18, 1975, pp.1-14.

Luikov, A.V. and Y.A. Mikhailov, Theory of Energy and Mass Transfer, Oxford, England: Pergamon Press, 1965.

Marciniak, T., et al., "Solid Desiccant Dehumidification Systems for Residential Applications," Final Report to GRI, Fauske & Associates, Inc. FAI/85-15, March 1985.

Miller, J.D. "Development and Validation of a Moisture Mass Balance Model for Predicting Residential Cooling Energy Consumption," ASHRAE Transactions, Vol. 90, Pt 2., 1984.

NBSIR 80-2184, "Energy Analysis of a Prototype Single-Family Detached Residence: the Effects of Climate, House Size, Orientation, Internal Heat Release, and Natural Cooling," U.S. Dept. of Commerce, Washington, DC, January 1981.

Peavy, B.A., "A Note on Response Factors and Conduction Transfer Functions," ASHRAE Transactions, Vol. 84 (ASHRAE, 1978), pp.688-690.

Scott, N.R., R.A. Parsons and T.A. Koehler, "Analysis and Performance of an Earth-Air Heat Exchanger," Presented at the Winter Meeting of American Society of Agricultural Engineers, 1965.

Sherwood, G.E., "Condensation Potential in High Thermal Performance Walls: Hot, Humid Summer Climate," U.S. Department of Agriculture, Forest Products Laboratory research paper No. FPL 455, Madison, WI, July 1985.

SOLMET, Hourly Solar Radiation Surface Meteorological Observations, Vol. 2, Washington, DC, 1979.

Sparrow, E.M., J. W. Ramsey and E.A. Mass, "Effect of Finite Width on Heat Transfer and Fluid Flow About an Inclined Rectangular Plate," Journal of Heat Transfer, Vol. 101, May 1979, p.204

Stephenson, D.G. and G.P. Mitalas, "Cooling Load Calculation by Thermal Response Factor Method," ASHRAE Transactions, Vol. 73 (ASHRAE, 1976).

Sterling, A., et al., "Criteria for Human Exposure to Humidity in Occupied Buildings," ASHRAE Transactions, Vol. 91, Pt I, 1984.

U.S. DOE, Economic Analysis Energy Performance Standards for New Buildings, Washington, DC, January 1980.

Vieira, R., S. Chandra and P.W. Fairey, "Residential Cooling Loads in Hot, Humid Climates," FSEC-PF-70-84, Proceedings 9th National Passive Solar Conference, Columbus, OH, September 24-26, 1984.

Vieira, R., "Energy Savings Potential of Dehumidified Roof Pond Residences, M.S. Thesis, Trinity University, San Antonio,TX, 1983.

Walton, G. TARP Reference Manual, NBSIR, 83-2655, Washington, DC: National Bureau of Standards, 1983.

Wexler, A., Humidity and Moisture, New York: Reinhold Publishing Co., 1965.